Role of the environment in establishment of definitive haematopoiesis

Jana Trávníčková

Collège Doctoral du Languedoc-Roussillon

THÈSE

Pour obtenir le grade de

Docteur

Délivré par UNIVERSITÉ DE MONTPELLIER

Préparée au sein de l'école doctorale ED-168 CBS2
Et de l'unité de recherche UMR 5235-DIMNP

Spécialité : Biologie santé

Présentée par Jana TRÁVNÍČKOVÁ

Rôle de l'environnement sur la mise en place de l'hématopoïèse définitive

Role of the environment in establishment of definitive haematopoiesis

Soutenue le 23 Septembre 2016 devant le jury composé de

Mme Cristina LO CELSO, DR, Imperial College London	Rapporteur
M Thierry JAFFREDO, DR, UMR-7622 CNRS, Paris	Rapporteur
Mme Mireille ROSSEL, MCF, U-1198 Inserm, Montpellier	Examinateur
Mme Karima KISSA, CR, UMR-5235 CNRS, Montpellier	Directeur de thèse

UNIVERSITÉ MONTPELLIER

Resumé

Rôle de l'environnement sur la mise en place de l'hématopoïèse définitive

L'hématopoïèse est le processus de formation des cellules souches hématopoïétiques (CSH); elle est conservée au cours d'évolution. Durant l'hématopoïèse embryonnaire, deux vagues hématopoïétiques se succèdent, la vague primitive et la vague définitive. La vague primitive produit des macrophages, des neutrophiles et des érythrocytes. Au cours de la vague définitive, les CSH émergent du plancher de l'aorte dorsale par une transition endothélio-hématopoïétique ou TEH, dans une région appelée aorte-gonades-mesonephros (AGM).

Ces dernières années, des études des organes hématopoïétiques chez les mammifères ont démontré que le microenvironnement joue un rôle crucial dans l'émergence et le devenir des CSH. Pendant ma thèse, je me suis intéressée au rôle du microenvironnement dans la mise en place de l'hématopoïèse définitive chez l'embryon de zebrafish. Dans l'AGM, j'ai caractérisé et évalué la contribution de différents acteurs dont deux populations en particulier, les macrophages et le système neuronal sympathique. Chacune de ces cellules joue un rôle spécifique durant la vague définitive de l'hématopoïèse. Les macrophages mobilisent des CSH de l'AGM afin de permettre leur intravasation et la colonisation des organes hématopoïétiques. Les catécholamines synthétisées par le système neuronal sympathique quant à elles contrôlent la TEH par l'activation des récepteurs beta2b et beta3 dans l'AGM.

En conclusion, nous avons démontré que le microenvironnement influence l'hématopoïèse définitive chez le zebrafish par différents mécanismes. Ces travaux ont pour objectif d'améliorer la compréhension du mécanisme de genèse des CSH et potentiellement de permettre un jour la production de CSH *in vitro*.

Mots-clés: Cellule souche hématopoïétique, Poisson zèbre, Microenvironnement, Macrophage.

Abstract

Role of the environment in establishment of definitive haematopoiesis

Haematopoiesis is the process of haematopoietic stem cell (HSC) generation conserved in all vertebrates. During the embryonic development, two successive waves of haematopoiesis occur – the primitive and the definitive wave. The first one gives rise to erythrocytes, macrophages and neutrophils. During the second one, HSCs emerge from the ventral wall of dorsal aorta (DA) in the aorta-gonads-mesonephros (AGM) region by a process called endothelial-to-haematopoietic transition or EHT.

In the last years, several studies performed in mammals have shown that the microenvironment plays a key role in haematopoiesis. During my thesis I have studied the role of the microenvironment in definitive haematopoiesis in the zebrafish embryo. I have described several cell components present in the AGM and evaluated their contribution to the haematopoiesis. I further analysed two of those players: macrophages and sympathetic nervous system. Each of them plays a specific role during the definitive wave of haematopoiesis. Macrophages mobilise nascent HSCs from the AGM to allow their intravasation and colonisation of haematopoietic organs. Catecholamines synthetized by sympathetic nervous system control EHT through the activation of beta2b and beta3 receptors in the AGM.

In conclusion, we have shown that the microenvironment can substantially influence the definitive haematopoiesis in the zebrafish by distinct mechanisms. These findings would help to understand the mechanism of HSC generation and potentially to allow *in vitro* HSC production.

Keywords: Haematopoietic stem cell, Zebrafish, Microenvironment, Macrophage.

Acknowledgements

At this moment, I would like to take the opportunity and acknowledge all the people without whom this project would not exist. The first and greatest thank belongs to Karima KISSA, my supervisor, who tutored and encouraged me through the whole time of my thesis. I thank her for all the advices and discussions, it was pleasure to work with her.

I gratefully acknowledge the University of Montpellier, the laboratory UMR 5235-DIMNP, all their members and their directors, Catherine BRAUN-BRETON and Georges LUTFALLA to accept me as a PhD student in their laboratory. Also I am thankful to the doctoral school CBS2 to allow me be its student and CBS2 student association for all the advices and event they organised.

I had a chance to work with many inspiring people whose ideas and suggestions allowed to accomplish this work. I am very grateful to all past and present members of Karima's team who supported and encouraged me through the whole time: Naoill ABDELLAOUI, Suma CHOORAPOIKAYIL, Laura FONTENILLE, Jean-Michel GIORGI, Magali GONZALEZ, Nadieh KUIJPERS, Etienne LELIEVRE, Sandra NICOLAS and Nausicaa POULLET. You were all great! Special thank belongs to Nausicaa and Etienne for their critical review of parts of my thesis manuscript.

During my PhD thesis I had the opportunity to co-supervise two master students, Sandra NHIM and Lukas HOCHTBERGER. They did a great job and helped to advance the research a lot. I hope they learned as much as I did during our work together. I wish them all the best in their future career.

This work could be performed thanks to several amazing collaborations. I would like to acknowledge:

- the group of Manuela TAVIAN in EFS in Strasbourg, France and especially her PhD student Emmanuelle JULIEN for the experiments on human embryos,
- the laboratory of Pertti PANULA for the tyrosine hydroxylase studies,
- Microscopy platform MRI CNRS and in particular Vicky DIAKOU, Elodie JUBLANC, Amélie SARRAZIN, Virginie GEORGET and Julio MATEOS-LANGERAK for their expertise in imaging techniques

- The group of Farida DJOUAD in IRBM, Montpellier, and her team members Mai NGUYEN-CHI, Béryl LAPLACE-BUILHE and Gautier TEJEDOR for their collaboration in the projects of macrophage behaviour and activation
- NeuroDialyTics platform and especially its director Sandrine PARROT in CRNL, Lyon, for catecholamine detection experiments
- The groups of Mireille ROSSEL and Alain GHYSEN in MNDM, Montpellier, for the collaboration and their expertise in nervous system in the zebrafish.

This research was supported by grants from the 'Ministère de l'Enseignement Supérieur et de la recherche' and from 'Fondation Recherche médicale' Nr. FDT20150532507 who provided my salary for four years. Other grants including ARC, ATIP-Avenir, FRM etc. allowed to perform the experiments.

I would like to express thank to my thesis committee members – Urszula HIBNER and Mireille ROSSEL for their advices and critical evaluation which always helped to advance our work. I thank very much to my thesis reviewers – Cristina LO CELSO and Thierry JAFFREDO – to evaluate my thesis manuscript and be part of the jury.

Working with animal model can be challenging sometimes and I wish to acknowledge the people who take care of the fish facility of helped us with troubleshooting any time we encounter a problem – Naoill ABDELLAOUI, Caty GONZALEZ, Stéphane CASTEL and Nicolas CUBEDO, you enabled us to work with the fish in the laboratory.

On a personal note, I would like to thank to PhD students and Post-Doc for the moments inside and outside the lab and all the inspiring discussion, particularly to Franciane PAUL, Anne-Laure GAGEZ, Tien QUANG-PHAN and Mariana ROSAS-OLVERA in addition to the team members mentioned above. Special thanks for the part 'DAA' for our 'research/gourmand' discussion with 'café frappé' in the afternoons.

Being far away from home can be sometimes very difficult. I wish to express my greatest thanks to my family for your never-ending support, encouragements and tolerance at any time during my stay in Montpellier. You were always the source of motivation. I wish to thank to my friends in Montpellier who made helped to feel like being at home.

Contents

List of figures

List of abbreviations

2D	two-dimensional
3D	three-dimensional

A

AGM	aorta gonad mesonephros
ANS	autonomic nervous system
ARG	arginase
Ascl1	achatae-acute complex homolog 1

B

BM	bone marrow
BMP-4	bone morphogenic protein 4
BSA	bovine serum albumin

C

CAR cells	CXCL-12-abundant reticular cells
ChAT	choline acetyl transferase
CHT	caudal haematopoietic tissue
CLP	common lymphoid progenitor
CMP	common myeloid progenitor
CNS	central nervous system
COMT	catechol O-methyl transferase
CXCR4	C-X-C chemokine receptor type 4

D

DA	dorsal aorta
DMSO	dimethyl sulfoxide
DβH	dopamine beta hydroxylase
	extracellular matrix

E

ECM	
EGF	epithelial growth factor
EHT	endothelial to haematopoietic transition
EMP	erythro-myeloid progenitors
EMT	endothelial to mesenchymal transition
EPO	erythropoietin

F

FGF	fibroblast growth factor

G

G-CSF	granulocyte colony stimulating factor
GM-CSF	granulocyte macrophage colony stimulating factor
Gr-1	Granulocyte differentiation antigen

H

Hh	Hedgehog
HM	hybridisation mix
hpf	hours post fertilisation
HSC	haematopoietic stem cell

I

ICM	intermediate cell mass
IFNɣ	interferon gamma
Igf	insulin like growth factort
Ihh	indian hedgehog
IL	interleukin

L

Lin	lineage
LSK	Lin/Sca/c-kit

LT-HSC	long term haematopoietic stem cell

M

MAPK	mitogen activated protein kinase
M-CSF	macrophage colony stimulating factor
MMP	matrix metalloproteinases
MO	morpholino
MPO	myoloperoxidase
MRC1	mannose receptor 1
MSC	mesenchymal stem cells

N

NCC	neural crest cell
Nes	nestin
NGF	neuronal growth factor
NK cell	natural killer cell
NO	nitric oxide
NOS2	inducible nitric oxide synthase

P

PBI	posterior blood islands
PBS	phosphate buffered saline
PCV	posterior cardinal vein
PECAM-1	platelet endothelial cell adhesion molecule
PGE2	prostaglandin E2
PKA	protein kinase A
PTU	phenylthiourea

S

SAP	subaortic patches
Sca-1	Stem cell antigen 1
SCF	stem cell factor

SCP	Schwann cell precursors
SDF-1	stromal cell derived factor 1
Shh	sonic hedgehog
SLAM	signalling lymphocytic activation molecule
ST-HSC	short term haematopoietic stem cell

T

TAM	tumour associated macrophages
TH	tyrosine hydroxylase

V

VAChT	vascular acetylcholine transporter
VEGF	vascular endothelium growth factor
VIP	vasoactive intestinal peptide

W

WASP	wiskott aldrich syndrome protein
WISH	whole mount in situ hybridisation

Y

Ym1	chitinase-3 like 3 protein

INTRODUCTION

Chapter 1: Introduction

1. Haematopoiesis

Blood is a connective tissue consisting of red blood cells, white blood cells and platelets suspended in plasma. The blood fulfils distinct roles, including oxygen and nutrient delivery, waste elimination, regulation of body temperature and pH. We can find in principle three groups of blood cells – erythrocytes, leukocytes (granulocytes, monocytes and lymphocytes) and platelets. All the differentiated cells are present in the blood in defined quantities with lifespan varying from few hours for granulocytes to several months for monocytes. Considering the relative short lifespan and continuous need of all blood cells, they renew constantly from the multipotent progenitor called haematopoietic stem cell (HSC).

1.1. Haematopoietic stem cell and its markers

The term "stem cell (in German Stammzelle)" had already appeared more than a century ago in 1868 when a German biologist, Ernest Haeckel proposed the stem cell as a unicellular organism from which all multicellular organisms evolved (rewieved by Ramalho-Santos and Willenbring, 2007). Later, he also used this term for the fertilized egg which gives rise to all cells of the organism (Ramalho-Santos and Willenbring, 2007). In the field of haematology, several scientist are credited for using the term stem cell as the multipotent progenitor of adult blood cells at the turn of the 20th century (Maximov, 1909; Pappenheim, 1896; reviewed by Ramalho-Santos and Willenbring, 2007). However, it lasted more than half of a century before the existence of HSCs was proved experimentally. In 1961, McCulloch and Till laboratory showed and quantified the presence of HSCs in the adult bone marrow (Becker et al., 1963; Till and McCulloch, 1961). They demonstrated that bone marrow cells after transplantation in the irradiated mouse form clusters of differentiated cells *in vitro*. These clusters are called colony forming units (CFU) and clonal analysis revealed the presence of all differentiated blood cell colonies as well as HSC self-renewal (Becker et al., 1963). The potential to differentiate into all blood cells is one of the characteristics of HSCs.

HSCs are characterised by their capacity of self-renewal, multi-lineage differentiation and production of all blood cells throughout the whole life (Yokota et al., 2012). This rare population of cells has attracted a large attention of scientists due to its high clinical application

potential, especially in order to treat haematological malignancies by transplanting HSCs or the whole haematopoietic tissues from healthy donors. Successful transplantation relies on the correct selection of HSCs. Therefore, the complete understanding of HSC biology as well as their unbiased identification by using accurate markers is essential. Until now, there is no unique surface marker that would allow to precisely identify HSCs, therefore a mix of several markers is currently used to identify and sort them (Yokota et al., 2012). A combination of markers called LSK is the most often adopted method for HSC identification. LSK stands for Lineage marker negative (Lin^-), Stem cell antigen-1 positive ($Sca\text{-}1^+$) and c-kit – also called Mast/stem cell growth factor receptor positive ($CD117^+$) (Ogawa et al., 1991; Spangrude et al., 1988; Yokota et al., 2012) . The term lineage marker includes markers specific for each of the differentiated blood cell populations, such as CD4 and CD8 for T-lymphocytes, B220 for B-lymphocytes, Gr-1 for granulocytes, Mac-1 for monocytes or glycophorin A-associated protein (Ter119) for erythrocytes (Spangrude et al., 1988). However, very soon after the establishment of those markers, it has been found that the LSK fraction is heterogeneous and contains both long-term and short-term HSCs as well as early progenitors (Yokota et al., 2012). Additional markers has been defined to specify the HSC fraction and enrich it for long-term HSCs which attracts the most attention (Yokota et al., 2012). Among those markers, we can count CD34 low-positive staining or an identification of HSCs activity by its ability to efflux DNA-binding dyes such as Hoechst33342 (Goodell et al., 1996; Yokota et al., 2012). An alternative combination of markers has been described recently and is based on the expression pattern of signalling lymphocytic activation molecules (SLAM) family – $CD150^+$, $CD48^-$ and $CD244^-$. The combination of the two systems, SLAM and LSK, leads to a gain of purity of the HSC population (increase of 50% compared to the single marker set) (Kiel et al., 2005; Oguro et al., 2013; Yokota et al., 2012). Since a combination of at least 4-5 markers is still required to identify a population highly enriched in HSCs, we are still seeking the unique and ideal marker of HSCs **(Figure 1)**. Today, discoveries and identification of new and potentially more specific markers are still published regularly. For instance, in the last 12 months, HoxB5 (Chen et al., 2016) and ESAM (Ishibashi et al., 2015) have been identified as new potential markers. Finally, we need to reconsider all the described markers from the distinct mammalian species point of view. All the markers mentioned above have been established using murine model and not all of them are conserved in human HSCs, for example the Sca1 or SLAM family (Larochelle et al., 2011).

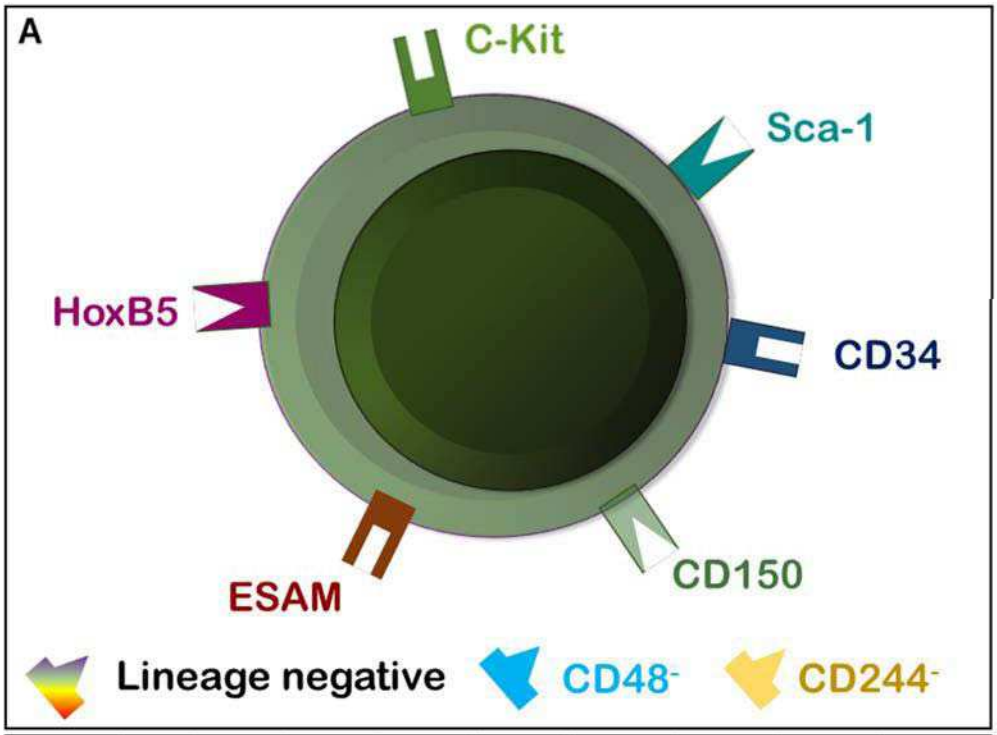

B	Lin-	C-Kit	Sca-1	ESAM	CD34	HoxB5	CD150	CD48-	CD244-
Human	√	low	x	√	√	?	x	x	x
Mouse	√	√	√	√	low	√	√	√	√

Figure 1 – Haematopoietic stem cells markers:
(A) Schematic representation of the surface markers identified as specific HSCs markers in mammals. Two main groups are represented in the scheme – LSK (Lineage, Sca-1 and c-kit) and SLAM (CD150, CD48 and CD244). Molecules designated under the drawing represent the negative markers used to eliminate other cell populations. (B) Table showing a comparison of markers in human and murine HSCs. SLAM family (CD150, CD48 and CD244) are not used for the identification of human HSCs. ESAM, endothelial cell-selective adhesion molecule; HSC, haematopoietic stem cell; Lin, lineage; Sca-1, stem cell antigen;

1.2. HSC and progenitor cell hierarchy

As previously stated, the search for specific markers has been dedicated mainly to identify a specific subpopulation of HSCs. HSCs can be divided into 2 groups regarding their activity – the long-term HSCs (LT-HSC, called also quiescent or dormant) and short-term HSCs (ST-HSC, dividing or active). LT-HSCs are the actual reserve of HSCs for the whole life – dividing only 5-6 times during life span – whereas ST-HSCs serve as a supply of blood cells – dividing actively to produce progenitors which will later differentiate into distinct blood cells. LT and ST-HSCs do not differ only in their activity but also in their localisation in the haematopoietic organs (Acar et al., 2015) and in the expression of specific markers. One of the

markers identified in the foetal liver to be specific for dividing HSCs is the GPI-80 (Prashad et al., 2015). Moreover, the level of expression of CD34 might help to distinguish between the LT and ST-HSCs. Low-level expressing cells show long-term reconstitution capacity, whereas high-level expressing cells exhibit only short-term differentiation corresponding to ST-HSCs (Osawa et al., 1996; Sudo et al., 2013). Foetal liver kinase 2 (Flk2 or CD135) is considered as another marker whose expression increases in ST-HSCs and reaches its highest level in multipotent progenitors (Boyer et al., 2011; Namikawa et al., 1996). ST-HSCs then give rise to oligo-potent progenitors: **common lymphoid progenitor** (CLP) and **common myeloid progenitor** (CMP), which have a more restricted differentiation potential. The CLP will give rise to lymphoid cells B and T, dendritic and natural killer cells (NK). The CMP, on the other hand, will differentiate into myeloerythroid cells, meaning monocytes and macrophages, granulocytes, erythrocytes and platelets (**Figure 2**). Each of the progenitors lacks the capacity to give rise to the blood cells originating from the other progenitor, confirming a more restricted fate for each population. In recent years, the HSC differentiation tree leading to more restricted fate at each step starts to be re-examined and new theories emerge. Most of the new theories considers the fate restriction less limited, suggesting that the progenitor cells would still keep the capacity to switch fate to give rise to cells from another branch (reviewed by Ceredig et al., 2009). The new concept of HSC hierarchy emerged thanks to evolving methods such as cell barcoding or single-cell transcriptomics (Grosselin et al., 2013; Paul et al., 2015; Wu et al., 2014). Each of these methods allowed precise single cell analysis and permitted to determine a detailed map of dynamic transcriptional states of progenitors. This revealed that cell fate is pre-determined from a very early stage but until full differentiation, the cell still keeps the capacity to switch into another cell fate.

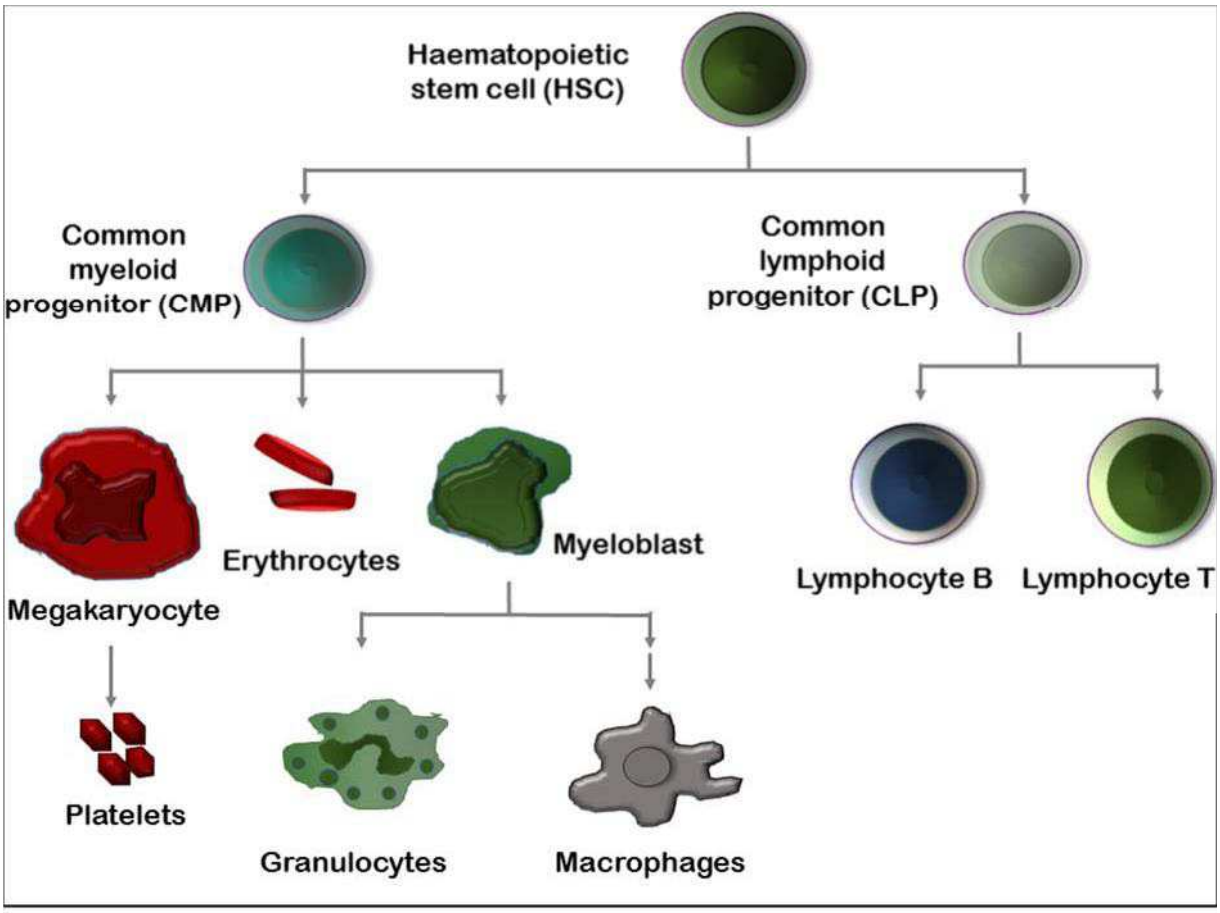

Figure 2 – HSC hierarchy:
Simplified tree representing the consecutive differentiation of mature blood cells from HSC. The exact hierarchy and progenitor stages not being the objective of this work, several multipotent and oligopotent progenitors have been omitted in this scheme.

Each of the differentiated cells then fulfil its specific role in the organism (as summarised in **figure 3**). **Erythrocytes**, called also red blood cells, differentiate progressively from erythroid progenitors through erythroblast and reticulocytes. The differentiation is dependent on several cytokines, including erythropoietin (EPO) and stem cell factor (SCF). Once differentiated, erythrocytes express Ter119, several globins and Gata1 on their surface (Lim et al., 2013). The function of erythrocytes is to transport oxygen bound to haemoglobin to all the cells and to eliminate carbon dioxide in the same way.

Platelets are fragments resulting from the large precursors called megakaryocytes. Megakaryocyte formation is based on repeated mitosis without being followed by cytokinesis. Megakaryocytes differentiate from HSPCs in presence of thrombopoietin, IL-6 or IL-11. After maturation, platelets express on their cell surface several markers, including CD41 (Lim et al., 2013). The main role of platelets is the clotting process and the prevention of bleeding.

Leukocytes, called also white blood cells are present in a small amount (they represent only 1% of total blood volume) but they are a highly heterogeneous blood population. They are required for the organism defence and are the key regulators of immunity. They differentiate from both branches of common precursors, the lymphoid and myeloid progenitors (Lim et al., 2013). **Granulocytes** represent the largest subgroup of leukocytes and further divide into neutrophils, eosinophils and basophils. A general commonly used marker for granulocytes is Granulocyte differentiation antigen (Gr-1). *In vitro*, differentiation of precursors into granulocytes is induced using the granulocyte colony stimulating factor (G-CSF), granulocyte-macrophage CSF (GM-CSF) and IL-6 (Lim et al., 2013). All three cell types are involved in innate immunity and are active phagocytes. The name granulocytes refers to their morphological characteristics as they are described as large cells with lobed nuclei and visibly stained granules. Neutrophils are the most common members of granulocytes and are directly involved in all acute and chronic inflammations. They are chemically attracted to the site of infection and fight against microorganisms via phagocytosis, reactive oxygen or nitrogen species, for example. The granule staining by Sudan black is one of the main markers for matured neutrophils together with the expression of myeloperoxidase (MPO). Eosinophils are more involved in parasitic infections, while basophils promote inflammation (both infectious and sterile) through histamine production.

Monocytes and their differentiated counterparts, **macrophages,** contribute to innate immunity as well as processes during embryonic development. They will be referred in details in Part 4. Macrophages differentiate from myeloid progenitors in the presence of macrophage CSF (M-CSF) through monocytes. Matured macrophages exhibit several markers such as the F4/80, CD11b, CD14 or CD115 (Lim et al., 2013).

Lymphocytes are the key players in adaptive immunity and regulation of the immune response. **T-lymphocytes** (T-cells) might be further divided into 3 groups: cytotoxic T-cells involved in the resolution of viral infections, memory T-cells (CD-4 and CD-8) providing memory of past infections and helper T-cells, which support the maturation or activation of other immune cells. T-lymphocytes differentiate and mature from the lymphoid progenitors in the thymus, one of the adult haematopoietic organs, in the presence of Flt-3 and IL-7 (Lim et al., 2013). Lymphoid precursors express the ikaros marker common for both T- and B-lymphocytes, while the matured T-cells might be recognised using markers such as T-cell receptor, CD-4 and 8 or recombination-activating genes (RAG-1 and 2) (Lim et al., 2013). **B-**

lymphocytes (B-cells) play a role in the humoral immunity. They display antigens and secrete various cytokines. B-cells differentiate under similar conditions as T-cells, in the presence of IL-6 or Flt-3, differentiating from common progenitors expressing the marker ikaros (Bonifer et al., 1998; Lim et al., 2013). The final step of maturation from pro-B-cells is controlled by Pax5 expression (Bonifer et al., 1998).

	Name	Number (cells/µl)	Life-spin (days)	Function
	Erythrocytes	4-6 million	120	Transport O_2 and CO_2
	Platelets	150 000 – 400 000	5-10	Blood coagulation
	Monocytes Macrophages	100 – 700	Months	Phagocytosis, innate immunity Lymphocyte activation
	Granulocytes	3000 – 7000	1-14	Phagocytosis, innate immunity, allergic reaction, Antiparasitic
	Lymphocytes B	1500 - 3000	hours to years	Antibody production
	Lymphocytes T	1500 - 3000	hours to years	Cell immunity

Figure 3 – Differentiated blood cell characteristics:
Table summarising the quantity of blood cells present in the blood, their average life-span and their main physiological function in adult human organism. Each cell population is associated to the drawing used in figure 2 – HSC hierarchy. Cell quantities are represented as number of cells in 1 µl. Life span is indicated in days if not specified in the line.

1.3. Embryonic haematopoiesis

Even though most of the studies on haematopoiesis was performed using mammalian embryos, other species also contributed to the research in the field. Non-mammalian models used for haematopoiesis studies are introduced in Chapter 2. In some cases, the observations in non-mammalian species preceded those done in mammals and for that reason they will be mentioned in this chapter to emphasise particular events.

The idea that blood cells are already formed in the embryo emerged more than a century ago. In 1912, Charles S. Minot in the Manual of Human embryology, which is the textbook addressed to embryologists and all physicians in general, suggested that the formation of intra-aortic blood clusters originated from the endothelium or at least adhered to the aortic endothelium in the human embryo (Minot, 1912). Yet, the exact origin of these cells remained unclear and the question of the origin of blood cells from the intra or extra-embryonic source arose. Both hypotheses of HSCs origin re-emerged in the 1970's when Moore and Metcalf described that the yolk sac mesoderm was capable to generate cells with haematopoietic activity while Dieter-Lievre suggested an embryonic origin of HSCs (Dieterlen-Lievre, 1975; Moore and Metcalf, 1970).

Today, a cascade of several waves with distinct haematopoietic activities during embryo development is a well-established consensus accepted by the majority of scientists in the field. During embryonic development, two successive waves of haematopoiesis occurs: the primitive and definitive waves. The **primitive wave** takes place prior to blood circulation in the extra-embryonic mesoderm, beginning around day E7 to E7.5 in mice and at day 21 in the human embryo (Medvinsky et al., 2011; Mikkola and Orkin, 2006). The yolk sac has been demonstrated experimentally as the first place with haematopoietic activity and has been considered for a while as the only source of haematopoietic cells (Moore and Metcalf, 1970). However, raising evidence on the intra-embryonic source of blood cells accumulated. In particular, it was shown that yolk-sac originating blood cells lack self-renewal capacity and that HSCs could be detected well after the peak of the primitive wave (Cumano et al., 1996; Medvinsky and Dzierzak, 1996). Indeed, the primitive wave give rise to a restricted number of blood cell populations such as primitive nucleated erythrocytes, macrophages and neutrophils (Palis et al., 1999). The interest to procure studies on the primitive wave of haematopoiesis declined after the discovery of the definitive wave and the description of HSCs. Currently, the importance of the primitive wave is being re-established. Recent studies showed that primitive macrophages play a role until adulthood as members of tissue-resident macrophage populations and that the primitive wave may influence the definitive wave (Espín-Palazón et al., 2014; Gomez Perdiguero et al., 2014). Around day E8.25, another wave of myelo-erythroid progenitors occurs. The myelo-erythroid progenitors then differentiate into two specific lineages, the erythrocytes and myeloid cells (Palis et al., 1999). The lineage fate decision is controlled by an antagonism between two transcription factors, GATA1 and PU.1. While

GATA1 represents a critical factor for the erythroid and megakaryocyte differentiation, PU.1 mediates myeloid cell differentiation. GATA1 and PU.1 transcription factors antagonise their respective activity and auto-regulate themselves, which permit to keep balance between numbers of erythroid and myeloid cells (Graf, 2002). Recently, new findings using long-term single cell tracking demonstrated that blood cell differentiation does not fully correspond to the balance of the two restriction factors. Their results suggest that this balance would rather be a supportive mechanism to the lineage choice decision of already partially restricted progenitors (Hoppe et al., 2016).

The **definitive wave** of haematopoiesis follows the primitive wave and is the only source of haematopoietic stem cells. It occurs at day E10.5 in the mouse and at day 28 in the human embryo in the aorta-gonad-mesonephros (AGM) (Gritz and Hirschi, 2016; Medvinsky et al., 2011; Miiller et al., 1994; Mikkola and Orkin, 2006; Tavian et al., 2010). Even though the AGM had been demonstrated as the intraembryonic site of definitive haematopoiesis already in the 1990s, the cellular origin of HSCs still remained an unanswered question (Cumano and Godin, 2007; Gritz and Hirschi, 2016). Two distinct theories about HSCs cellular origin emerged. While the first one considered the mesodermal cells underlying the dorsal aorta as the precursor of the HSCs, the second one favoured the endothelial origin (Cumano and Godin, 2007; Tavian et al., 2010). The first theory described the presence of sub-aortic patches (SAP), structures located below the aortic floor (**Figure 4A**). These structures then migrate toward the aortic floor to intercalate and reach the bloodstream in order to later colonise the haematopoietic organs (Cumano and Godin, 2007; Tavian et al., 2010). The second theory relied on the **endothelial origin**. In this theory, the **haemogenic endothelium** is the common precursor for two populations – the vascular endothelium and the HSCs (**Figure 4B**). The haemogenic endothelium appears to differentiate from a common precursor of all endothelium – the vascular and the haemogenic one, called the haemangioblast. The endothelial origin of the HSCs was confirmed recently by several laboratories using different animal models. For this reason, only this model will be introduced in details in the following paragraphs.

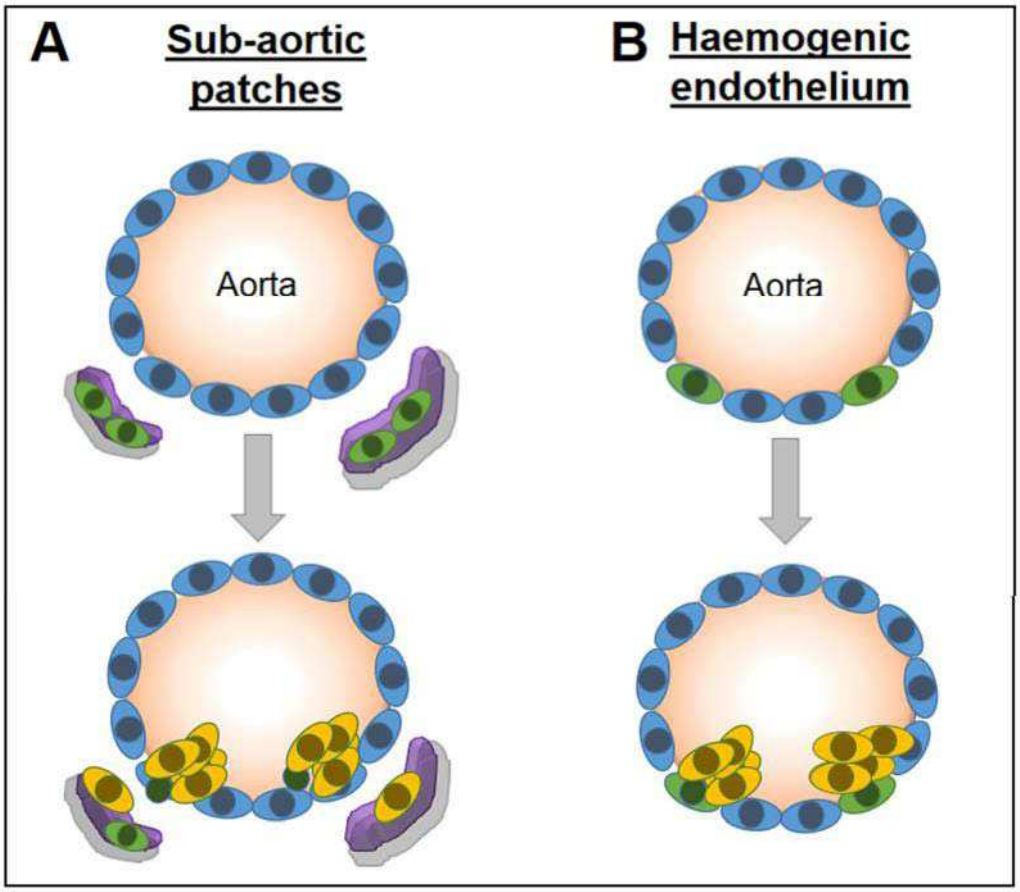

Figure 4 – Two distinct theories of HSCs embryonic origin:
(A) The sub-aortic patches theory proposing the mesodermal origin of the HSCs migrating from the sub-aortic patches (green/purple) to intercalate in the vascular endothelium and give rise to intra-aortic clusters of HSCs (yellow). (B) The haemogenic endothelium theory suggesting the common progenitor for vasculature and blood cells.

1.4. Endothelial origin of HSCs

The lineage relationship between endothelium and HSCs has been proposed based on the fact that they share a number of surface markers such as Flk1 (Kabrun et al., 1997). An additional feature that supports the connection between HSCs and endothelium is the time of HSC development. The vascular endothelium specification precedes HSC emergence, therefore the endothelium might play a direct role in blood cell development (Dieterlen-Lièvre et al., 2006; Gritz and Hirschi, 2016; Jaffredo et al., 1998; Oberlin et al., 2002). The theory proposing the emergence of HSCs directly from vascular endothelium led to the definition of the haemogenic endothelium. This idea emerged already in the beginning of the 20th century based on the observations performed in pig embryo (Jordan, 1916). The haemogenic endothelium has been characterised as a cell population expressing endothelial markers, such as Flk1, VE-Cadherin, or KDR and being part of the vascular endothelium, but at the same time having the

capacity to produce HSCs (Oberlin et al., 2002). Recently, several studies has demonstrated that HSCs originate from the haemogenic endothelium by a trans-differentiation process based on the increase of haematopoiesis-specific markers and the decrease of vascular markers **(Figure 5)**. These studies excluded at the same time the origin of HSCs from the underlying mesenchyme (Boisset et al., 2010; Bruijn et al., 2002; Lancrin et al., 2012; Zovein et al., 2008). The haemogenic endothelium specification is govern by SCL gene (also called TAL-1), which was first identified as a T-cell oncogene and later proved to be expressed in the blood, endothelium and brain. SCL expression already controls definitive haematopoiesis at very early stage as a crucial factor of the haemangioblast to haemogenic endothelium step. The key function during this step has been described for the first time in the zebrafish embryo before being confirmed with additional details in mouse embryos (Gering et al., 1998; Lancrin et al., 2009). GATA2 and ETV2 range among the transcription factors co-expressed with SCL in the early mesoderm to expand haemangioblast and initiate definitive haematopoiesis **(Figure 5)**. GATA2 appears to affect all steps of haematopoiesis including yolk sac-derived haematopoiesis and definitive haematopoiesis in the AGM. GATA2 and FLI-1 form a complex which bind to SCL and induce haemogenic endothelium specification. It also induces the BMP4 pathway (Ling et al., 2004; Lugus et al., 2007; Shi et al., 2014).

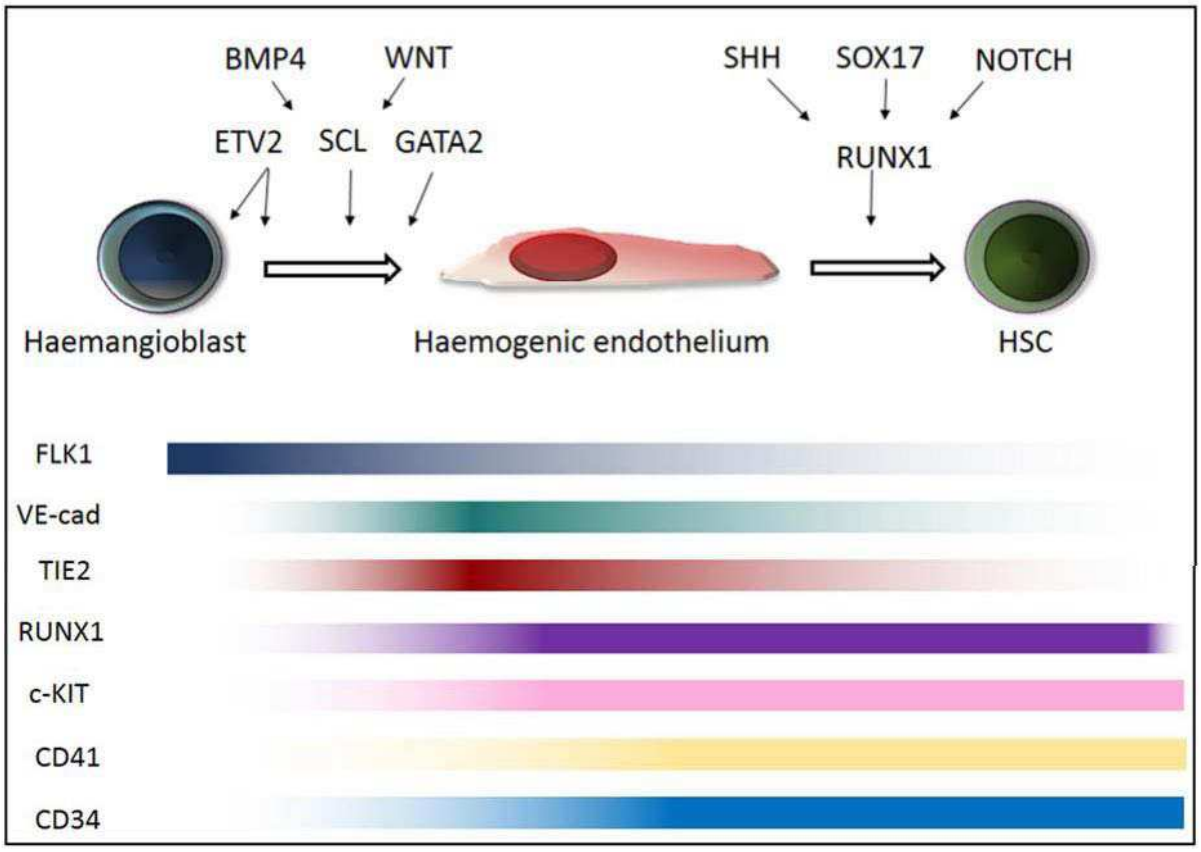

Figure 5 – HSC embryonic development:
Differentiation of HSCs from haemangioblast through haemogenic endothelium by increasing HSC markers and decreasing vascular markers. The upper part represents the signalling molecules involved in the individual steps of HSC emergence while the lower part describes the evolution of endothelial and HSC markers. Relative increase/decrease of marker expression is indicated by saturation/transparency of colour over time. BMP4, Bone Morphogenetic Protein 4, Etv2, Ets Variant gene 2; FLK1, Foetal Liver Kinase 1; HSC, haematopoietic stem cell; SHH, Sonic Hedgehog; TIE2, Tyrosine kinase with Immunoglobulin-like and EGF-like domains 2; VE-cad, Vascular Endothelium Cadherin,

Once the haemogenic endothelium is specified, HSC emergence occurs. The process of HSCs production itself is referred as the endothelial-to-haematopoietic transition. This process has been described concurrently in the mouse and zebrafish embryos (Bertrand et al., 2010a; Boisset et al., 2010; Kissa and Herbomel, 2010), which confirms once again the conserved mechanism of haematopoiesis in vertebrates. The endothelial cell starts to separate from a uniform endothelial cell layer, polarises, bends and slowly detaches from the endothelium to form intra-aortic clusters. This process as well as the specification of haemogenic endothelium is dependent on Runx1 transcriptional factor and several signalling pathways (**Figure 5**), including Notch, Wnt and Hedgehog (Gritz and Hirschi, 2016).

1.5. Signalling pathways

Notch signalling pathway is involved in many aspects of embryonic development and plays a role in cell fate decision and cell differentiation. It was identified for the first time in *Drosophila* mutants, but it is evolutionary conserved in most species including mammals. Notch is a family of transmembrane receptors containing 4 different receptors in mammals named Notch1-4. It binds to a ligand located on the surface of the same cell or the adjacent one for the juxtacrine signalling (Bigas and Espinosa, 2012). At least 5 functional Notch ligands exist in vertebrates. They are divided into 2 groups – Delta or Delta-like (Dll 1, 3, 4) and Jagged (1 and 2). Each ligand has a different expression pattern and a distinct resulting signalling. During embryonic haematopoiesis, Notch plays a crucial role in the determination of the haematopoietic fate but also in the arterial fate. Three Notch ligands, Jagged 1, Jagged 2 and Delta 4 are expressed in aortic endothelium. The two cell fates – hematopoietic versus arterial – are controlled by specific Notch ligands. Jagged 1 mutants still express endothelial markers but fail to produce HSCs, demonstrating that Jagged 1 is involved in HSC production. On the other hand, Jagged 2 and Delta 4 are required for arterial specification (Bigas and Espinosa, 2012; Kim et al., 2013).

Similarly to the Notch pathway, **Wnt signalling** is also involved in many areas of embryonic development. The Wnt family consists of 19 ligands that bind to Frizzled receptors to activate one of the distinct downstream pathways. These downstream pathways are divided into either canonical group, such as β-catenin, or non-canonical pathway, for example JNK and PKC. Wnt/ β-catenin activity is transiently required for the emergence of LT-HSCs in the AGM. It seems that a transient activation is required for the specification of the haemogenic endothelium in the AGM and is gradually down-regulated once the haemogenic endothelium starts to undergo EHT to form HSCs (Gritz and Hirschi, 2016; Ruiz-Herguido et al., 2012).

Hedgehog signalling (Hh) also belongs to pathways playing an essential role during embryonic development. Initially identified in *Drosophila* as a single Hh gene, Hedgehog signalling has 3 ligands in vertebrates, Sonic hedgehog (Shh), Indian hedgehog (Ihh) and Desert hedgehog (Dhh). Ihh has been identified as the ligand present in haematopoietic cells among other tissues (Lim and Matsui, 2010). Hh signalling plays a role during both the primitive and definitive waves of haematopoiesis. Ihh is required for the formation of blood islands during

the primitive wave, while Shh seems to affect several aspects of definitive haematopoiesis, ranging from proliferation to differentiation (Lim and Matsui, 2010).

Transforming growth factor beta (TGF-β) and especially its member bone **morphogenetic protein 4 (BMP-4)** regulates HSC generation. Mice lacking BMP4 die *in utero* prior the blood formation, suggesting that BMP4 is crucial during early development. Moreover, studies in other species such as *Xenopus* have confirmed the role of BMP4 signalling in the primitive and definitive waves. Its expression may induce the expression of a number of HSC-associated transcription factors, including SCL, GATA-2 or LMO-2. Another point of interest is the polarized expression of BMP4 spatially in the AGM. BMP4 expression is restricted to the ventral part of the AGM, corresponding perfectly to the exclusive region of HSC emergence and formation of intra-aortic clusters in human (Durand et al., 2007; Marshall et al., 2000; Sadlon et al., 2004). This suggest that BMP4, which is described as a ventralising factor during the early development, may equally contribute to intra-aortic clusters specific ventralisation (Dale et al., 1992). BMP4 may play role during late phases of EHT as nascent HSCs increasingly express BMP4 ligands (Durand et al., 2007). Interestingly, the mouse embryo is the only known exception for this expression pattern among all vertebrates. Indeed, in the AGM of the mouse embryo, BMP4 is expressed in the whole aorta and concomitantly, the formation of the intra-aortic clusters is not restricted to the ventral part (Yokomizo and Dzierzak, 2010).

Other signalling molecules have been proposed to play a role during definitive haematopoiesis. **Homeobox genes**, such as SOX and HOX have been shown to determine cell identity during embryonic development. Hox paralogue group 3 (Hoxa3) affects endothelial and cardiovascular development and seems to play a role in the maintenance of the endothelium prior to haematopoietic transition (Iacovino et al., 2011). Sox17 is a downstream target of Hoxa3 and is equally required for HSCs emergence, probably through Notch1 signalling, because a loss of Sox17 decreases Notch1 expression (Clarke et al., 2013; Gritz and Hirschi, 2016).

The activation of these signalling pathways leads to the expression of transcription factors which are essential regulators of EHT, as well as markers currently used for embryonic HSCs identification (Gritz and Hirschi, 2016). The principal transcription factor, **RUNX1** (AML1) governs the determination of haematopoietic fate from the haemogenic endothelium.

Its expression precedes EHT and is therefore considered as one of the earliest markers of HSCs. RUNX1 is specifically required to induce EHT but not thereafter when HSC markers are expressed (Chen et al., 2009). Nevertheless, RUNX1 expression is not limited exclusively to the haemogenic endothelium in the mouse embryo. It is also found in mesenchymal cells in the dorsal aorta and in the AGM, in the placenta, in haematopoietic cell clusters, in vitelline and umbilical arteries (North et al., 1999, 2002).

1.6. Embryonic HSCs markers

Apart from Runx1, other markers have been used to identify embryonic HSCs. Another principal marker proposed for HSC identification is the integrin alpha-IIB, also called CD41 or ITGA2B. Unlike other markers, CD41 protein is expressed only by nascent HSCs, while mature HSCs have lower CD41 expression (Mikkola et al., 2003; Robin et al., 2011). In the mouse embryo, HSCs do not express CD41 anymore in the foetal liver (Robin et al., 2011). CD41 expression later become restricted to megakaryocytes (Mikkola et al., 2003). The transcription factor cMyb also lines up to nascent HSCs markers and its lack impairs definitive haematopoiesis, specifically HSCs maintenance and differentiation (Gritz and Hirschi, 2016). Endoglin (CD105) is another marker reported in the embryonic aortic region and nascent HSCs. Moreover, its level of expression differs according to the type of HSCs. Short-term HSCs and progenitors express intermediate levels of CD105 while high expression is restricted to the long-term HSCs (Roques et al., 2012). Several markers currently used for adult HSCs are expressed in both adult and nascent cells including CD34, PECAM-1 and c-kit **(Figure 6)**. C-kit is one of the few markers whose expression level does not differ during development and might be used for identification of both embryonic and adult HSCs. On the other hand, CD34 expression decreases during adulthood and its higher level of expression becomes restricted to ST-HSC (McKinney-Freeman et al., 2009; Osawa et al., 1996).

Contrary to the previously described markers, CD45 is upregulated during HSC maturation and might be used to distinguish pre-mature from mature cells (McKinney-Freeman et al., 2009). CD150 and CD48 also count among the markers whose expression increases with HSC maturation and during haematopoietic organ colonisation. Their differential expression permits to distinguish HSCs at different stages of maturation (McKinney-Freeman et al., 2009).

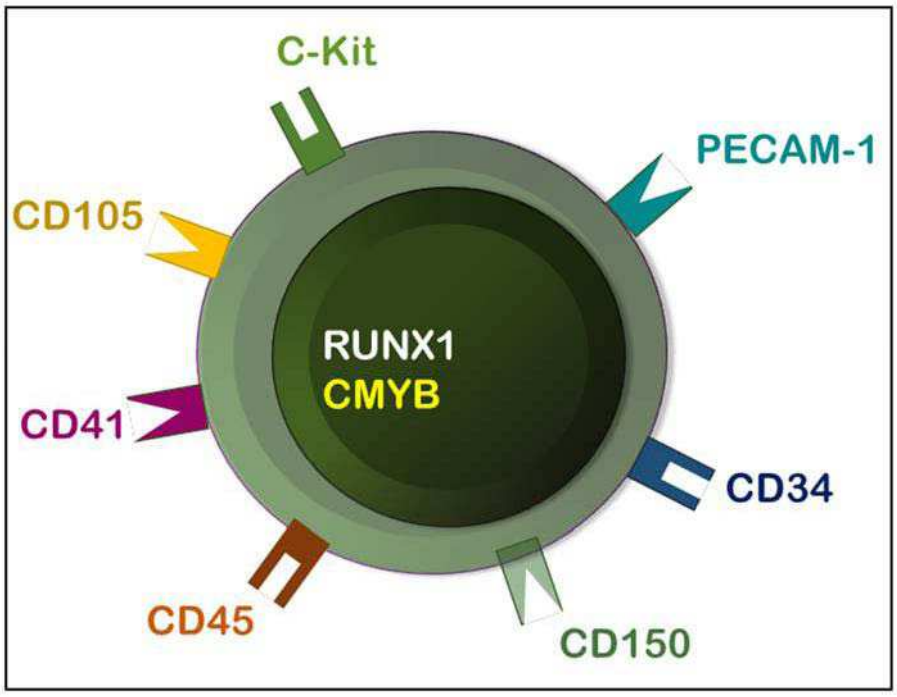

Figure 6 – Embryonic HSC markers:
The surface markers and transcription factors used to identify embryonic HSCs in mammals. The markers are differentially expressed during successive steps of HSC emergence and maturation. RUNX1, cMyb and CD41 are expressed during early phases and in nascent HSCs, while CD105, C-kit, CD34 and PECAM-1 remains until adulthood.

1.7. The HSC journey

The AGM region is considered as the only intraembryonic source of HSCs. In mammals, haematopoietic activity has been described in placenta in addition to the AGM. The placenta is an extraembryonic tissue forming the interface between the foetus and the mother. This highly vascularised tissue has been identified as an important source of HSCs which do not originate from the AGM (Dzierzak and Robin, 2010; Gekas et al., 2005; Robin et al., 2009). As the placenta is a specific organ of mammalian development and is not present in lower vertebrate species, it will not be detailed in this introduction.

After emergence and maturation, HSCs first seed the foetal liver which is an embryonic or transitory haematopoietic organ (**Figure 7**) before colonising the definitive haematopoietic organs (**Figure 7**). HSCs localised in the sub-aortic clusters within the dorsal aorta become mobile and join the blood circulation. The circulating HSCs seed the foetal liver from day E11.5 for the mouse and E30 for the human embryo (Mikkola and Orkin, 2006). The **foetal liver** is a haematopoietic organ exclusively during embryonic development and during postnatal stages the liver's function becomes restricted to metabolism.

In the transitory haematopoietic organ, HSCs highly proliferate. Throughout the whole ontogeny, the proliferation rate of HSCs is at its highest in the foetal liver (Ema and Nakauchi, 2015). The number of cells reaches its maximum around day E16 in the mouse embryo and then starts to decline (Mikkola and Orkin, 2006). The behaviour of HSCs in foetal liver differs from the one of HSCs seeded in definitive haematopoietic organs, where they are mostly quiescent while in the foetal liver proliferation predominates. In the foetal liver, cells are actively cycling and specific signals might be required to promote symmetric divisions. Several factors have been shown to contribute to cell expansion such as insulin-like growth factor 2 (Igf2) or angiopoietin-like proteins (Mikkola and Orkin, 2006; Zhang and Lodish, 2004; Zhang et al., 2006).

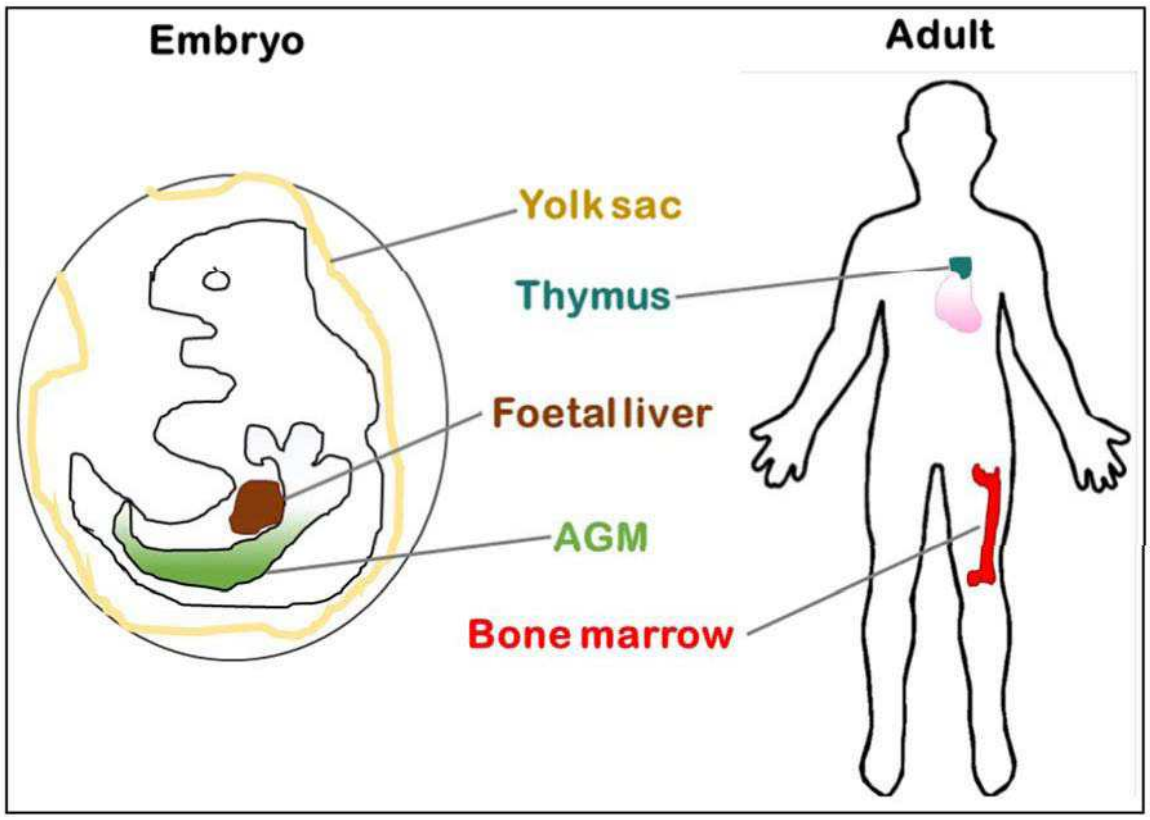

Figure 7 – Haematopoietic organs:
Schematic representation of sites of primitive (yolk sac, yellow) and definitive (AGM, green) haematopoiesis and the haematopoietic organs seeded by HSCs throughout embryonic (foetal liver, brown) and adult (thymus, blue and bone marrow, red) development. Heart is shown in pink.

The **thymus** develops shortly after the foetal liver and is considered as one of the first definitive haematopoietic organs to be colonised. The development of the thymus is induced by the colonisation of the first T-cell (Itoi et al., 2001; Ramond et al., 2014). Epithelial cells

forming the thymus tissue together with mesenchymal cells through several layers, remodel with the first precursors from polarised layers to clusters. The epithelial clusters later become the site where T-cell precursors home (Itoi et al., 2001). Once the thymus has matured, the second wave of various precursors, consisting of multi-lineage progenitors, CLP and CMP, migrate and seed this tissue (Ramond et al., 2014).

Starting at day E17.5 in the mouse embryo, HSCs appears in the **bone marrow** (BM), which is considered as the principal definitive haematopoietic organ. Few days earlier, the skeletal development has begun, starting from mesenchymal cells through chondrocytes to osteoblast differentiation. From very early stages of development, bone formation is accompanied by vascularisation (Mikkola and Orkin, 2006). The homing of HSCs to the bone marrow is a relatively fast process occurring during 1-2 days while HSCs actively pass the blood/BM endothelial barrier to enter the BM. Although the initial process of homing is rapid and simple, the engraftment and seeding in the BM requires the contribution of many factors and their mutual interaction (Lapidot et al., 2005). One of the key signalling molecules identified to control HSCs homing is the CXCL12 chemokine/CXCR4 receptor pairing. CXCR4, stands for C-X-C chemokine receptor type 4 and is expressed on the surface of HSCs. It is required for stem cell migration and for the journey from foetal liver to the BM. In the BM, the stromal cell derived factor (SDF-1 or CXCL12) expression creates a gradient, that allows the cell chemo-attraction (Lapidot, 2001; Lapidot et al., 2005; Whetton and Graham, 1999). To allow HSCs seeding and adhering within the tissue, several adhesion molecules are expressed on the HSC surface. These include CD44, platelet-endothelial cell adhesion molecules (PECAM-1, CD31), heparin binding protein and L-selectin (Whetton and Graham, 1999). Distinct cell types, growth factors, cytokines and matrix components are required to create specific conditions supporting HSCs maturation, survival and stemness. Those specific conditions, called HSCs niche, are defined in detail in Part 3.

In the last decades, the studies of embryonic and adult haematopoiesis in mammalian models revealed most of the current knowledge on HSC origin and fate. Many specific markers have been defined and enable a better characterisation of HSCs and their neighbouring subpopulations. Recently, two new aspects of the studies have attracted researchers' attention. First, new non-mammalian models to study embryonic haematopoiesis start to emerge and allow to reveal additional information and a new point of view. Second, the importance of stem-cell microenvironment during their emergence, maturation and homing in the haematopoietic

organs start to be taken into account and studied deeply to characterize all the cells and their signals that can control HSC ontogeny. These two aspects will be described and discussed in the following two parts.

2. Animal models used to study the embryonic haematopoiesis

Haematopoiesis research has been performed using several vertebrate models, both mammalian and non-mammalian. All of them have extended our knowledge of the haematopoietic system during the last years. While each model has its own advantages and limitations, combining them permitted to understand the haematopoietic processes which could not be elucidated by a single model. Among the vertebrate models frequently utilised for haematopoiesis research, we can find the mouse, zebrafish, xenopus and chick (Medvinsky et al., 2011). While the mouse is the most often used model for its closest similarity to the human organism, each of the other models have brought new aspects thanks to their advantages. First of all, each of them has external embryonic development enabling the study of embryonic haematopoiesis. External development allows direct observation of embryogenesis during which haematopoiesis occurs. For instance, the use of chimeric chick embryos permitted to demonstrate the embryonic origin of adult haematopoietic system (Dieterlen-Lievre, 1975). Furthermore, xenopus and zebrafish embryos enabled a detailed characterization of the AGM as the site of HSCs emergence, including its spatial origin prior to studies performed in mammalian models thanks to the possibility of rapid genetic analysis (Ciau-Uitz et al., 2000; Gering et al., 1998).

2.1. Chicken embryo

The chicken embryo has a long history as a model in developmental biology. It contributed to several breakthroughs in the field of haematopoiesis. Its use confirmed that definitive haematopoiesis has an intra-embryonic origin and showed for the first time that HSCs derived from the haemogenic endothelium (Dieterlen-Lievre, 1975; Jaffredo et al., 1998). Despite the common key points during the establishment of haematopoiesis between avian and mammalian embryos, several aspects have been so far described exclusively in the avian embryo and may be unique to this species. Detailed study of the avian dorsal aorta revealed its very specific composition. In the chicken embryo, somite-derived endothelium contributes to the remodelling of the dorsal aorta, which in the other species has been describe so far to originate from the splanchnopleural mesoderm (Jaffredo et al., 2010; Pouget et al., 2006). In the chicken embryo, the somitic cells migrate toward the aorta to participate to the endothelium

remodelling (**Figure 8**) into two distinct phases. Firstly, somitic cells form the dorsal part of the aorta and secondly they replace the haemogenic endothelium which meanwhile gave rise to HSCs (Pouget et al., 2006). This two-step remodelling act on the aorta dorso-ventral polarity. The discoveries in the field of haematopoiesis using the avian animal model could be obtained thanks to methods exclusively developed within this species such as chimeric transplantation or unilateral *in ovo* electroporation.

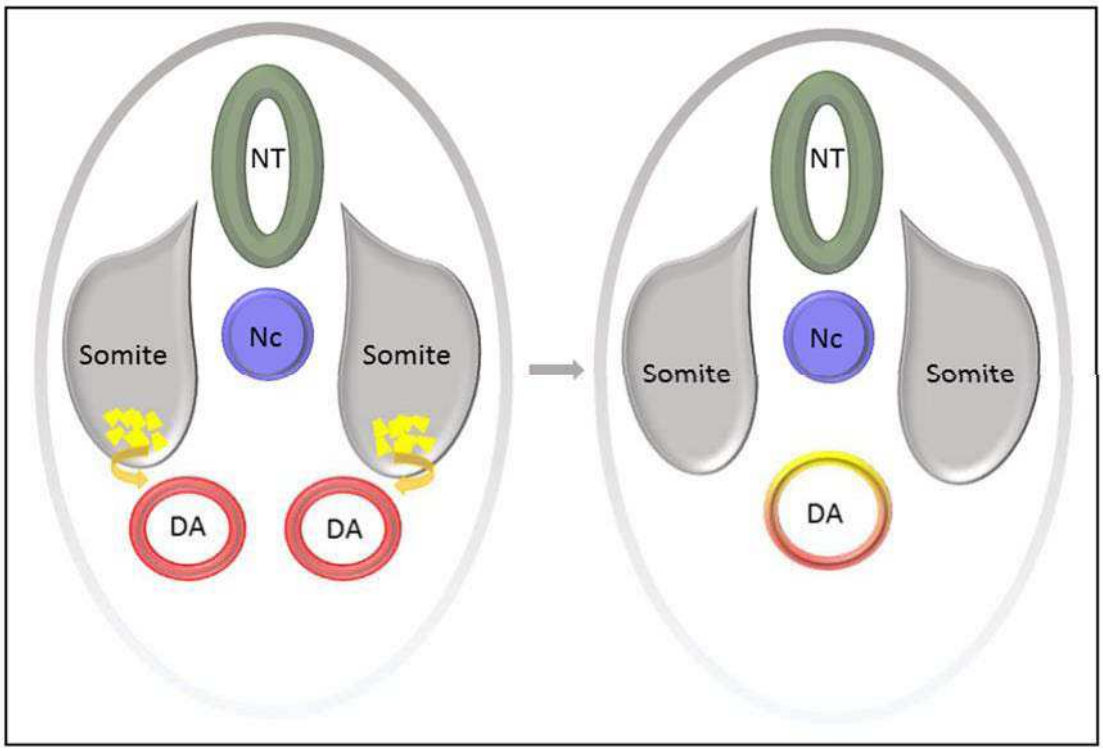

Figure 8 – Composition of the aorta in the chicken embryo:
Transversal sections of chicken trunk during embryonic development. The somitic cells (yellow) migrate ventrally from somites (grey) to the aorta (red) to participate to the aorta remodelling (red/yellow). NT, neural tube; Nc, notochord; DA, dorsal aorta.

2.2. Zebrafish embryo

During my PhD thesis, I have used the zebrafish embryo as an animal model to study haematopoiesis. For this reason, I will highlight in the following paragraphs embryonic haematopoiesis in zebrafish with impact on conserved mechanism between vertebrates. Zebrafish (or *Danio rerio*) is a small tropical freshwater fish belonging to the family *Cyprinidae*. Its natural habitat is in South Asia (Himalayan region) where it lives in 28°C slowly

flowing water. It possesses several characteristics which made it a suitable and very promising animal model for development (**Figure 9**). First of all, its small size is an important aspect for a laboratory animal. As the size is directly proportional to the amount of material, food and place required for housing to establish the husbandry, zebrafish can be raised and maintained in high-density aquarium systems minimising the price and place requirements compared to mice housing. Then, the zebrafish like avian and amphibian embryos has external development making it an ideal candidate for developmental studies including haematopoiesis. In particular, during the first days of development, the zebrafish embryo is transparent and pigment formation can be abolished by soaking embryos in melanin synthesis inhibitor phenylthiourea (PTU). This allow the use of various imaging techniques and real-time tracking. A couple of adult fish might give several hundred eggs every week which develop very rapidly. During the first five days, all major organs are developed and start to function. Finally, the zebrafish genome has been sequenced and shares 70% orthology with human genes (Howe et al., 2013). One of the main differences compared to mammals is a genome duplication occurred in teleosts. Because of that, many human genes are found in duplicates in the zebrafish. The sequenced genome allowed to perform genetic manipulation, such as nucleotide sequence knockdown, mutagenesis and transgenesis. The last two characteristics in particular place the zebrafish as a pertinent animal model to study haematopoiesis.

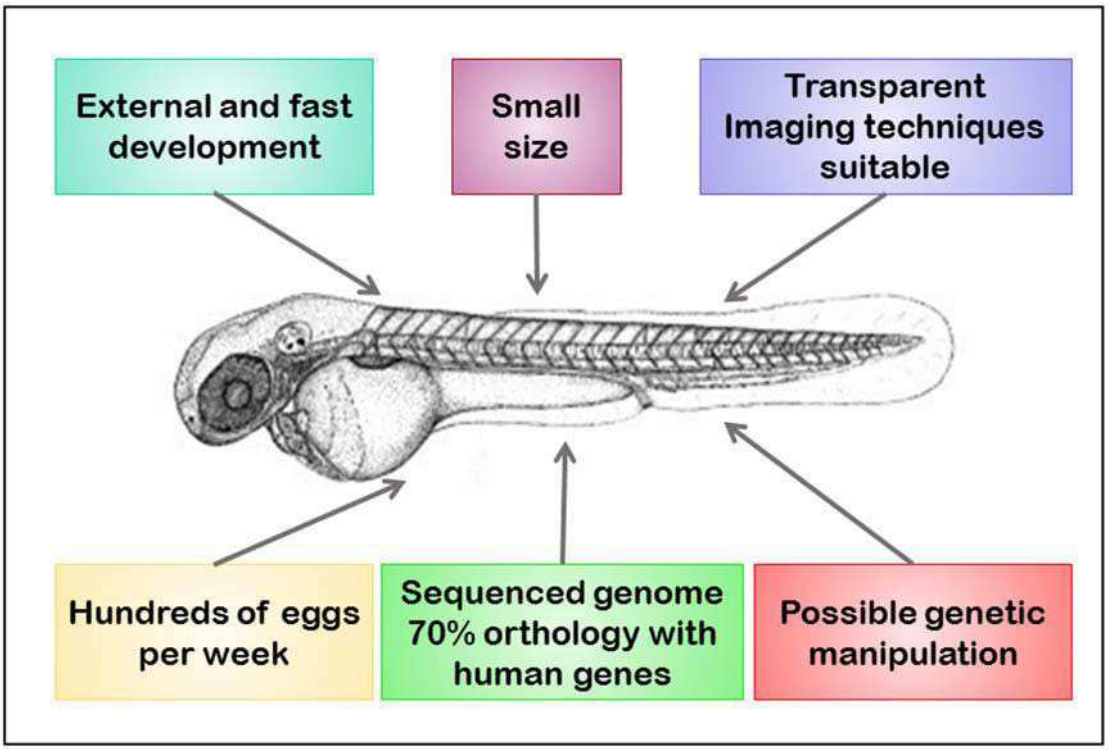

Figure 9 – Zebrafish model advantages:
Characteristics of the zebrafish embryo which make it a suitable model for embryonic haematopoiesis research

Zebrafish embryogenesis shares many similarities with the higher vertebrates including humans and other mammals. The main stages of zebrafish embryonic development has been well characterised and described thanks to non-invasive imaging techniques (Kimmel et al., 1995). The ability to stage embryo precisely allow micromanipulations at the exact stage of interest. It also permit to accelerate or slow down embryonic development through temperature variation. The standard developmental rate is measured at 28.5°C, whereas increasing temperature to 33°C accelerates development by 25% and decreasing it to 24°C slow down development by 25% (Kimmel et al., 1995).

The zebrafish early development can be divided into several stages, which can be further sub-divided. The main stages are as followed: zygote period, cleavage period, blastula, gastrula, segmentation, pharyngula and hatching period. The first 4 periods are represented in **Figure 10**. The segmentation period (10.33-24 hpf) consists of somitogenesis. The body becomes recognisable and primary organs are formed including the nervous and cardiovascular system (**Figure 11**). The embryo continues to elongate during the pharyngula period (24-48 hpf). The organs start to be functional and most importantly blood circulation starts (25 hpf) and definitive

haematopoiesis occurs. At last, the organs continue to develop in the hatching period (48-72 hpf, **Figure 11**), with the formation of first cartilage and bone, and the hatching of the embryos from their chorions (Kimmel et al., 1995).

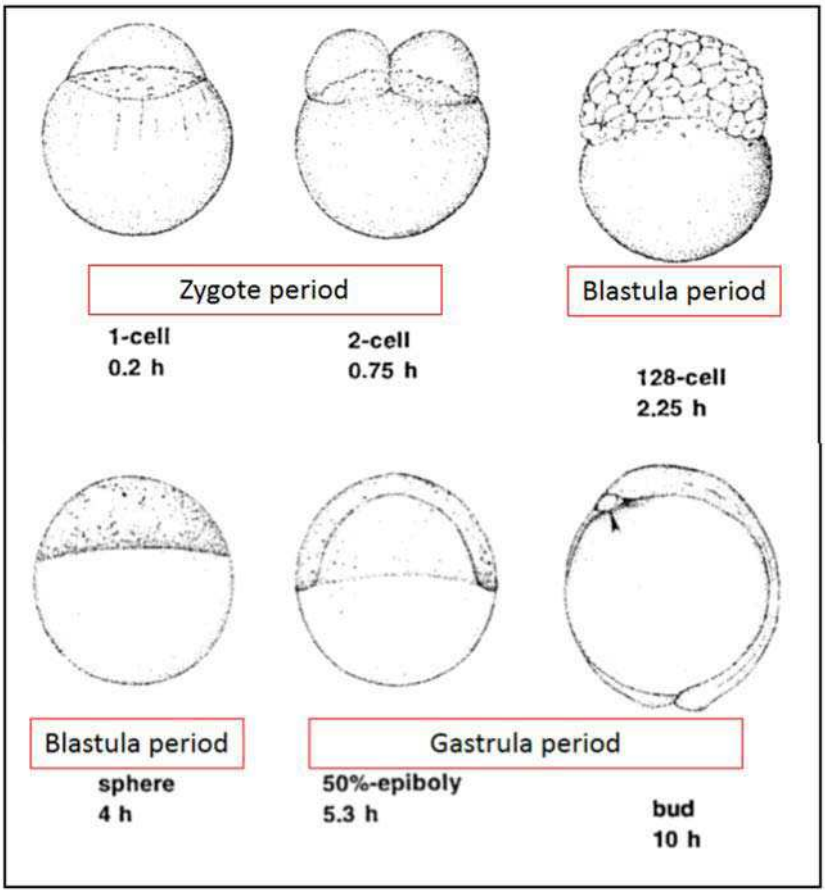

Figure 10 – Zebrafish development stages:
Representative drawing of several developmental stages during very early zebrafish development from 1-cell stage to the beginning of the somitogenesis (Bud, 10 hpf). Adapted from Kimmel, 1995 (Kimmel et al., 1995).

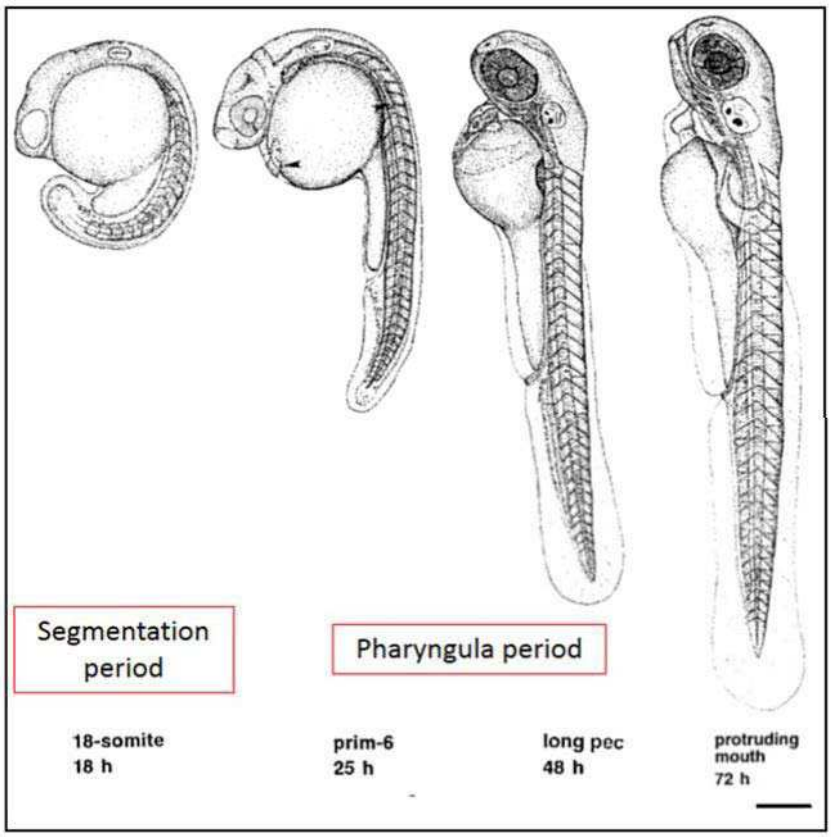

Figure 11 – Zebrafish development stages – part 2:
Representative drawing of several developmental stages during zebrafish development after somitogenesis – Segmentation and pharyngula period. Scale bar = 250µm. (Adapted from Kimmel et al., 1995).

2.3. Zebrafish haematopoiesis

Regarding embryonic haematopoiesis in the zebrafish, all the key points are comparable to mammalian embryos. Embryonic haematopoiesis occurs in two successive waves, the primitive and the definitive wave. The **primitive wave** takes place around 18 hpf (**Figure 12**) at two distinct places, contrary to an unique place in mammalian embryos. The primitive erythrocytes are formed in the intermediate cell mass (ICM) in the trunk of the embryo, while the primitive macrophages and neutrophils arise from the cephalic mesoderm. Primitive macrophage and neutrophils then migrate to the yolk sac syncytial layer and colonise the whole embryo to ensure tissue remodelling and innate immunity (Herbomel et al., 1999). Erythrocytes enter the vessel lumen with the beginning of circulation at 25 hpf.

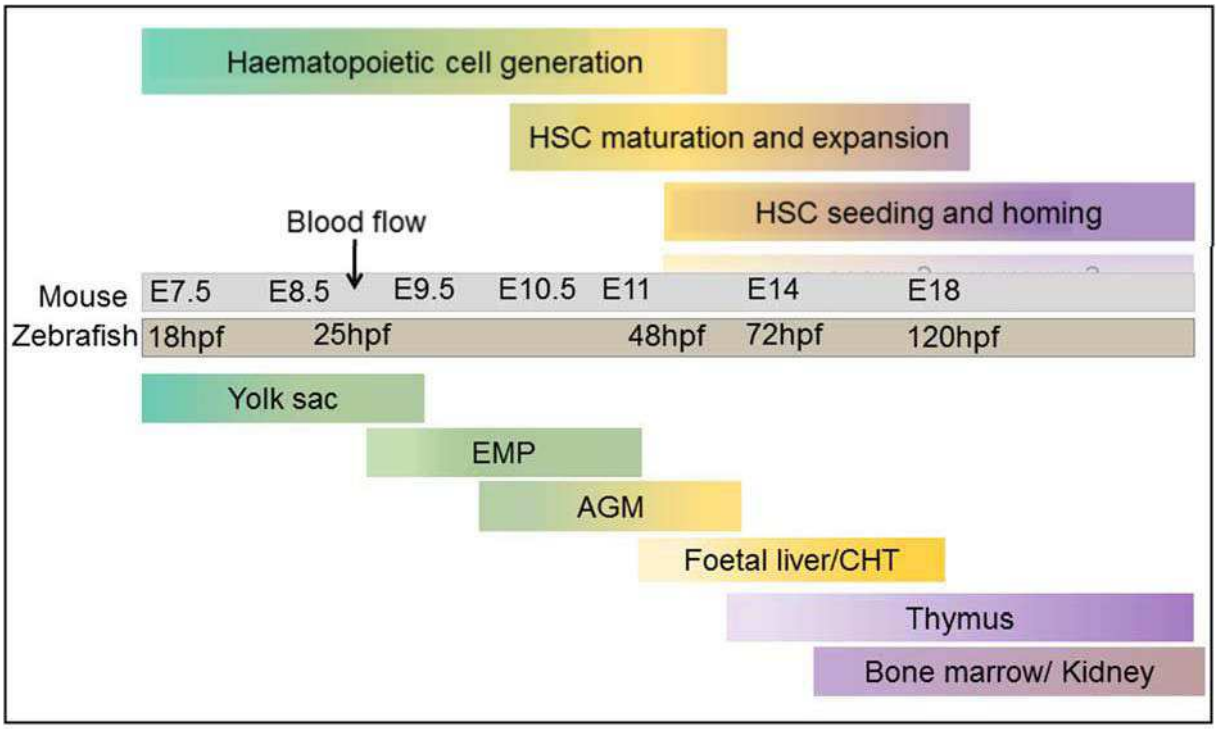

Figure 12 – The haematopoiesis timing:
Diagram representing the comparison of developmental stages in the murine and zebrafish embryo with the approximate specification of each major step of embryonic haematopoiesis. The grey line shows the time scale of development in days for the mouse embryo and in hours for the zebrafish embryo. HCS or progenitors are generated during development in three phases at distinct sites – Yolk sac, ICM (Intermediate cell mass for EMP) and AGM. HSCs then mature in the AGM and proliferate in foetal liver/CHT (yellow) to finally home in thymus and bone marrow/kidney (violet). AGM, Aorta-Gonad-Mesonephros; CHT, Caudal haematopoietic tissue; EMP, erythro-myeloid progenitors; HSC, Haematopoietic stem cell.

An **intermediate wave** of haematopoiesis completes the two principal waves and occurs in the posterior blood islands (PBI) at 30 hpf (**Figure 12**). This wave gives rise to erythro-myeloid progenitors (EMPs) which later differentiate into macrophages, neutrophils and erythrocytes (Bertrand et al., 2007). EMPs are considered by several authors as a part of the definitive wave of haematopoiesis due to their time of appearance and their multipotent potential and despite their inability to seed definitive haematopoietic organs or to differentiate into lymphoid cell population (Bertrand et al., 2007).

The **definitive wave** of haematopoiesis which gives rise to HSCs starts at 30 hpf in the zebrafish embryo. It takes place in the AGM, like in mammalian embryos and other vertebrates. The haemangioblast which is the common precursor of haematopoietic and endothelial cells,

depends on the expression of the SCL gene (Gering et al., 1998). HSCs emerge from the ventral wall of the dorsal aorta (**Figure 13A**) by the specific trans-differentiation process called the endothelial-to-haematopoietic transition which was imaged in real time for the first time in the zebrafish embryo (Bertrand et al., 2010a; Kissa and Herbomel, 2010). The observed process confirmed the endothelial origin of HSCs which was already described in other species (Jaffredo et al., 1998; Lancrin et al., 2009; Oberlin et al., 2002). The endothelial cell start to bend and to lose its polarity (**Figure 13B**). The cell slowly rounds up while the neighbouring cells migrate toward each other to ensure the aorta integrity (**Figure 13C**). Finally the junctions break, the cell detaches from its neighbours and is released in the sub-aortic space of the AGM (**Figure 13D**). Live imaging in the zebrafish embryo enables the detailed description of each individual step of EHT. It also gives an estimated duration of the whole process as well as the extrapolated quantification of the number of emerging cells in the whole organism. When extrapolating from the imaged 2-somite-length to the total 12-somite-length of the AGM, real-time imaging revealed approximately 3 HSCs emerging per hour in the AGM (Kissa and Herbomel, 2010).

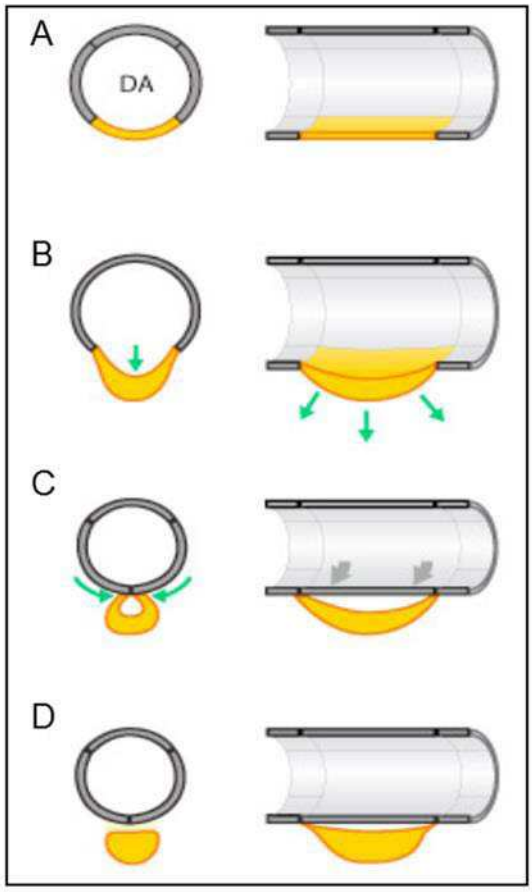

Figure 13 – Endothelial-to-haematopoietic transition:
Individual steps of EHT. (A) The endothelial cell in the ventral floor of dorsal aorta (DA) starts to bend from the endothelium layer (B), the cell loses its polarity and becomes round (C) to finally detach completely from the junctions of the neighbouring cells which approach together to replace the emerging cell. Adapted from Kissa and Herbomel, 2010 (Kissa and Herbomel, 2010).

Many genetic factors influencing embryonic haematopoiesis have already been elucidated and confirm the conserved mechanism of haematopoiesis between vertebrate species. The haemogenic endothelium and aortic specification rely on Notch signalling by two distinct mechanisms. Notch1a governs the artery specification whereas Notch1b is involved in the HSCs fate (Bertrand et al., 2010b; Kim et al., 2014). In addition, Notch3 also affects HSCs emergence but indirectly through Wnt16 in the sclerotome prior the haemogenic endothelium formation (Clements et al., 2011). The last member of the Notch family, Notch2, is dispensable for haematopoiesis. Notch1 expression in the haemogenic endothelium induces Runx1 expression which allows EHT. Notch signalling is located downstream of Vegf and Hedgehog signalling. Apart from the signalling already described in mammalian models, other factors have been suggested to affect definitive haematopoiesis in the zebrafish embryo. Prostaglandin

E2 (PGE2) has been one of the factors discovered during a high-throughput chemical screening (North et al., 2007). PGE2 seems to affect both embryonic and adult HSCs homeostasis, likely through the Wnt canonical signalling (Goessling et al., 2009; North et al., 2007). Aside from signalling molecules, physical factors have been proposed as key players to initiate EHT. Mutant screening showed that lack of blood flow and/or heartbeat impairs the initiation of EHT (Ransom et al., 2004). Blood circulation appears to induce NO production by shear stress which then initiate HSC emergence (North et al., 2009).

Several specific markers are used to identify embryonic HSCs in the zebrafish embryo. Similar to murine embryos, no single marker exclusively expressed in HSCs exists so far. Runx1 is considered as the earliest HSC marker in the zebrafish embryo, its expression being detected in the AGM from 24 hpf (Lam et al., 2009). Later, after the initiation of EHT, two other markers appear with the trans-differentiation of stem cells, cd41 (also called itga2b) and cmyb. Currently, a combination of two or three of the mentioned markers together with endothelium-specific markers is used to identify HSCs. Despite the high similarity between animal models, the zebrafish orthologue for CD34 has not yet been described in zebrafish.

Contrary to the mammalian embryos, in the zebrafish embryo, HSCs emerge outside the dorsal aorta and join the blood stream through the posterior cardinal vein (PCV) (Kissa et al., 2008). HSCs then migrate through the AGM toward the vein wall, they intravasate into the vein and join the blood stream to reach the haematopoietic organs through circulation. The **caudal haematopoietic tissue** (CHT, **Figure 14**) is the first organ to be colonised by HSCs during embryonic development (Murayama et al., 2006). HSCs leave the blood stream in the caudal part of the body, by extravasating into the CHT. The CHT is formed and remodel progressively with the first HSCs arriving to seed this haematopoietic tissue. HSCs first arrive in the CHT from 48 hpf onwards, with the peak of colonisation between 3 and 4 dpf (Murayama et al., 2006). HSCs first adhere to the endothelial wall, then extravasate rapidly to the abluminal side of the endothelial wall within minutes. Once outside the circulation several endothelial cells remodel around a single HSC to form a pocket called endothelial cuddling to create an appropriate environment for cell division (Tamplin et al., 2015).

During the following journey, HSCs reach the **thymus** (**Figure 14**), which is the first definitive haematopoietic organ, from 54 hpf (Kissa et al., 2008). The thymus homes the lymphoblasts, which are the lymphoid progenitors, similar to the mammalian embryos. Once

there, they proliferate and differentiate to give rise to rag-positive T-lymphocytes through ikaros positive precursors (Kissa et al., 2008). Finally HSPCs colonize the kidney (**Figure 14**), which is the definitive haematopoietic organ corresponding to the mammalian bone marrow. The **kidney marrow** is seeded from 4 dpf and it remains the site of haematopoiesis throughout the rest of the larval and whole adult life (Ellett and Lieschke, 2010; Song et al., 2004).

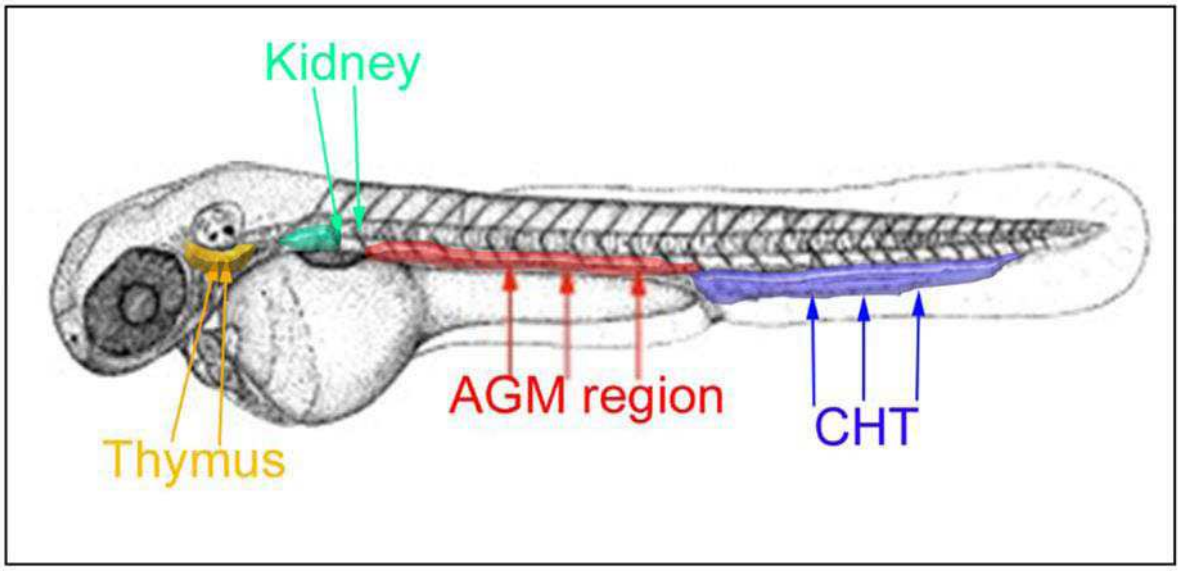

Figure 14 – Zebrafish embryo haematopoietic organs:
Drawing showing the localisation of the sites of HSC origin, the AGM region (red), the embryonic haematopoietic organ, CHT (blue) and definitive haematopoietic organs, thymus (yellow) and kidney marrow (green).

Despite the lack of extensive studies on the kidney marrow, we might postulate that mechanism of HSC regulation during the adult life is conserved. The functional analysis and comparison of the zebrafish kidney marrow niche to the mammalian bone marrow still remains to be elucidated. The tissue structure and haematopoietic organ microenvironment will be detailed in part 3.

3. HSCs environments

The production of blood cells relies on active and functional HSCs. HSC emergence, proliferation, migration and maturation take place in several haematopoietic sites in the embryo and adult; each step occurs in a different temporal window. The diversity of anatomical sites makes the understanding of all aspects of haematopoiesis very challenging. Every distinct location is characterised by its cell and extracellular composition with specific signalling and is defined as HSCs environment, also named HSCs niche.

3.1. Yolk sac environment

During embryonic development, the first haematopoietic precursors emerge in the yolk sac which represents the first anatomical site of haematopoiesis. Despite its relatively simple structure, the bilayer organ that envelops the developing embryo substantially controls primitive haematopoiesis. Indeed, haematopoietic activity occurs in the inner layer – the visceral mesoderm - while the outer layer – the visceral endoderm - contributes to haematopoiesis by Indian hedgehog (IHH) secretion. IHH activates the bone morphogenic protein-4 (BMP4) leading to the initiation of haematopoietic activity. In addition, this tissue is highly vascularised, like all the other future haematopoietic tissues (Al-Drees et al., 2015; Sugiyama et al., 2011).

3.2. AGM environment

The site of HSC emergence in all vertebrate embryos is located in a region co-localising three different structures – the vasculature, the reproductive and excretory organs – called aorta-gonad-mesonephros or AGM. In the AGM, several factors and cell populations have already been described to influence distinct steps of the onset of definitive haematopoiesis. The HSCs themselves originate exclusively from the ventral wall of the aorta *in vivo*, revealing a polarisation of this vessel. This localisation plays a key role. Indeed, the ventral wall exhibits either the haematopoietic activity or the supportive role (Peeters et al., 2009) whereas the dorsal wall only provides supportive signalling. Interestingly, the dorsal part of aorta can exhibit haematopoietic activity *in vitro* if co-cultured with the tissues surrounding the ventral part of

the aorta *in vivo* (Souilhol et al., 2016). These findings emphasise the importance of the aorta microenvironment in HSC emergence. After their emergence, HSCs accumulate in intra-aortic clusters which represent another heterogenic structure supporting HSCs. Intra-aortic clusters contain, in addition to the stem cells themselves, pre-HSCs, progenitors and cells with limited lineage potential, stromal cells and others (Boisset et al., 2014). In addition to the heterogeneity of clusters, several types of cells are found outside the clusters, such as stromal cells, neurons, leukocytes or smooth muscle cell precursors (**Figure 15**).

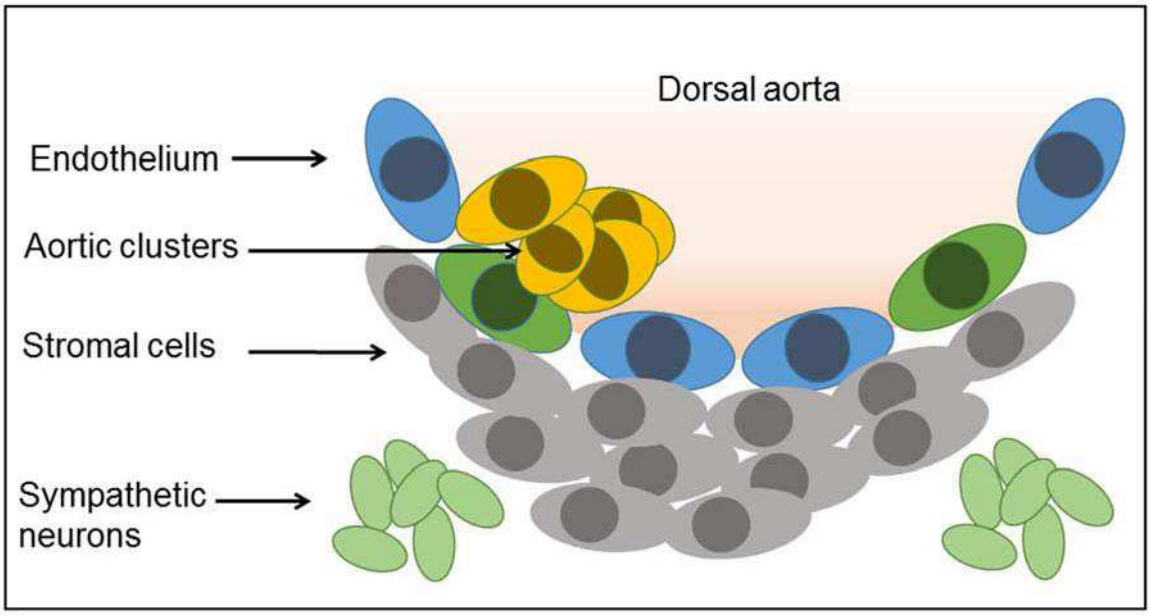

Figure 15 – Orthogonal view of the AGM to visualise the cells surrounding the dorsal aorta: Vascular and haemogenic endothelium forming the vessel (blue and green) and giving rise to the intra-aortic clusters (yellow), stromal cells enveloping the vessels (grey) and the sympathetic neuron clusters in the sub-aortic region (pale green).

Many soluble factors including cytokines and pro-inflammatory factors, growth factors or neurotransmitters have been detected in the AGM and each of them was found to be crucial for the establishment of definitive haematopoiesis. Similarly to the yolk sac, BMP-4 signalling as well as Hh pathway are both expressed in the AGM (Crisan et al., 2016; Marshall et al., 2000). BMP-4 and Hh affect differentially HSCs activity. Based on their dependence to these signals, we can distinguish two distinct HSC types in the AGM: BMP4-responsive and non-BMP4-activated HSCs. Except for the HSC-factors expression which they have in common, the two populations differ by their gene expression. While the BMP4-activated HSCs maintain a high expression level of endothelial factors, such as Pecam1, VE-Cad, Tie-2, endoglin, and a

detected expression of HSC factors, the non-BMP4-activated (but Hh dependent) population expresses in higher level HSC markers, including c-kit or cd41 and no or low level of EHT inducing transcription factor Sox17. The functional difference between the two populations remains to be elucidated (Crisan et al., 2016).

Signalling from sympathetic nervous system innervating the dorsal aorta in the mouse embryo from day E10 regulates HSC emergence (Fitch et al., 2012). The sympathetic precursors migrate ventrally from the neural crest to the aorta and the transcription factors Gata3 and Hand2 initiate their differentiation into sympathetic neurons to form ganglions. Each of those factors has been shown to influence indirectly haematopoiesis through the sympathetic nervous system development. The neurons then synthetize catecholamines, the neurotransmitters associated with the sympathetic system. The released catecholamines activate EHT through the adrenergic receptors on the surface of future HSCs (Fitch et al., 2012). The detailed description of sympathetic development and its role in haematopoiesis is developed in part 5.

Pro-inflammatory signalling controls HSC emergence via the Notch pathway in the zebrafish embryo. Tumour necrosis factor alpha (TNFα), produced and released by primitive neutrophils present in the AGM, activates TNF receptor type 2 expressed by endothelial cells and activates NF-κB and Notch pathways (Espín-Palazón et al., 2014). The Notch activation then initiates HSC emergence in the AGM. Together with TNFα, another inflammatory cytokine, interferon gamma (IFNɣ) contributes to definitive haematopoiesis in the AGM. IFNɣ expression impairment decreases the number of emerging HSCs in both mouse and zebrafish embryos. Finally, the combined impairment of both signalling IFNɣ and TNFα acts synergistically and causes a greater decrease of HSCs emergence measured by Runx1 expression (Li et al., 2014). Interleukin 3 (IL-3) is another cytokine detected in the AGM during HSC emergence in the mouse embryo. IL-3 is expressed by all major vessels and HSCs and controls the survival and expansion of nascent HSCs as a downstream target of Runx1 expression factor (Robin et al., 2006).

3.3. Foetal liver and CHT environment

The foetal liver (FL), or the CHT in the zebrafish embryos, serve as a transitory haematopoietic organ in which HSCs mature and proliferate. The haematopoietic niche contains

a high variety of cells including HSCs themselves, progenitors, endothelial cells, fibroblasts, macrophages and neutrophils, stromal cells and hepatoblasts (in case of FL). Hepatoblasts express and release several growth factors – SCF, EPO and IL-6 or IL-7 – supporting cell differentiation, especially into erythroid or lymphoid lineage (Al-Drees et al., 2015). The FL macrophages create a supportive microenvironment by migrating from the sinusoids to the parenchyma. There, by interaction with the erythroblasts, macrophages allow the final step of erythrocyte differentiation and enucleation mediated by erythroblast macrophage protein. Perivascular fibroblasts are located around the blood vessels. Their co-localisation with the vessel suggests that they may be involved in myeloid cell differentiation. In addition, fibroblasts contribute to the microenvironment extracellular organisation through the production of matrix components, such as fibronectin and collagen (Payushina, 2012).

The vascular endothelium affects foetal liver haematopoiesis through several aspects. Similarly to the other haematopoietic tissues, the vascular endothelium together with smooth muscle cells control tissue permeability permitting the migration and homing of the HSCs. Furthermore, endothelial cells maintain erythrocyte and myeloid cell differentiation *in vitro*. In the zebrafish embryo, the endothelial cells present in the CHT redistribute themselves around HSCs to form a specific microenvironment supporting HSCs proliferation (**Figure 16**). This specific endothelial cell behaviour and remodelling have been called cuddling by the authors of the study (Tamplin et al., 2015).

In addition to the vascular endothelium, stromal cells contribute to the maintenance and expansion of HSCs in embryonic haematopoietic organs. Recent studies in zebrafish and mouse models showed the presence of stromal cells in proximity to the seeded HSCs (Khan et al., 2016; Murayama et al., 2015). Interestingly the cells do not originate from the same precursors. In the zebrafish CHT, the stromal cells derive from the caudal somites, whereas in the mouse foetal liver, nestin$^+$ stromal cells suggest a neural crest origin (Khan et al., 2016; Murayama et al., 2015). In zebrafish embryos, somite-derived stromal cells contribute to the formation of the CHT niche (**Figure 16**). Those progenitors originate from the ventral border of caudal somites. After trans-differentiating by EMT, they interact with endothelial cells and support the formation of the caudal vein sinusoid plexus (Murayama et al., 2015). In mouse embryos, nestin$^+$ stromal cells allow HSCs expansion in the foetal liver during embryonic development while after birth the foetal liver niche is reorganised with the loss of these stromal cells (Khan et al., 2016).

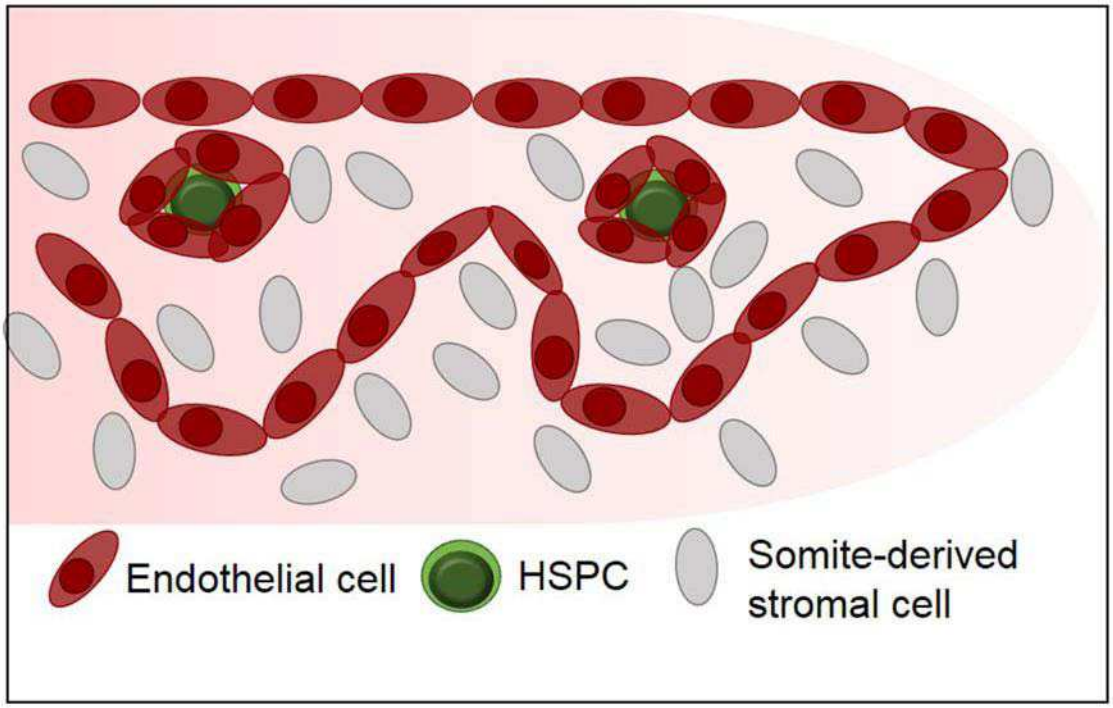

Figure 16 – The zebrafish CHT environment:
Structure of the CHT niche with the somite-derived stromal cells (grey) contributing to the HSPC (green) maintenance and expansion and endothelial cells (red) enclosing HSPCs to create a cell-division promoting microenvironment.

3.4. Bone marrow niche

Bone marrow (BM) represents a complex structure consisting of several distinct cell types which provides a beneficial environment for HSCs homing, proliferation and differentiation. Arteriolar vessels and capillaries, endothelial cells, macrophages, osteoblasts, osteoclasts and stromal cells form a unique three-dimensional scaffold that support haematopoietic clusters (Calvi and Link, 2014). The concept of 'niche' had been already proposed in 1978 to describe the place where specific cells establish close interactions with HSCs to maintain stem or progenitor cell behaviour (Schofield, 1978).

HSCs can be found in most regions of long bones. However we can distinguished at least two distinct anatomical sites seeded preferentially by specific cell populations: the endosteal niche close to the bone surface and the perivascular niche associated with the arterioles close to the bone centre (Al-Drees et al., 2015). The two distinct locations suggest different cell fate restriction depending on the factors and signalling molecules specific for each

region. Nevertheless, the theory of two distinct niche regions has been complicated by two facts. First, HSCs unlike most other adult stem cells are extraordinarily mobile and often migrate from one compartment to the other (Hsu and Fuchs, 2012). Second, the bone morphology may differ depending on the type of bone studied. While in the long bones we can distinguish the endosteal and perivascular zone with well limited boundaries, in the calvarium, the microarchitecture exclude the distinction between the two zones (Lo Celso et al., 2009; Xie et al., 2009).

In the long bones, *ex-vivo* live imaging revealed the preferential localisation of HSCs in the **endosteal region** where the cells remain mostly quiescent due to the presence of several factors. The niche exhibits specific physiological properties including hypoxia due to the long distance from the blood vessels and a high concentration of free calcium ion coming from the bone surface (Adams et al., 2006; Nombela-Arrieta et al., 2013). The main cells present are the osteoblasts which are in direct contact with HSCs and appear to promote their maintenance and quiescence. (Visnjic et al., 2004).

The **perivascular zone** of the BM niche is composed of several cell populations, including the arterioles, perivascular mesenchymal cells, pericytes, sympathetic nerves and non-myelinating Schwann cells. In the long bone, the activated HSCs or progenitors are preferentially localised in the perivascular zone, more precisely in close proximity to the arterioles. When they are needed, the HSCs in the bone marrow start to proliferate, enter the blood stream and differentiate in the circulation. However, not all HSCs are designated to enter the bloodstream and some are retained from mobilisation by CXCL12 signalling (Sugiyama et al., 2006).

Regarding the calvarium, the morphological structure differs from the long bones, therefore we cannot distinguish two regions in the BM. *In vivo* imaging of mouse calvarium revealed the dynamic and non-random positioning of the HSCs relative to the niche cell components. Similarly to the long bone seeding, LT-HSCs were localised in the closest proximity to osteoblasts, whereas HSC maturation occurs in a distant area from osteoblasts. However, because osteoblasts are localised in the vicinity of the vessels, we cannot assume the presence of endosteal and perivascular niche, but rather refer to periendosteal-perivascular niche (Lo Celso et al., 2009).

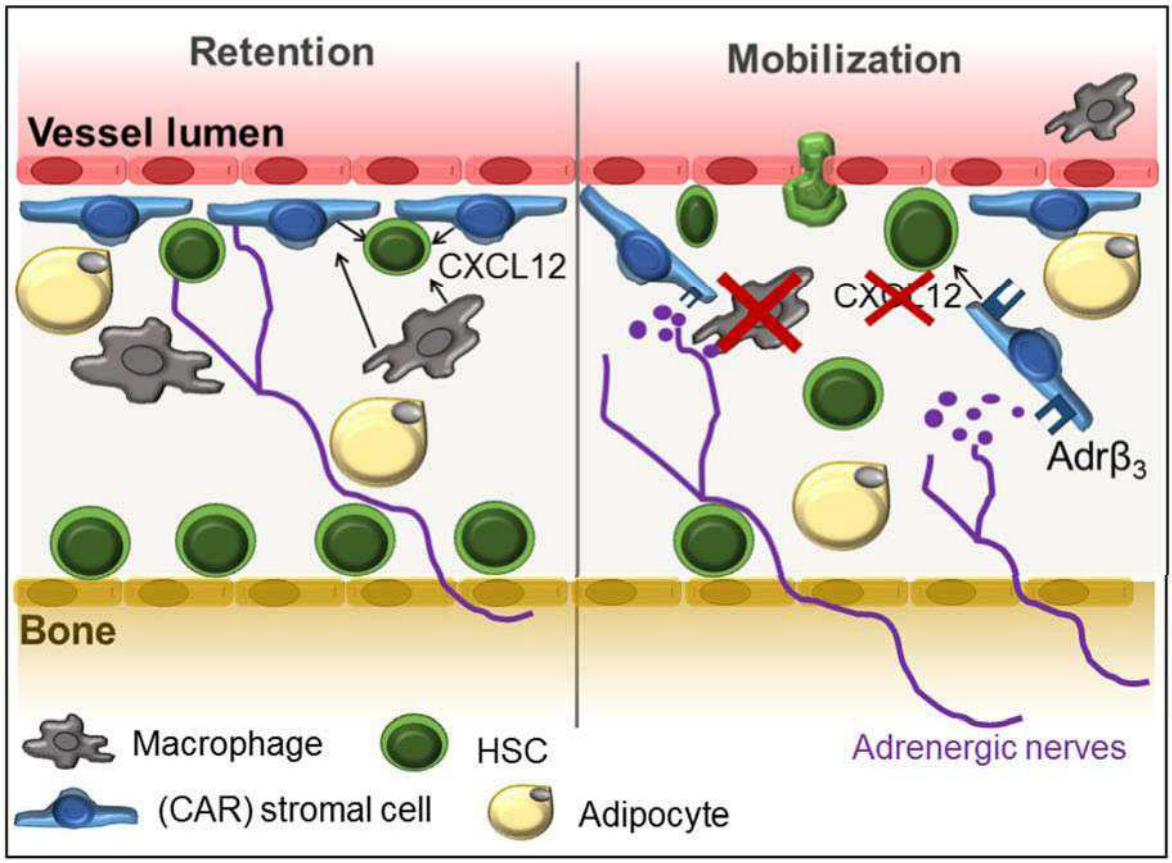

Figure 17 – The bone marrow niche:
The cellular composition of the environment where HSCs home in the bone marrow and the factors that contribute to their retention/mobilisation. Left side: HSCs (green) are retained in the bone marrow due to CXCL12 signalling from CAR stromal cells. Expression and release of CXCL12 is controlled by macrophages (grey) or negatively by adrenergic nerves (violet). Right side: Loss of macrophages or adrenergic nerve activity reduce CXCL12 expression from CAR stromal cells. It results in HSC mobilisation.

Apart from two specific distinct niches in the BM, each cell population specifically contributes to HCS homeostasis (**Figure 17,** reviewed by Mendelson and Frenette, 2014). **Endothelial** cells form the surface of blood vessels and together with perivascular cells constitute a natural barrier for intra and extravasation. Moreover, endothelial cells secrete factors to induce HSC expansion, such as the E-selectin adhesion molecule (Winkler et al., 2012).

Mesenchymal stem cells (MSC) and their derivatives are a heterogeneous cell population that still lacks precise definition and characterisation. As multipotent precursors, MSCs could differentiate into osteolineage cells, adipocytes, chondrocytes, perivascular or

stromal cells. MSCs are represented by their differentiated members in both niches where they play unique and indispensable roles.

As previously stated, **osteoblasts** are a major component of the endosteal region of the BM niche. They originate from the mesenchymal stem cells (MSC), confirming the complex role of MSCs in all the compartments of the BM. Osteoblasts appear to maintain HSCs and also to support their long-term reconstitution capacity after transplantation (Calvi and Link, 2014). The **osteoclasts**, the other member of osteolineage cells, seem to be dispensable for HSC maintenance.

Perivascular cells are localised on the surface of vessels, close to HSCs and sympathetic nerves. A subpopulation of perivascular cells, called CXCL12-abundant reticular (CAR) cells are the main source, as the name indicates, of CXCL12 chemokine. This chemokine is the key player in HSC retention in the BM niche. Though the exact characterisation of **CAR cells** remains unclear, they are described as cells expressing nestin (Nes), leptin receptor or myxovirus resistance-1 (Mx-1). CXCL12 expression and its interaction with its partner receptor CXCR4 expressed by HSCs are so far the principal manner to retain HSCs in their specific niche. CAR cells, as the major producers of CXCL12, attract HSCs – 94% of HSCs stay in contact or interact with CAR cells (Sugiyama et al., 2006).

Macrophages are considered as other significant players in the bone marrow niche. They are located in close proximity to HSCs and their presence ensure HSCs retention through CXCL12 signalling. Macrophage depletion by clodronate liposome or G-CSF treatment in mice promotes the mobilisation of HSCs and their release in the blood stream. HSC retention by macrophages seems to be mediated through nestin^{+} (Nes^{+}) stromal cells (probably CAR cells). Indeed, those cells are the source of CXCL12 chemokine whose expression level is controlled by macrophages (Chow et al., 2011; Winkler et al., 2010). **Neutrophils**, the other principal member of myeloid leukocytes, are also present in the BM niche. Their role in HSCs mobilisation appears to be minor and dispensable compared to the role of macrophages (Calvi and Link, 2014).

Interestingly, macrophages are not the single player controlling CXCL12 signalling. **Sympathetic nervous system** signalling has been proved to influence this pathway as well. The bone marrow is highly innervated by sympathetic nerves which are located close to the perivascular region. The neurons release neurotransmitters which act through adrenergic

receptors specifically expressed in distinct cell populations. While the β_2 receptor is localised on the surface of osteoblasts and HSCs themselves, the β_3 receptor is expressed by Nes^+ stromal cells (Katayama et al., 2006). The nervous system neurotransmitters activate β_3 receptor on Nes^+ stromal cells, induce Sp1 signalling which leads to the decrease of CXCL12 expression (Mendez-Ferrer et al., 2008). The HSC egress is therefore controlled by two distinct manners which act independently through CXCL12 expression. Indeed, macrophage depletion may still partially mobilise HSCs in the sympathectomised bone marrow (Chow et al., 2011). The β_2 receptor signalling appears to be dispensable in this process. The sympathetic nervous system in general and its distinct role in haematopoiesis are introduced in part 5.

The sympathetic nerves in the BM are ensheathed with nonmyelinating **Schwann cells**. These neural crest derivatives, defined also as glial cells might be one of the potential players in HSC dormancy regulation. Their function is based on activation of TGFβ signalling. Whereas the latent TGFβ is produced by most of BM cells, the active form is restricted to Schwann cells laying in parallel to the vessels. The active TGFβ signals trigger Smad2 and Smad3 signalling in HSCs by direct cell-to-cell contact. This ensures that only cells in direct contact will enter the dormancy state. Interestingly, only 25% of Smad2/3 activated cells were found in the direct contact with Schwann cells, supporting the theory that HSC are highly migrating within the bone marrow regions (Yamazaki et al., 2011).

Adipocytes represent a large part of the adult bone marrow in human and their proportion increases with age. The role of the adipocytes in HSCs homeostasis remains controversial. The quantity of adipocytes increases with age while concomitantly HSC activity decreases, suggesting a negative regulation of haematopoiesis by adipocytes. Consistent with this hypothesis, specific adipocyte ablation in the marrow improves HSC engraftment after transplantation as well recovery after injury (Naveiras et al., 2009). However, in contrary to those findings, adipocytes secrete adiponectin, whose receptor is expressed in HSCs and whose activation increases HSC proliferation (Calvi and Link, 2014; DiMascio et al., 2007).

HSCs go through or home in several different environments during their journey. These so-called niches represent a supportive environment for each step during development and homeostasis, such as HSCs emergence, expansion, maturation, quiescence and mobilisation. Each of the environments contains several cellular as well as molecular components. The complexity of the niche makes HSC research challenging but also very stimulating. Two

cellular components contributing to HSC niches among other roles, the macrophages and peripheral nervous system, will be closely introduced in the following two chapters.

4. Macrophages

Macrophages, as one the major players in innate immunity, have been described for the first time in 1892. They have been identified as phagocytic cells responsible for pathogen elimination (Metchnikoff, 1892). Through the following decades, it has been shown that macrophages possess much more capacities than just phagocytosis. Despite their primary phagocytic function, macrophages also express a high variety of cytokines and growth factors. They are involved in acute and chronic inflammation and contribute to many non-immune processes including angiogenesis, tissue remodelling, regeneration, matrix degradation, metabolism and general tissue homeostasis (reviewed by Pollard, 2009; Wynn et al., 2013). Macrophages can achieve all these distinct roles, because they possess two important characteristics – a high plasticity (or heterogeneity) and the ability to invade most tissues (Ebert and Florey, 1939).

During development, macrophages emerge from the two haematopoietic waves. The first wave gives rise to the primitive macrophages (also called yolk-sac derived macrophages) which play a crucial role during early development, including angiogenesis or tissue remodelling. They can remain until the adult stage as they colonise most tissues to differentiate into tissue-resident macrophages like microglia in the brain, alveolar macrophages in lungs or Küpffer cells in liver (**Figure 18**).

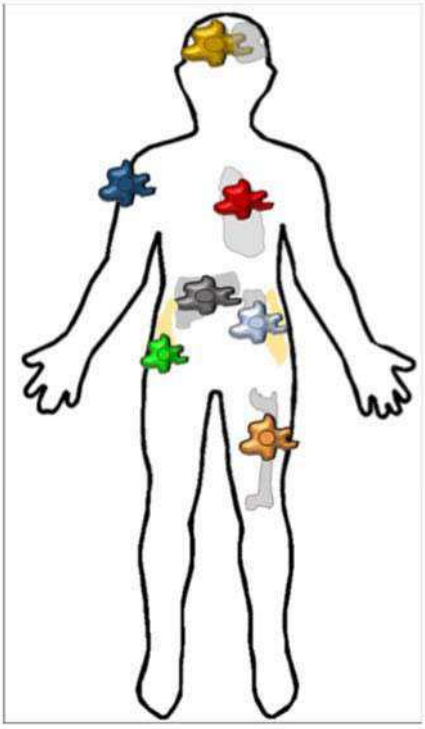

Name	Location	Role
Microglia	Brain	Neuronal survival
Kupffer cells	Liver	Erythrocyte clearence
Red pulp m.	Spleen	Erythrocyte clearence Iron metabolism
Alveolar m.	Lungs	Surfactant clearance
Osteoclasts	Bone	Bone resorbtion
Adipose associated m	Adipose tissue	Thermogenesis
Lagerhans c.	Skin	T-lymphocyte interaction

Figure 18 – Tissue resident macrophages:
List of tissue resident macrophages, their organ location and principal function. Each colour represents resident macrophages in the distinct tissues indicated in the second column.

During the second wave, HSCs are generated which can later differentiate into all blood cells including macrophages. Definitive macrophages called bone marrow derived macrophages (BMDM) are formed by a sequence of differentiation steps from HSCs. The common myeloid progenitors (CMP) first give rise to monocytes in the blood circulation. Monocytes exhibit several markers such as Ly6C high and low, CD11b, CD14, CD115 and chemokine receptors CCR2 or CX3CR1. In the circulation, monocytes progressively lose the Ly6C expression, suggesting that several monocyte subsets may exists. Monocytes then extravasate to actively infiltrate tissues upon chemokine-induced attraction. Depending on the local environment, monocyte differentiate and polarized into macrophages with specific phenotype. Macrophages arisen from the BM then keep their capacity to perform several functions depending on their environment (Gordon and Taylor, 2005; Yang et al., 2014).

4.1. Macrophage activation

The different response of macrophages to the local signalling always triggered the scientists' interest and promoted their efforts to categorise them. This led to the concept of

macrophage polarisation toward a specific phenotypes later called M1 and M2. More than 20 years ago, it has been shown that once macrophages infiltrate the tissue, they activate themselves in response to local signalling. The two extreme activation profiles have been defined as the classical activation caused principally by the interferon gamma (IFNγ) and lipopolysaccharide (LPS) or the alternative activation induced by the interleukin-4 (IL-4) or 10 (IL-10) (Stein et al., 1992). Macrophages then start to express specific markers in response to different signalling and exhibit different nitrogen metabolism. This differences permitted their description and classification. Classically-activated macrophages, called also M1 macrophages express mainly inflammatory factors, such as tumour necrosis factor alpha (TNFa), interleukin-1 (IL-1), interleukin-6 (IL-6), interleukin-12 (IL-12), interleukin-23 (IL-23). They also express inducible nitric oxide synthase (NOS2) which metabolises nitrogen. Those macrophages are generally considered as pro-inflammatory macrophages based on their expression profile their behaviour (**Figure 19**).

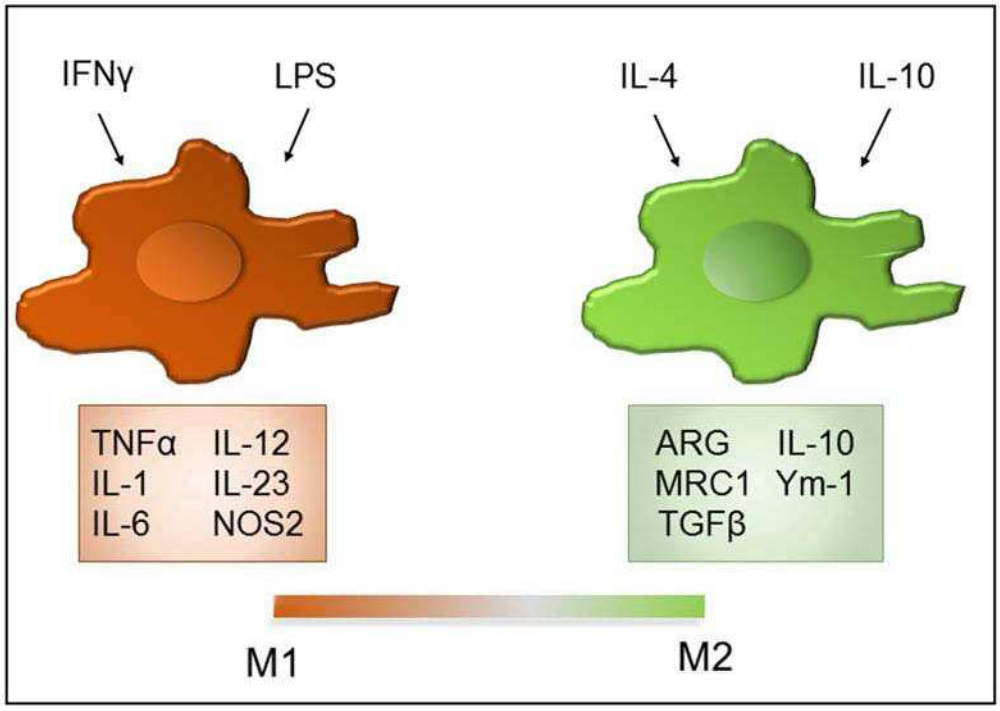

Figure 19 – M1/M2 macrophage polarization:
The activation of specific cytokines and expression factors in response to distinct cytokines summarized in coloured tables. Macrophages polarise toward M1 phenotype (orange) in response to IFNγ or LPS signalling and start to express specific markers summarised in the orange table. Macrophages polarise toward M2 phenotype (green) after IL-4 or IL-10 signalling and start to express markers summarised in the green table. Two coloured scale shows that M1/M2 phenotype activation only represents two edges of a continuum of intermediate states.

On the other hand, the alternative-activated macrophages or M2 macrophages (**Figure 19**) are often called anti-inflammatory macrophages as they express more metabolism-related markers or growth factors such as mannose receptor (MRC1 or CD206), galactose receptor, Arginase (ARG), TGFb or interleukin-10 (IL-10). While M1 macrophages show a high uniformity across species and different infectious conditions, M2 macrophages display a high variability and plasticity even inside their own category. For this reason, some studies proposed a system of further subcategorising M2 macrophages into M2a, b, c and d, according to their functions, marker expression and activators. M2a macrophages are polarized in response to IL-4 and 10 and play role in parasite immune control. M2b macrophages are considered as immune-regulators and also express pro-inflammatory factors similarly to M1 macrophages such as IL-1 and 6. M2c macrophages are involved in tissue repair and remodelling and possess the characteristics which have been most often associated with M2 macrophages historically. The last subcategory, M2d are macrophages described and involved in tumour progression, called tumour-associated macrophages (TAM).

The concept of macrophage polarisation state has been established on human and murine macrophages. As the process of haematopoiesis and blood cell differentiation is conserved among all vertebrates, the diversity of macrophage polarisation might be conserved too. Several studies have shown that macrophages in lower vertebrates also express pro-inflammatory factors during acute inflammation and M2-like factors, such as arginase in non-inflammatory conditions. In addition, in invertebrates such as *Drosophila*, phagocytes which are the equivalent of macrophages in vertebrates express chitinase-3 like 3 protein (Ym1) which is a M2 marker in mouse macrophages (Rőszer, 2015). Together, these results suggest that macrophage activation diversity might be conserved or possess comparable parameters through the animal kingdom.

The macrophage polarisation concept is based on the studies performed on bone marrow-derived macrophages. As previously stated, we distinguish two types of macrophages depending on their origin. Whether the M1/M2 concept might be extrapolated to tissue-resident or generally to yolk sac-derived macrophages remains to be elucidated. Considering that the activation depends greatly on the local microenvironment and the present factors, we can assume that these macrophages may equally exhibit a diversity according to the tissue they infiltrated. Several studies have shown that tissue-resident macrophages express few M2

markers, with a peak of expression at neonatal stage and consecutive decrease with age (Hung et al., 2002; Rőszer, 2015).

4.2. Macrophage functions

The macrophage heterogeneity originates from the number of functions they can fulfil (**Figure 20**). The first described role, **phagocytosis,** gave their name to macrophages as big eaters (from Greek makros = big and phagein=eat). Phagocytosis serve to engulf all foreign substances, from debris to unicellular organisms, and protect the organism from outside and inside danger. Concomitantly, the expression of **cytokines** contributes to pathogen elimination by killing the microorganisms or attracting other immune cells. IL-1, TNFa or NOS2 induce the synthesis and release of reactive oxygen and nitrogen species which help to the clearance of pathogens. Furthermore, IL-1, 6 and 12 contribute to lymphocyte activation and IL-8 to T-lymphocyte attraction to the infected site.

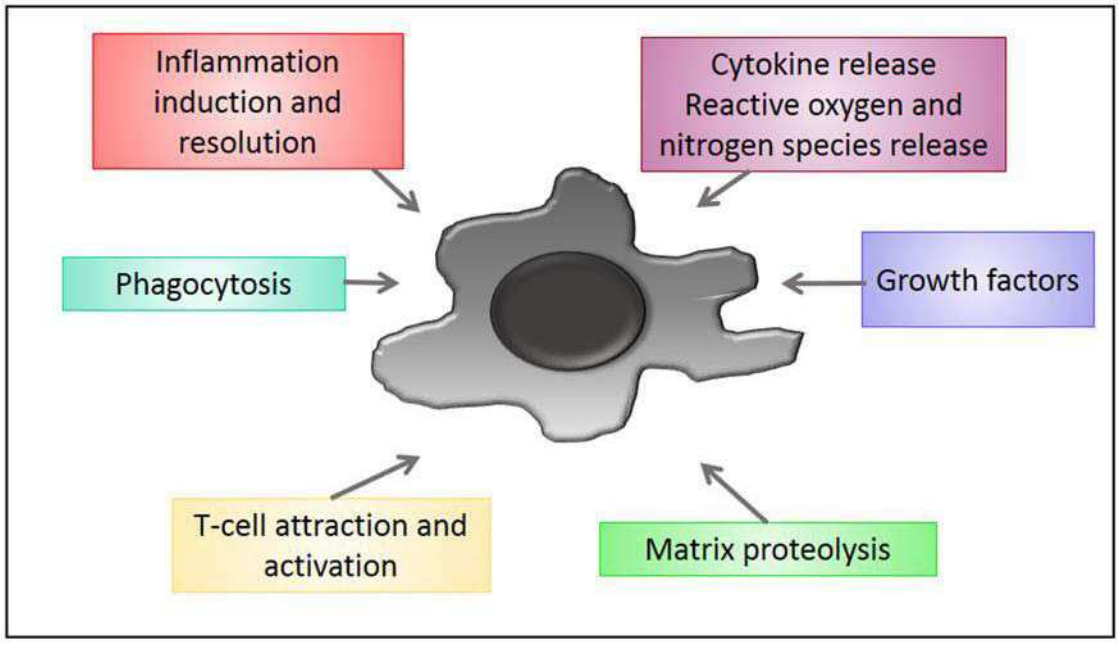

Figure 20 – Macrophage functions:
List of various functions that macrophages can achieve

In addition to cytokine synthesis, macrophages also produce and release **growth factors** and other signalling molecules, including prostaglandins, TGFb, EGF or FGF. The expression factor depends on the macrophage subpopulation as well as the environment. The nervous

system-specific resident macrophages, called microglia, express the neuronal growth factor (NGF). The macrophages present in tumours, TAM, express at once several growth factors, such as epithelial growth factor (EGF), vascular endothelium growth factor (VEGF) or fibroblast growth factor (FGF) which all promote cancer cell progression and metastasis initiation in a specific way (Wynn et al., 2013).

Finally, synthesis and release of **proteolytic enzymes** by macrophage enable them to achieve their role during tissue remodelling and matrix degradation. Tissue remodelling ruled by macrophage-induced proteolysis is an important part of tissue organisation during embryogenesis but also during several chronic pathologies, especially the ones affecting cardiovascular system such as atherosclerosis, myocardial infarct and aneurysm.

Proteolytic enzymes can be divided into six groups according to their mechanism of action – serine, threonine, cysteine, aspartate, glutamic acid proteinases and Matrix metalloproteinases (MMP) (Quillard et al., 2011). Macrophages express principally MMP and serine proteinases (Cathepsins). MMPs can be further divided according to their structure into secreted (MMP-1 - MMP-13) and membrane-associated, named also MT-MMPs (MMP-14 - MMP-17), or according to their activity into collagenases, gelatinases, stromelysins etc. As previously stated, MMPs main function is ECM degradation. In addition to this role, MMPs influence several cellular processes, most often by cleaving a molecule to activate or deactivate its function. Specific matrix degradation might therefore modulate cell migration and its behaviour, but also the signalling based on the integrin-mediated cell contact or cell proliferation and apoptosis (Vu and Werb, 2000). Blood-circulating monocytes and differentiated macrophages can express the majority of MMPs with predominant expression of the MMP-1, MMP-2, MMP-3, MMP-9 and MMP-10 (**Figure 21**). MMP-9 has been the first proteinase described in human macrophages and associated to macrophage specification (Welgus et al., 1990).

Name	Alternative name	Substrate	Zebrafish orthology
MMP-1	Collagenase-1 Fibroblast collagenase	Collagen I-III,VI-VII,X, Gelatin, Fibronectin, Vitronectin, Lamilin, TNF prec.	No orthologue described
MMP-2	Gelatinase A 72kDa gelatinase	Collagen I, III-V, VII, X-XI, Gelatin, Lamilin, Fibronectin, TNF prec., SDF-1	Yes
MMP-3	Stromelysin-1	Collagen III-IV, IX-XI, Gelatin, Lamilin, Fibronectin, TGFB1, TNF prec., osteopontin	No orthologue described
MMP-9	Gelatinase B 92kDa gelatinase	Collagen IV-V, VII, X, Gelatin, Lamilin, Fibronectin, ZO-1, TGFB1, TNF prec., proIL-1b, IL-8	Yes
MMP-10	Stromelysin-2	Collagen III-V, IX-X, Gelatin, Fibronectin,	No orthologue described

Figure 21 – MMPs expressed by macrophages
List of matrix-metalloproteinases (MMPs) secreted by monocytes and macrophages, their substrates and presence of orthologues in zebrafish genome. IL-8, Interleukin 8; SDF-1, Stromal-cell Derived Factor 1 (also called CXCL12); TGFB1, Transforming Growth Factor Beta 1; TNF prec., Tumour Necrosis Factor precursor; ZO-1, Zona Occludens 1

The zebrafish embryos appear to have 25 *mmps* genes in its genome, which is more than in the human genome (24 MMPs). However, this elevated number is associated to the teleost genome duplication and therefore not all human orthologues have been described in the zebrafish so far. For example, the majority of collagenases and stromelysin family members, such as MMP-1, 3, 8 or 10, which are also monocyte-associated enzymes, have not been found yet. On the other hand, the collagenase mmp-13 and stromelysin mmp-11 are duplicated and might at least partially take over the function of the missing MMPs, especially as the mmp-13 and mmp-9 expressions have been detected in zebrafish myeloid cells (Wyatt et al., 2009; Yoong et al., 2007; Zhang et al., 2008).

4.3. Macrophage migration

Macrophages infiltrate most tissues to fulfil their role. Their capacity to migrate through different matrices distinct them from other blood cells and allow them to fulfil their role. The

type of cell migration is separated in two main categories defined by the tissue architecture: 2-dimensional (2D) and 3-dimensional (3D), which we can be further subdivided into mesenchymal and amoeboid (**Figure 22**). Each of these categories possesses specific behavioural characteristics and cell cytoskeleton structure. 2D migration takes place when macrophages are migrating along flat or smooth tissues such as epithelium or inner vessel wall (inside vasculature). 3D migration is established inside tissues containing ECM scaffold with heterogeneous composition (Cougoule et al., 2012; Friedl and Weigelin, 2008). The scaffold composition seems to be one of the major factors in the decision of which pattern of migration macrophage will use. It has been shown *in vitro* that macrophage can adopt different migration pattern according to the characteristics of the surrounding tissue and combine both types of 3D migration –amoeboid and mesenchymal modes (Guiet et al., 2011).

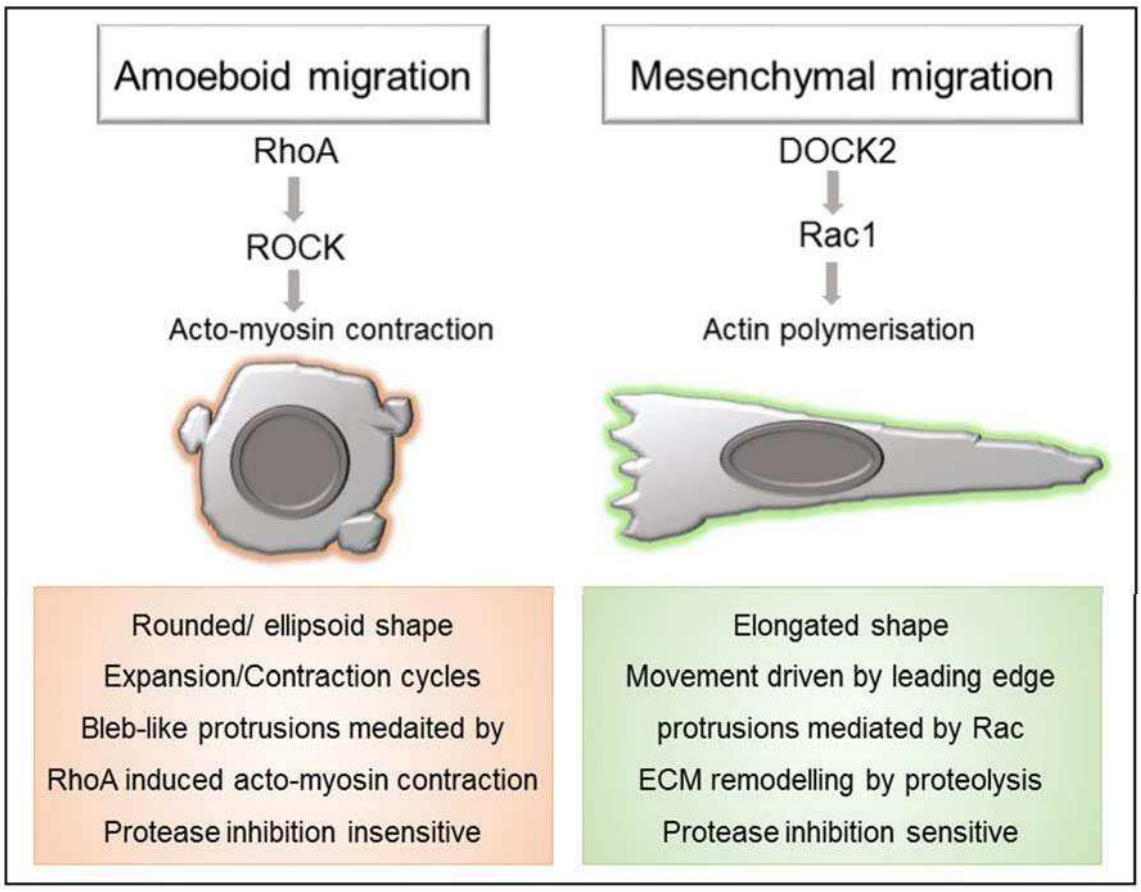

Figure 22 – Macrophage migration:
Specific characteristics and cell morphology in amoeboid (orange) versus mesenchymal (green) migration. Amoeboid migration is induced by RhoA and ROCK signalling, cells adopt rounded or ellipsoid shape and migrate via acto-myosin contraction cycles and bleb-like protrusions. Mesenchymal migration is adopted after Rac1 activation, cells become elongated and form a leading edge. Migration is mediated by ECM remodelling by proteases.

Although the type of migration seems to be dependent on the environment, the classification has been primarily based on the cell morphology during migration. This parameter was later extended to other parameters such as cytoskeleton implication, cell-matrix interactions and matrix modification (Friedl, 2004; Friedl and Wolf, 2010). Amoeboid migration is characterized by rounded or ellipsoid shape and a movement that mimics the behaviour of the amoeba *Dictyostelium discoideum*. Thus, the cell translocates very rapidly by alternating cycles of expansion and contraction (Friedl, 2004). This type of movement is also called crawling, and weak or no interaction with the matrix are observed. The amoeboid migration requires the actomyosin repetitive contraction which are dependent on small GTPase RhoA and its downstream effector ROCK (Figure 22). Recently, a subdivision of this mode has been proposed to distinguish two additional categories. A first type which is represented by a very round shape and blebby fast movements with no interactions with the matrix. A second mode adopts a more elongated or ellipsoid shape with an actin-rich structure at the leading edge permitting weak adhesive interactions with the ECM (Friedl and Wolf, 2010).

In contrast, mesenchymal migration is defined by elongated to spindle shapes and uses proteinases to remodel and digest ECM to allow migration. As a result, we can observe modified ECM structure along the track of the migrating cell. The ECM remodelling is mediated through focal contacts which occur slowly (up to several dozens of minutes) resulting in relatively slower migration compared to the amoeboid type (Friedl, 2004). The remodelling process during migration is governed by synthesis and release of proteolytic enzymes, mostly MMPs, cathepsins and urokinase-type plasminogen activator (Guiet et al., 2012; Vérollet et al., 2011). Especially MMP-2, 9, 12 and 13 have been shown to play a substantial role in mesenchymal migration and tissue infiltration by macrophages (Gong et al., 2008). Interestingly, the set of proteinases involved in the mesenchymal migration might depend on environmental conditions, especially the structure and composition of the tissue. It has been shown that while in matrigel or gelled collagen, macrophages degrade the matrix by predominantly using cathepsins, in the 3D multicellular spheroid, their migration requires MMP-mediated degradation (Van Goethem et al., 2010; Guiet et al., 2011; Vérollet et al., 2011).

ECM remodelling mediated though the focal adhesion to the matrix requires the formation of specific subcellular structures called podosomes. Podosomes exhibit very specific and complex architecture permitting the focal release of proteolytic enzymes (Wiesner et al., 2014). The podosome formation as well as their polarized morphology during mesenchymal migration involves a specific cytoskeleton structure and the contribution of several small GTPases including Rac1 and 2 or Cdc42 (Keely et al., 1997; Sanz-Moreno and Marshall, 2010; Wheeler et al., 2006).

4.4. Macrophage cytoskeleton

As previously mentioned, macrophage migration and morphology represent two tightly connected and inseparable features. Depending on the migration mode, macrophages adopt either a rounded shape – and mediate no or very few adhesions, generally integrin-based – or an elongated shape with ECM focal adhesions.

The rounded shape during amoeboid migration requires a specific organisation of the macrophage cytoskeleton. The cells migrate through gaps existing in the ECM. Therefore, they keep a high capacity of deformation and lack stable contacts. Their shape change is mediated by cortical filamentous actin (F-actin), responsible for the dynamics as well as cell body stiffness. During migration, macrophages change their shape from round to ellipsoid. This change requires actin polymerization along the plasma membrane to stiffen and contract the cell cortex. These cortical actin dynamics are governed by RhoA and its effector molecule ROCK (Friedl, 2004). Rho induces actomyosin contractility (**Figure 23**) via the Rho-kinase called ROCK and phosphorylation of MLC kinase (MLCK). Each of these kinases influence the actin filaments at different position. ROCK acts in the cell body whereas MLCK is required at the cell periphery. Moreover, Rho acts on F-actin through further kinases to induce actin accumulation or stress fibre formation (Ridley, 2001).

The ECM degradation associated with mesenchymal migration depends on the formation of dynamic focal adhesions, the podosomes. Podosomes are defined as actin-rich adhesive structure belonging to the group of invasion-mediating adhesions. They can be formed during 2D as well as 3D migration with minor morphological differences caused by matrix structure (Wiesner et al., 2014). They consist of an F-actin-rich core with actin-associated proteins, such as Arp2/3 complex or cortactin, surrounded by a ring structure with adhesion

plaque proteins including vinculin, paxillin or talin. In the podosomes associated with mesenchymal 3D migration (also called 3D podosomes), the ring and core structure are not as well defined as in 2D migration though the molecular composition remains identical. This less precisely defined structure might be related to the technically-challenging high-resolution imaging. Despite their relatively complex structure, podosomes stay highly dynamic with a life span of approximately 5 minutes. Single cell forms around 2-9 podosomes which are localised at the tip of long protrusions (Wiesner et al., 2014).

Podosome assembly is controlled by several signalling molecules including the Rac GTPases (**Figure 23**). Both Rac1 and Rac2 affect podosome formation, each in its specific way. Rac2 impairment completely disables podosome assembly whereas without Rac1 the F-actin foci are formed but lack the adhesion proteins, especially paxillin. Interestingly, the absence of podosome formation did not impair macrophage migration on plate. On the contrary, macrophages exhibited higher speed, suggesting that the migratory properties might have been modified and depend on other signalling molecules (Wheeler et al., 2006). In agreement with the podosome formation modifications, the overall morphology of the macrophages changed. The single Rac1 or Rac2 disruption enhanced the elongated shape, while dysfunction of both Rac1 and 2 caused two extreme states – either the rounded shape or the stellate one with extended protrusions in several direction simultaneously (Wheeler et al., 2006). Cdc42 kinase ranges among the other small GTPases involved in podosome assembly (**Figure 23**). Its activation is required for the formation of focal complexes, filopodia and fine actin cables running in parallel to the membrane along the nucleus. In addition, it interacts directly with Rac GTPase and act in parallel of podosome formation (Jones, 2000).

During mesenchymal migration, macrophages adopt the elongated shape, suggesting that mesenchymal migration induce higher cell polarity compared to amoeboid migration. The cell actively forms its leading edge to allow directed migration. The unilateral accumulation of F-actin permits the induction of cell polarity and the creation of the leading edge. Wiskott Aldrich Syndrome protein (WASP) is a member of the small GTPase kinase family complex responsible for actin monomer recruitment and thus for the formation of the leading edge. This protein was discovered for the first time as a product of the gene mutated in the Wiskott Aldrich syndrome. During this X-linked auto-immune disease, patients exhibit among other symptoms an abnormal cytoskeletal organisation including a lack of podosomes in myeloid cells. Indeed, in the WASP null mice, the myeloid cells fail to polarise and to assemble podosomes. The

substitution of the WASP protein rescue cell polarity. The leading edge formation concept is based on the contact of myeloid cells with a rigid substratum. This is then followed by a chemotactic factor that initiate asymmetric extension of protrusions together with WASP recruitment (Monypenny et al., 2011).

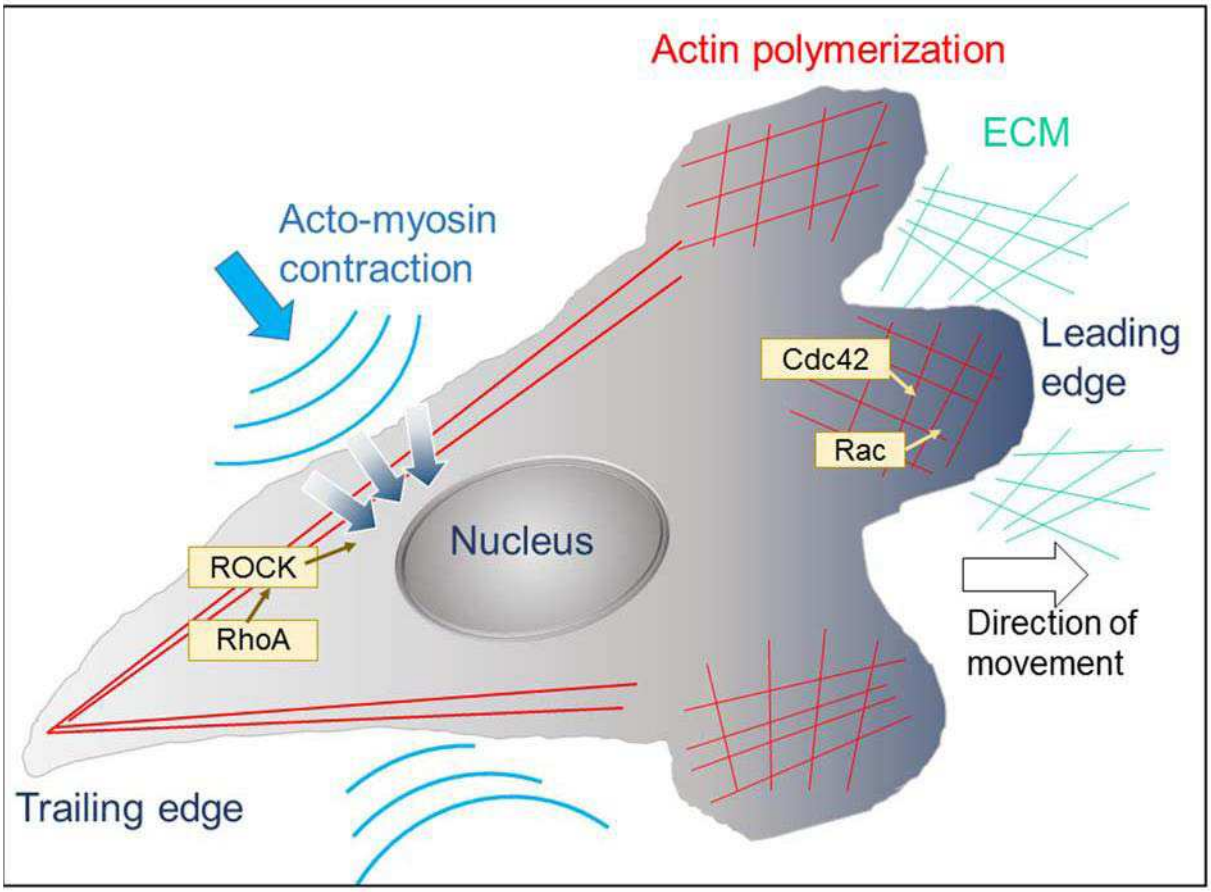

Figure 23 – Macrophage cytoskeleton:
Cell components contributing to specific macrophage morphology and to their migration. Macrophage migration and shape are influenced by several factors. After morphological polarisation, macrophage forms leading and trailing edge. The leading edge determines the direction of movement where proteases will be released to degrade ECM (green). Specific membrane extensions such as podosomes are formed in the leading edge. For ECM-remodelling independent migration, RhoA induces acto-myosin (blue) contractions along the central part of the cell.

In recent years, the studies performed *in vitro* as well as *in vivo* using different animal models led us to a rapid advance in understanding macrophage heterogeneity and plasticity. Their heterogeneity based on their effective adaptation to the local environment and its signalling allows the macrophage to accomplish their multiple roles. Deciphering all the intrinsic and extrinsic factors influencing the polarization and behaviour would help us to

understand and predict the specific role of macrophages during development, homeostasis and pathologies.

5. Autonomic nervous system

The autonomic nervous system (ANS) refers to the part of the nervous system that regulate the function of all internal organs and is not controlled by volition or conscious reaction. As the ANS innervate the vast majority of internal organs, it contributes significantly to homeostasis. It regulates, among other things, blood pressure, gastrointestinal responses to food, contraction of the urinary bladder, eye focus or thermoregulation. The ANS belongs to the peripheral nervous system, which means that all the neurons are localised outside the brain and spinal cord. Based on its functional unit and morphology, the ANS can be divided into two groups: sympathetic and parasympathetic system (Mccorry, 2007). The sympathetic system is often referred to as the sympatho-adrenal system, suggesting that the hormonal organ adrenal medulla participates to the ANS. The adrenal medulla is an endocrine organ synthetizing the same molecules as the sympathetic nervous system and contributing to the effects of the sympathetic nervous system (Saito and Takahashi, 2015).

Many tissues are innervated by both systems – sympathetic and parasympathetic nerves - which act typically opposite to each other to ensure the precise control of homeostasis. In addition, both systems are tonically active, which allow the activation or the inhibition of their activity following the appropriate signalling. While the sympathetic system predominates in emergency conditions – often referred to as the "fight-or-flight" reaction – the parasympathetic system is effective during quiet, resting conditions to conserve and store energy (Mccorry, 2007). Morphologically, the two systems exhibit distinct structures despite the common concept of the two neurons units, which means that a preganglionic neuron innervates a ganglion outside CNS and from this ganglion a postganglionic neuron innervates the targeted tissue. The sympathetic system is composed of short preganglionic neurons, which in both cases – sympathetic and parasympathetic systems - are mediated by the same neurotransmitter, the acetylcholine, the ganglions are structured in ganglion chain and the postganglionic neurons are long and terminate on the targeted tissue. The parasympathetic system, on the other hand, is formed by long preganglionic neurons with the ganglia at the vicinity of the targeted tissue. From the synaptic ganglion only very short neurons innervate the tissue (Mccorry, 2007).

5.1. Autonomic nervous system development

The origin of the ANS is common in all vertebrates and arises from evolutionary conserved mechanism. All the peripheral autonomic nerves originate from the neural crest cells (NCCs), except from cranial parasympathetic neurons. NCCs are a transient population arising between the neuronal and non-neuronal ectoderm during early development. The NCCs give rise to a high variety of differentiated cells, including the sensory, autonomic and enteric nerves, adrenal medulla, melanocytes or skeletal, connective, adipose and endocrine cells (Green et al., 2015; Takahashi et al., 2013; Young et al., 2011). NCCs undergo epithelial-to-mesenchymal transition to delaminate from the ectoderm tissue to participate to the formation of different organs. They possess specific molecular signature. Sox10 and FoxD3 transcription factors or Wnt1 signalling are characteristic of NCCs at their stem or early progenitor stage and required for their maintenance prior to the commitment into specific lineages (Green et al., 2015; Kim et al., 2003).

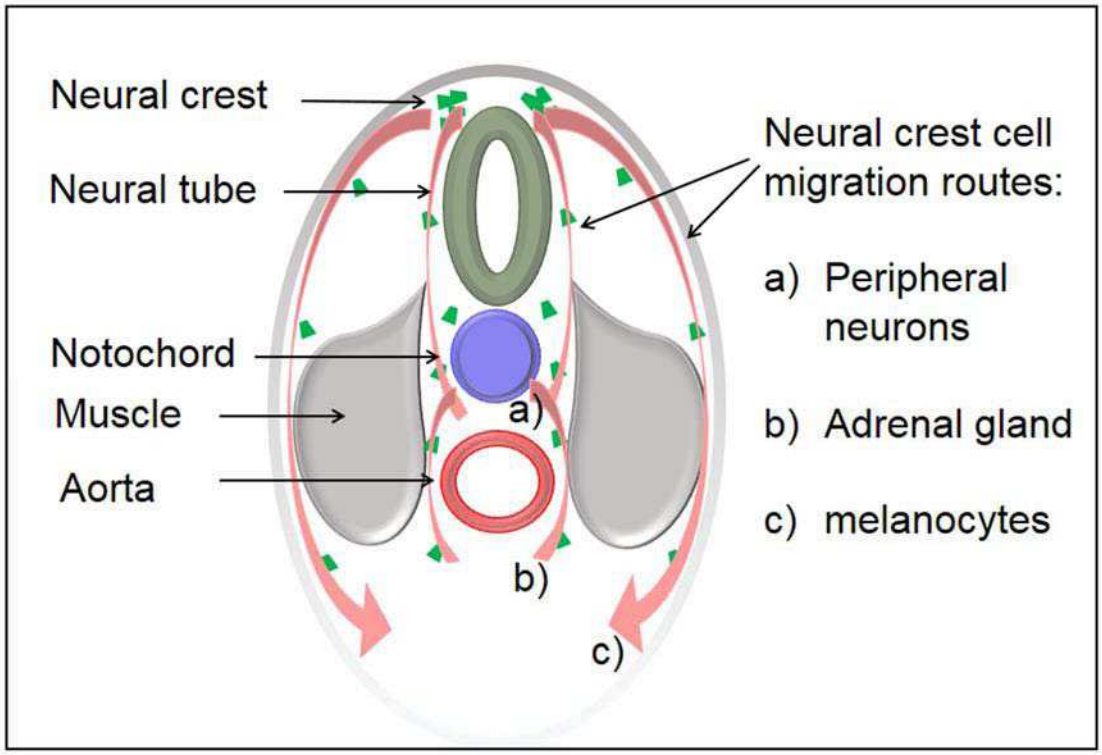

Figure 24 – Migration of the neural crest cells to colonise the organism:
Two ventral migration routes to settle to the final location – the dorso-ventral migration gives rise to the peripheral neurons (**a**) and adrenal gland (**b**) and the dorso-lateral migration initiates the first wave of pigmentation (**c**).

The **sympathetic system** arises from trunk NCCs that migrate ventrally (**Figure 24**) in the direction of the dorsal aorta, which is the first formed embryonic vessel (Saito et al., 2012; Young et al., 2011). The early progenitors, which will later give rise to both the sympathetic ganglions and adrenal medulla (sympatho-adrenal or SA progenitors), migrate actively in the ventral direction attracted by multiple factors present in the dorsal aorta region. BMP produced by the aorta induce the SDF-1 and neuregulin-1 expression in the para-aortic region which as a result guide the SA progenitor migration in mouse and chicken embryos (Saito et al., 2012). Once the SA progenitors reach the dorsal aorta, they become restricted to a specific cell fate. The sympathetic progenitors remain near the aorta, while the adreno-medullary precursors continue to migrate ventrally to form adrenal gland (Saito and Takahashi, 2015). In the zebrafish embryo, similar mechanism occurs with few exceptions. Chromaffin cells - the homologue for the adrenal medulla in the zebrafish - are localised more dorsally than aorta compared to the mammalian embryos, inside the anterior part of the kidney. Thus, the SA precursor migrate toward the kidney region in the cervical part and only the sympathetic progenitors then continue ventrally to reach the dorsal aorta (An et al., 2002).

BMP signalling is not only required for sympathetic precursor migration but also to induce their differentiation into mature sympathetic neurons. BMP signalling activates several transcription factors including the paired homeodomain factors Phox2A and Phox2B, the basic helix-loop-helix transcription factors Hand2 and achaete-acute complex homolog 1 (Ascl1) or zinc finger factors Gata2/3 (Morikawa et al., 2009). Whereas sympathetic and parasympathetic are both dependent on Phox2 and Ascl1 transcription expression factor, Hand2 and Gata2/3 activations (**Figure 25**) are restricted to the sympathetic system lineage (Howard, 2005). Those factors induce cAMP and MAPK signalling leading to neurotransmitter synthesis and therefore maturation of the neurons (Apostolova and Dechant, 2009). The sympatho-adrenal system neurotransmitters are noradrenaline and adrenaline, commonly referred, together with dopamine, as catecholamines due to their chemical structures. Catecholamine synthesis is executed by a cascade of enzymatic reactions mediated by the following enzymes: tyrosine hydroxylase (TH), dopamine-β-hydroxylase (DβH) and catechol-O-methyl transferase (COMT). These synthetizing enzymes are currently used as mature sympathetic system markers (Apostolova and Dechant, 2009).

The exact origin of the **parasympathetic system** remained unclear for much longer than the sympathetic system development. Recently, two independent groups have unveiled the

parasympathetic system origin simultaneously (Dyachuk et al., 2014; Espinosa-Medina et al., 2014). Like all autonomic neurons, the parasympathetic system arises from the neural crest. However, the preganglionic and postganglionic neurons each exhibit distinct mechanisms of development. The preganglionic neurons arise in the same way as sympathetic neurons, but the postganglionic neurons originate from Schwann cell precursors (**Figure 25**). Despite the distinct mechanism of formation, the development of preganglionic and postganglionic neurons is closely associated. Indeed, disruption of the preganglionic nerves also impairs the ganglion and following nerves formation. Schwann cell precursors (SCP) express Schwann cell specific markers, but also general neural crest markers like Sox10 and autonomic neural cell marker Phox2B (Espinosa-Medina et al., 2014). According to the distance of SCPs from the central nervous system (CNS) the different cell fate is adopted. At the vicinity to the CNS, SCPs downregulate the paired-like homeobox 2b (Phox2B) expression and differentiate into Schwann cells or melanocytes. In the distant areas from the CNS, they keep the Phox2B expression and decrease the Sox2 – a melanocyte marker – to become parasympathetic postganglionic neurons (Adameyko et al., 2012).

During their differentiation, parasympathetic neurons depend on the expression of proneural bHLH transcription factor, which increases the expression of Phox2B transcription factor, and Ascl1, which define the autonomic nervous system commitment (Dyachuk et al., 2014). Once differentiated, parasympathetic neurons exhibit specific cholinergic neurotransmitter features, such as expression of choline acetyl transferase (ChAT), vesicular acetylcholine transporter (VAChT) and vasoactive intestinal peptide (VIP). These molecules are required for neurotransmitter synthesis and are used to identify parasympathetic neurons (Arvidsson et al., 1997; Stanke et al., 2005). Once differentiated, parasympathetic neurons start to express and release acetylcholine, the parasympathetic neurotransmitter, and thus become functional (Stanke et al., 2005).

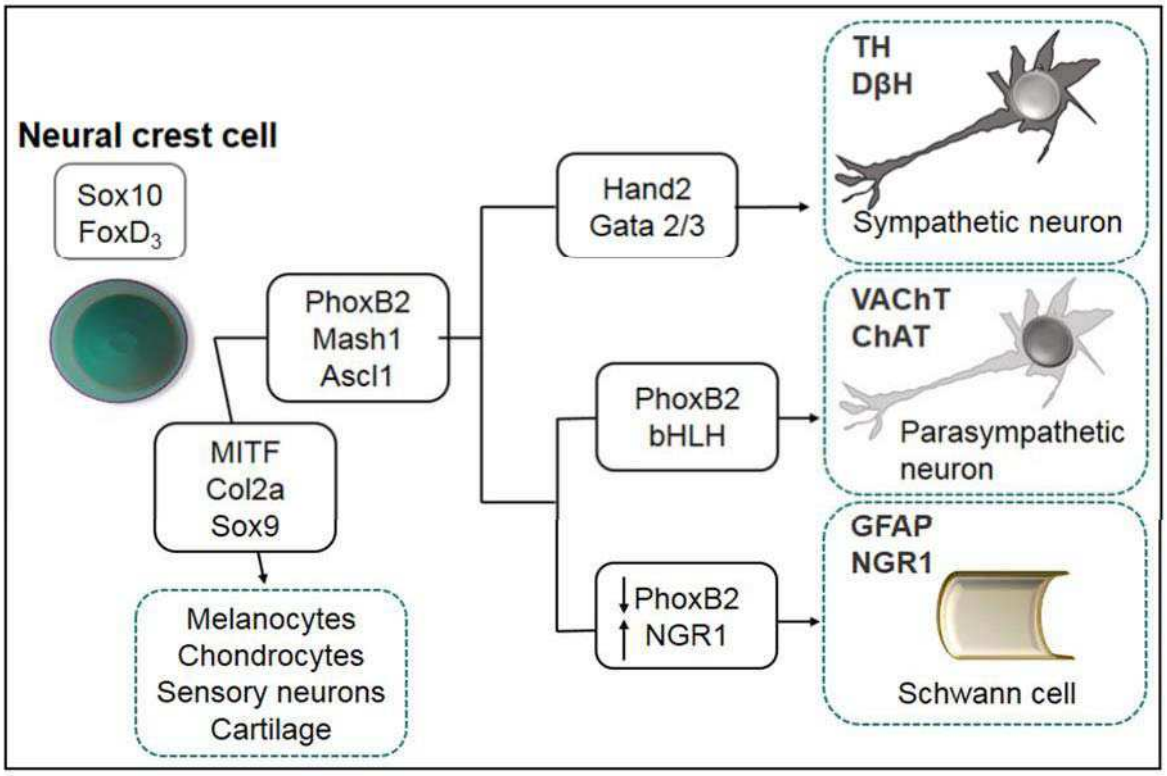

Figure 25 – Neural crest cell differentiation:
The transcription factors delineating the lineage specification and differentiation into neurons or Schwann cells. Sox10 and FoxD3 specify neural crest cell. Increase of MITF, Col2a or Sox9 expressions lead to the differentiation toward non-neural cells, such as melanocytes, chondrocytes or cartilage. PhoxB2, Mash1 and Ascl1 induce differentiation to the common progenitors of autonomic neurons and Schwann cells. Sympathetic neurons differentiate in response to Hand2, Gata 2 and 3 signalling while parasympathetic neurons after PhoxB2 and bHLH activation. Downregulation of PhoxB2 and increase of NGR1 signalling lead to Schwann cell differentiation. Ascl1, Achaete-scute homolog 1; bHLH, basic Helix-Loop-Helix protein; ChAT, Choline Acetytransferase; Col2a, Collagen type 2a; DβH, Dopamine beta Hydroxylase; GFAP, Glial Fibrillary Acidic Protein; Hand2, Heart and Neural Crest Derivates Expressed 2; NGR1, Neuregulin-1; PhoxB2, Paired-like Homeobox B2; TH, Tyrosine Hydroxylase; VAChT, Vesicular Acetylcholine transporter

5.2. Sympatho-adrenal nervous system

The sympathetic nervous system has been described to be present in several haematopoietic niches and to contribute to HSCs homeostasis, whereas the parasympathetic system has not been yet fully described and is likely dispensable during the haematopoiesis. For this reason, only sympathetic nervous system and its signalling will be introduced in details in this chapter. The sympathetic system is sometimes referred as sympatho-adrenal to include neuronal and hormonal system sharing the common features of catecholamine synthesis and signalling pathway.

5.3. Neurotransmitters

As previously mentioned, the sympatho-adrenal system activity is mediated by catecholamines, which are specific neurotransmitters that affect the targeted tissues. The two principal mediators are produced by the enzymatic complex of the sympatho-adrenal system, noradrenaline and adrenaline, both being members of the catecholamine family. Noradrenaline, the precursor of adrenaline during synthesis, is the main neurotransmitter produced by the sympathetic nervous system. It is produced by neurons, delivered in the vesicles to the terminal axon synapse where it is locally released and activates the proximal receptors in the tissue. Adrenaline, on the other hand, is the terminal product of catecholamine synthesis and is preferentially produced in the adrenal gland by chromaffin cells. Adrenaline is released when needed in the circulation and activates the receptors on the targeted tissue by the blood stream. The action through blood circulation enables the activation of a high variety of the tissues in parallel (Mccorry, 2007).

5.4. Adrenergic receptors

The catecholamines act on the adrenergic receptors localised on the surface of the targeted cells. Adrenergic receptors consist of 2 classes, alpha and beta which further divide into two and three receptors respectively, α_1, α_2, β_1, β_2 and β_3 (**Figure 26**). Some studies suggest the existence of a 4th β-receptor but it has not been confirmed yet and it may simply be a distinct conformation of another β receptor (Granneman, 2001). Adrenergic receptors are all composed of 7-transmembrane proteins coupled to G-protein and second messenger system inducing intracellular signals (Li and Cho, 2011; Mccorry, 2007; Wikberg, 1982). While the α-receptors are activated preferentially by noradrenaline, adrenaline binds with higher affinity to the β-receptors. The zebrafish embryo sympathetic system is composed of 5 β-receptors, β_1, β_{2a}, β_{2b}, β_{3a} and β_{3b} compared to 3 mammalian receptors due to the genome duplication in teleost. Zebrafish β receptors share a relatively high percentage of sequence identity with their human orthologues – in average around 50% – but even higher in the 7-transmembrane domain (Wang et al., 2009).

	Localisation	Role	Agonist	Antagonist
α_1	Smooth muscle	Constriction	Noradrenaline	Doxasosine
α_2	CNS	Regulatory role	Clonidine	Yohimbine
β_1	Cardiomyocyte	Contraction	Dobutamine	Metoprolol
β_2	Smooth muscle	Relaxation	Salbutamol Isoprenaline	Propranolol
β_3	Adipocytes	Lipolysis	BRL 37344	SR59230A

Figure 26 – Adrenergic receptors' list:
List of adrenergic receptors, their main localisation in the adult organism, the role associated with their activation and an example of specific activator and inhibitor of the receptor.

The α_1 protein is considered more as an excitatory receptor and is localised in a high variety of peripheral tissues, such as smooth muscle including the smooth muscle of the peripheral blood vessels, bladder neck or prostate. It is mainly responsible for the smooth muscle contraction as a result of second messenger cAMP activation. The α_1 receptor may be further divided into 4 subpopulations with distinct expression patterns and binding site structures (Bylund, 1992). On the other hand, the α_2 receptor is localised more centrally and its role might be referred more as a regulatory receptor. Its activation leads to cAMP inhibition. Therefore α_2 acts in a contrary or regulatory fashion to the α_1 receptor.

The β_1 receptor is expressed predominantly by cardiomyocytes and partially by the adipose tissue. It influences substantially all the heart characteristics – the heart rate, the strength and duration of the contraction (Fairchild and Shea, 2011; Frielle et al., 1988). The β_1 receptor shows an equal affinity to both catecholamines, adrenaline and noradrenaline, whereas the β_2 receptor is generally activated by adrenaline. The β_2 receptor is expressed by lung, liver and smooth muscle cells and at low level by brain. The β_2 receptor signalling pathway may be mediated through two distinct downstream pathways. Most of the receptor appear to act through cAMP second messenger inducing protein kinase A (PKA) signalling. However, a small proportion of the signalling is mediated through the p38 mitogen-activated protein kinase (MAPK) (Johnson, 2006). The β_3 receptor is expressed predominantly by adipose tissue, vascular endothelium, heart and gastro-intestinal system. Its activation through cAMP second

messenger induce a signalling leading to PKA activation followed by MAPK pathway. In the vascular endothelium and heart, the β_3 receptor activation results in NO synthesis and following vasodilatation or reduced contractile force of myocardium (Coman et al., 2008).

5.5. Sympatho-adrenal system and haematopoiesis

As previously mentioned, several β-receptors are expressed either on the surface of HSCs at specific stages or within the haematopoietic niche. In the murine AGM (**Figure 27A**), the local sympathetic innervation at the vicinity of the dorsal aorta activates β_2 and β_3 receptors within the niche. While the β_3 receptor is expressed by stromal cells and its function remains unclear, the β_2 receptor is expressed by both endothelial cells and HSCs themselves. The activation of the β_2 receptor is required for HSC emergence (Fitch et al., 2012).

Despite being less described than other niches, the T-lymphocyte homeostasis in the thymus is also dependent on the sympathetic innervation (Leposavić et al., 2008). Interestingly, catecholamine synthesis is not exclusively produced by sympathetic neurons in the case of the thymus niche. The non-neuronal cells, such as macrophages and other leukocytes are also able to produce and liberate locally catecholamines. The differentiating thymocytes and the surrounding cells express two different receptors, α_1 and β_2. Both of them appear to play a role during thymocytes maturation, however at different stages. The α_1 receptor activation plays a role during the early differentiation phase and its expression decreases with cell maturation. On the other hand, the β_2 receptor expression level increases with lineage differentiation, suggesting that it rather affects the late stages (Leposavić et al., 2008).

Bone marrow is a highly innervated haematopoietic organ, and sympathetic nerves with nonmyelinating Schwann cells are localized within perivascular bone marrow niche close to the arteries. Two types of receptors are present in the BM: the β_2 receptor expressed on the surface of HSCs and the β_3 produced by Nes+ CAR cells (Katayama et al., 2006). Neurotransmitters released from the sympathetic neurons activate the β_3 receptor on those CAR stromal cells. The downstream Sp1 pathway downregulates CXCL12 expression, which leads to mobilisation of HSCs, followed by their intravasation and differentiation into blood cells (**Figure 27B**). Moreover, the whole process is controlled by circadian rhythm which contribute to the sympathetic system regulation (Mendez-Ferrer et al., 2008). The β_2 receptor activation

might also play a role in HSC mobilisation but its exact mechanism remains unclear (Dar et al., 2011).

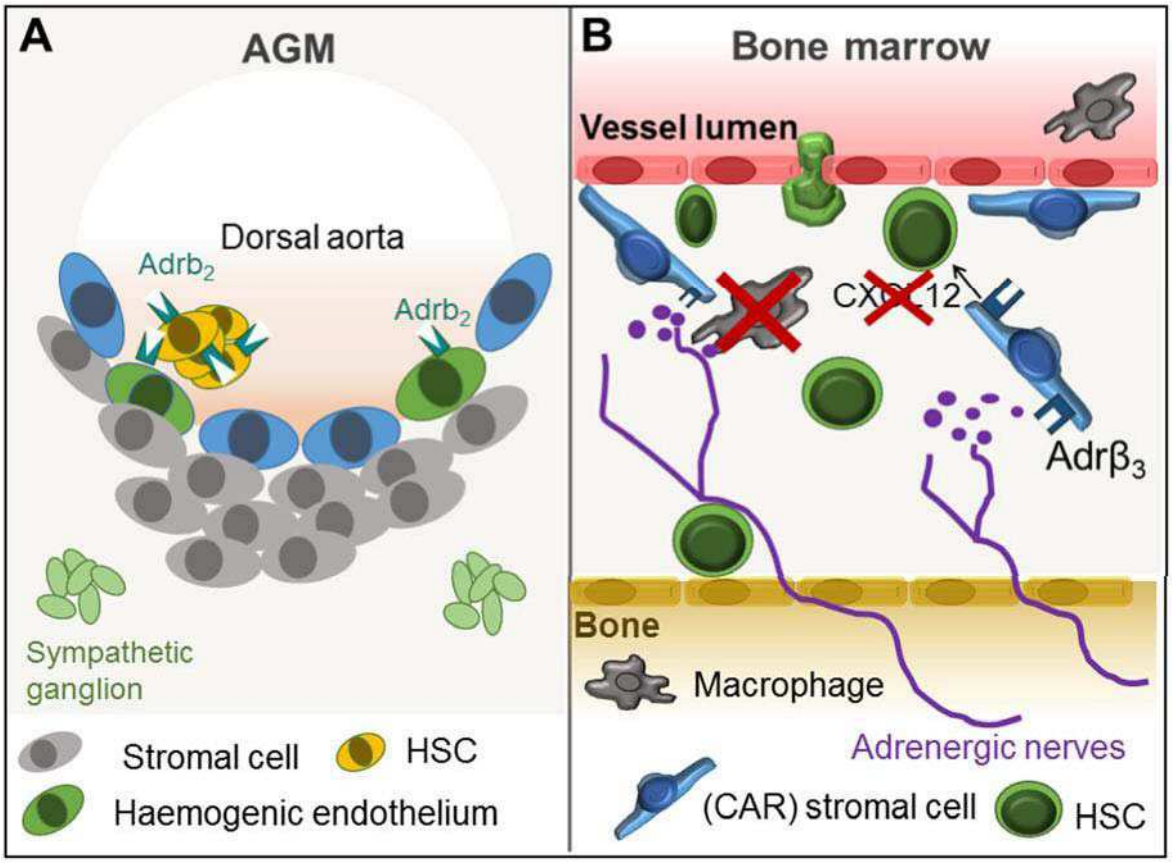

Figure 27 – The role of the sympathetic nervous system in different stages of haematopoiesis:
(A) The AGM orthogonal view with the endothelium (blue and green), stromal cells (grey) and the sympathetic ganglions (pale green). (B) Bone marrow niche with the sympathetic nerves (violet) close to the vessels (pink), CAR stromal cells (blue) and macrophages (grey), all contributing to HSCs (green) retention and mobilisation.

The peripheral nervous system acts as one of the main controller of inner organ homeostasis. Regarding the cardiovascular system, the sympathetic nervous system plays a fundamental role in heart beat characteristics and vessel tension. Moreover, HSC emergence and maintenance appears to be influenced by the sympathetic nervous system through the β_2 and β_3 receptor activation. Therefore, the peripheral nervous system needs to be considered as an important part of the HSC microenvironment together with the other cell compartments.

MATERIALS AND METHODS

Chapter 2: Materials and methods

Zebrafish Husbandry

Wild-type and transgenic lines were maintained in compliance with the Institutional Animal Care and Use protocols. All experiments were performed in accordance with the protocol CEEA-LR-13007 approved by the Animal Care and Use Languedoc-Roussillon Committee. Embryos were obtained from pairs of adult fish by natural spawning and raised at 28.5°C. Embryos were raised and staged according to Kimmel et al. (Kimmel et al., 1995). Wild type fish (AB) were obtained from ZIRC.

Medium	**Ingredients**	**Final concentration**
Egg's water	Distilled water	
	Instant Ocean Aquarium salt	60 µg/ml
	HEPES pH 7.3	500 µM
	Methylene blue	0.3 µl/ml
PTU egg's water	Distilled water	
	Instant Ocean Aquarium salt	60 µg/ml
	HEPES pH 7.3	500 µM
	phenylthiourea	200 µM

Transgenic lines

Transgenic lines used in this study are listed in the table below

Tg line	**Reference**
Tg(kdrl:Has.HRAS-mCherry) = Tg(kdrl:caax-mCherry)	(Chi et al., 2008)
Tg(kdrl:eGFP)	(Beis et al., 2005)
Tg(cd41:eGFP)	(Lin et al., 2005)
Tg(runx1:GFP)	(Lam et al., 2009)
Tg(mpx:eGFP)	(Renshaw et al., 2006)
Tg(mpeg1:mCherry-f)	(Ellett et al., 2011; Travnickova et al., 2015)
Tg(mpeg1:Gal4FF // UAS-E1b:Eco.NfsB-mCherry)	(Palha et al., 2013)
Tg(Xia.Tubb:DsRed) = Tg(NBT:DsRed)	(Peri and Nüsslein-Volhard, 2008)
Tg(Foxd3:GFP)	(Gilmour et al., 2002)
Tg(Sox10:GFP)	(Dutton et al., 2008)

Live Imaging

Embryos were anesthetised with 0.016% tricaine solution (MS-222, Sigma Aldrich) and mounted in 0.7% low melting point temperature (LMP) agarose in glass bottom dish (WPI). Embryos were positioned laterally, rostral to the left). Embryos were imaged at confocal microscopes Leica SPE, Leica SP5, Zeiss LSM510 or DeltaVision OMX.

Immunofluorescence and actin staining

Manually dechorionated anesthetised embryos were fixed at desired stage with PFA 4% sucrose 4% for at 3 hours at room temperature while rocking or overnight at +4°C. After PBS 1x/Tween 20 0.1% (PBST) washes embryos were permeabilised with 1% Triton for 2 hours at room temperature. Blocking step then followed using blocking solution (PBST/1% DMSO/1% BSA/10% Serum) overnight at +4°C. Embryos were incubated with primary antibodies – TH1 (1/200, Merck Millipore), TH2 (Semenova et al., 2014), Rac1 (1/100,), Rac2 (1/200, Santa

Cruz), Vinculin (1/200, Sigma), GFP (1/500, BLM), DsRed (1/500, Clontech) – followed by Alexa Fluor Goat Anti-mouse or Anti-rabbit IgG antibody (1/1000, Life Technologies).

For Actin staining, embryos were fixed with 4% PFA, permeabilised with 1% Triton and then stained with ActinGreen (Life Technologies, 2 drops per ml) in staining buffer (PBS 1x, 0.1% Tween 20, 1% DMSO, 1% Triton) for 5 hours in dark and washed with PBS/Tween 0.1%. Embryos were mounted in 90% glycerol and images at confocal Zeiss LSM510.

Whole mount *in situ* hybridization (WISH)

WISH was performed according to Thisse (http://zfin.org/zf_info/zfbook/chapt9/9.82.html). Embryos at 48 hpf were fixed, dehydrated with methanol, digested with proteinase K (New England Biolabs) and fixed again. Prehybridization was performed at 68°C in HM+ buffer (50% formamide, 5X saline sodium citrate, 0.1% Tween-20, 50 µg ml^{-1} heparin, 500 µg ml^{-1} yeast tRNA) and followed by hybridization with 0.5 ng μl^{-1} digoxigenin-labelled antisense RNA probe in HM+ buffer. The probes were detected with alkaline phosphatase-conjugated anti-digoxigenin antibodies (1/5,000; Roche Applied Science) using nitro blue tetrazolium chloride/5-bromo-4-chloro-3-indolyl-phosphate, toluidine-salt (Roche Applied Science). After staining embryos were mounted in 90% glycerol prior imaging. Zebrafish Mmp-9 and 13a plasmids were gifts from L. Ramakrishnan laboratory, mmp-2 from A. Noel laboratory.

WISH coupled to IF

WISH was performed as previously and embryos were incubated with blocking buffer containing 10% goat serum overnight at +4°C. Primary antibody – anti-L-plastin (1/10 000, gift from M. Redd) or anti-GFP (1/500, MBL) or anti-GFP (1/500, BLM) – were added to the embryos at indicated concentration and incubated at +4C for 3 days while rocking. After PBST washes AlexaFluor 488 Goat anti-rabbit IgG antibody (Life Technologies, 1/1000) was added for 1 night at +4°C while rocking. After PBST washes embryos were mounted in 90% glycerol between glass slides prior imaging.

Morpholino oligonucleotide knockdown

Morpholino oligonucleotides (MO) were purchased from GeneTools. The following MOs at defined doses were used to block gene translation or splicing. MO dissolved in MO buffer (H_2O with KCl 12mM and HEPES 20mM) with phenol red were injected with micro-injector system (Tritech Research Inc.) into zebrafish embryo at 1-4 cell stage.

Name	5'-3' sequence	Type	Concentration	Reference
Adrb1	GGT AGC CCG TCT CCC ATG ATT TGG A	ATG	0.4mM	(Wang et al., 2009)
Adrb2a	GTA TTG AGG ACC TTA TGT TTC CCA T	ATG	0.8mM	(Wang et al., 2009)
Adrb2b	TCA GCG TAT TCT CTC CCT CCA TGA G	ATG	0.3mM	(Wang et al., 2009)
Adrb3a	TCA TGG TGT GCA GCT TTT CAA GGC A	ATG	0.4mM	*Designed for the study*
Adrb3b	GTT GGC GCT CAT CCT GAG AGG AAG C	ATG	0.3mM	(Wang et al., 2009)
TH1	CAC AGG TTA ACA GAC TTA CAT TTG A	Splice	1mM	(Reimer et al., 2013)
TH2	CTG TTG TTC ACT TAC AGG GTG ATC C	Splice	0.6mM	(Semenova et al., 2014)
TH2 bis	TTA TGC ATT GTA CGT ACG GTT CAG G	Splice	0.6mM	(Semenova et al., 2014)
FoxD3	CAC CGC GCA CTT TGC TGC TGG AGC A	ATG	0.5mM	(Stewart et al., 2006)

Pharmacological treatment

Embryos were manually dechorionated, transferred into 24-well-dish with 1 ml PTU Egg's water and soaked in the chemical compound until the evaluation. The compound was diluted in desired concentration in egg's water containing maximally 1% DMSO. The control embryos have been soaked in equivalent amount of DMSO as treated embryos. All used compounds, their final concentrations and producer are listed below.

Compound name	Producer	Target	Used concentration
GM6001	Milipore	Broad spectrum MMP inhibitor	200 µM
SB-3CT	Enzo	MMP-2 and 9 inhibitor	10 µM
Y27632	Tocris	ROCK inhibitor	50 µM
NSC23766	Tocris	Rac inhibitor	50 µM
DSP-4	Enzo	Adrenergic neurotoxin	40 µM
6OHDA	Sigma	Dopaminergic and adrenergic neurotoxin	200 µM
ICI 118551	Abcam	AdrB2 inhibitor	100 µM
Procaterol	Abcam	AdrB2 agonist	100 µM
SR 59230A	Sigma	AdrB3 inhibitor	30 µM
BRL 37344	Enzo	AdrB3 agonist	100 µM

Chemical macrophage depletion

Macrophages were depleted by injecting 5 nl of clodronate liposome (L-clodronate) suspension (clodronate concentration 5 mg/ml) into the caudal vein (gift from M. Daeron Laboratory) at 26 hpf. L-PBS was injected as a control. Embryos with L-clodronate aggregates causing vessel occlusions and shortcuts were discarded.

Genetic macrophage depletion

Metronidazole-mediated depletion was performed as described (Palha et al., 2013). Double transgenic fish *Tg(mpeg1:GAL4//UAS:NfsB-mCherry)* were crossed with *Tg(cd41:eGFP)* to evaluate the effect of macrophage depletion on cd41+ cells. Embryos were manually dechorionated and soaked with metronidazole 12mM in 0.1% DMSO/PTU Egg's water solution in dark from 18 hpf to evaluation, then rinsed with PTU Egg's water. *Tg(cd41:eGFP//mpeg1:mCherry*) embryos treated with 12mM metronidazole as well as *Tg(mpeg1:GAL4//UAS:NfsB-mCherry//cd41:eGFP)* treated with DMSO 0.1% were used as control.

In vivo zymography

In vivo zymography has been performed according to Pilgrim and Crawford (Crawford and Pilgrim, 2005). We decided to use gelatin as a substrate of proteolytic enzymes instead of collagen. Gelatin is an intermediate degradation product of collagen metabolism owning several advantages such as low molecular weight and easier degradation down to amino-acids. Highly quenched fluorescein labeled gelatin (Gelatin-FITC) was injected into the muscle between 4th and 5th somite counted from head of zebrafish transgenic embryos just prior the imaging. Embryos were immediately mounted in 0.7% LMP agarose and imaged at confocal microscope as describe above.

RNA extraction

30-35 embryos were treated using Rac and MMP-2 and 9 inhibitors or DMSO as previously mentioned, from 25 hpf and used at 48 hpf for RNA extraction. Embryos were manually transected to remove the tail and head regions. The zebrafish trunks were then lysed using Qiagen RLT solution with 1% 2-mercaptoethanol. RNA was extracted using a Qiagen RNeasy mini kit.

RT-qPCR

30-35 embryos were treated using Rac and MMP-2 and 9 inhibitors or DMSO as previously mentioned, from 25 hpf and used at 48 hpf for RNA extraction. Embryos were manually transected to remove the tail and head regions. The zebrafish trunks were then lysed using Qiagen RLT solution with 1% 2-mercaptoethanol. RNA was extracted using a Qiagen RNeasy mini kit. 2µg of mRNA was used for reverse transcription. QPCR were performed on a LightCycler® 480 system following the manufacturer's recommendations (SYBR Green format, Roche Applied Science, Meylan, France) and using primers listed in Table S2. Expression levels were determined using LightCycler analysis software from 5 independent experiments. The relative expression of specific genes in DMSO- treated or Rac inhibitor-treated embryos was indicated normalised to *ef1a* reference gene expression.

Zebrafish primer			
Gene	Accession	Name primer	Nucleotide sequence (5' → 3')
ef1a	ENSDARG00000020850	zEF1a.5	TTCTGTTACCTGGCAAAGGG
		zEF1a.3	TTCAGTTTGTCCAACACCCA
tnfa	NM_212859	zTNFa.54	TTCACGCTCCATAAGACCCA
		zTNFa.34	CCGTAGGATTCAGAAAAGCG
tnfb	NM_001024447.1	zTNFalp.51	CGAAGAAGGTCAGAAACCCA
		zTNFalp.3	GTTGGAATGCCTGATCCACA
il1b	NM_212844.2	zIL1b.5	TGGACTTCGCAGCACAAAATG
		zIL1b.3	GTTCACTTCACGCTCTTGGATG
il6	NM_001261449.1	zIL6.5	TGAAGACACTCAGAGACGAGCAGTT
		zIL6.3	AGGTTTGAGGAGAGGAGTGCTGAT
arg1	NM_001045197.1	ARG1 5.3	ACGGCCAGCCGATGTCTTAC
		ARG1 3.3	TCCACGTCTCGGAGTCCAAT
arg2	NM_199611.1	ARG2.5	GAAGCCGTTCCTGTCTGCCA
		ARG2.3	TCGGCCTTTGCTTCCTTGCC
tgfb1	ENSDARG00000041502	TGFb1a 5.3	CAACCGCTGGCTCTCATTTGA
		TGFb1a 3.3	ACAGTCGCAGTATAACCTCAGCT
mrc1a	XM_002662968	MRC1a.5	AGCTTGCGTGTACATCGACACA
		MRC1a.3	TGGCATCTGAGGTGGGTCTGT

Laser ablation

Manually dechorionated *Tg(NBT:dsREd)* and 0.016% tricaine anesthetised embryos at 26 hpf were mounted in 1% agar in concavity slides and neuron body was localised with Zeiss Axioplan 2 microscope equipped with a 40x water immersion objective. The neuron body was ablated using coumarin 440 nm, 5mM in methanol, as a laser medium. The ablation was performed on three following somites bilaterally in the zebrafish trunk. Embryos were then freed from agar and kept at 28°C in the PTU Egg's water until the imaging.

Catecholamines biochemical detection

The embryos at 30 h.p.f. were manually dechorionated and anesthetised with the cold Egg's water. The 200 embryos were decapitated using a pair of needles. The heads and the zebrafish bodies were snap-frozen separately. The 150 snap-frozen embryos were used to compare the whole organism with the peripheral part. The HPLC system consisted of an ESA liquid chromatography pump (ESA, Bedford, UK) coupled to an ESA Coulochem II detector (ESA, Chelmsford, USA) equipped with a 5014 high-performance analytic cell (ESA Bedford). The detector potential at the analytic cell was set at +0.4 V. HPLC analysis was performed on a C18 Spherisorb ODS2 Nucleosil HD reverse phase column (Macherey-Nagel EURL, France; 5 µm pore size, 4.6 mm internal diameter, 25 cm long). The mobile phase consisted of 0.1 M NaH2PO4, pH 3, containing 0.1 mM of EDTA, 1.7 mM 1-octane sulphonic acid sodium salt and 10% acetonitrile. The flow rate was 0.9 mL/min. Concentrations of NE were determined by comparison of chromatographic peak areas with calibration curves derived from authentic standards of NA, using data analysis software (Baseline 810, Waters).

Post-acquisition analysis

Cell enumeration

For the HSCs quantification in the AGM, 2 sets of z-stacks were acquired using the 20x air immersion objective and resolution of 1024x256 pixel with 1 µm z-interval. The maximum intensity projections were then used for the manual counting of cd41+ cells with the Fiji cell counter plugin. For HSCs quantification in the CHT, photos from fluorescent microscope Zeiss V12 were acquired and counted using the Cell counter plugin in Fiji.

3D view and colour-depth projection

3D volume view was performed either using Fiji plugin 3D view for confocal z-stacks with the size under 10GB or using Imaris 7 Software for more voluminous files or 3D animations. For colour-depth projection confocal stacks of membrane-labelled macrophages

were re-ordered to replace time over z-stack and then projected using temporal colour-code plugin with 6shades LUT.

Speed measurement and cell tracking graphs

Maximum intensity projections of 60 minute time-lapses acquired every minute were analysed using a manual tracking plugin in Fiji. Measured data were transferred into a Chemotaxis and Migration tool programme (Ibidi) to design tracking and rose plots. A rose diagram maps single counts of the position of every macrophage in a selected area (black and grey sectors of angle $\pi/18$) every minute over 60 minutes with an (x,y 0,0) starting point. The tracking plot diagram represents the migration path and distance of macrophages in the AGM with an x,y 0,0 starting point, being measured every minute over 60 minutes. The average of single macrophage velocities ($\mu m\ min^{-1}$) during 15-60 minutes were used for analysis. The evaluation of the directionality was performed using a Rayleigh statistical test for the uniformity of a circular distribution of points (end points of single macrophages). All analyses were conducted using the Chemotaxis and Migration tool software (Ibidi).

Shape analysis

Confocal stacks of membrane-labelled macrophages were projected using a maximum intensity projection and 2D images were binarised using an automatic threshold. The following shape descriptors were evaluated using the Fiji plugin Particle analysis: area (μm^2), perimeter (μm), circularity and roundness. The elongation factor was manually measured by dividing the longest axis of the object by its longest perpendicular axis (x/y). Objects with an area under 80 μm^2 were excluded from the further analysis. Circularity was calculated using the following formula: 4π x (area/perimeter^2). This parameter varied from 0 (linear polygon) to 1 (perfect circle). Circularity was used to set apart round objects (circularity > 0.2) and roundness and elongation factor enabled us to break down non-round subjects into 3 subgroups: elongated, amoeboid and star-like shaped. Roundness was calculated using the following formula: 4 x {area/ [π x (major axis)^2]} and varied from 0 (linear polygon) to 1 (perfect round).

Shape dynamics analysis

Time-lapse confocal acquisitions of membrane-labelled macrophages (*Tg(mpeg1:mCherry)*) were projected using a maximum intensity projection and every 5th stack (every 5 minutes) was binarised using an automatic threshold. Then the same shape descriptors were evaluated as previously for each macrophage present in the acquired area for more than 20 minutes. For each analysed time frame the shape category was attributed to the followed macrophage and the shape dynamics was demonstrated as shape category over time evolution. The statistical analysis of the dynamics were performed by quantifying the number of adopted morphologic categories and by quantifying the number of changes between the distinct categories.

Statistical analysis

Normal distributions were analysed by the Shapiro-Wilk test. Non-gaussian data were analysed with a Wilcoxon or Kruskal-Wallis test, Gaussian with student t-test or ANOVA followed by Holm's multiple comparison. $P<0.05$ was considered as statistically significant (symbols: **** $p<0.0001$; *** $p<0.001$; ** $p<0.01$, * $p<0.05$) Statistical analysis were performed using R software with data transferred from excel file.

AIM OF THE THESIS

Chapter 3: Aim of the thesis

HSCs are generated during the embryonic development and give rise to all blood cells for the whole life of the organism. During the definitive wave of embryonic haematopoiesis HSCs emerge from the haemogenic endothelium on the ventral side of the dorsal aorta by a trans-differentiation called endothelial to haematopoietic transition. This process is conserved in all vertebrates. The cellular origin of HSCs was elucidated in recent years *ex vivo* and *in vivo*. In all vertebrate species, it has been demonstrated that HSCs are generated from the haemogenic endothelium, which is the common bi-potential progenitor of endothelial and haematopoietic stem cells.

HSC production relies on the specific signalling at precise time. Several pathways were described to play a role during the transition from the haemangioblast through haemogenic endothelium to HSCs including BMP4, WNT, SOX17 and NOTCH which all control the initiation of the EHT. In addition to the time specific signalling, the spatial restriction of their expression was shown to be important. These findings suggest that deciphering the composition of the AGM and surrounding tissues may help to our understanding of control of HSC emergence. While the studies of the bone marrow revealed a complex regulation of the haematopoiesis by the microenvironment surrounding the HSCs, the role of the environment in the AGM remained less characterised.

The microenvironment of the aorta during definitive haematopoiesis represents the principal focus of my PhD work. I used the zebrafish embryo to identify and describe the cells presents in the AGM and their role. The zebrafish embryo possesses several characteristics which makes it appropriate model for the microenvironment study. Its transparency, fluorescent transgenic lines and external development permit the live real-time non-invasive imaging and analysis of reciprocal cell interaction. The zebrafish AGM contains several cell populations (**Figure 28**).

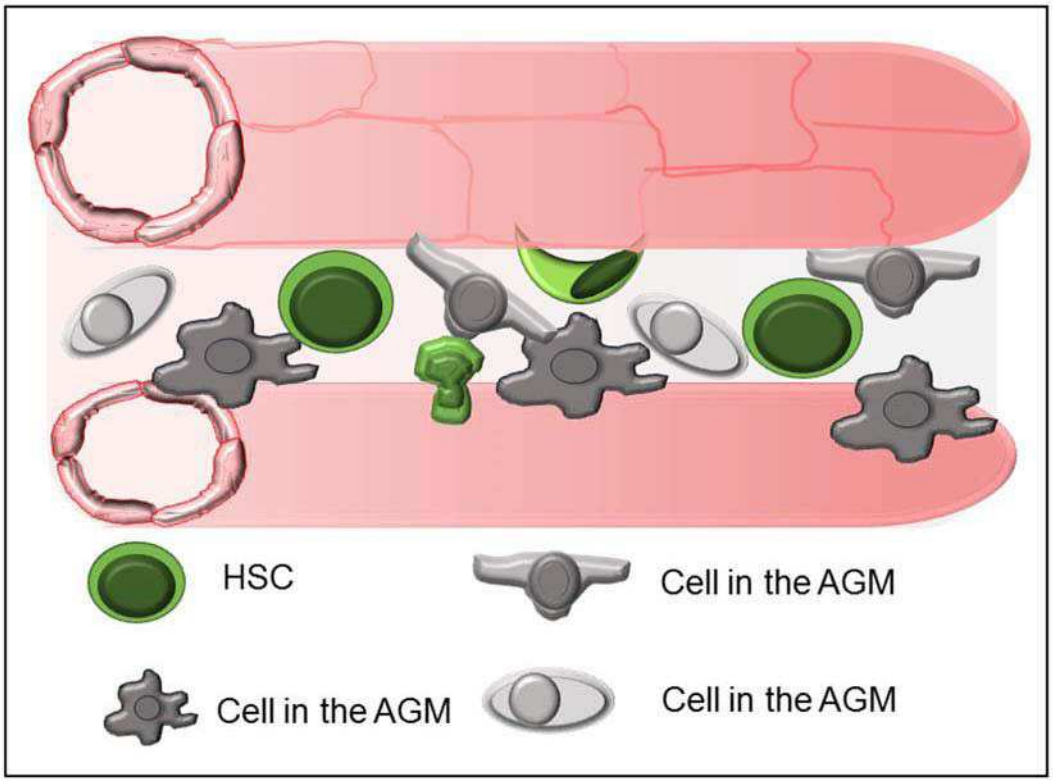

Figure 28 – AGM haematopoietic environment:
Drawing shows the heterogeneous cell composition of the AGM during definitive haematopoiesis in the zebrafish embryo. The thesis objective is to identify and characterise these cell populations and evaluate their role.

During my thesis I have described and characterised cell populations found at the vicinity of the dorsal aorta or nascent HSCs. The results are presented in 3 main parts completed with an appendix chapter.

Part 1 describes the macrophages - first cell population that we characterised in the AGM – and their contribution to the establishment of definitive haematopoiesis. We show the substantial role of the macrophages in particular step during haematopoiesis, in the migration of HSPCs to the haematopoietic organs.

Part 2 contains the direct continuation of the story introduced in the part 1. It describes the morphology and migration of macrophages in the AGM, shows their behaviour and the factors influencing the migration and morphology. We demonstrate for the first time an *in vivo* mesenchymal migration of macrophages in the zebrafish embryo and its dependence on rac and Mmp signalling.

Part 3 presents the sympathetic nervous system, specifically the catecholamine synthesising cells which control the first steps of EHT in the zebrafish embryo. We show that

catecholamine activation of adrenergic beta receptors, Adrb2b and Adrb3 initiates HSC emergence. Moreover, we propose that the local innervation is not required for the receptor activation.

The appendix contains the work performed in collaboration with another group, and where I was involved in the description of macrophages. We show that zebrafish macrophages polarise toward a pro-inflammatory or regulatory phenotype in the response to the environment. The concept of macrophage polarisation has been profoundly described in the mammalian macrophages but remained unresolved in lower vertebrates.

RESULTS

Chapter 4: Results

1. Primitive macrophages and their impact on definitive haematopoiesis

1.1. Article 1: Primitive macrophages control HSPC mobilisation and definitive haematopoiesis

Primitive macrophages control HSPC mobilisation and definitive haematopoiesis

Jana Travnickova*, Vanessa Tran Chau*, Emmanuelle Julien, Julio Mateos-Langerak, Catherine Gonzalez, Georges Lutfalla, Manuela Tavian and Karima Kissa

* The authors contributed equally to this work

Nature Communications, 2015, 6:6227, DOI: 10.1038/ncomms7227

Graphical abstract:

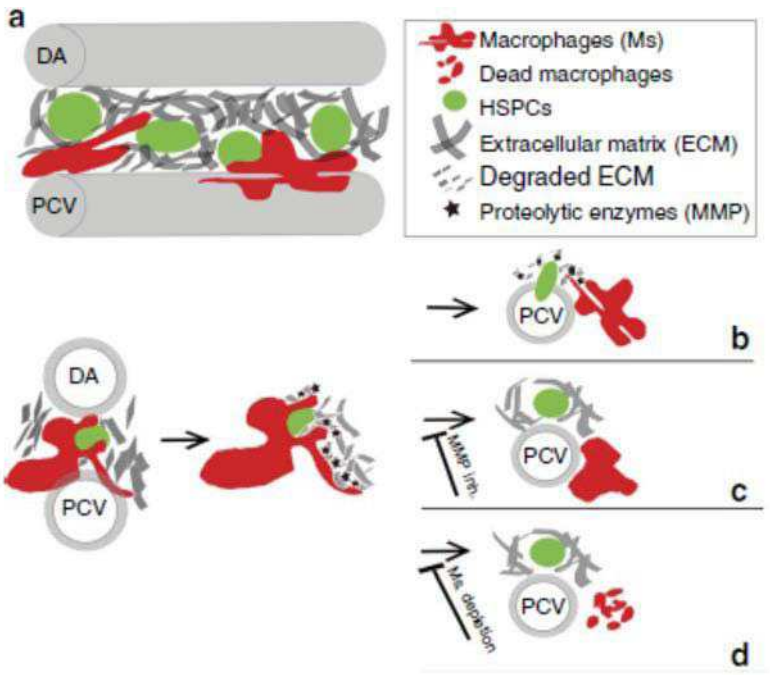

Key points:

- Macrophages interact with HSPCs in the AGM during haematopoiesis
- Macrophage depletion impairs the haematopoietic organ colonisation
- Macrophages produce and secrete Mmp-9 whose inhibition mimics the phenotype of macrophage depletion
- Macrophages degrade the ECM around the HSPCs through the Mmp-9 secretion

nature COMMUNICATIONS

ARTICLE

Received 23 Jul 2014 | Accepted 7 Jan 2015 | Published 17 Feb 2015

DOI: 10.1038/ncomms7227

Primitive macrophages control HSPC mobilization and definitive haematopoiesis

Jana Travnickova[1,2,3,*], Vanessa Tran Chau[1,2,3,4,5,*], Emmanuelle Julien[6,7,8], Julio Mateos-Langerak[9], Catherine Gonzalez[1,2,3], Etienne Lelièvre[1,2,3,10], Georges Lutfalla[1,2,3], Manuela Tavian[6,7,8] & Karima Kissa[1,2,3,10]

In vertebrates, haematopoietic stem/progenitor cells (HSPCs) first emerge in the aorta–gonad–mesonephros (AGM) before colonizing transitory and subsequently definitive haematopoietic organs allowing haematopoiesis throughout adult life. Here we identify an unexpected primitive macrophage population accumulated in the dorsal mesenteric mesoderm surrounding the dorsal aorta of the human embryo and study its function in the transparent zebrafish embryo. Our study reveals dynamic interactions occurring between the HSPCs and primitive macrophages in the AGM. Specific chemical and inducible genetic depletion of macrophages or inhibition of matrix metalloproteinases (Mmps) leads to an accumulation of HSPCs in the AGM and a decrease in the colonization of haematopoietic organs. Finally, in vivo zymography demonstrates the function of primitive macrophages in extracellular matrix degradation, which allows HSPC migration through the AGM stroma, their intravasation, leading to the colonization of haematopoietic organs and the establishment of definitive haematopoiesis.

[1] CNRS UMR 5235, F-34095 Montpellier, France. [2] Universite Montpellier 2, Dynamique des Interactions Membranaires Normales et Pathologiques, F-34095 Montpellier, France. [3] Universite Montpellier 1, F-34000 Montpellier, France. [4] Institut Pasteur, Unité Macrophages et Développement de l'Immunité, Département de Biologie du Développement, F-75015 Paris, France. [5] CNRS, URA2578, F-75015 Paris, France. [6] INSERM UMR_S949, F-67000 Strasbourg, France. [7] Universite de Strasbourg, F-67000 Strasbourg, France. [8] Etablissement Français du Sang-Alsace, F-67000 Strasbourg, France. [9] Montpellier RIO Imaging, F-34396 Montpellier, France. [10] INSERM, DIMNP, F-34095 Montpellier, France. * These authors contributed equally to this work. Correspondence and requests for materials should be addressed to K.K. (email: karima.kissa@univ-montp2.fr).

Blood cells are continuously produced from self-renewing progenitors with multi-lineage differentiation potential, called haematopoietic stem/progenitor cells (HSPCs). In vertebrates, haematopoiesis occurs as two waves. The 'primitive' wave produces only myelo-erythroid cells, whereas the 'definitive' wave gives rise to HSPCs[1–4]. In zebrafish, from 16 hours post fertilization (h.p.f.), primitive haematopoietic cells produce macrophages and neutrophils that initiate innate immunity[5–7]. Zebrafish first HSPCs appear in the aorta–gonad–mesonephros (AGM), between the dorsal aorta (DA) and the posterior cardinal vein (PCV) by 30 h.p.f. (refs 3,8) where they start to express cd41 marker[9]. These HSPCs originate from aortic endothelial cells[10,11] through a process called endothelial haematopoietic transition or EHT[11]. Live imaging of mouse embryo sections[12], cell sorting and differentiation experiments in human embryo have shown haemogenic endothelial cells to be at the immediate origin of haematopoietic cell clusters sprouting from the ventral side of the aorta[13], which suggest that this process is conserved throughout evolution. We have previously documented that zebrafish HSPCs migrate from the AGM, enter the circulation and colonize the caudal haematopoietic tissue (CHT), analogous to the mammalian fetal liver. There they proliferate before colonizing the definitive haematopoietic organs, thymus and kidney[9]. HSPCs emerging between 30 and 55 h.p.f. give rise to all mature blood cell populations, including the second wave of macrophages.

Macrophages from the first and second waves of haematopoiesis play important roles in development, tissue homeostasis[14], innate and adaptive immunity and wound healing. In adults, they are also involved in the pathologies including chronic diseases[15] and cancer metastasis[16,17].

Macrophage-related processes are associated with their ability to migrate throughout the body and remodel surrounding stroma[18] by degrading the extracellular matrix (ECM) via the secretion of matrix metalloproteinases (MMPs for human and Mmps for zebrafish) and cathepsins[19]. MMPs have been shown to play important roles in tissue remodelling, or pathological processes[20], especially MMP-2, 9 and 13. In zebrafish embryos, Mmp-9 and 13a are expressed by myeloid cells from 19 h.p.f. (refs 21,22).

In this study, we imaged the accumulation of primitive macrophages in the AGM of both human and zebrafish embryos and analysed their interactions with emerging HSPCs. We demonstrated that primitive macrophages play a major role in the establishment of definitive haematopoiesis by permitting HSPC mobilization and colonization of haematopoietic organs via Mmps secretion and ECM remodelling.

Results

Macrophages accumulate in AGM during HSPC emergence. Human HSPCs emerge between the 27th and the 40th day of development in the AGM as clusters of CD34 þ CD45 þ cells adhering to the ventral wall of the DA[23]. Immunohistochemistry in human embryos at 34 days of development (n ¼ 2) showed an intriguing accumulation of CD68 þ macrophages in the mesenchyme beneath the ventral part of the CD34 þ aortic endothelium (Fig. 1a–a^{00}, b–b^{00}) and in the HSPC containing intra-aortic clusters (Fig. 1b^{0},b^{00}). The number of macrophages in these locations, increased between 26 and 37 days of gestation, that is, in concomitance with the emergence of HSPCs (Supplementary Fig. 1; n ¼ 3).

We took advantage of zebrafish embryo remarkable optical properties to study the possible role of these macrophages during definitive haematopoiesis.

In vivo imaging of Tg(cd41:eGFP//mpeg1:mCherry) zebrafish embryos at 43 h.p.f. (green HSPCs and red macrophages) showed a similar accumulation of primitive macrophages along the entire length of the trunk in the direct vicinity of the ventral wall of the DA (Fig. 1c).

Macrophage quantification confirmed their tissue-restricted accumulation in zebrafish AGM compared to surrounding tissues (Fig. 1d, n ¼ 20). Interestingly, this accumulation was concomitant with HSPC/cd41:eGFP þ emergence in the AGM between 30 and 55 h.p.f. (ref. 11).

Macrophages actively patrol in the AGM. To assess if macrophages play a role in HSPC emergence, we imaged the behaviour of HSPCs and macrophages in Tg(cd41:eGFP//mpeg1:mCherry) zebrafish embryos at 43 h.p.f. (Fig. 1e–l). As previously described, endothelial cells from the ventral wall of the aorta first bend then egress into the subaortic space to become free HSPCs[11]. At this stage, we observed that macrophages (Fig. 1f) continuously patrolled between the DA and the PCV, and intimately interacted with emerging HSPCs/cd41:eGFP þ (Fig. 1e–l, Supplementary Movies 1 and 2). Live imaging of Tg(cd41:eGFP//mpeg1:mCherry) zebrafish embryo at 55 h.p.f. showed a macrophage/mpeg1:mCherry þ migrating in the AGM around an HSPC/cd41:eGFP þ during 32 min, before joining the PCV (Supplementary Movie 2, time code 00:56 to 1:00). This HSPC/cd41:eGFP þ would then join the PCV following the same route (Supplementary Movie 2). A quantification of 112 HSPCs/cd41:eGFP þ (from 12 embryos) in the AGM revealed that 95.6% of them directly interacted with macrophages suggesting that macrophages could play an important role in emergence of HSPCs in the AGM.

Figure 1 | Accumulation of macrophages in the AGM at the onset of definitive haematopoiesis. (a–b^{00}) Immunostained transverse sections of AGM region in 34-day human embryos (n ¼ 2). (a,a^{0}, b,b^{00}) CD34 labels position of aortic endothelium (arrowhead) and HSPCs (a^{0}, asterisks and arrows). (a^{0}–a^{0}) Higher magnification of a, black box. CD68 stains macrophages (a^{00},b^{0}, arrow). (b^{00}) Higher magnification of b, white box. Double CD34/CD68 immunofluorescence shows accumulation of macrophages (arrow and empty arrow), respectively, in the ventral wall of the DA and in HSPCs intra-aortic clusters (red arrow). (c) Maximum projection of confocal z-stack acquisitions in a Tg(cd41:eGFP//mpeg1:mCherry) zebrafish embryo at 43 h.p.f. (10 mm depth); bright field is merged with green and red fluorescence. HSPCs/cd41:eGFP þ (arrow) and macrophages/mpeg1:mCherry (arrowhead) accumulate between the DA and the PCV. (d) Graph representing the specific accumulation of macrophages in the AGM during EHT compared with macrophages present in the intersomitic vessels and in pronephric ducts area. Data are shown as average ±s.e.m, n ¼ 20 (from two independent experiments). P values are calculated for the difference between AGM and both intersomitic vessels and pronephric duct area at 40, 45 and 50 h.p.f. and for the difference of macrophage number in the AGM between 30 and 40 h.p.f. (underlined asterisks). *** Po0.001 (Kruskal–Wallis test for the whole evaluation and Student's t-test followed by Holm's multiple comparison for individual stages). (e–l) Time-lapse confocal imaging of Tg(cd41:eGFP//mpeg1:mCherry) zebrafish embryo at 43 h.p.f. (higher magnification of c, black box). (f–j) A macrophage (arrowhead) actively patrols in the AGM around a HSPC/cd41:eGFP þ (arrow) for 20 min, before heading toward another HSPC/cd41:eGFP þ (k,l). CV, cardinal vein; DA, dorsal aorta; ISV, intersomitic vessels; Mn, mesonephros; Nc, notochord; NT, neural tube; PCV, posterior cardinal vein; Pd, pronephric ducts; Ye, yolk extension. Scale bars, 50 mm (a,b^{0},b^{00}), 25 mm (a^{0},a^{00},c,e–l), and 100 mm (b). See also Supplementary Fig. 1 and Supplementary Movies 1 and 2.

Macrophages are essential for definitive haematopoiesis. To characterize their role in HSPC emergence, we chemically and genetically depleted primitive macrophages before or during definitive haematopoiesis at 25 and 45 h.p.f., respectively (before maturation of the second wave of macrophages).

Liposome encapsulated clodronate (L-clodronate) has been widely used to specifically induce the death of phagocytic macrophages in vitro and in vivo in mice and recently in zebrafish[24,25]. We first set about testing its efficiency, toxicity and specificity. Injection of 5 nl of L-clodronate stock suspension into the vein was sufficient for thorough macrophage depletion in embryos between 25 and 96 h.p.f. (Supplementary Fig. 2b, n ¼ 200), compared with control embryos injected with PBS liposomes (L-PBS; Supplementary Fig. 2a, white arrows, n ¼ 25). The fate of macrophages in the AGM and in the CHT was examined during 18 h after L-clodronate injection. This

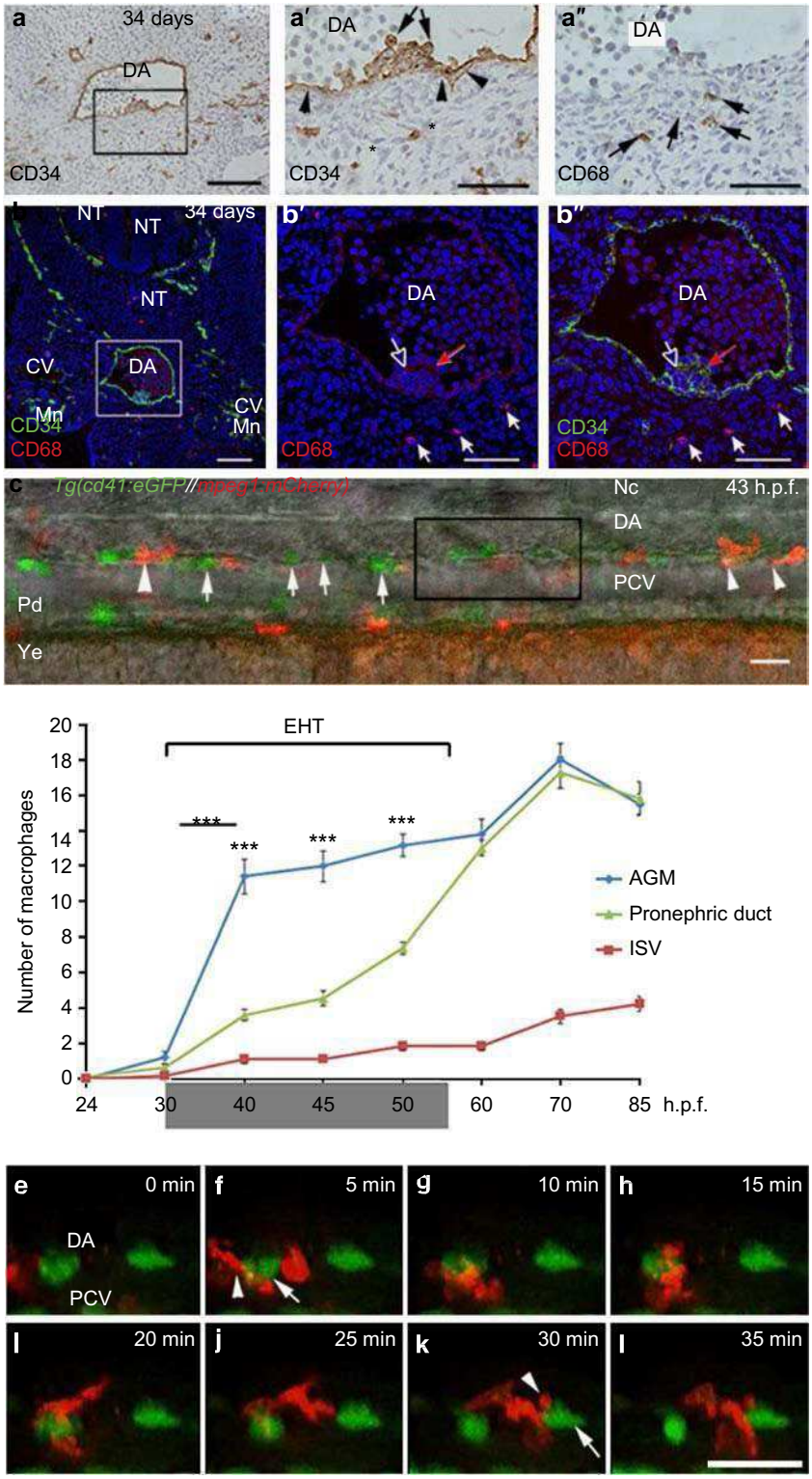

revealed the steady decrease to complete disappearance of macrophages while passing through vacuolization and fragmentation (Supplementary Fig. 2g). No toxic effect was noticed on blood vessel organization (Supplementary Fig. 2c,d, Tg(kdrl:caax:mCherry), n ¼ 15) nor on the evolution (Supplementary Fig. 2h), differentiation and function of primitive wave neutrophils[5], the other myeloid cell population present in the embryo at this stage of development (Supplementary Fig. 2e,f, arrow, Tg(mpx:eGFP), n ¼ 35).

To evaluate the effect of macrophage depletion on HSPC emergence (Fig. 2a–d), we injected L-clodronate in Tg(cd41:eGFP) embryos at 25 h.p.f. and observed that macrophage depletion did not prevent HSPCs/cd41:eGFP þ emergence in the AGM (Fig. 2b versus a), but led instead to their accumulation at 48 h.p.f. (Fig. 2n, þ 60%, n ¼ 20). Whole-mount in situ hybridization (WISH) of c-myb confirmed the unaffected HSPC emergence in the AGM (Fig. 2d versus c). By contrast, macrophage depletion led to a very substantial decrease in the number of HSPCs/cd41:eGFP þ colonizing the CHT (Fig. 2g,h versus e,f and n; – 89%, n ¼ 28) and the thymus at 72 h.p.f. (Fig. 2l, versus k and n; – 91%, n ¼ 28), while injecting L-clodronate at 45 h.p.f. (Fig. 2i) caused less marked effects (– 72% in CHT: Fig. 2j,n, n ¼ 28; and – 50% in the thymus: Fig. 2m,n, n ¼ 22). The partial colonization observed after late L-clodronate injections was likely due to HSPCs that had already left the AGM before macrophage depletion. It further proved that L-clodronate was not toxic for HSPCs (Fig. 2j).

To fully validate the effect of macrophage depletion on haematopoietic organ colonization, we set inducible nitroreductase genetic depletion of macrophages[26] as an alternate

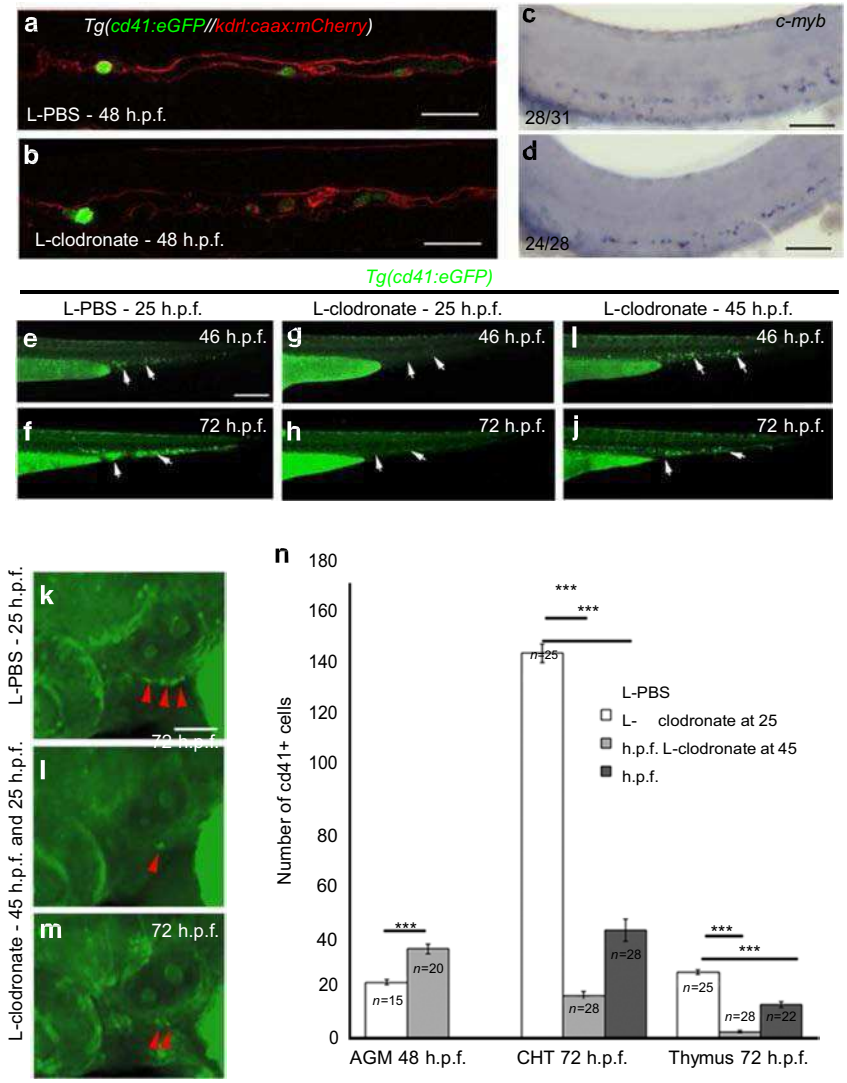

Figure 2 | Depletion of primitive macrophages reduces CHT and thymus colonization. (a,b) Macrophage depletion by L-clodronate injection at 25 h.p.f. does not affect HSPC/cd41:eGFP þ emergence in the AGM (48 h.p.f.). (c–d) WISH of c-myb shows normal HSPC emergence in the AGM after macrophage depletion (N ¼ 21±0.72, n ¼ 15) compared with control embryos (N ¼ 14.9±0.51, n ¼ 15; Po0.001; Wilcoxon test). N stands for the number of c-myb cells per embryo, n for the number of embryos. (e–m) Macrophage depletion by L-clodronate injection at 25 or 45 h.p.f. decreases HSPC/cd41:eGFP colonization at 46 and 72 h.p.f. of the CHT (g–j, white arrow) and thymus (l–m, red arrowhead) compared with control injected with L-PBS (e,f,k). (n) Macrophage depletion by L-clodronate injection at 25 h.p.f. causes HSPC/cd41:eGFP þ accumulation in the AGM at 48 h.p.f. (left column, þ 60%), while injection at 25 or 45 h.p.f. substantially reduces HSPC/cd41:eGFP þ colonization of the CHT at 72 h.p.f. (- 89 and - 72%, respectively) and thymus colonization at 72 h.p.f. (- 91 and - 50%, respectively) compared with the control injected with L-PBS. Data are shown as average ±s.e.m. *** Po0.001 (Wilcoxon test), n ¼ number of embryos of minimal three independent experiments. Scale bars, 30 mm (a,b), 100 mm (c,d, k–m) and 250 mm (e–j). See also Supplementary Fig. 2.

experimental approach. Expression of E.coli nitroreductase under the control of mpeg1 promoter allows the inducible tissue specific and reversible depletion of macrophages by soaking embryos in the prodrug metronidazole. Similar to L-clodronate, metronidazole macrophage depleted embryos (Fig. 3b versus a) exhibited an impaired CHT colonization by HSPCs/cd41:eGFP þ (Fig. 3b^0 versus a^0, – 68% at 60 h.p.f., Fig. 3c, n ¼ 24) as well as an accumulation of HSPCs/cd41:eGFP in the AGM (Supplementary Fig. 3a, þ 71% at 60 h.p.f., n ¼ 11). Macrophages still present after 42 h of metronidazole treatment (Fig. 3b) result either from partial depletion or delayed depletion or both and most likely explain the partial CHT colonization by HSPC compared with embryos injected with L-clodronate (Fig. 3b^0 and Fig. 2g,h).

As the genetic depletion is reversible by removing metronidazole from the medium, we measured macrophage reappearance during the 2 days following prodrug withdrawal (Fig. 3d–g) and its effect on haematopoiesis in the CHT (Fig. 3d,e^0,f^0,g^0). Indeed the number of HSPCs/cd41:eGFP þ accumulated in the CHT was directly correlated with both the reappearance of macrophages in embryos (Fig. 3d and Supplementary Fig. 3b) and the decrease of the HSPCs/cd41:eGFP accumulation in the AGM (Supplementary Fig. 3a).

Altogether these results demonstrated the crucial role of macrophages in haematopoietic organ colonization.

Mmps allow HSPC intravasation then organ colonization. Various proteases, especially MMP-2 and -9 that share high similarity in protein sequence with their zebrafish orthologs (90 and 73%, respectively)[21,27] have been shown to be associated with ECM degradation and cell intravasation mediated by

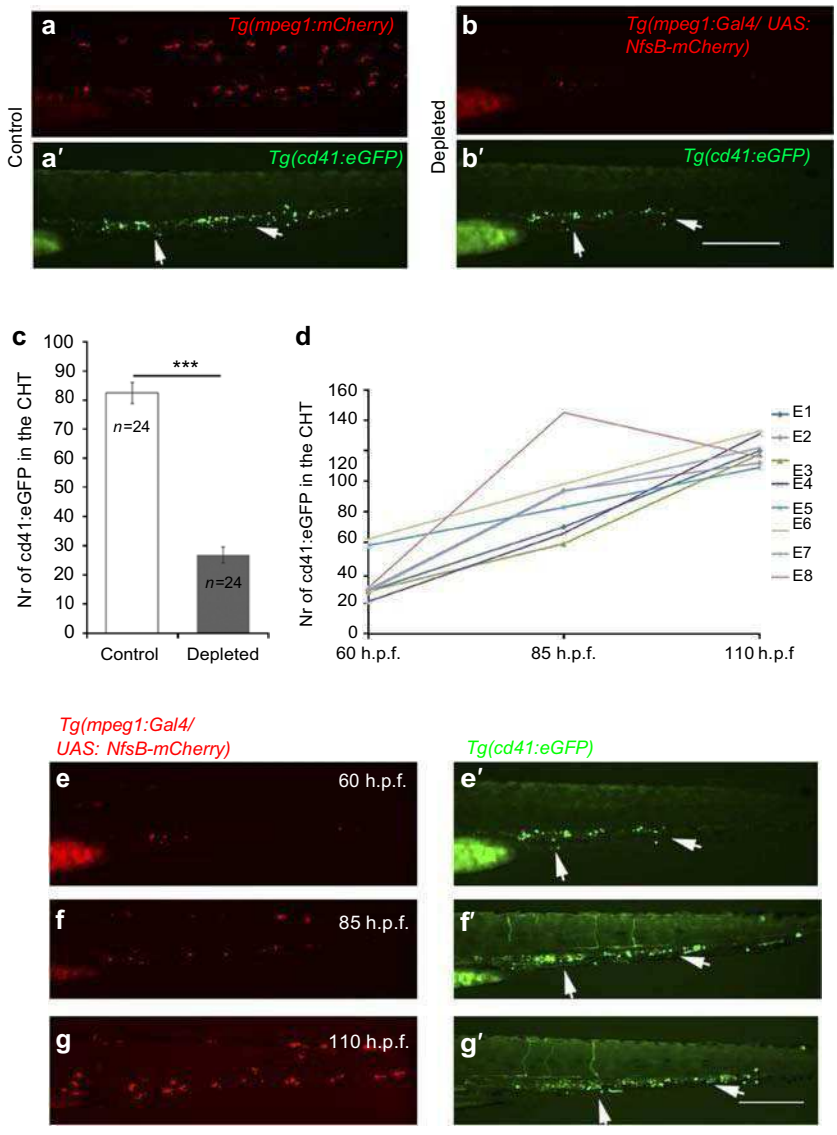

Figure 3 | Rescue of CHT colonization after macrophage reappearance. (a,b^0) Metronidazole induced depletion of macrophages (a,b) results in the decrease of CHT colonization (a^0,b^0). (c) Metronidazole induced macrophage depletion substantially reduces HSPC/cd41:eGFPþ colonization of the CHT (–68%) at 60 h.p.f. compared with the control Tg(cd41:eGFP//mpeg1:mCherry) embryos treated with metronidazole. Data are shown as average ±s.e.m. *** Po0.001 (Wilcoxon test), n ¼ number of embryos of minimal three independent experiments. (d) Rescue of CHT colonization is held due to metronidazole withdrawal at 60 h.p.f. Graph represents number of HSPCs/cd41:eGFPþ accumulated in the CHT at 60, 85 and 110 h.p.f. Data are shown as longitudinal study of single embryo, n ¼ 8. (e–g) Reappearance of macrophages is detected after the metronidazole wash-out during the following 2 days (25 (f) and 50 h post withdrawal (g)). The increasing number of HSPCs/cd41:eGFPþ accumulated in CHT (e^0–g^0) is directly connected to reappearance of macrophages in the embryo (e–g). Scale bar, 250 mm. See also Supplementary Fig. 3.

macrophages. To study the role of MMPs, Tg(cd41:eGFP) embryos were soaked from 38 h.p.f. in two different MMP inhibitors; GM6001, a general MMP inhibitor[28] or SB-3CT, a specific inhibitor of MMP-2 and 9 (Gelatinases A and B)[29]. This inhibition resulted in HSPCs/cd41:eGFP þ accumulation in the AGM at 60 h.p.f. (Fig. 4e,f and Supplementary Fig. 4d, þ 26% and þ 51% for GM6001 and SB-3CT respectively) compared with control embryos (Fig. 4d), while it led to a consequent decrease in HSPCs/cd41:eGFP colonization of the CHT at 60 h.p.f. (Fig. 4a–c; – 43 and -66% respectively, Supplementary Fig. 4d, n ¼ 42 and n ¼ 44) and the thymus at 72 h.p.f. (Supplementary Fig. 4a–d, -44 and -75%; respectively, n ¼ 30 and 29).

We thus concluded that both primitive macrophages and Mmps secretion are essential for HSPC mobilization and consequently haematopoietic organ colonization.

Mmp-9 and mmp-13a are expressed by macrophages. To establish a direct connection between macrophages and mmps expression in the AGM, we combined L-plastin immunostaining (a leukocyte marker) with WISH of 48 h.p.f. embryos using mmp-2, mmp-9 and mmp-13a probes. Mmp-9 and -13a expression patterns (Fig. 4g–j) matched to myeloid cells (Fig. 4g^0–h^{00}, n ¼ 10) but not mmp-2 expression (Supplementary Fig. 4e,f, n ¼ 10), which gave a broader pattern in the trunk region (Supplementary Fig. 4e–e^{00}).

As L-plastin is expressed by different myeloid populations, we analysed mmps expression in embryos injected with L-clodronate. We observed in the AGM that mmp-2 expression profile (Supplementary Fig. 4g,g^0) was unchanged after macrophage depletion while mmp-13a (Figs 4l,l^0) was significantly reduced and mmp-9 completely disappeared (Fig. 4k,k^0).

We concluded that macrophages expressing mmp-9 are unambiguously associated with HSPC mobilization and intravasation.

Macrophage-mediated ECM degradation. WISH showed that mmp-9 is expressed by primitive macrophages, but no direct demonstration was made of macrophage-mediated matrix degradation. We therefore decided to visualize matrix degradation by in vivo zymography[30] using gelatin as an intermediate product of collagen degradation. We injected highly quenched fluorescein-labelled gelatin (Gelatin-FITC) into the muscles of Tg(mpeg1:mCherry) embryos (Fig. 5a, n ¼ 10). Degradation of this substrate releases FITC from its quencher resulting in green fluorescence. Specific punctiform green fluorescence was observed around spherical cells that appeared as unlabelled ghosts (Fig. 5b,c, blue dots and arrow), while embryos soaked in MMP inhibitors did not show any FITC signal fluorescence (Supplementary Fig. 5a–c, middle and right, Supplementary Movie 5) nor did L-clodronate injected embryos (Supplementary Fig. 5d,e). Time-lapse imaging showed co-localization of macrophage trails and emitted FITC fluorescence (Fig. 5c^0–f, j–m, Supplementary Movies 3–4 and Supplementary Fig. 5f, n ¼ 3, 79% of liberated FITC was correlated to macrophages). Figure 5i provides a schematic diagram of a macrophage migrating around the HSPC and leaving a trail of degraded gelatin (Fig. 5c^0 –h, Supplementary Movie 3), followed by the migration and intravasation of a round cell between two spots of degraded gelatin (Fig. 5f–h, arrow; Supplementary Movie 3). To confirm

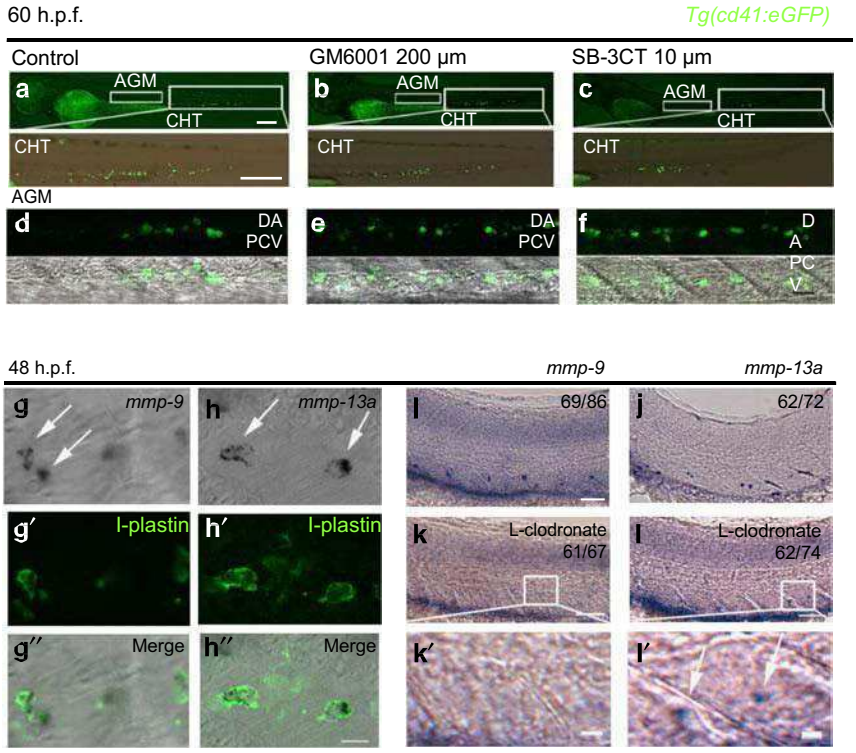

Figure 4 | Role of MMPs in HSPC mobilization and colonization of the CHT. (a–f) Inhibition of MMPs impairs HSPC mobilization and the colonization of CHT. (a) HSPCs are present in Tg(cd41:eGFP) embryo at 60 h.p.f. (bottom, enlarged CHT). Small box shows the AGM imaged by confocal microscopy in d. (d) Green fluorescence shows the presence of cd41:eGFP cells in the AGM at 60 h.p.f. (bottom, merged with transmission channel). (b,c) Treatment with GM6001 (b, n ¼ 42) or SB-3CT (c, n ¼ 44) reduces CHT colonization by HSPCs/cd41:eGFP þ cells compared with control (a, n ¼ 45). (e,f) Confocal imaging of the AGM reveals accumulation of HSPCs/cd41:eGFP þ cells in AGM compared with the control (d) (d–f, n ¼ 23; three frames combined). Confocal imaging of WISH (g,h, arrows) combined with L-plastin immunofluorescence (green) (g^0,h^0) are merged in g^{00} and h^{00}. (i–l) WISH of mmp-9 (i) and mmp-13a (j) in the AGM in control embryos and after macrophage depletion by L-clodronate (k,l). Close-ups of macrophage depleted embryos in k^0,l^0 (arrow). Scale bar, 250 mm (a–c), 30 mm (d–f), 50 mm (i–l), 10 mm (g,h^{00}, k^0,l^0). See also Supplementary Fig. 4.

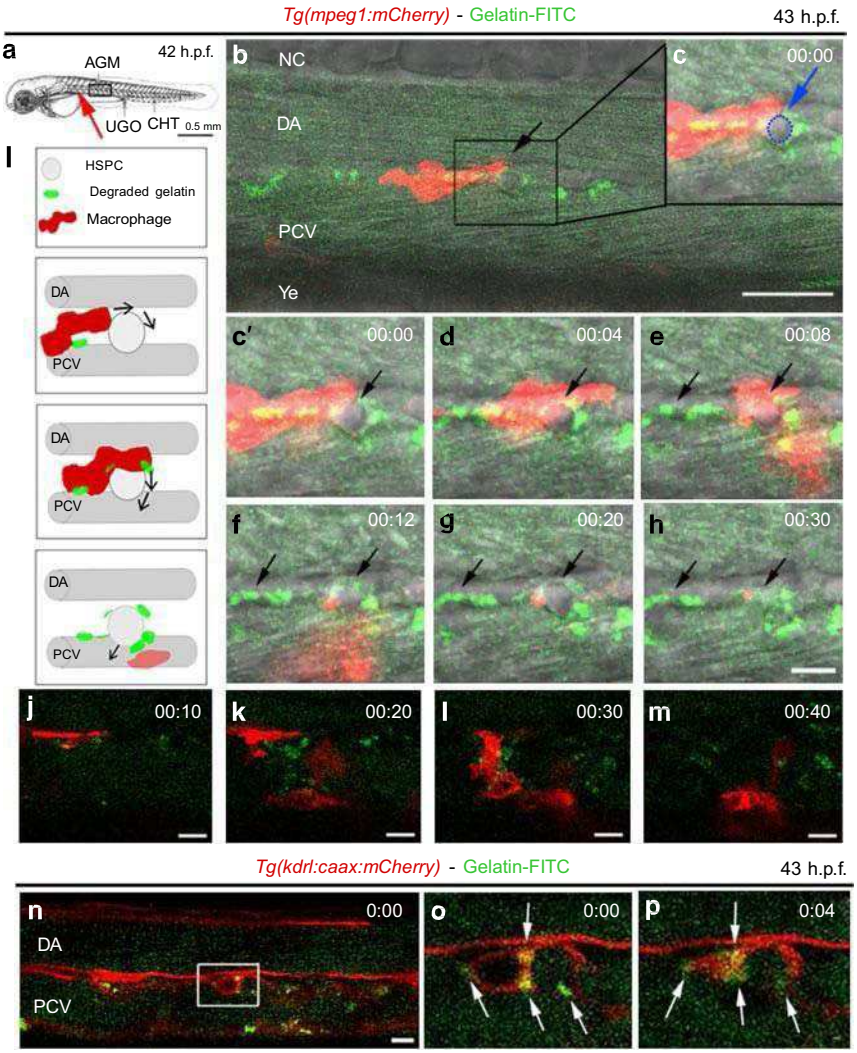

Figure 5 | In vivo zymography shows macrophage-induced proteolysis of the ECM. (a) Drawing indicates the site of intramuscular injection of Gelatin-FITC (red arrow) and the area imaged in b (black box). (b–h) In vivo imaging of the AGM at 43 h.p.f. was carried out just after gelatin-FITC injection in Tg(mpeg1:mCherry). Green staining indicates gelatin degradation after macrophage migration (red) in c–h (n¼10). (c–h) Close-ups (b, black box) show a patrolling macrophage (red) that degrades gelatin (green dots), induces HSPC migration through the ECM (arrow), followed by intravasation (Supplementary movie 3). (c) Arrow shows unlabelled round cells corresponding to HSPCs (blue dots). (i) Schematic view of gelatin degradation by a red macrophage around a light gray HSPC in the AGM. First diagram shows macrophage migration around an HSPC. Macrophage migration results in green spots corresponding to gelatin degradation, followed by HSPC intravasation (f–h, Supplementary Movie 3). (j–m) Zoomed imaging shows two macrophages in the AGM-degrading Gelatin-FITC during their passage (Supplementary Movie 4). (n) Gelatin degradation is localized around an emerging HSPC/mCherry þ cell after injection of gelatin-FITC in a Tg(kdrl:caax:mCherry) embryo. (o,p) Close-ups of emerging HSPC/mCherry þ intravasation in the vein (inset, n) after ECM degradation in 4 min. Time code in hours and minutes, upper right corner. White arrows point the FITC liberation next to the intravasating HSPC/mCherry þ cells. UGO, urogenital opening. Scale bars, 0.5 mm (a), 30 mm (b) and 10 mm (c^0-n). See also Supplementary Fig. 5 and Supplementary Movies 3–5.

that these migrating round cells are HSPCs, we injected Gelatin-FITC into Tg(kdrl:caax:mCherry) embryos in which vascular endothelium and HSPCs express the mCherry protein[10]. We observed the same specific punctiform fluorescence around HSPCs/mCherry þ cells emerging from the wall of the aorta (Fig. 5n–p, n¼4).

In vivo zymography therefore provided a final demonstration of matrix degradation in the AGM by macrophage secreted proteases followed by HSPC mobilization and vein intravasation.

Discussion

The studies described herein show an unexpected accumulation of primitive macrophages in the AGM region (ventrally to the DA) of human and zebrafish embryo.

We previously reported that zebrafish HSPCs emerge in the subaortic mesenchyme then enter the PCV circulation through peculiar structures, which facilitate HSPC intravasation[9]. Live imaging in HSPC-cd41:eGFP þ /macrophage-mpeg1:mCherry þ zebrafish embryo shows these tiny entry points are created by macrophages during their migration through the stroma, which will allow HSPCs to join the PCV.

Macrophage depletion at early stages of development (25 h.p.f.) prevents the colonization of haematopoietic organs without affecting EHT in the AGM, while late depletion (45 h.p.f.) leads to less pronounced effects. Because zebrafish definitive haematopoiesis occurs between 30 and 55 h.p.f. (ref. 3), the partial colonization observed after late depletion is likely due to HSPCs which had already left the AGM before macrophage depletion.

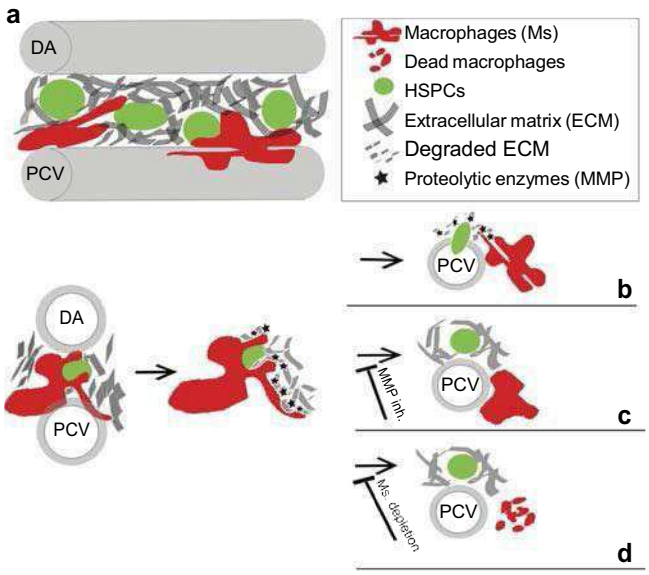

Figure 6 | Primitive macrophages in HSPC mobilization and definitive haematopoiesis. (a) Macrophages (red) interact with HSPCs (green) in the AGM during haematopoiesis. (b) ECM degradation by macrophages enables HSPC mobilization, intravasation and haematopoietic organ colonization. Mmps inhibition (c) or macrophage depletion (d) result in HSPC accumulation in the AGM. inh., inhibition.

We show here that these entry points are formed by Mmps-secreting macrophages. Specific chemical Mmps inhibition together with combined WISH and immunofluorescence staining established that macrophages are involved in HSPC mobilization via Mmp-9 secretion.

Therefore, our data suggest that primitive macrophages play an essential role in definitive haematopoiesis by inducing Mmps-mediated degradation of the ECM around HSPC in the AGM region. Matrix degradation allows mobilization and migration of HSPC into the stroma, driving their intravasation into the vein, leading ultimately to the colonization of haematopoietic organs and the establishment of definitive haematopoiesis (as summarized in Fig. 6).

Another intriguing observation of this report is that a specific accumulation of primitive macrophages is also detected in the human embryo. CD68þ macrophages are indeed concentrated in the mesenchyme beneath the ventral wall of the human embryonic aorta but also associated with the intra-aortic HSPC clusters. Even if, in the human, like any mammalian embryo the mobilization of HSPCs occurs within the DA circulation[1], this accumulation of macrophages observed in the AGM, suggests that they could play a role in the establishment of definitive haematopoiesis also in these species. Therefore, we speculate that in human embryo, macrophages can facilitate the release of HSPCs from intra-aortic clusters, through a process evolutionary conserved.

Recent findings have demonstrated that macrophages maintain HSCs in adult bone marrow niches and their depletion mobilizes HSPCs in the bloodstream[31,32]. Our data show that during development, macrophages may have the opposite function by mobilizing HSPCs from the AGM followed by their intravasation and colonization of haematopoietic organs. This mobilization involves ECM degradation by the local secretion of Mmps.

Recent studies have shown that tumour-associated macrophages play a role in ECM remodelling in tumour stroma through the release of proteases from invadopodia, (mainly MMP-2 and 9) (ref. 18,19). These enzymes degrade the rigid stroma of tumours and enable CICs (cancer-initiating cells) to intravasate and seed secondary sites, that is, metastasis[33]. Our observations show marked similarities with this process, suggesting that HSPC and CIC migration might be comparable. It will thus be interesting to explore whether HSPCs also release factors that attract macrophages and what are their nature.

Methods

Human tissues and immunostaining. Human embryos were obtained from voluntary abortions performed according to guidelines and with the approval of the French National Ethics Committee. Patients gave their written consent for the embryos to be used for research purposes. Embryo sections (5 mm) were incubated with anti-CD34 (3.2 mg ml^{-1}, Miltenyi) or anti-CD68 (10 mg ml^{-1}, eBioscience) antibodies, then with biotinylated secondary antibodies (10 mg ml^{-1}, Immunotech) and with peroxidase-labelled streptavidin (0.6 mg ml^{-1}, Immunotech). Fluorescence-conjugated secondary antibodies (0.5 mg ml^{-1}, Biolegend) were used for double staining.

Zebrafish transgenic lines and live imaging. Wild-type AB, Tg(kdrl:Has.HRAS-mCherry) (here cited as kdrl:caax:mCherry)[34], Tg(cd41:eGFP)[35], Tg(mpx:eGFP)[36], Tg(mpeg1:mCherry-f) (here cited as mpeg1:mCherry; see below) and Tg(mpeg1:Gal4FF//UAS-E1b:Eco.NfsB-mCherry) (here cited as mpeg1:GAL4//UAS:NfsB-mCherry)[26] transgenic embryos were staged as described by Kimmel et al.[37] All experiments were carried out following the protocol CEEA-LR-13007 approved by the Animal Care and Use Committee Languedoc-Roussillon.

Human and zebrafish embryos (lateral views, rostral to the left) were imaged on Leica SP5 confocal (Fig. 1a–b^{0}^{0}, Fig. 5, Supplementary Fig. 1 and Supplementary Movies 3 and 4), Leica SPE confocal (Fig. 1c; Fig. 4d,g–h^{0}^{0} and Supplementary Fig. 4a–c, e–e^{0}^{0}, Supplementary Fig. 5d,e), DeltaVision OMX (Applied Precision; Figs 1e–l and Supplementary Movie 1), Zeiss LSM510 confocal (Fig. 2a,b, Supplementary Fig. 5a–c, Supplementary Movies 2 and 5), Zeiss V12 (Fig. 2c,d, Fig. 3a–b^{0} and e–g^{0}), Trophos Plate Runner (Figs 2e–m), Olympus MVX10 (Fig. 4a–c and Supplementary Fig. 2a–f) and Zeiss AxioImager Z.1 (Fig. 4i–l^{0} and Supplementary Fig. 4f–g^{0}).

Generation of mpeg1:mCherry-f transgenic Zebrafish line. A 1.9-kb mpeg1 promoter fragment encompassing the mpeg sequences driving promoter activity specifically in macrophages[38] was amplified by PCR using following forward 5^{0}-TTGGAGCACATCTGAC-3^{0} and NotI-introducing reverse 5^{0}-TTATAGCGG CCGCGAAATGCTCTTGACTTCATGA-3^{0} primers. Resulting product was digested by NotI and ligated to farnesylated mCherry protein coding sequence so that Mpeg1 ATG initiation codon would be in frame with downstream mCherry-F cds in a Tol2 derived vector. The resulting plasmid was injected along with transposase mRNA in one cell stage zebrafish embryos to achieve germline integration.

Macrophage chemical and inducible genetic depletion. Macrophages were depleted by injecting 5 nl of L-clodronate into the caudal vein (gift from M. Daeron Laboratory). L-PBS was injected as a control. Embryos with L-clodronate aggregates causing vessel occlusions and shunts were discarded.

Metronidazole-mediated depletion was performed by using double transgenic fish Tg(mpeg1:GAL4//UAS:NfsB-mCherry)[26] crossed with Tg(cd41:eGFP) to evaluate the effect of macrophage depletion on cd41þ cells. Embryos at 18 h.p.f. were treated with freshly prepared 10 mM metronidazole (Sigma) in 0.1% DMSO (dimethylsulphoxide) solution protected from light until the evaluation (60 h.p.f.), then rinsed with embryo water. Tg(cd41:eGFP//mpeg1:mCherry) embryos treated with 10 mM metronidazole were used as control.

MMP inhibition assay. Embryos were soaked in GM6001 (200 mM, Merck Millipore), SB-3CT (10 mM, Enzo Life Sciences) or DMSO (0.2%) as a control from 38 h.p.f. until observation.

WISH and immunofluorescence staining. WISH was performed according to Thisse (http://zfin.org/zf_info/zfbook/chapt9/9.82.html). Embryos at 48 h.p.f. were fixed, dehydrated with methanol, digested with proteinase K (New England Biolabs) and fixed again. Prehybridization was performed at 68 °C in HMþ buffer (50% formamide, 5× saline sodium citrate, 0.1% Tween-20, 50 mg ml^{-1} heparin, 500 mg ml^{-1} yeast tRNA) and followed by hybridization with 0.5 ng ml^{-1} digoxigenin-labelled antisense RNA probe in HMþ buffer. The probes were detected with alkaline phosphatase-conjugated anti-digoxigenin antibodies (1/5,000; Roche Applied Science) using nitro blue tetrazolium chloride/5-bromo-4-chloro-3-indolyl-phosphate, toluidine-salt (Roche Applied Science). After staining embryos were mounted in 90% glycerol prior imaging.

Zebrafish Mmp-9 and 13a plasmids were gifts from L. Ramakrishnan laboratory, mmp-2 from A. Noel laboratory. For immunostaining, embryos were incubated with anti-L-plastin antibody (1/10,000, gift from M. Redd), followed by Alexa Fluor 488 Goat Anti-Rabbit IgG antibody (1/1,000, Life Technologies).

In vivo zymography. In vivo zymography was performed according to Crawford's protocol[30]. FITC conjugated gelatin (Gelatin-FITC, Anaspec) 1 mg ml^{-1} in PBS was injected (4–8 ng) into muscle between somite 4 and 5 at 42 h.p.f. Imaging was performed just after injections. Control embryos were either incubated with MMP inhibitors during 4 h prior injections or injected with L-clodronate 17 h prior Gelatin-FITC injections.

Statistical analysis. Normal distributions were analysed using Shapiro–Wilk test. Non-gaussian data were analysed using Wilcoxon or Kruskal–Wallis test, Gaussian with Student's t-test or analysis of variance followed by Holm's multiple comparison. P<0.05 was considered as statistically significant (symbols: ***P<0.001; **P<0.01; *P<0.05). Statistical analyses were performed using R software.

References

1. Tavian, M., Biasch, K., Sinka, L., Vallet, J. & Péault, B. Embryonic origin of human hematopoiesis. Int. J. Dev. Biol. 54, 1061–1065 (2010).
2. Cumano, A. & Godin, I. Ontogeny of the hematopoietic system. Annu. Rev. Immunol. 25, 745–785 (2007).
3. Murayama, E. et al. Tracing hematopoietic precursor migration to successive hematopoietic organs during zebrafish development. Immunity 25, 963–975 (2006).
4. Mikkola, H. K. a. & Orkin, S. H. The journey of developing hematopoietic stem cells. Development 133, 3733–3744 (2006).
5. Guyader, D. L. e. et al. Origins and unconventional behavior of neutrophils in developing zebrafish origins and unconventional behavior of neutrophils in developing zebrafish. Blood 111, 132–141 (2008).
6. Herbomel, P., Thisse, B. & Thisse, C. Ontogeny and behaviour of early macrophages in the zebrafish embryo. Development 126, 3735–3745 (1999).
7. Gering, M., Rodaway, A. R., Göttgens, B., Patient, R. K. & Green, A. R. The SCL gene specifies haemangioblast development from early mesoderm. EMBO J. 17, 4029–4045 (1998).
8. Gering, M. & Patient, R. Notch signalling and haematopoietic stem cell formation during embryogenesis. J. Cell Physiol. 222, 11–16 (2005).
9. Kissa, K. et al. Live imaging of emerging hematopoietic stem cells and early thymus colonization. Blood 111, 1147–1156 (2008).
10. Bertrand, J. Y. et al. Haematopoietic stem cells derive directly from aortic endothelium during development. Nature 464, 108–111 (2010).
11. Kissa, K. & Herbomel, P. Blood stem cells emerge from aortic endothelium by a novel type of cell transition. Nature 464, 112–115 (2010).
12. Boisset, J.-C. et al. In vivo imaging of haematopoietic cells emerging from the mouse aortic endothelium. Nature 464, 116–120 (2010).
13. Oberlin, E., Tavian, M., Blazsek, I. & Péault, B. Blood-forming potential of vascular endothelium in the human embryo. Development 129, 4147–4157 (2002).
14. Wynn, T. a., Chawla, A. & Pollard, J. W. Macrophage biology in development, homeostasis and disease. Nature 496, 445–455 (2013).
15. Mantovani, A., Biswas, S. K., Galdiero, M. R., Sica, A. & Locati, M. Macrophage plasticity and polarization in tissue repair and remodelling. J. Pathol. 229, 176–185 (2013).
16. Lin, E. Y., Nguyen, A. V., Russell, R. G. & Pollard, J. W. Colony-stimulating factor 1 promotes progression of mammary tumors to malignancy. J. Exp. Med. 193, 727–740 (2001).
17. Pollard, J. W. Tumour-educated macrophages promote tumour progression and metastasis. Nat. Rev. Cancer 4, 1–8 (2004).
18. Linder, S. The matrix corroded: podosomes and invadopodia in extracellular matrix degradation. Trends Cell Biol. 17, 107–117 (2007).
19. Vérollet, C. et al. Extracellular proteolysis in macrophage migration: losing grip for a breakthrough. Eur. J. Immunol. 41, 2805–2813 (2011).
20. Kessenbrock, K., Plaks, V. & Werb, Z. Matrix metalloproteinases: regulators of the tumor microenvironment. Cell 141, 52–67 (2010).
21. Yoong, S. et al. Characterization of the zebrafish matrix metalloproteinase 9 gene and its developmental expression pattern. Gene Expr. Patterns 7, 39–46 (2007).
22. Qian, F. et al. Microarray analysis of zebrafish cloche mutant using amplified cDNA and identification of potential downstream target genes. Dev. Dyn. 233, 1163–1172 (2005).
23. Tavian, M., Hallais, M. F. & Péault, B. Emergence of intraembryonic hematopoietic precursors in the pre-liver human embryo. Development 126, 793–803 (1999).
24. Bernut, A. et al. Mycobacterium abscessus cording prevents phagocytosis and promotes abscess formation. Proc. Natl Acad. Sci. USA 111, E943–E952 (2014).
25. Mancardi, D. a. et al. The high-affinity human IgG receptor FcgRI (CD64) promotes IgG-mediated inflammation, anaphylaxis, and antitumor immunotherapy. Blood 121, 1563–1573 (2013).
26. Palha, N. et al. Real-time whole-body visualization of Chikungunya Virus infection and host interferon response in zebrafish. PLoS Pathog. 9, e1003619 (2013).
27. Zhang, J., Bai, S., Zhang, X., Nagase, H. & Sarras, M. P. The expression of gelatinase A (MMP-2) is required for normal development of zebrafish embryos. Dev. Genes Evol. 213, 456–463 (2003).
28. Bai, S. et al. Matrix metalloproteinase expression and function during fin regeneration in zebrafish: analysis of MT1-MMP, MMP2 and TIMP2. Matrix Biol. 24, 247–260 (2005).
29. Krüger, A. et al. Antimetastatic activity of a novel mechanism-based gelatinase inhibitor. Cancer Res. 65, 3523–3526 (2005).
30. Crawford, B. D. & Pilgrim, D. B. Ontogeny and regulation of matrix metalloproteinase activity in the zebrafish embryo by in vitro and in vivo zymography. Dev. Biol. 286, 405–414 (2005).
31. Winkler, I. G. et al. Bone marrow macrophages maintain hematopoietic stem cell (HSC) niches and their depletion mobilizes HSCs. Blood 116, 4815–4828 (2010).
32. Chow, A. et al. Bone marrow CD169 þ macrophages promote the retention of hematopoietic stem and progenitor cells in the mesenchymal stem cell niche. J. Exp. Med. 208, 261–271 (2011).
33. Condeelis, J. & Segall, J. E. Intravital imaging of cell movement in tumours. Nat. Rev. Cancer 3, 921–930 (2003).
34. Chi, N. C. et al. Foxn4 directly regulates tbx2b expression and atrioventricular canal formation. Genes Dev. 22, 734–739 (2008).
35. Lin, H.-F. et al. Analysis of thrombocyte development in CD41-GFP transgenic zebrafish. Blood 106, 3803–3810 (2005).
36. Renshaw, S. a. et al. A transgenic zebrafish model of neutrophilic inflammation. Blood 108, 3976–3978 (2006).
37. Kimmel, C. B., Ballard, W. W., Kimmel, S. R., Ullmann, B. & Schilling, T. F. Stages of embryonic development of the zebrafish. Dev. Dyn. 203, 253–310 (1995).
38. Ellett, F., Pase, L., Hayman, J. W., Andrianopoulos, A. & Lieschke, G. J. Mpeg1 promoter transgenes direct macrophage-lineage expression in zebrafish. Blood 117, e49–e56 (2011).

Acknowledgements

We thank V. Diakou, V. Georget and the MRI facility for their assistance; D. Mancardi and M. Daeron for the L-clodronate gift; A. Meijer for mpeg1:Gal4 fish; L. Ramakrishnan for mmp-9 and mmp-13 plasmids; A. Noel for mmp-2 plasmid; M. Redd for L-plastin antibody; and M. Rossel for discussions. We thank P. Herbomel for hosting the initial phase of this work at Institut Pasteur. This work was supported by ARC and Fish-ForPharma (EU, FP7). J.T. was supported by a fellowship from the MESR, VTC by a fellowship from the DARRI, Institut Pasteur and by a fellowship from the Région Languedoc-Roussillon, Chercheur d'Avenir.

Author contributions

J.T., V.T.C., E.J., J.M.-L., E.L., M.T. and K.K. designed and performed the experiments. C.G. and G.L. generated the mpeg1:mCherry transgenic fish line. J.T., E.L. and K.K. wrote the manuscript with input from G.L. and M.T.

Additional information

Supplementary Information accompanies this paper at http://www.nature.com/naturecommunications

Competing financial interests: The authors declare no competing financial interests.

Reprints and permission information is available online at http://npg.nature.com/reprintsandpermissions/

How to cite this article: Travnickova, J. et al. Primitive macrophages control HSPC mobilization and definitive haematopoiesis. Nat. Commun. 6:6227 doi: 10.1038/ncomms7227(2015).

Supplementary Data

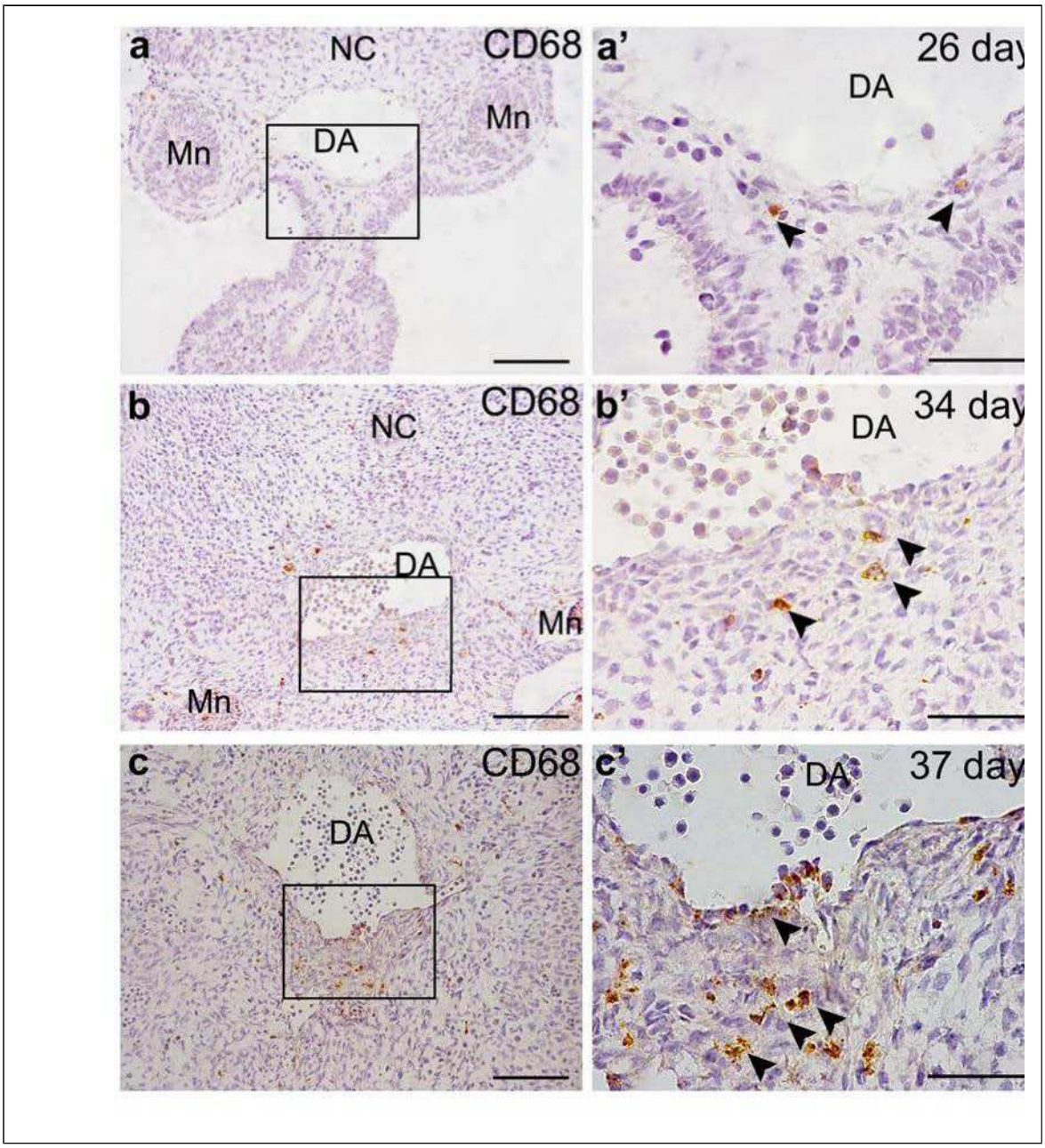

Supplementary Figure 1. Accumulation of macrophages in the ventral wall of the human aorta during the emergence of HSPCs, related to Figure 1.

(a-c') Transverse sections through the DA of 26 (**a-a',** n=3), 34 (**b-b'**, n=2) and 37-day human embryos (**c-c'**, n=3). Immunostaining by anti-CD68 reveals that the number of macrophages (arrowhead) in the mesoderm beneath the aorta increases with development. (**a', b', c'**) Higher

magnification of black box in **a, b, c**. DA, dorsal aorta; Mn, mesonephros, NC, notochord. Scale bar: 100 µm (**a-c**); 50 µm (**a'-c').**

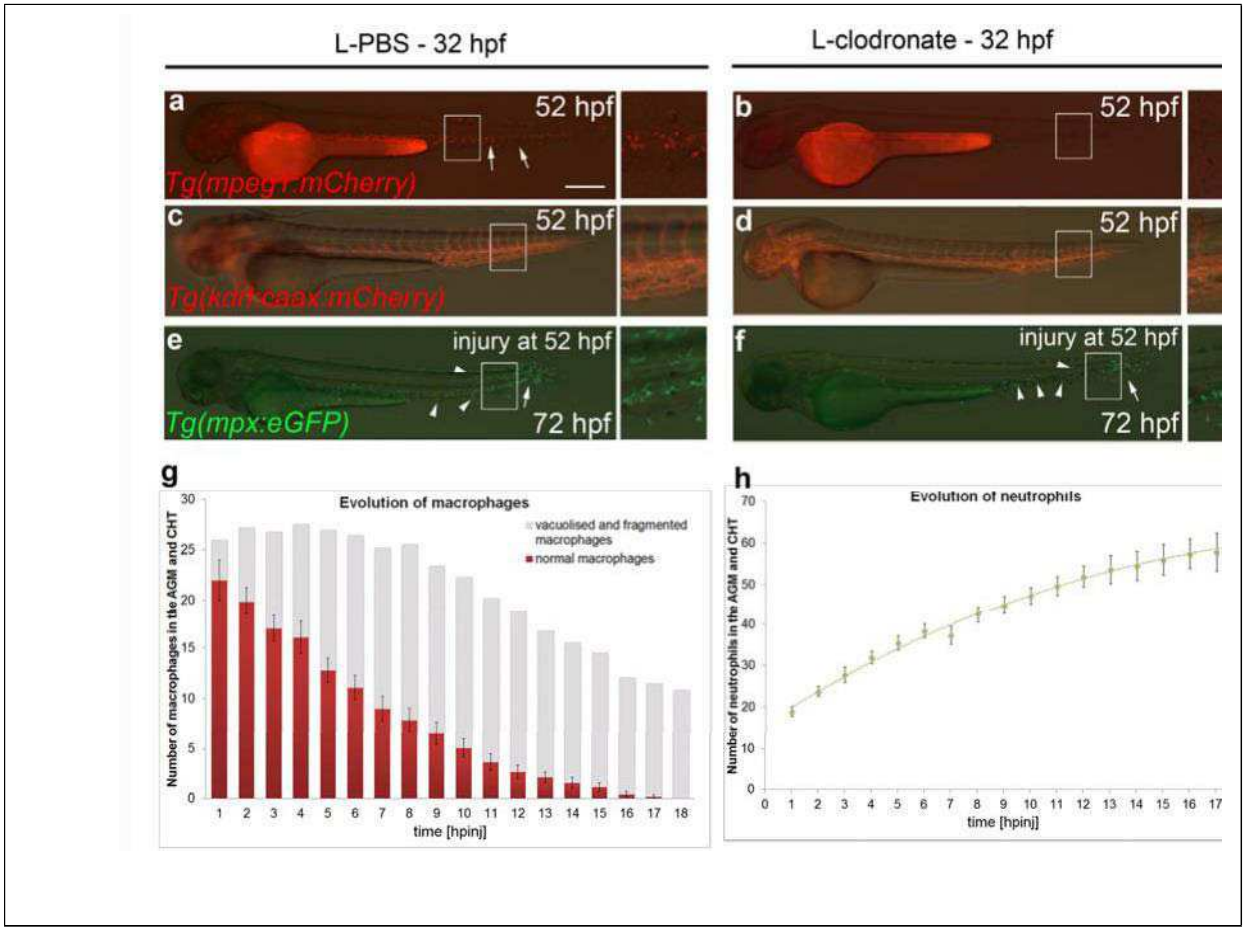

Supplementary Figure 2. Macrophage depletion by L-clodronate has no toxic effect on zebrafish vasculature nor on neutrophil emergence and functions, related to Figure 2.

(**a-b**) L-clodronate injection at 32 hpf *Tg(mpeg1:mCherry)* specifically depletes macrophages (**b,** 52 hpf, high magnification, n=200) compared to injection with L-PBS (a, white arrow, high magnification, n=25) but has no effect on vasculature development (**d vs c**, n=15**)**, *Tg(kdrl:caax:mCherry)*, 52 hpf, high magnification) nor neutrophil survival (arrowhead) and function (arrow) as shown by the tail wound test (**f vs e**, *Tg(mpx:eGFP)*, 72 hpf, high magnifications, n=35).

Scale bar: 250 µm (**a**). AGM, aorta gonad mesonephros; CHT, caudal haematopoietic tissue.

(g) Graph represents the evolution of macrophages (n=10) in the AGM and the CHT every hour during 18 hours after L-clodronate injection. Red columns stand for normal macrophages, grey for vacuolated or fragmented macrophages. Data shown as an average ± SEM.

(h) Graph represents the evolution of neutrophils in the AGM (n=10) and the CHT every hour during 18 hours after L-clodronate injection. Data shown as an average ± SEM.

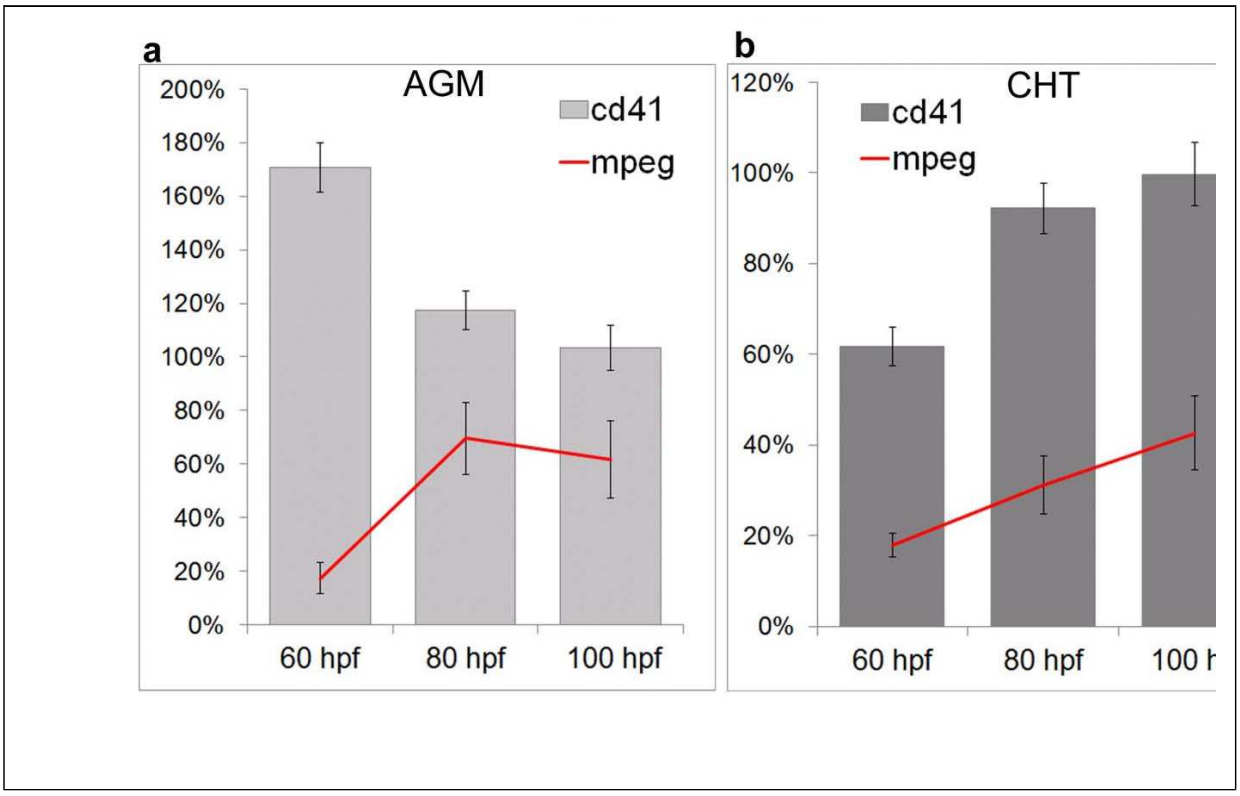

Supplementary Figure 3. Re-appearance of macrophages in genetically depleted embryos directly rescues mobilisation of HSPCs/cd41:eGFP+ cells and haematopoietic organ colonisation. Related to Figure 3.

(**a-b**) Graphs represent the evolution of the number of macrophages/mpeg:mCherry+ (red line) and HSPCs/cd41:eGFP+ (columns) in the AGM (**a**) and CHT (**b**) over the time after metronidazole

removal (at 60 hpf, then 20 and 40 hours after removal respectively at 80 hpf and 100 hpf, n=11). Data shown as relative ratio ± SEM compared to control embryos represented as 100% (n=9).

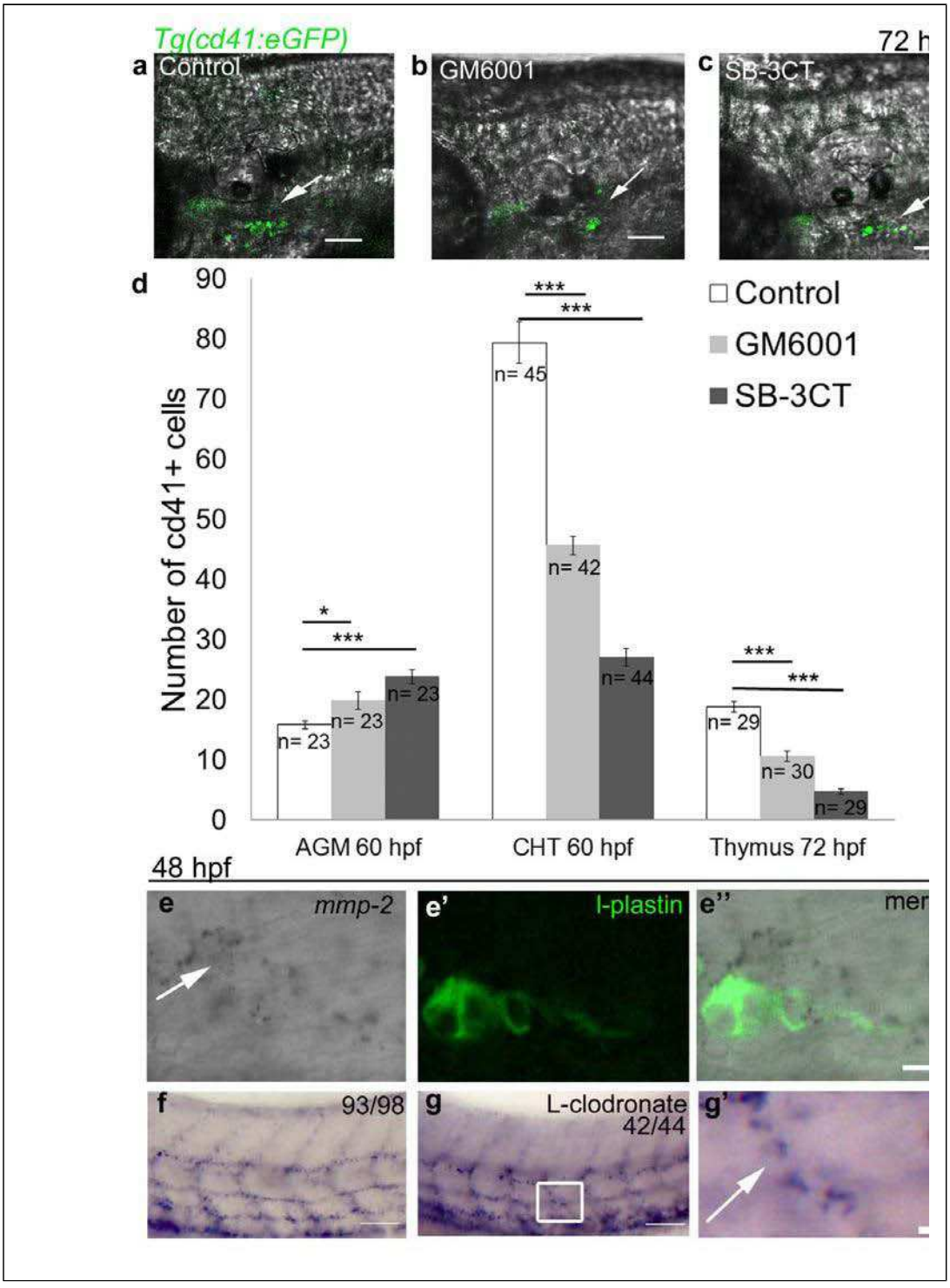

Supplementary Figure 4. Mmps expressed by macrophages affect colonisation of haematopoietic organs by HSPCs/cd41:eGFP+. Related to Figure 4.

(**a-c**) Accumulation of HSPC/cd41:eGFP+ cells in the thymus (arrow) at 72 hpf. Control embryo (**a**), treated with GM6001 (**b**) or SB-3CT (**c**). Fluorescence is merged with transmitted light.

(**d**) Quantification of the HSPC/cd41:eGFP+ number after treatment with Mmps inhibitors from 38 hpf compared to control. Graph shows HSPC/cd41:eGFP+ accumulation in the AGM at 60 hpf, induced by GM6001 or SB-3CT (+26% and +51% respectively), decrease of colonisation in the CHT at 60 hpf (-43% and -66% respectively) and in the thymus at 72 hpf (-44% and -75% respectively). Data are shown as average ±SEM. * $P < 0.05$; *** $P < 0.001$ (Student's t-test for AGM and Wilcoxon test for CHT and thymus); n = number of embryos from minimum 3 independent experiments.

(**e-e''**) Confocal imaging of WISH for *mmp-2* (**e**) combined with L-plastin immunofluorescence (green) (**e'**) are merged in **e''**. (**f-g'**) WISH for *mmp-2* in the AGM in control embryos (**f**) and after macrophage depletion by L-clodronate (**g**). Close-up of macrophage depleted embryo in **g'**. Arrow indicates the presence of *mmp-2* expressing cells. Scale bar: 50µm (**a-c, f-g**), 10 µm (**e-e'', g'**).

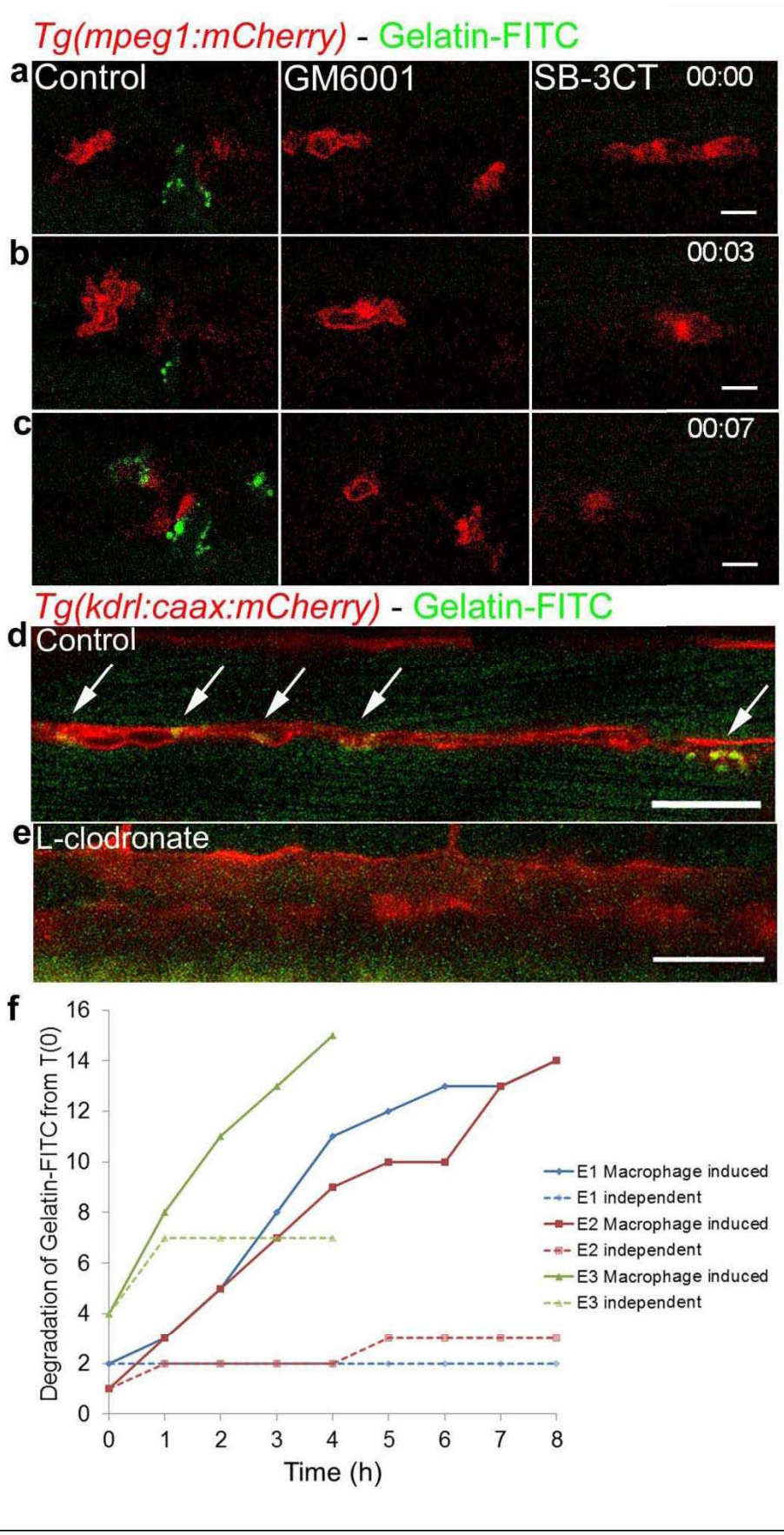

Supplementary Figure 5. Gelatin degradation depends on macrophage-expressing mmps.

Related to Figure 5.

(a-c) Release of FITC signals from degraded gelatin-FITC in the AGM in *Tg(mpeg1:mCherry)* after macrophage passage (red cells) is disrupted by treatment with MMP inhibitors GM6001 (middle column) and SB-3CT (right column) (n=4).

(d-e) Degradation of gelatin-FITC in the AGM in *Tg(kdrl:caax:mCherry)* (**d**, arrow) is impaired after chemical L-clodronate mediated macrophage depletion (**e**, n=4).

(f) Graph represents the number of FITC+ foci appearing either after macrophage passage (macrophage induced, full line) or without macrophage interaction (independent, spaced line) every hour during over-night time-lapse (n=3). h, hour. Scale bar: 10µm (**a-c**), 50µm (**d-e**)

2. Macrophage migratory dynamics in the zebrafish embryo

2.1. Article 2: Real time imaging of macrophage *in vivo* behaviour

Real time imaging of macrophage *in vivo* behaviour

Jana Travnickova, Sandra Nhim, Maï Nguyen-Chi, Naoill Abdellaoui, Farida Djouad and Karima Kissa

Manuscript submitted

Key points:

- Macrophage morphology might be categorised into 4 groups *in vivo*
- Macrophage dynamically change their morphology during their migration in the physiological conditions
- MMP or Rac inhibition abolish the mesenchymal migration of macrophages
- Rac inhibition impairs the macrophage migration and their ability to degrade ECM matrix
- MMP inhibition induce the transition of movement to the amoeboid type of migration

Real time imaging of macrophage *in vivo* behaviour

Jana Travnickova[1,2], Sandra Nhim[1,2], Maï Nguyen-Chi[2,3], Naoill Abdellaoui[1,2], Farida Djouad[2,3] and Karima Kissa[1,2,*].

[1]CNRS UMR 5235, DINMP F-34095 Montpellier, France.

[2]Université de Montpellier, F-34095 Montpellier, France.

[3]Inserm U 1183, IRMB, F-34295, Montpellier, France

*Correspondence:

Karima Kissa, PhD

UMR5235, Université de Montpellier

Place Eugène Bataillon, Bat. 24, cc107

34095 Montpellier cedex 5, France

karima.kissa@univ-montp2.fr

Phone +33 467 14 92 03

Abstract

In vitro, depending on extracellular matrix (ECM) architecture, macrophages migrate either in amoeboid or mesenchymal mode; while the first is a general trait of leukocytes, the latter is associated with tissue remodelling via Matrix Metalloproteinases (MMPs). To assess whether these stereotyped migrations could be also observed in the more complex context of a live organism, we used the zebrafish embryo and monitored macrophage morphology and behaviour associated with the mobilisation of haematopoietic stem/progenitor cells (HSPCs). Morphometric analysis identified 4 different cell shapes. Live imaging revealed that macrophages successively adopt all four shapes as they migrate through ECM. Treatment with inhibitors of MMPs or Rac GTPase to abolish mesenchymal migration, suppresses both ECM degradation and HSPC mobilisation while differently affecting macrophage behaviour. This study depicts real time macrophage behaviour in a physiological context and reveals extreme reactivity of these cells constantly adapting and switching migratory shapes to achieve HSPCs proper mobilisation.

Introduction

Macrophages were for the first time identified as phagocytic cells responsible for pathogen elimination (Metchnikoff, 1892). Over the past century, they were associated with homeostasis, innate and adaptive immune responses, inflammation, tissue remodelling and cytokine production (Gordon and Taylor, 2005; Wynn et al., 2013). Macrophages are the most plastic haematopoietic cells present in all tissues; their diversity depends upon their location, their morphology, their membrane receptors or surface markers (Wynn et al., 2013). Depending on tissue composition they infiltrate and environmental constraints, macrophages adopt different migration modes (Vérollet et al., 2011). In the course of a three-dimensional (3D) migration, macrophages can either adopt an amoeboid or a mesenchymal migratory mode. In case of an amoeboid migration, cells take on a round or polarised shape and migrate through the extracellular matrix (ECM). Such a migration is Rho/Rock GTPases dependent. During mesenchymal migration, macrophages degrade the ECM through proteinases secretions (e.g. Matrix Metalloproteinases or MMPs) and cells take on an elongated shape. This second migratory mode is Rac GTPase signalling dependent (Sanz-Moreno and Marshall, 2010; Vérollet et al., 2011).

In mouse and human, macrophage characterization was mainly performed *in vitro* using bone marrow derived macrophages. Recently, the zebrafish model was used to resolve specific issues during the developmental process or to address accurate pathologies. The transparency of zebrafish embryos enables the live imaging and real time tracking of cell populations. We and other groups have shown that two main waves of macrophages emerge from primitive and definitive haematopoiesis during the zebrafish development (Gering and Patient, 2005; Herbomel et al., 1999; Murayama et al., 2006). The initial wave takes place between 18 and 25 hours post fertilization (hpf) in the yolk sac (Herbomel et al., 1999). The second wave occurs

between 30 and 55 hpf in the aorta-gonad-mesonephros (AGM) (Gering and Patient, 2005; Murayama et al., 2006) and generates the haematopoietic stem/progenitor cells (HSPCs) (Bertrand et al., 2010a; Kissa and Herbomel, 2010) which later will differentiate into all blood cells including macrophages. Finally, a transient hematopoietic wave is initiated in the posterior blood island, giving rise to the multilineage progenitor cells and erythromyeloid progenitors, which develop into both erythroid and myeloid cells (Bertrand et al., 2007).

Recently, we demonstrated *in vivo* that primitive macrophages are crucial in the establishment of a definitive haematopoiesis (Travnickova et al., 2015). Macrophages that accumulated in the AGM degrade the ECM located in the vicinity of HSPCs via matrix metalloproteinase 9 (MMP-9) secretions, thereby enabling them to migrate, enter the blood stream and colonise haematopoietic organs.

In the present study, we provide an extensive analysis of macrophages in zebrafish embryos. Using morphological analysis we were able to distinguish for the first time different macrophage subtypes *in vivo*. By combining morphological analysis with live imaging we succeeded in visualizing the dynamic behavioural patterns of individual macrophages during their migration through the ECM.

Results

Macrophage shape heterogeneity in the zebrafish embryo

During the establishment of the definitive haematopoiesis, macrophages accumulated in the AGM between 30 and 60 hpf degrade the ECM surrounding HSPCs via Mmp-9 secretions which result in the mobilization of HSPCs (Travnickova et al., 2015). Using this physiological model, we analysed the shape and behaviour of proteolytic macrophage in order to establish a potential correlation. We first described the position and shape of macrophages in the AGM using the *kdrl:eGFP//mpeg1:mCherry-F* double transgenic lines where the GFP protein highlighted vessels and mCherry-F macrophage membranes (**Fig. 1A-B**). Figure 1A provides a schematic view of the vessel and macrophage position as shown in Figure 1B. Using a 3D view (**Fig. 1B**) we were able to determine the position of macrophages (white arrows) in the outer layer of the vein wall between the vein and the aorta floor with different morphologies. The particle analysis of macrophages from a maximum projected confocal acquisitions enabled us to distinguish and quantify the various macrophage shapes. Three main morphological criteria were identified: circularity, roundness and elongation factor (**Fig. 1C and Suppl. Table 1**). They revealed the existence of 4 main shapes whose images are shown in **Figure 1D**. We named these 4 subgroups - round (1), amoeboid (2), star-like (3) and elongated shape (4). While the round and elongated shapes had already been described *in vitro*, the two remaining shapes might represent either subgroups present *in vivo* or intermediate stages between round and elongated shapes. The main difference between the amoeboid and star-like shapes lied in the presence in the amoeboid shape of a main axis, i.e. polarity. The quantification of each shape revealed that amoeboid, star-like and elongated shapes were equally present whereas the round shape remained sparse (**Fig. 1E**).

Dynamics of macrophage migration *in vivo*

The analysis of macrophage shapes revealed the existence of four morphological subgroups distributed in the zebrafish AGM. To assess the behaviour of each macrophage subgroup, we imaged *Tg(Mpeg1:mCherry)* embryos over the course of one hour (acquisition every minute; **Video 1.**). We selected time frames in colour depth projection that illustrated the dynamics of macrophages able to adopt different shapes within fifteen minutes (**Fig. 2A-F and Video 1,** colour code scale). The outlines represent the shape of macrophages in the imaged area at the 9th minute and enable us to draw a direct comparison with following time points. The colour depth projection of confocal imaging enabled us to determine the depth of macrophage positions *in vivo* and to demonstrate their ability to migrate in 3D patterns (**Video 1**). *In vivo* tracking of all macrophages within a 60 minute timeframe demonstrated that no specific directionality was maintained during their migration (**Fig. 2G**, n=23) as opposed to macrophages attracted to a wound site as an example of typical oriented migration (**Fig. 2H**, n=27). The speed of migration remained the same in both cases (data not shown). Subsequently, we quantified the evolution of macrophage shapes over time. Every single macrophage in the AGM reveals an ability to change shape within a very short time span (measured every 5 minutes) and to pass repeatedly through distinct shape subgroups over a 30 minutes course (**Fig. 2I**, n=10). The round shape appeared less frequently than others and live imaging showed that cells often adopted a round shape under two specific conditions: during cell division or once the macrophage entered the bloodstream.

In conclusion, macrophage real time imaging completes the characterisation of mesenchymal migrating macrophages and shows for the first time that they can adopt successive morphologies for their migration in the 3D matrix.

Rac inhibition modifies macrophage behaviour and function

Using *in vivo* imaging we showed that macrophages exhibited morphological plasticity during their migration. This high plasticity depended on both, external (the stroma rigidity) and intrinsic parameters (cytoskeleton dynamics) (Vérollet et al., 2011). One intrinsic factor associated with mesenchymal migration is the small GTPase- Rac signalling. We thus investigated the effect of Rac chemical inhibition on macrophage shape and migration patterns. The macrophage shape distribution in Rac inhibitor (NSC23766) treated embryos did not significantly differ from that of DMSO treated control (**Fig. 3A**, N_{DMSO}=10 and $N_{Rac\ inh.}$=15 embryos). Selected images from **Video 2** (colour, depth, projection, bottom) demonstrated that the macrophage migration was much slower than that of control embryos (**Fig. 3B-E, Video 2**, top). Macrophage speed measured over 60 minutes in the AGM confirmed a decrease in velocity from 2.37 ± 0.13 µm.min^{-1} to 1.13 ± 0.16 µm.min^{-1} (**Fig. 3F**).

The tracking plot diagram illustrated macrophage migration path and distance in control and Rac-inhibited embryos (**Fig. 3G-H,** n=15 macrophages from 4 embryos, position measured every minute over 1 hour) and revealed that Rac inhibition reduced macrophage moves from 130.9 ±7.5 µm to 56.8 ± 7.8 µm. Moreover, the analysis of macrophage shape dynamics, revealed a reduction in macrophage plasticity over time as macrophages were no longer able to consecutively adopt different shapes (**Fig. 3I, right**; n= 7) versus control (**Fig. 3I, left**; n= 7). However, in spite of reduced plasticity levels, membrane extensions were still formed at the same rate and with similar length as in control macrophages. Rac inhibition resulted in an increase in single extension span (from 2.8 ± 0.3 min to 11.0 ± 1.9 min, $n_{extension}$= 45) as opposed to that of control macrophages.

As macrophage migration and morphological plasticity were significantly affected by Rac inhibition, we decided to evaluate the functionality of these macrophages. The main role

of AGM macrophages is to degrade the ECM and to enable HSPC migration (Travnickova et al., 2015). *In vivo* zymography of *Tg(Mpeg1:mCherry)* embryos at 48 hpf, revealed a significant reduction in gelatin degradation and thereby a lower gelatinase activity (decreased number of green dots of cleavage-revealed FITC) in Rac inhibited embryo compared to control (**Fig. 3J**). Since the proteolytic function of macrophages in the AGM is essential to HSPC mobilisation, we assessed the effect of Rac inhibition on haematopoietic organ colonisation. We noticed an increase in HSPCs accumulated in the AGM at 48 hpf (+70±8%, n=6) and consequently a decrease in HSPC accumulated in the CHT at 55 hpf (-41±2%; n=5).

MMP inhibition affects macrophage shape, behaviour and function.

Rac inhibition has an impact on macrophage proteolytic activity and consequently on their function. To assess whether direct inhibition of macrophage proteolytic activity induces a similar behaviour, we soaked embryos in a medium containing SB-3CT MMP inhibitor. We previously demonstrated that ECM degradation occurred as a result of macrophage-secreted MMP-9 around HSPCs to enable their intravasation. We evaluated the direct impact of MMP inhibition on macrophage morphology and noticed a variation in shape distribution: an increase in round shape number and a decrease in star-like and elongated shapes (**Fig. 4A**). Moreover, MMP inhibition affected macrophage migration and behaviour (**Fig. 4B-E**, **Video 3**). Selected images from **Video 3** displayed a typical example of macrophage migration pattern. Using Colour depth projection we were able to visualise the 3D migration of macrophages in the AGM and noticed that in MMP-9 inhibited embryos, macrophages migrated mainly in 2D. At a given point in time, they adopted a single colour whereas in control embryos we observed dynamic

changes indicated by the presence of several colours at one time point (**Fig. 2A-F**). Moreover, **Video 3** showed the macrophages adopted different migration pattern resembling to the leukocyte crawling on vein vessel.

Furthermore, we observed that MMP inhibition affected macrophage velocity and directionality. The speed of migration increased more than 3 times compared to the control (from 2.20 ± 0.11 $\mu m.min^{-1}$ to 7.80 ± 0.92 $\mu m.min^{-1}$**; Fig. 4F**). Finally, a tracking plot diagram which illustrated the migration path and distance of macrophages in the AGM in control and MMP-inhibited embryos (**Fig. 4G** and **H)** revealed that migration directionality increased from 0.27 to 0.66. Cell tracking showed that macrophages migrated along the vein, in the same direction as the blood flow. We concluded that, MMP inhibition affected both macrophage shape and migration patterns. They adopted a MMP independent migration pattern with increased velocity which was reminiscent of an amoeboid type of migration.

Discussion

In this study we characterised in zebrafish embryos the macrophage population present in the AGM with a known proteolytic function (Travnickova et al., 2015). We reported the existence of four macrophage morphological subgroups. Previous studies performed *in vitro* described two major morphological types, elongated and rounded shapes (McWhorter et al., 2013). Using *in vivo* analyses we were able to identify two additional morphological shapes: amoeboid and star-like shapes. *In vivo* observations revealed the presence of a higher number of macrophage subgroups in contrast to conclusions drawn from assays on 3D matrices, thereby suggesting the importance of *in vivo* modelling to complete results obtained *in vitro*. Using high resolution live imaging in conjunction with macrophage shape descriptor analysis we devised a novel tool that enabled to quantify *in vivo* the dynamics and morphological plasticity of macrophages.

While macrophages were thought to exclusively migrate using an amoeboid mode (Friedl and Weigelin, 2008), Dr Parini's group demonstrated their capacity to also use a mesenchymal migration mode (Cougoule et al., 2012). In line with this last study, we describe the mesenchymal macrophage migration process *in vivo* in zebrafish embryos. Macrophages revealed an increase in shape plasticity which confirmed the outcome of previous studies performed *in vitro* (Cougoule et al., 2012).

Previous studies highlighted the significance of the role played by Rac signalling in cytoskeleton organisation during the mesenchymal migration of cells (Sanz-Moreno and Marshall, 2010). Our study performed *in vivo* during the establishment of haematopoiesis in zebrafish embryos also demonstrated that the mesenchymal migration of macrophages was Rac signalling dependent. Going further, we observed that Rac signalling inhibition affected not

only macrophage migration but also their proteolytic function and their phenotype. Indeed, upon Rac inhibition macrophages lose their ability to degrade the ECM matrix. We also observed that this treatment significantly reduced macrophage velocity and morphological plasticity. Moreover, live imaging revealed that macrophages develop and keep longer membrane extensions and that they remained longer in a specific location. Our study confirmed previous *in vitro* observations showing that Rac1-/- macrophages cultured on plastic exhibited additional membrane extensions when compared to control macrophages (Wheeler et al., 2006).

We finally observed that the inhibition of the macrophage proteolytic function induces their transition into a different type of migration mode corresponding to the adaptation of macrophages to their new environment. They adopted a round shape with an amoeboid migration. Macrophages were no longer able to migrate within the AGM stroma and they moved along the vein wall.

Proteolytic macrophages in the AGM exhibited a high functional similarity to macrophages found in solid tumours referred to as tumour associated macrophages (TAM). TAM play a significant part in ECM remodelling through proteinase releases (mainly MMP-2 and 9) and allow tumour cells to join the bloodstream and to seed in secondary sites (Condeelis and Pollard, 2006). Therefore, a current strategy is to target *TAM* to combat cancer (Panni et al., 2013). Several approaches based on macrophage depletion (clodronate liposomes) or functional modification (broad spectrum MMP inhibitors) did not succeed and failed during clinical trials due to low specificity and the amount of side effects (Panni et al., 2013; Turk, 2006). Expanding our knowledge from a purely molecular standpoint toward an in-depth understanding of behaviour and requirements in migration and site infiltration using adapted *in vivo* models, would complement existing studies and enable us to develop more targeted immunotherapeutic solutions.

Materials and Methods

Zebrafish husbandry

Wild-type and transgenic lines were maintained in compliance with the Institutional Animal Care and Use protocols. The following transgenic lines were used in this study: *Tg(Mpeg1:mCherry-F)* (Ellett et al., 2011; Travnickova et al., 2015) for macrophage membrane marking and *Tg(kdrl:eGFP)* (Beis et al., 2005) for vessel endothelium labelling. Embryos were kept in the presence of 1-phenyl-2-thiourea to prevent melanin pigmentation (Westerfield, 2000) and staged as described by Kimmel et al (Kimmel et al., 1995). All experiments were performed in accordance with the protocol CEEA-LR-13007 approved by the Animal Care and Use Languedoc-Roussillon Committee.

Live Imaging

Zebrafish embryos (lateral views, rostral to the left) were embedded in 0.7% low melting agarose and imaged using a Zeiss LSM510 confocal microscope through a 40x water immersion objective with a 1024x256 pixel resolution at 28°C. All live imaging experiments were performed at 46-48 hpf and all time-lapse imaging occurred at an acquisition rate of one minute at a 1µm z-interval. The image acquisitions were performed using ZEN2009. Image post-acquisition processing such as maximum intensity projections, 3D view, and overall image contrast adjustment were performed using Fiji software.

Inhibitor treatment

Embryos were soaked in MMP-2 and 9 inhibitors SB-3CT (Enzo Life Sciences) 9 µM or NSC23766 Rac inhibitor (Tocris) 50 µM or DMSO 0.25% as a control from 5-prim stage (25 hpf) to 46-48 hpf. For stock solution, inhibitors were dissolved in DMSO at a 10mM concentration and stored at -20°C.

Image processing and macrophage shape analysis

Confocal stacks of membrane-labelled macrophages were projected using a maximum intensity projection and 2D images were binarised using an automatic threshold. The following shape descriptors were evaluated using the Fiji plugin Particle analysis: area (µm²), perimeter (µm), circularity and roundness. The elongation factor was manually measured by dividing the longest axis of the object by its longest perpendicular axis (x/y). Objects with an area under 80 µm² were excluded from the further analysis. Circularity was calculated using the following formula: 4π x (area/perimeter²). This parameter varied from 0 (linear polygon) to 1 (perfect circle). Circularity was used to set apart round objects (circularity > 0.2) and roundness and elongation factor enabled us to break down non-round subjects into 3 subgroups: elongated, amoeboid and star-like shaped. Roundness was calculated using the following formula: 4 x {area/ [π x (major axis)²]} and varied from 0 (linear polygon) to 1 (perfect round). Supplementary table 1 shows the mean values of circularity, roundness and elongation factor measured for each of the above listed subgroups.

Cell tracking and velocity measurement

Maximum intensity projections of 60 minute time-lapses acquired every minute were analysed using a manual tracking plugin in Fiji. Measured data were transferred into a Chemotaxis and Migration tool programme (Ibidi) to design tracking and rose plots (Figure 2G-H for rose plots, 3G-H and 4G-H for tracking plots). A rose diagram maps single counts of the position of every macrophage in a selected area (black and grey sectors of angle $\pi/18$) every minute over 60 minutes with an (x,y 0,0) starting point. The tracking plot diagram represents the migration path and distance of macrophages in the AGM with an x,y 0,0 starting point, being measured every minute over 60 minutes. The average of single macrophage velocities ($\mu m\ min^{-1}$) during 15-60 minutes were used for analysis. The evaluation of the directionality was performed using a Rayleigh statistical test for the uniformity of a circular distribution of points (end points of single macrophages). All analyses were conducted using the Chemotaxis and Migration tool software (Ibidi).

Fin amputation for oriented migration analysis

Caudal fin amputation was performed with a sterile scalpel at 44 hpf, posterior to muscle and notochord under anaesthesia with 0.016% Tricaine (ethyl 3-aminobenzoate, Sigma Aldrich). 4 h post amputation embryos were mounted and imaged as described above.

In vivo zymography

The *In vivo* zymography was performed according to Crawford's protocol (Crawford and Pilgrim, 2005). A working solution, 1 mg ml^{-1} of fluoresceinated gelatin (Gelatin-FITC,Anaspec) in PBS was injected (4-5 ng) into muscles between 4^{th} and 5^{th} somite at 42 hpf.

Imaging was performed following the injections. Embryos were incubated in DMSO or Rac inhibitor from 25 hpf up to the Gelatin-FITC injections.

Statistical analysis

Normal distributions were analysed using the Shapiro-Wilk test. Non-Gaussian data were analysed using the Wilcoxon test, Gaussian with Student t-test. $P<0.05$ was considered as statistically significant (symbols: ****$p<0.0001$ *** $p<0.001$; ** $p<0.01$; * $p<0.05$) Statistical analyses were performed using the R software.

Acknowledgements

We would like to thank E. Lelièvre, M. Rossel and G. Lutfalla for their critical review of this manuscript; V. Diakou and the MRI facility for their assistance, A. Sahuquet for his help in the particle analysis. This work was supported by grants from the ARC, Chercheur d'Avenir - Région Languedoc-Roussillon, FRM and ATIP-Avenir. J.T. was supported by a fellowship from the MESR and FRM (FDT20150532507), M.N.-C. by a fellowship from the Université de Montpellier.

Author contributions

J.T., and K.K. designed the project and the experiments, J.T., S.N., M.N.-C and N.A. performed the experiments and analysed the results. J.T. and K.K. wrote the manuscript with the input of S.N., M.N.-C. and F.D.

Ethics

All animal experiments described in the present study were conducted at the University of Montpellier in compliance with European Union guidelines for handling of laboratory animals (http://ec.europa.eu/environment/chemicals/lab_animals/home_en.htm) and were approved by the Direction Sanitaire et Vétérinaire de l'Hérault and Comité d'Ethique pour l'Experimentation Animale under reference CEEA-LR-13007.

Disclosure of Conflicts of Interest

The authors declare no competing financial interests.

Abbreviations

AGM, Aorta-Gonad-Mesonephros

HSPC, Haematopoietic stem and progenitor cells

MMP, Matrix metalloproteinases

TAM, Tumour associated macrophages

Figure Legends

Figure 1: Macrophages in the AGM can be divided into 4 morphological subgroups.

(A) The drawing shows a 3D view of vessels and macrophages (red) imaged in B. (B) 3D view of the AGM in the mid-trunk region of a *Tg(kdrl:eGFP//mpeg1:mCherry-F)* zebrafish embryo at 48 hpf showing the position of vessels (endothelium in green) and macrophages (in red, white arrows) in the outer side of the vein and in between the dorsal aorta and the cardinal vein. (C) Diagram of the 4 categories of macrophages delineated according to shape attributes– circularity, roundness and elongation factor. (D) Representative confocal images (maximum intensity projections) of individual categories with an outline drawing from particle analysis on the right. (E) Graph representing the percentage distribution of the different shape categories per AGM. Data are represented as percentage average ± s.e.m. N= 20 embryos. C, caudal; D, dorsal; DA, dorsal aorta; PCV, posterior cardinal vein; R, rostral; V, ventral. See also supplementary table 1.

Figure 2: Macrophages in the AGM migrate in the mesenchymal way and undergo dynamic transition between different shapes over time.

(A-F) Selected images from Video 1 illustrate the macrophage migration and shape transformation over time. Numbers point to individual macrophages. Time code is expressed in hours and minutes. White outlines on panel B-F indicate the shape and position of macrophages from panel A (9^{th} minute). (G-H) Rose plot diagrams show the directionality of macrophage migration in the AGM compared to the oriented migration of macrophages in the tail region after tail fin cut injury. A diagram represents the single counts of the position of each macrophage in the selected area (black and grey sectors of angle $\pi/18$) every minute over 60

minutes with a (x,y 0,0) starting point. n= 23 macrophages for the control and n=27 for directed migration. (I) Graph showing the shape evolution of individual macrophages during a 30 minutes course with 5 minutes interval measurements. Every line represents a single macrophage (n= 10). See also Video 1. Scale bar, (A-F) 30 µm.

Figure 3: Rac inhibition leads to a loss of macrophage plasticity and motility.

(A) Graph comparing macrophage shape distribution in the AGM of NSC23766 Rac-inhibited embryos (Rac Inh) to DMSO treated embryos (control) shows no significant change of distribution. N=10 embryos for control and 15 for Rac inh. Data are represented as the mean of the percentage of each shape type in the total macrophage population in the AGM ± s.e.m. NS = not significant. (B-E) Selected cropped images from Video 2 showing the shape and migration of macrophages over time. Time code in hours and minutes. White outlines on panel C-E indicate the shape and position of macrophages from panel B (21st minute) (F) Graph showing the velocity of macrophages in control and Rac-inhibited embryos. Data are represented as a mean ± s.e.m., n= 15 macrophages from 4 different embryos, ****p<0.0001. (G-H) Tracking plot diagram representing the migration path and distance of macrophages in the AGM in control and Rac-inhibited embryos measured every minute for 60 minutes. Scale in µm, n=15 macrophages from 4 different embryos. (I) Graph shows the shape evolution of individual macrophages during a 30 minute course with 5 minutes interval measurements, Control to the left, Rac inhibitor to the right. Each line represents a single macrophage (n= 7). Statistically significant differences exist in the number of shapes adopted during a 30 minute measurement course (P=0.003) as well as in the number of changes between two different shapes (P=0.006). (J) *In vivo* zymography in *Tg(Mpeg1:mCherry)* embryos at 48 hpf reveals the degradation of

inserted gelatin (green dots of cleavage-revealed FITC) in control embryos and a highly reduced degradation after Rac inhibition. See also Video 2. Scale bar: 30 µm.

Figure 4: MMP-9 inhibition induces a change in macrophage shape and a transition towards an amoeboid-like migration.

(A) Graph compares the macrophage shape distribution in the AGM of MMP-2 and 9 (SB-3CT) -inhibited embryos (MMP inh) to DMSO treated embryos (control) shows an increase in round shape and a decrease in star-like and elongated shapes in MMP inh embryos. N=10 embryos for control and 15 for MMP inh. Data represent the percentage mean for each shape type out of the total number of macrophages in the AGM ± s.e.m. NS = not significant; *p<0.05; ****p<0.0001. (B-E) Selected cropped images from Video 3 displays macrophage shape and migration patterns over time. Numbers point to individual macrophages, time code is expressed in hours and minutes. Grey outlines on panel C-E show the shape and position of macrophages from panel B (3rd minute). (F) Graph showing the velocity of macrophages in control and MMP-inhibited embryos. Data are represented as a mean ± s.e.m., n= 17 macrophages for control and 14 for MMP inhibitor from 4 different embryos, ****p<0.0001. (G-H) Tracking plot diagram represents the migration path and distance of macrophages in the AGM in control and MMP-inhibited embryos measured every minute over 60 minutes. Scale in µm, n=17 macrophages for control and 14 for MMP inhibitor from 4 different embryos. See also Video 3. Scale bar 30 µm. DA, dorsal aorta; PCV, posterior cardinal vein.

Supplementary table 1: Measured average values (± s.e.m.) of shape descriptors for each shape subgroup. N = 20 embryos.

Video 1: Macrophage 3D migration in the AGM during haematopoiesis.

Representative time-lapse colour-depth projections of *Tg(mpeg1:mCherry*) embryo at 46 hpf illustrate macrophages migration occurring in a non-directional manner and through different depth by appropriately changing colour . Image stacks were acquired every minute over 60 minutes at a 1 µm interval with 1024x256 pixel resolution using the LSM510 Zeiss confocal microscope equipped with a 40x water immersion objective. Scale bar 30 µm, time code in hours and minutes.

Video 2: The migratory behaviour of macrophage changes after Rac inhibition.

Combined representative time-lapse colour-depth projections of *Tg(mpeg1:mCherry)* embryos at 46 hpf draws a comparison between macrophage migration in DMSO-treated (control, top) embryos and that of Rac-inhibitor (Rac inh, bottom) treated embryos. Rac-inhibited macrophages display slower migration modes. They change shapes and migration direction less often, and form very long membrane extensions. Image stacks were acquired every minute over 60 minutes at a 1 µm interval with 1024x256 pixel resolution using the LSM510 Zeiss confocal microscope equipped with a 40x water immersion objective. Scale bar 30 µm, time code in hours and minutes.

Video 3: MMP inhibition induces mesenchymal-amoeboid transition of macrophage migration.

Combined representative time-lapse colour-depth projections of *Tg(mpeg1:mCherry*) embryos at 46 hpf draw a comparison between macrophage migration in DMSO-treated (control, top) and MMP-2 and 9 inhibitor (MMP inh, bottom) treated embryos. MMP-inhibited macrophages migrate faster, adopt a round shape, change the depth of their displacement less often and

migrate partially inside the bloodstream. Image stacks were acquired every minute over 60 minutes at 1 μm interval with 1024x256 pixel resolution using the LSM510 Zeiss confocal microscope equipped with a 40x water immersion objective. Scale bar 30 μm, time code expressed in hours and minutes.

Figure 1

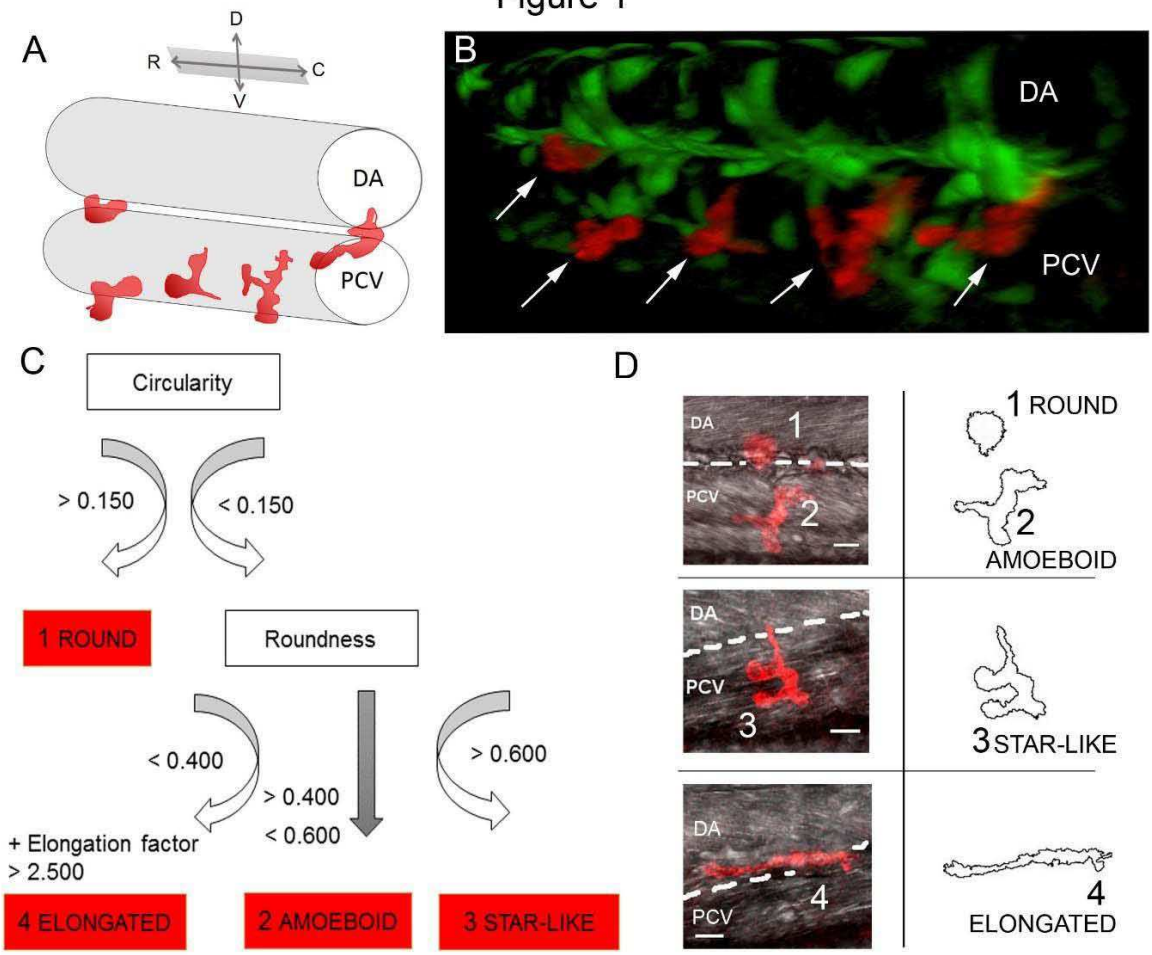
A
D
R
C
V
DA
PCV
B
DA
PCV
C
Circularity
> 0.150
< 0.150
1 ROUND
Roundness
< 0.400
> 0.400
< 0.600
> 0.600
+ Elongation factor
> 2.500
4 ELONGATED
2 AMOEBOID
3 STAR-LIKE
D
DA
PCV
1
2
3
4
1 ROUND
2
AMOEBOID
3 STAR-LIKE
4
ELONGATED

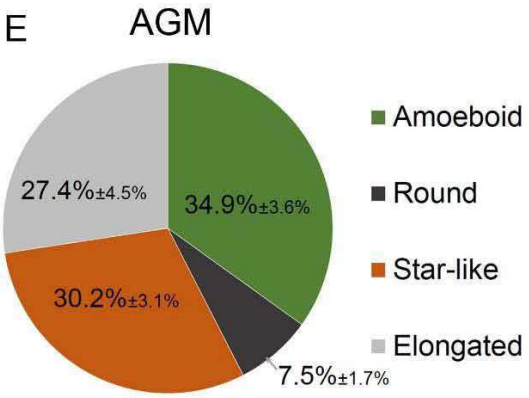
E
AGM
27.4%±4.5%
34.9%±3.6%
30.2%±3.1%
7.5%±1.7%
Amoeboid
Round
Star-like
Elongated

Figure 2

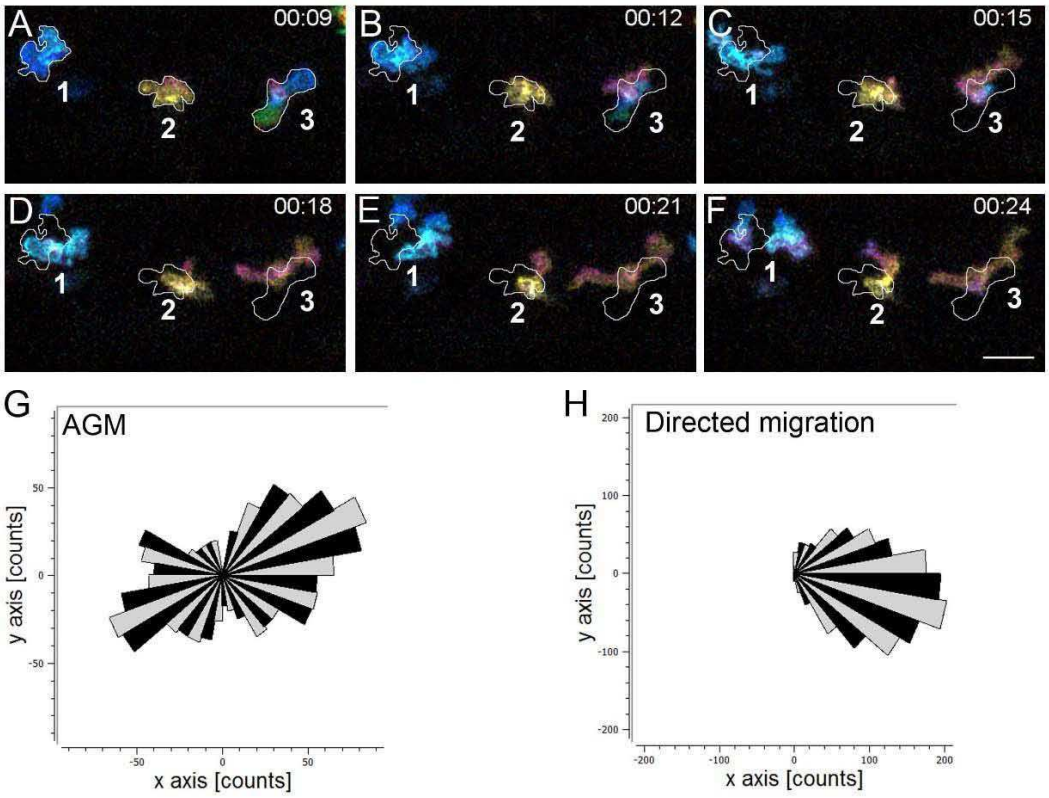
A
00:09
1
2
3
B
00:12
1
2
3
C
00:15
1
2
3
D
00:18
1
2
3
E
00:21
1
2
3
F
00:24
1
2
3
G
AGM
y axis [counts]
x axis [counts]
H
Directed migration
y axis [counts]
x axis [counts]
I
Elongated
Star-like shape
Amoeboid
Round
M1
M2
M3
M4
M5
M6
M7
M8
M9
M10
0
5
10
15
20
25
30 min

Figure 3

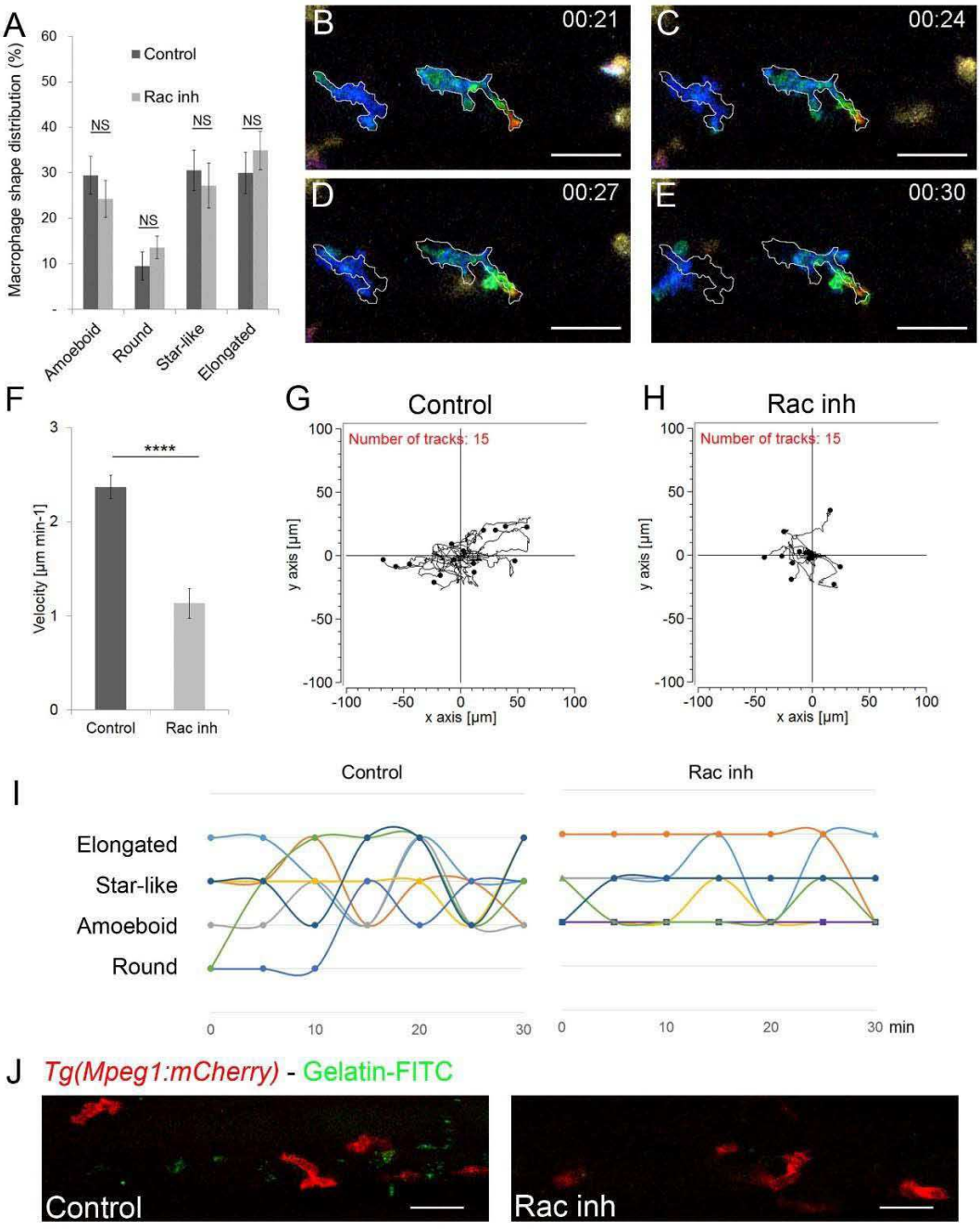
A
Macrophage shape distribution (%)
Control
Rac inh
NS
Amoeboid
Round
Star-like
Elongated
B
00:21
C
00:24
D
00:27
E
00:30
F
Velocity [µm min-1]
****
Control
Rac inh
G
Control
Number of tracks: 15
y axis [µm]
x axis [µm]
H
Rac inh
Number of tracks: 15
y axis [µm]
x axis [µm]
I
Control
Rac inh
Elongated
Star-like
Amoeboid
Round
min
J
Tg(Mpeg1:mCherry) - Gelatin-FITC
Control
Rac inh

Figure 4

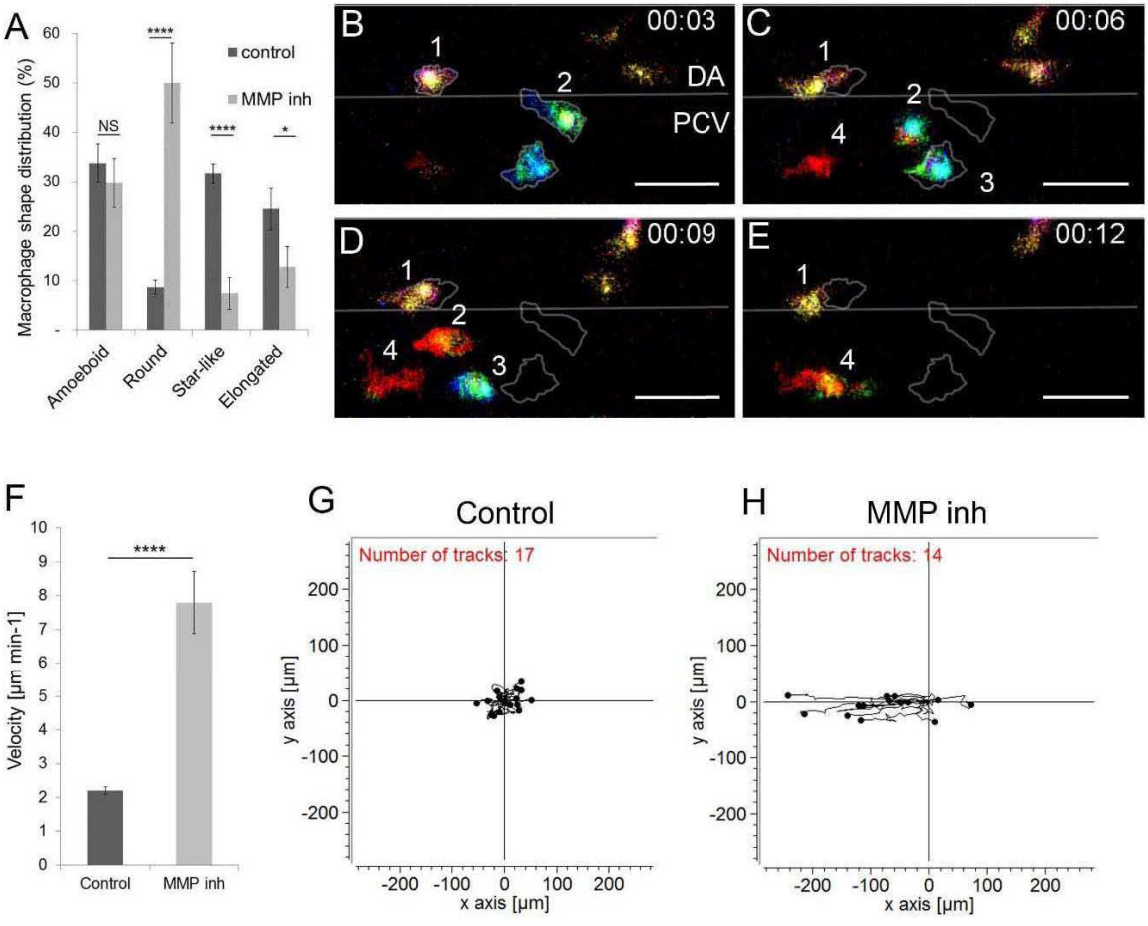
A
Macrophage shape distribution (%)
control
MMP inh
NS
****
****
*
Amoeboid
Round
Star-like
Elongated
B
00:03
DA
PCV
C
00:06
D
00:09
E
00:12
F
Velocity [µm min-1]
****
Control
MMP inh
G
Control
Number of tracks: 17
y axis [µm]
x axis [µm]
H
MMP inh
Number of tracks: 14
y axis [µm]
x axis [µm]

Supplementary Table 1.

Shape	Circularity	Roundness	Elongation factor
Round	0.19 ± 0.01	0.65 ± 0.04	1.55 ± 0.10
Amoeboid	0.07 ± 0.004	0.49 ± 0.01	2.04 ± 0.05
Star-like	0.07 ± 0.004	0.70 ± 0.01	1.56 ± 0.07
Elongated	0.07 ± 0.005	0.35 ± 0.01	3.45 ± 0.14

2.2. Dynamics of macrophage migration: complementary results

In the manuscript "Real time imaging of macrophage *in vivo* behaviour" we analysed the morphology and behaviour of zebrafish macrophages in the AGM. These macrophages degrade the ECM to mobilise the HSPCs from the AGM. This specific function of macrophages was described and analysed in the part 1 of results. In the part 2, the morphometric analysis identified 4 different cell shapes present *in vivo*, while *in vitro* most often only two categories were used. Live imaging revealed that macrophages successively adopt all four shapes as they migrate through the AGM. Treatment with inhibitors of MMPs or Rac, which are indispensable for mesenchymal migration of cells, suppressed both ECM degradation and HSPC mobilisation. They differently affected the macrophage behaviour. While Rac inhibition impaired the migration but did not affect the shape distribution significantly, the MMPs inhibition induced the changes in both, the shape distribution and the migratory behaviour.

Here I am presenting several complementary results which are not part of the manuscript but might give several perspectives of my project. First of all, we identified four shape categories present in the AGM. Regarding the macrophage morphology *in vitro*, the most often described shapes were the round and the elongated shape (McWhorter et al., 2013). We observed much higher diversity in the macrophage shape during the morphometric analysis *in vivo* in the zebrafish AGM. To confirm that these shapes can be found also in different zebrafish tissues, we performed macrophage morphometric analysis in the zebrafish tail region, in the CHT respectively at 48 h.p.f. All 4 shape categories are present in the CHT but the distribution differs. The proportion of round shape predominates while the elongated and the star-like shapes remain in minority (**Figure 29**). The data suggest the high diversity of macrophage shapes *in vivo* in all tissues. The percentage distribution then differs accordingly to the distinct tissue composition and the signalling factors.

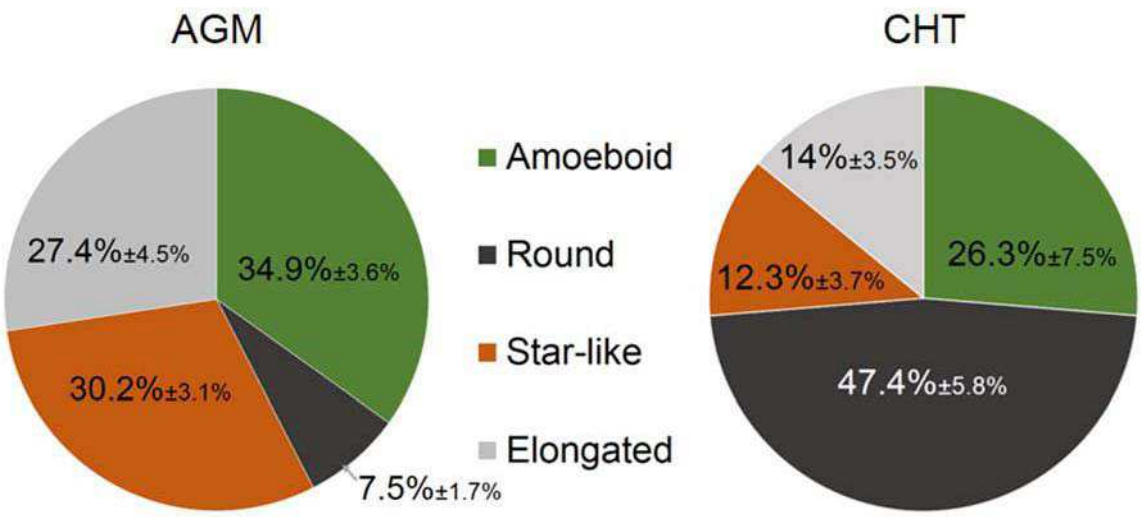

Figure 29 – Macrophage shape distribution in the different zebrafish tissues:
The quantification of the 4 macrophage shape categories in the AGM (this graph is copied from the panel Figure 1E of the manuscript – for the purpose of the direct comparison) and in the CHT. The data represented as percentage average ± s.e.m. AGM, Aorta-gonad-mesonephros; CHT, caudal haematopoietic tissue.

The cell shape and the cell migration are dependent on several factors which can be divided into 2 groups – extrinsic factors such as the signalling pathways and ECM characteristics and - intrinsic factors including the cytoskeleton architecture of the cell. We analysed several components of macrophage cytoskeleton. We primarily focused on the actin because the actin polymerisation and acto-myosin contraction differently control the type of migration and the cell protrusion formation. The F-actin staining of macrophages showed the specific accumulation of actin at the edge of the macrophage membrane in physiological conditions (**Figure 30A**). Those actin rich structures resemble to the protrusions at the leading edge of macrophages during their mesenchymal migration. However, other markers, such as vinculin and paxilin need to be analysed to confirm if this structures might be podosomes on the leading edge. Unfortunately, the preliminary experiments using the commercially available antibodies were not successful and zebrafish specific antibodies have to be synthetized.

After Rac or MMP inhibition, the actin rich structures were still found in macrophages, but the localisation differed. Rac-inhibited macrophages formed the actin accumulations on the membrane without the specific localisation to the edge (**Figure 30B**). This observation is in agreement to the live imaging and membrane extension analysis and confirms the loss of macrophage polarity and the leading edge. The MMP inhibition did not impair the actin accumulation neither. In contrary, the accumulations were found in higher

density and dispersed at large area of the membrane (**Figure 30C**). The observed structures resemble to the actin polymerisation along the plasma membrane to increase the cell stiffness which is one of the factors of amoeboid migration. This result is again in the accordance to the live imaging, which showed the predominating round shape and increased speed of migration of macrophages - other markers of amoeboid migration. Although the actin staining helped to the characterisation of macrophage cytoskeleton, the additional markers are also required to fully confirm the identity of the actin structures and their function. Moreover, live imaging of actin dynamics during their migration would significantly improve our understanding of macrophage behaviour during their migration in physiological and non-physiological conditions.

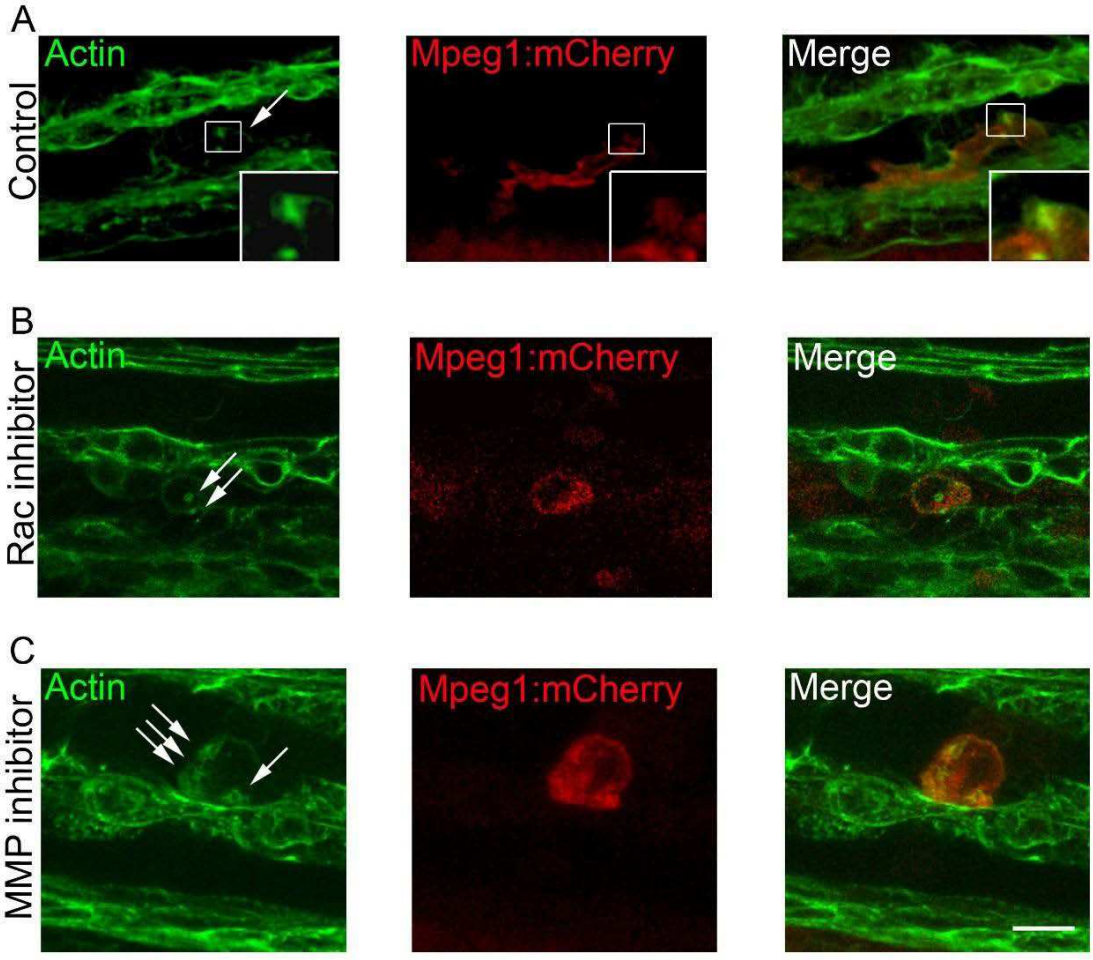

Figure 30 – Actin staining of macrophages at different conditions:
(A) F-actin accumulates at the edge of a macrophage membrane in the physiological conditions. (B) Several structures of F-actin accumulation are present in macrophages after Rac inhibiton and distributed more randomly than in control. (C) Actin rich structures are more dispersed and localised in relatively large area in macrophages after MMP inhibition. Scale bar = 10 μm, white arrows – actin accumulation.

Macrophage behaviour is importantly affected after the Rac or MMP inhibition. Their shape, cytoskeleton, polarity, speed and way of migration changed with the treatment. Recently, increasing attention has been paid to the possible correlation between macrophage shape and molecular phenotype. *In vitro* studies showed that mechanically induced elongated shape of macrophages was associated with the increased expression of M2-like polarisation markers, such as arginase or CD206 (McWhorter et al., 2013). We analysed if the morphological and behavioural changes are also associated with the changed polarization marker expression. When we compared by quantitative RT-PCR the mRNA profile between control and Rac inhibited embryo, we detected increased expression of several pro-inflammatory markers such as *tnfa*, *tnfb*, *il1b* and *il6* in the zebrafish trunk region compared to control (**Figure 31**). The expression of M2 like polarization markers, such as *Arg1* and *2*, *mrc1a* or *tgfb* did not differ from the control. These results suggest that Rac inhibition does not only affect the migratory capacity and plasticity of macrophages but it also decreases their proteolytic activity and polarizes them toward a more pro-inflammatory identity. Interestingly, the MMP inhibition did not significantly alter the expression of the pro-inflammatory markers in trunk region with the exception of *il6*. Therefore, the changes in expression of polarization markers appear to be specific for the Rac inhibition in the embryo.

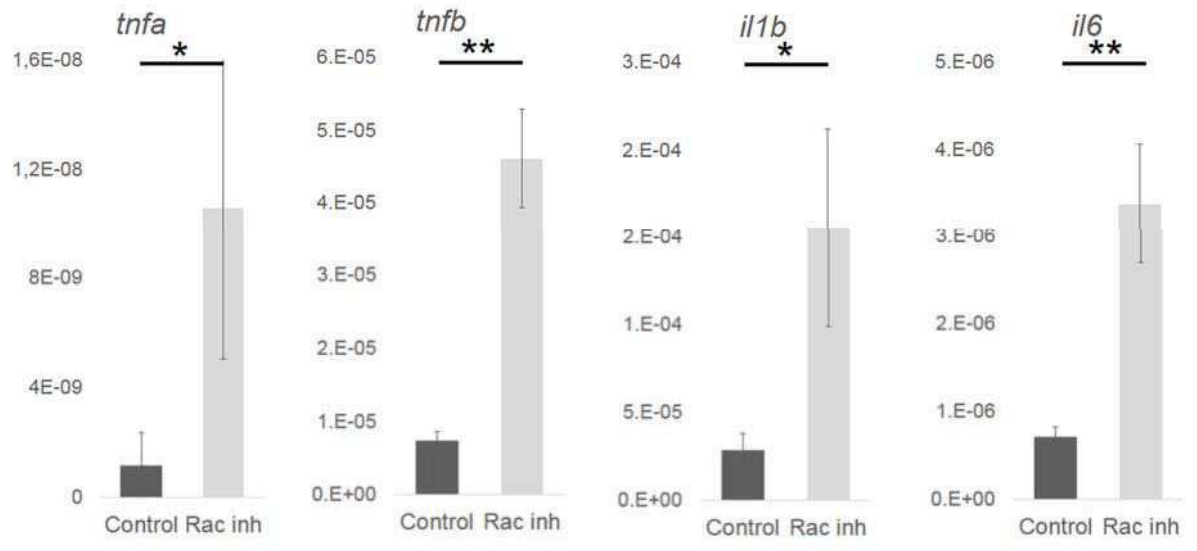

Figure 31 – mRNA expression of pro-inflammatory marker:
Quantitative RT-PCR (qPCR) analysis shows an increased mRNA expression of pro-inflammatory markers (*tnfa, tnfb, il1b and il6*) in the zebrafish trunk region after Rac inhibition. Relative expression of specific genes in DMSO treated or Rac inhibitor-treated embryos is indicated normalized to *ef1a* reference gene expression. Data represent mean ± s.e.m. from 5 independent experiments of N= 35 embryos per condition. * P<0.05; **P<0.01.

The increased expression of pro-inflammatory markers after rac inhibition coincidences with the changes in the behaviour and migration of macrophages. Currently, it is difficult to postulate if the two events are directly correlated or if the rac inhibition affect several parameters independently. In addition, the analysis of the markers was not restricted to sorted macrophage but done in RNA extracted from the whole trunks. The analysis of sorted macrophages would confirm their pro-inflammatory phenotype.

The results presented in this part complete the manuscript and these preliminary observations propose future directions of experiments. The use of zebrafish embryo will permit an *in vivo* analysis of macrophages and their direct tracking in their natural ECM scaffold. Therefore, it may serve as a suitable model completing the striking analysis already performed *in vitro*.

3. Nervous system and definitive haematopoiesis

3.1. Article 3: Catecholamines control definitive haematopoiesis in the zebrafish embryo

Catecholamines control definitive haematopoiesis in the zebrafish embryo

Manuscript in preparation

Graphical abstract:

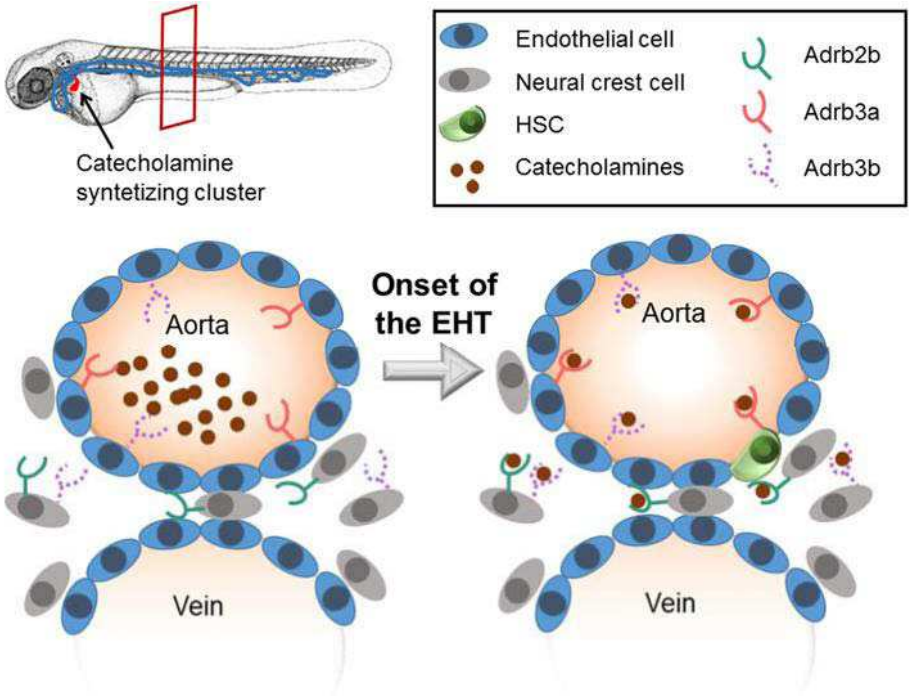

Key points:

- All adrenergic beta receptors are expressed in the AGM at the time of EHT
- Knock-down of Adrb2b and Adrb3 completely or partially impairs the EHT and haemogenic endothelium identity
- The sympathetic local innervation is established after the initiation definitive haematopoiesis
- The catecholamines produced by TH2 expressing cells activate through the blood circulation the beta receptors in the AGM

Introduction

Haematopoietic stem cells (HSCs) are self-renewing stem cells giving rise to all blood cell lineages. The generation of HSCs is initiated in the aorta-gonads-mesonephros (AGM) region at 30 hours post fertilisation (h.p.f.) in the zebrafish embryo. HSCs emerge from the haemogenic endothelium in the ventral wall of the dorsal aorta in a process conserved among all vertebrates (Bertrand et al., 2010a; Boisset et al., 2010; Kissa and Herbomel, 2010; Lam et al., 2010). The haemogenic endothelial cells, which are specified by the runx1 marker (Chen et al., 2009; Lam et al., 2010) transdifferentiate into HSCs by a process called endothelial-to-haematopoietic transition (EHT). During this transition, the endothelial cells lose their polarity, start to bend and get round before to detach from aorta and to express haematopoietic markers, such as cd41 (Kissa and Herbomel, 2010; Kissa et al., 2008).

The role of the environment in the regulation of haematopoiesis had been the subject of many researches in last years. The sympathetic nervous system has been recently described in the haematopoietic microenvironment (Fitch et al., 2012; Katayama et al., 2006). The sympathetic nervous system is part of the peripheral nervous system and arises from the neural crest (Douarin and Smith, 1988). The sympathetic precursors delaminate from the neural crest and migrate ventrally toward the dorsal aorta (Theveneau and Mayor, 2012). At this stage they express neural crest specific markers, such as, Sox10 or FoxD3 (Rohrer, 2011; Stewart et al., 2006). Once they reach the aorta, they start to differentiate into sympathetic neurons, synthetize and release catecholamines. Catecholamines are produced by an enzymatic cascade in which tyrosine hydroxylase (TH) is the first rate limiting step of synthesis. In zebrafish, two TH proteins have been described with distinct location and have been encoded TH1 and TH2 (Semenova et al., 2014). The family of catecholamines consists of three transmitters – dopamine, noradrenaline and adrenaline (Goridis and Rohrer, 2002).

Adrenaline and noradrenaline are the transmitters of the sympatho-adrenal system which combines the role of two different systems – the nervous system represented by sympathetic nerves and the hormonal system represented by the adrenal medulla which synthetises and releases adrenaline to the organism. Catecholamines then activate adrenergic receptors in the target tissue to initiate a cellular response. Two classes of adrenergic receptors exist in vertebrates and are called alpha – adra1 and adra2 – and beta – adrb1, adrb2 and adrb3, seven transmembrane proteins (Muthu et al., 2007). The majority of these receptors is associated with the cardiovascular system. However, only Adrb2 and Adrb3 are receptors playing a role in haematopoiesis (Fitch et al., 2012; Katayama et al., 2006; Muthu et al., 2007).

In mouse embryo, sympathetic nervous system regulates definitive haematopoiesis through the Adrb2 receptor. Adrb2 and Adrb3 are expressed in the AGM at the onset of definitive haematopoiesis. The first receptor is expressed by endothelial cells and HSCs whereas the second one predominates in mesenchymal cells. The Adrb receptors are activated by catecholamines released locally from the sympathetic nerves present in sub-aortic region (Fitch et al., 2012).

In zebrafish embryo – due to the genome duplication in teleosts - 5 beta receptors are expressed: adrb1, adrb2a, adrb2b, adrb3a and adrb3b (Wang et al., 2009). Zebrafish adrb receptors share relatively high percentage of sequence identity with their human orthologs with in average 50% homology. They are all already expressed at 18 h.p.f., therefore they might be involved in the embryonic haematopoiesis in zebrafish. Their expression in adult organs differs upon the receptor type. Adrb1 and adrb2a are expressed in high a variety of organs, while adrb2b remains restricted to the muscle, pancreas, liver and blood and both adrb3 receptors show the highest expression in the blood (Wang et al., 2009).

Considering the studies performed in the mouse embryo and the importance of the sympathetic nervous system in definitive haematopoiesis, we hypothesised that it may also be involved in definitive haematopoiesis in the zebrafish embryo. We therefore characterised the expression of the adrenergic receptors in the zebrafish embryo and analysed their role during definitive haematopoiesis. Interestingly, we described that despite the lack of dorsal aorta sympathetic innervation during the first steps of HSC emergence, adrenergic receptors are activated. Therefore, we propose a new way of catecholamine mediated activation from the distant area through the blood circulation delivery.

Results

Adrenergic receptors are expressed in the zebrafish AGM

Zebrafish beta adrenergic receptors are expressed in the embryos from early stages of development. They are already detected from 18 h.p.f. by quantitative RT-PCR (Wang et al., 2009). This timing corresponds to the onset of haematopoiesis which suggests that the receptors may be involved in this process. Using whole mount *in situ* hybridisation (WISH) we detected all 5 beta adrenergic receptors localised in the AGM at 30 h.p.f. (**Figure 1-2**) in the zebrafish embryo. The expression pattern of individual receptors differs in the zebrafish trunk. The *Adrb1* and *Adrb2a* receptors show a diffuse pattern through the whole trunk and predominantly in the muscles (**Figure 1A-B**). The *Adrb2b* and *Adrb3b* also exhibit a diffuse pattern but with higher expression in the ventral part of the trunk corresponding to the AGM region (**Figure 1C-D**).

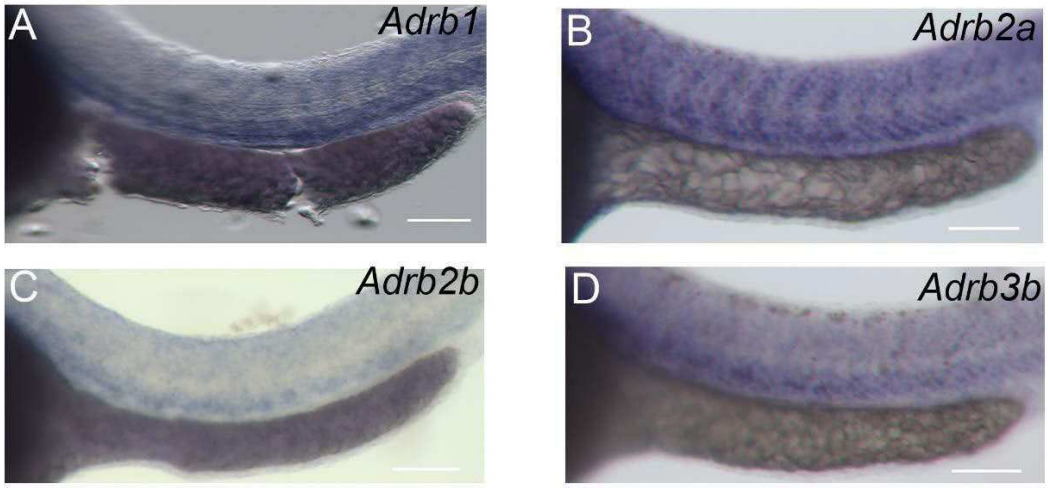

Figure 1: Adrenergic receptors are expressed in the zebrafish trunk. The zebrafish pattern of (A) *Adrb1*, (B) *Adrb2a*, (C) *Adrb2b* and (D) *Adrb3b* receptors at 30 h.p.f. Scale bar = 100 µm

Interestingly, *adrb3a* is exclusively expressed in the AGM region (**Figure 2A**). The high resolution imaging revealed that the receptor is expressed on the surface of erythrocytes (**Figure 2B**) and potentially on vascular endothelium. To further confirm the endothelium specific expression, we performed WISH coupled to immunostaining of kdrl endothelial marker.

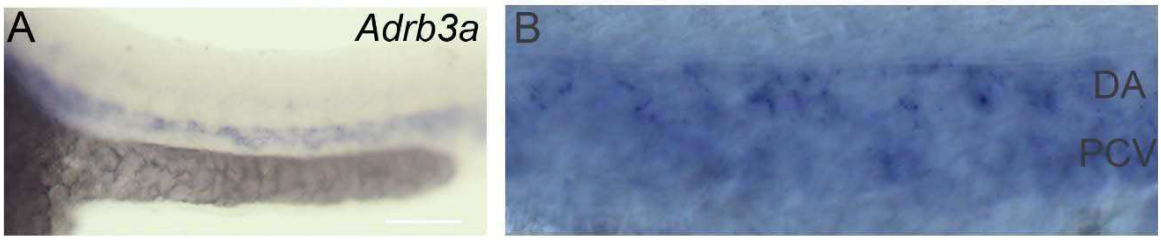

Figure 2: Adrenergic receptor *adrb3a* is expressed in the AGM region. (A) The expression patters of *adrb3a* receptor in the zebrafish trunk at 30 h.p.f. Scale bar = 100 µm. (B) High magnification of the AGM shows expression in the erythrocytes and vessels. DA, dorsal aorta; PCV, posterior cardinal vein.

Co-staining of WISH with the kdrl endothelial cell marker allowed to confirm the expression of *adrb3a* receptor by aortic endothelial cells (**Figure 3B**). We used the same approach for the *adrb2b* and *adrb3b* receptors to further evaluate the localisation of these receptors. However, the expression patterns of *Adrb2b* and *Adrb3b* receptors did not allow to clearly identify their co-localisation with the vascular endothelium (**Figure 3A and C**). The co-localisation assay of WISH with an immunofluorescence staining still remains a challenging experiment depending on the expression pattern of detected RNA. Strong diffuse signal may not permit to perform a detailed analysis of cells. An adaptation of the protocol should permit us to decrease the background associated with this double staining. Thus, at this stage of our study, we can only suggest that some endothelial cells expressed *adrb3b* (white arrows, **Figure 3C**). We propose to complete this experiment with transversal sections of embryos to more accurately determine the cell expressing *adrb2b* and *adrb3b* receptors. Determining the cell type expressing the receptors would permit to understand precisely how they can be involved in the process of haematopoiesis. The expression of the beta receptors decreases in later stages of the embryo development and becomes restricted to the central nervous system and heart at 48 h.p.f. which corresponds to the peak of the HSC emergence (data not shown). This suggests that none of the beta receptors is expressed on the surface of nascent HSCs. The high expression at 30 h.p.f. during the initial steps of haematopoiesis and following by a decrease correspond to

temporal expression of transcription factors controlling the EHT initiation. Runx1 is one of these factors and its temporal expression matches to the expression of adrb receptors. We can hypothesise that these receptors could play a role in the regulation of EHT initiation.

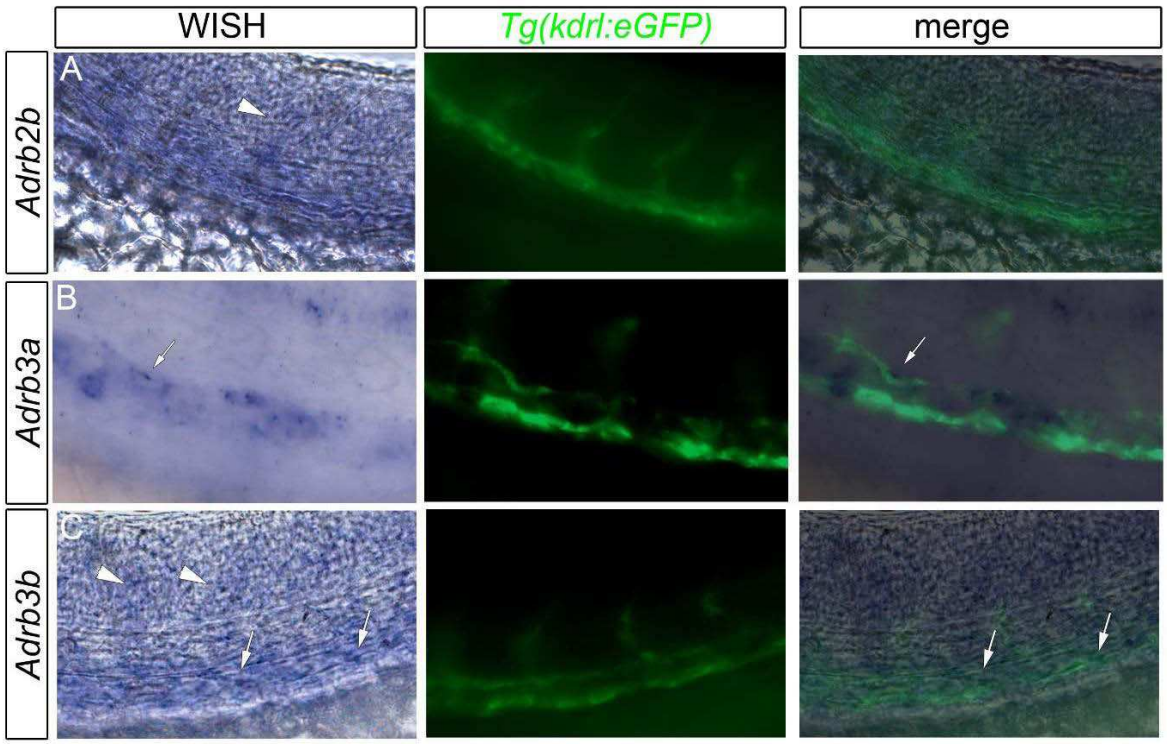

Figure 3: Adrenergic receptors are expressed in the AGM. Co-staining of adrenergic receptor expression with vascular endothelium. (A) *Adrb2b* WISH, (B) *Adrb3a* WISH and (C) *Adrb3b* WISH combined with the GFP immunofluorescence (green) in *Tg(kdrl:eGFP)* embryos at 30 h.p.f. White arrows indicate co-localisation with the endothelial cells, white arrowheads point signal in somitic muscles

The Adrb2b and Adrb3 receptors are required for definitive haematopoiesis

The expression of all receptors in the AGM suggested that they may be involved in the process of haematopoiesis. Therefore we performed a functional analysis of all receptors. The morpholino induced genetic knock-down of Adrb1 and Adrb2a did not affect HSC emergence. Indeed the number of cd41 cells in the AGM at 48 h.p.f. did not significantly differ from the number in control embryos (data not shown). In contrary, the Adrb2b morpholino severely impaired definitive haematopoiesis. The number of cd41 cells decreased of 89% compared to

the control (**Figure 4A-B**). This result was confirmed by the runx1 expression – one of the earliest marker of HSC identity - which was reduced in morphant embryos at 30 h.p.f. (**Figure 4C**). This results emphasise how important will be to determine the *adrb2b* receptor localisation.

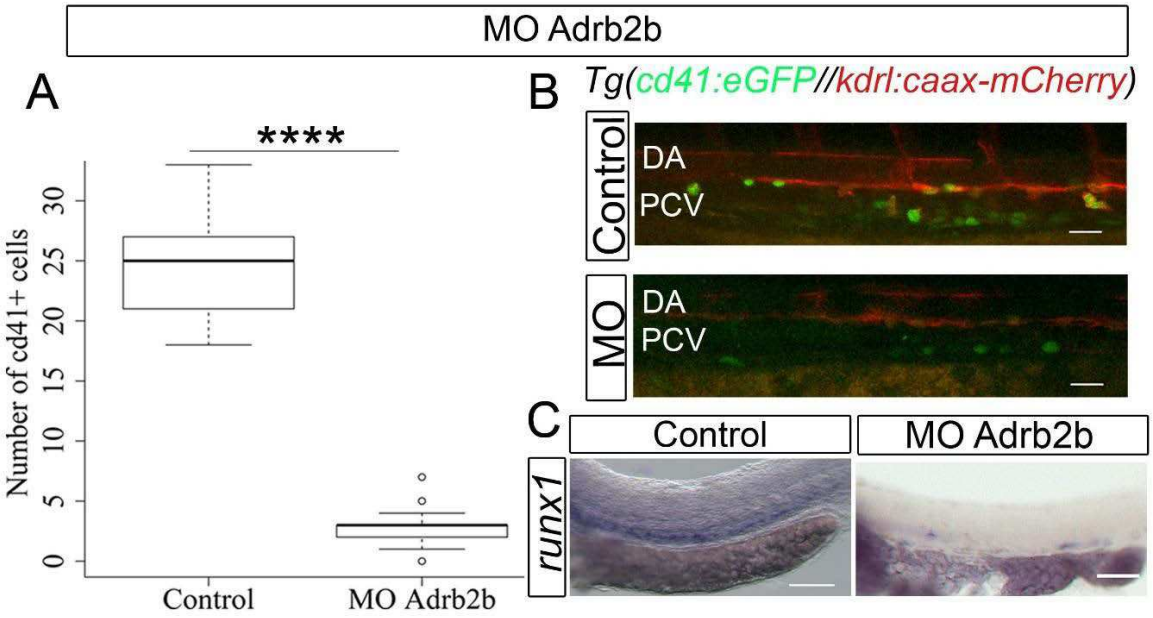

Figure 4: Absence of Adrb2b receptor impairs definitive haematopoiesis. (A) Morpholino Ardb2b disrupts HSC emergence counted as cd41+ cells in the AGM at 48 h.p.f. Data are represented in a boxplot showing minimum (lower whisker) and maximum (upper whisker), as well as 1st and 3rd quartile (bottom and top of box, respectively), and median (central thicker line). N=13 embryos. (B) Representative maximum projections of the AGM region show the cd41+/HSCs (green) and vascular endothelium (red) in control (top) and morphants (bottom). (C) The *runx1* expression in the AGM at 30 h.p.f. in control (left) and morphants (right). Scale bars = 30 µm (B) and 100 µm (C). **** $p < 0.0001$.

The genetic knock-down of Adrb3a and Adrb3b also affected HSC emergence. The number of HSCs in the AGM decreased of 50% and 68% respectively (**Figure 5A-D**). Runx1 expression was altered at 30 h.p.f. suggesting that both receptor activation are important during the early stages of the EHT (**Figure 5E**). The genetic knock-down of adrb receptors revealed that only three receptors play a role during definitive haematopoiesis – adrb2b, adrb3a and adrb3b although all five receptors are expressed in the zebrafish trunk region at 30 h.p.f.

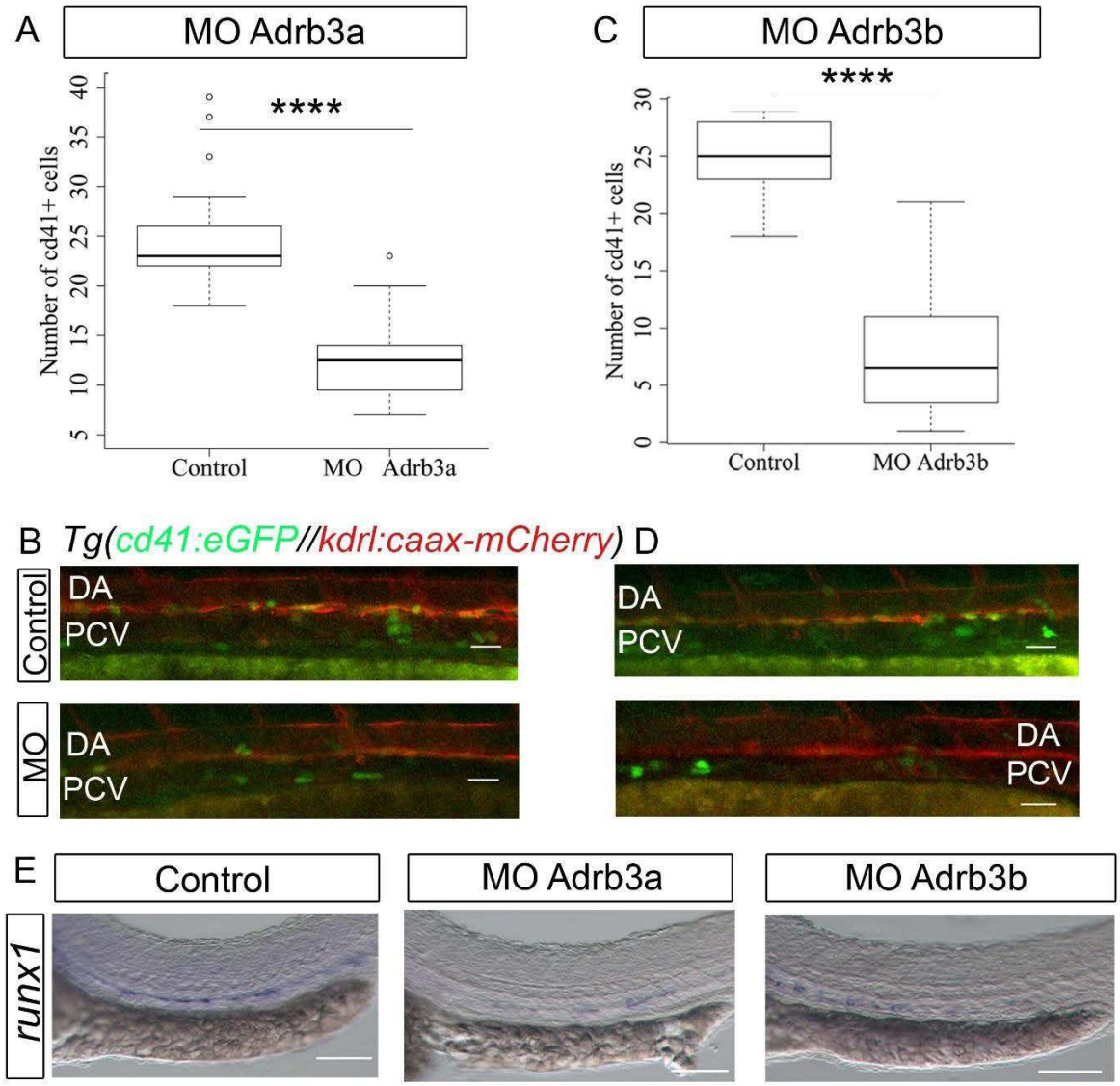

Figure 5: Absence of Adrb3a and Adrb3b receptors impairs definitive haematopoiesis. (A) Morpholino Adrb3a decrease HSCs emergence counted as the cd41+ cells in the AGM at 48 h.p.f. Data are represented in a boxplot. N= 20 (B) Representative maximum projections of the AGM region show the cd41+/HSCs (green) and vascular endothelium (red) in control (top) and morphants (bottom). (E) Morpholino Adrb3b decreases HSCs emergence counted as the cd41+ cells in the AGM at 48 h.p.f. Data are represented in a boxplot. N=9 for control and N=8 for MO Adrb3b. (F) Representative maximum projections of the AGM region show the cd41+/HSCs (green) and vascular endothelium (red) in control (top) and morphants (bottom). (E) The *runx1* expression in the AGM at 30 h.p.f. in control and morphants. Scale bars =30 µm (B) and 100 µm (C).

To further confirm the role of Adrb2b receptor, we used a pharmacological inhibitor of beta 2 receptor ICI-118,551 at the concentration which was already demonstrated in the zebrafish embryo (Kumai et al., 2012). We observed a decreased number of HSCs in the AGM

of 50% compared to DMSO treated control (**Figure 6A-B**). The less pronounced effect can be explained by the use of human ADRB2 specific inhibitor, whose affinity to the zebrafish receptors has not been evaluated. It would be also interesting to evaluate whether the inhibitor impairs the *runx1* expression alike the morpholino.

We also evaluated the specific role of Adrb3 receptors by using their pharmacological inhibitor SR59230A. The concentration of inhibitor was determined experimentally according to its effect/toxicity ratio. The pharmacological inhibition exhibited same effect on the HSC number in the AGM as in the morphants (-49% cd41 cells, **Figure 6C-D**).

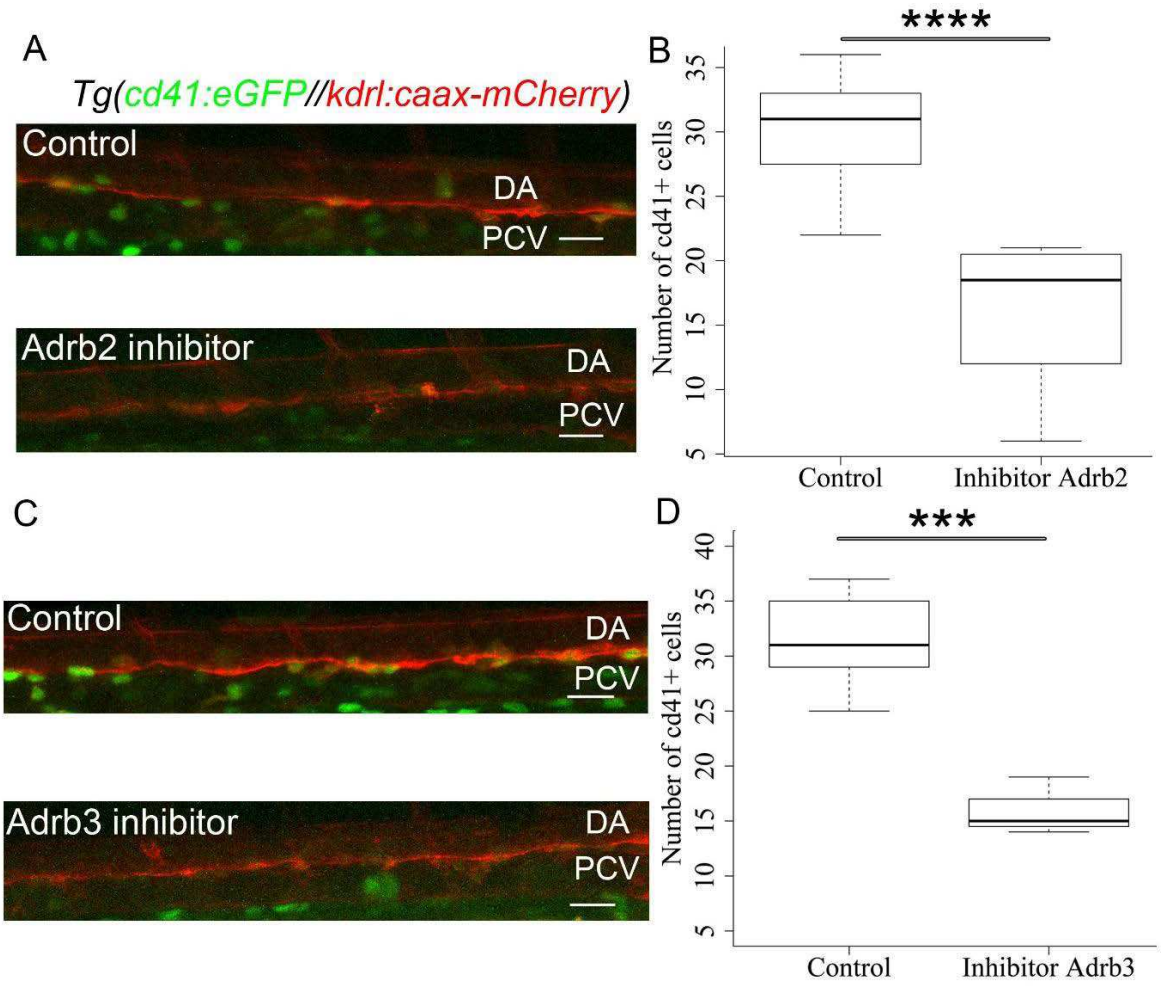

Figure 6: Adrb2 and Adrb3 inhibitors decrease HSC emergence. (A) Representative maximum projections of the AGM region show the cd41+/HSCs (green) and vascular endothelium (red) in DMSO treated control (top) and adrb2 inhibitor (bottom). Scale bar = 30 µm (C) The quantification of the HSC emergence counted as cd41+ cells and represented in a boxplot. N= 8 embryos. **** $p < 0.0001$.
(C) Representative maximum projections of the AGM region show the cd41+/HSCs (green) and vascular endothelium (red) in DMSO treated control (top) and adrb3 inhibitor (bottom). Scale bar = 30 µm (D) The quantification of HSC emergence counted as cd41+ cells and represented in a boxplot. N= 10 embryos for control and N= 3 embryos for inhibitor. *** $p < 0.001$.

To analyse the reason of decreased HSC number in the AGM we performed a live imaging of EHT events from the aortic endothelium. We observed several fragmented endothelial cells in the dorsal aorta in morphants. The fragmented cells were localised exclusively at the ventral side of the aorta and prior to HSC specification. Endothelial cells broke into fragments before they started to bend and lose their polarity or express cd41 marker (**Figure 7, Supplementary movies 1-3**). It remains to be evaluated which mode of the cell

death was detected in endothelial cells. Markers of apoptotic cells will be applied. This suggests that the adrenergic receptors play a major role in the haemogenic endothelium survival. In addition to the fragmented cells, we observed decreased HSC emergence in morphants and part of the emerging cells did not succeed to finish the EHT process.

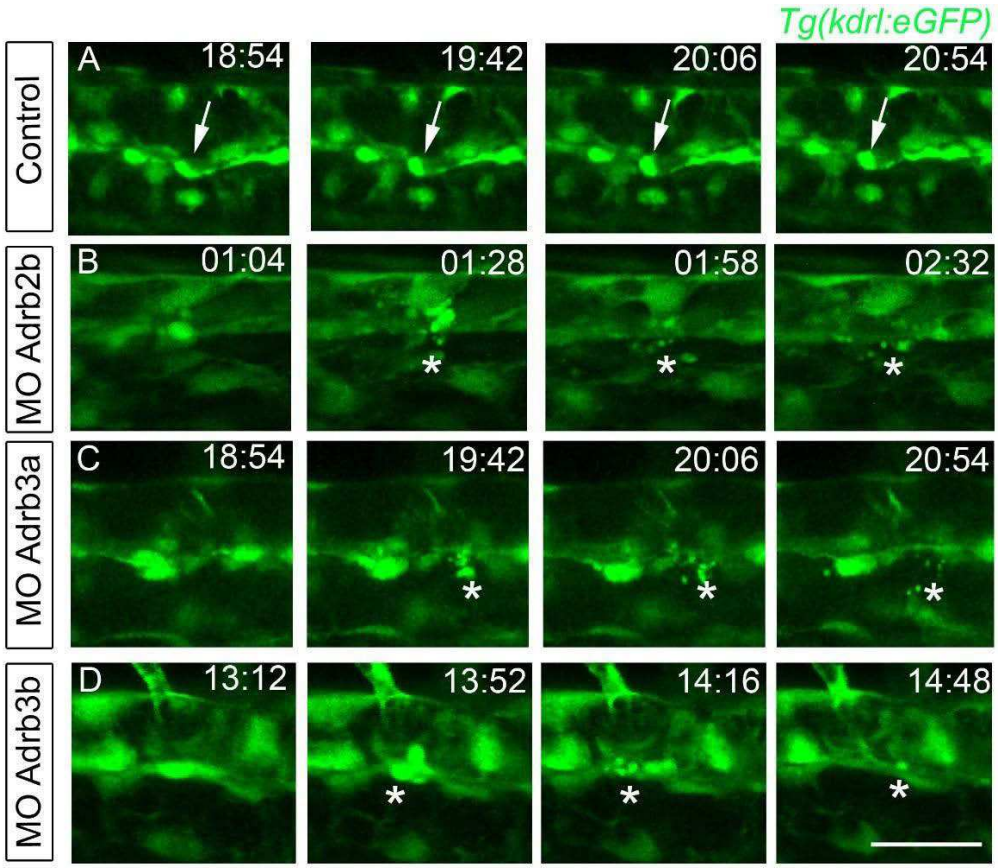

Figure 7: Endothelial cell fragmentation in absence of Adrb2 and 3 receptors. (A) An EHT event (white arrow) in the physiological conditions. (B-D) The examples of the endothelial cell fragmentations (white asterisks) of ventral wall of dorsal aorta in absence of Adrb2b (B), Adrb3a (C) or Adrb3b (D) expression. The photo sequences were cropped from the supplementary movies 1-3. Time is indicated in hours and minutes counted from the beginning of the acquisition at 30 h.p.f. Scale bar: 30 µm. See also supplementary movies 1-3.

During EHT process, the DA diameter exhibit specific changes summarised as a dilation followed by contraction at the peak of HSC emergence corresponding to 48 h.p.f. (Kissa and Herbomel, 2010). In the absence of adrb receptors the aorta dilation corresponding to the initial

steps of EHT is impaired. A detailed analysis of Adrb3a morphants showed missing dilation step whereas the contraction still occurred (**Figure 8**). As a result of the impaired dilation, the diameter of the aorta during the whole period of EHT was smaller than in control embryos. The effect of other receptors was not evaluated in details but preliminary results suggest that the dilation is also impaired (**Supplementary movies 1 and 3**). Further analysis is required to determine if all three receptors influence the aorta dilation and if we can establish a correlation between impaired dilation and HSC emergence. Results of live imaging suggest that several mechanisms controlling the establishment of haematopoiesis should be considered, including cell survival, aorta dynamics during EHT and impaired EHT process itself.

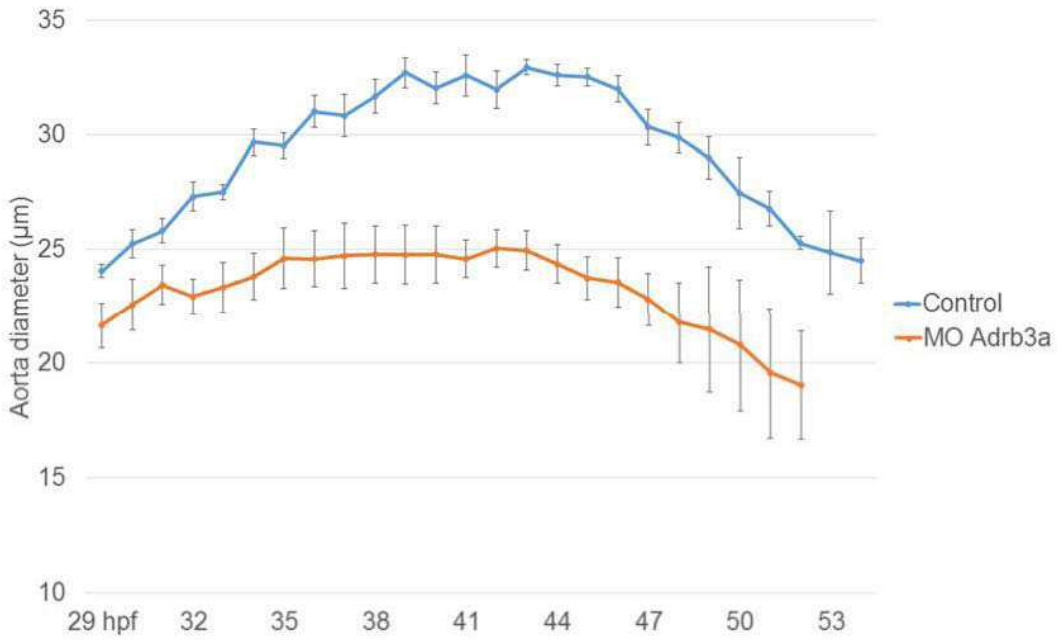

Figure 8: Dynamic shrinking of dorsal aorta. The measurements of aorta diameter (average of 10 measures per aorta) in control and morphants adrb3a every hour for 24 hours. Data represented as average ± s.e.m. of N=4 embryos.

Sympathetic nerves start to innervate the DA after the onset of definitive haematopoiesis

The adrenergic receptors are effectors of the sympathetic nervous system action. The catecholamines released from the nerve synapsis activate the receptors and induce the downstream signalisation. In the zebrafish AGM region, the first matured sympathetic neurons were found at 48 h.p.f. at vicinity of the dorsal aorta (**Figure 9A**). These sympathetic neurons originated from the neural crest cells as described earlier (Stewart et al., 2006) and as we confirmed by the FoxD3 marker co-localisation (**Figure 9A**). However, the receptors appear to play a role at 30 h.p.f. regarding the previous results and at this stage the dorsal aorta is not locally innervated (**Figure 9B**). We can already detect the presence of the neural crest cells in the AGM, but negative for sympathetic system markers (**Figure 9B**).

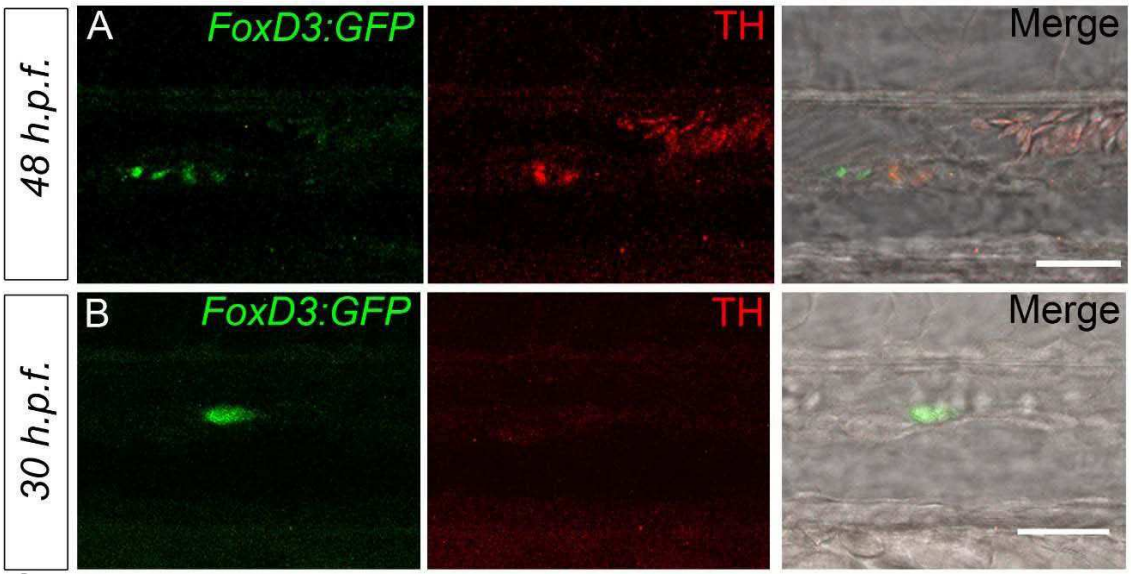

Figure 9: Tyrosine hydroxylase expression in the AGM (A) The TH protein is found in the AGM in neural crest cells at 48 h.p.f. but is absent at 30 h.p.f. (B). Scale bar = 30 µm.

We then used HPLC combined with electrochemical detection to evaluate the level of the synthetized catecholamines present in the embryo. Indeed, we detected noradrenaline already at 30 h.p.f. suggesting a presence of catecholamine synthetizing cells (**Figure 10**). To

exclude the role of neurotransmitters present is the central nervous system, which is known to be one of the first organ releasing catecholamines, we repeated the catecholamine detection in the decapitated embryos. We concluded that the noradrenaline was also present in the peripheral tissues (**Figure 10**). Even though adrenaline was not detected in embryos at 30 h.p.f. it can still be produced but at low level technically not detectable by this method. The detection of catecholamines in zebrafish embryo was very challenging experiment due to the sample size. It is not technically possible to use single embryo for detection because a minimum of 50 milligrams of material is required, which correspond approximately to 150 embryos at 30 h.p.f. The previous studies performed using the 48 h.p.f. zebrafish embryos showed that adrenaline is present at 2-4 fold lower concentration compared to noradrenaline and is at the limit of detection at this stage (Steele et al., 2011). For this reason, we suppose that adrenaline can be already produced in the embryo but under the detection limit of method. To confirm this supposition, an assay using a higher number of embryos could permit to reach the detection limit and potentially to measure the adrenaline presence in the embryo.

Condition	Amount (pg)	Peak area	Concentration (mol/l)
Whole embryos	**3.4241**	185488	3.4896E-08
Decapitated embryos	**1.5879**	82222	2.0405E-08

Figure 10: Noradrenaline detection is measured by HPLC coupled with electrochemical detection in whole and decapitated embryos.

To determine which cells were synthetizing the catecholamines, we performed a TH1 immunostaining. We detected the presence of 2 areas of TH1 expression –the central nervous system (**Figure 11A**) and 2 symmetric clusters of cells localised at vicinity of the lateral dorsal aorta (**Figure 11B-C**). This structure was symmetrically placed at the each side of the yolk sac. The high resolution 3D view revealed the localisation of TH1 clusters at the direct contact to

the blood vessels (**Figure 11B-C**, white arrow, and **Supplementary movie 4**). We postulated that this particular location permits the catecholamines to be released to the blood circulation and to be delivered to all tissues of the embryo including the AGM. The TH1 clusters originated from the neural crest (**Figure 11D**) alike the sympatho-adrenal system. The size of one cluster in the periphery corresponds approximately to the half of the CNS clusters. The two peripheral clusters can potentially produce the same quantity of catecholamines as the CNS. It is in agreement with the results we observed in biochemical catecholamine detection. Whole embryo contained twice the amount of catecholamines compared to decapitated embryos.

Due to genome duplication in teleosts, zebrafish embryo produces 2 TH enzymes. Previous results showed that the both TH enzymes are expressed in the CNS and localised close to each other (Semenova et al., 2014). We expect similar results also in the peripheral tissues with the expression of TH2 in the proximity to the clusters expressing TH1. However, TH2 localisation in the peripheral tissue is required to confirm this hypothesis. We are establishing a collaboration with the laboratory of Prof. Panula who developed zebrafish specific TH2 antibody in order to perform the immunostaining of the zebrafish embryo at 30 h.p.f. (Semenova et al., 2014). In addition to our results, another study demonstrated that the sympathetic innervation of dorsal aorta is established at 2 d.p.f. They used dopamine-β-hydroxylase for the detection which is the second enzyme after TH in the cascade of catecholamines and is not duplicated in the zebrafish (An et al., 2002). This additional information support our hypothesis of catecholamine synthesis in a distant region and following delivery through the blood circulation.

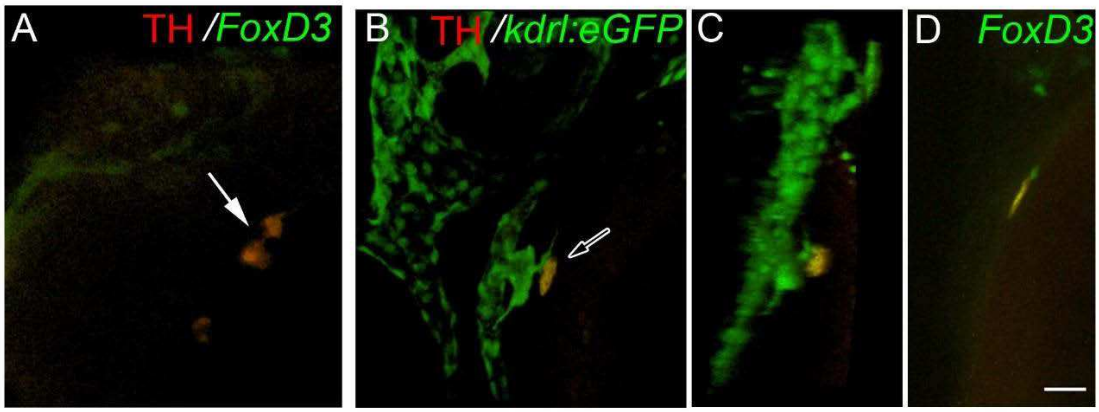

Figure 11: TH1 localisation in the zebrafish embryo. (A) Localisation of a cluster of TH expressing cells (white arrow) in the central nervous system at 28 h.p.f. (B-C) The co-staining of the TH expressing cell clusters (white arrow) with the vascular endothelium using the *Tg(kdrl:eGFP)* embryo – the lateral (B) and orthogonal view (C) - and (D) the co-localisation with the neural crest marker using the *Tg(FoxD3:GFP)* embryo at 30 h.p.f. Scale bar = 30µm

Absence of catecholamine synthesis impairs HSC emergence

To further demonstrate the effect of catecholamines on HSC emergence, we performed a MO knockdown of each TH. Due to TH duplication in the zebrafish we used a specific MO for each enzyme separately to analyse their contribution to haematopoiesis. The TH1 knock-down did not impair definitive haematopoiesis, the number of cd41 cell even slightly increased in the AGM (**Figure 12A**). The combination of 2 splice-blocking TH2 morpholino decreased the number of HSCs in the AGM of 53% compared to control (**Figure 12A**). The combined knock-down of TH1 and TH2 did not induce more profound effect than TH2 morpholino alone (data not shown). This result suggests that only TH2 enzyme is crucial for catecholamine synthesis at this stage and plays a role in definitive haematopoiesis.

In order to directly correlate the catecholamines synthesis and release with HSC emergence, we performed a rescue assay of haematopoiesis. We added Adrb2 specific agonist, Adrb3 specific agonist or adrenaline to the TH2 morphants at 18 h.p.f. to replace the missing TH-mediated synthesis by an external source. We observed a minor increase of the cd41 cells

in the AGM (approximately 32 – 36% increase depending on agonist) suggesting a partial rescue of haematopoiesis. Even though the difference was not statistically significant probably due to the low number of samples and high variability, all the conditions showed a same tendency of the increased HSC number (**Figure 12B**). The only partial rescue can be explained by several factors. The external source of catecholamines was mediated by adding the specific human agonists whose affinity to the zebrafish receptor has not been evaluated. We can presume that the human agonist will be less efficient than the zebrafish specific agonist. The concentration was used upon the published results in the zebrafish larva (Steele et al., 2011), but the range of different concentrations was not performed. Finally, we propose that catecholamines could activate the receptor through the blood circulation because of the absence of local innervation. Until now, chemical compounds were added in the zebrafish medium. Therefore, introducing the pharmacological agonist directly to the blood circulation by intravenous injection can mediate a more important rescue of HSC emergence compared to the simple soaking.

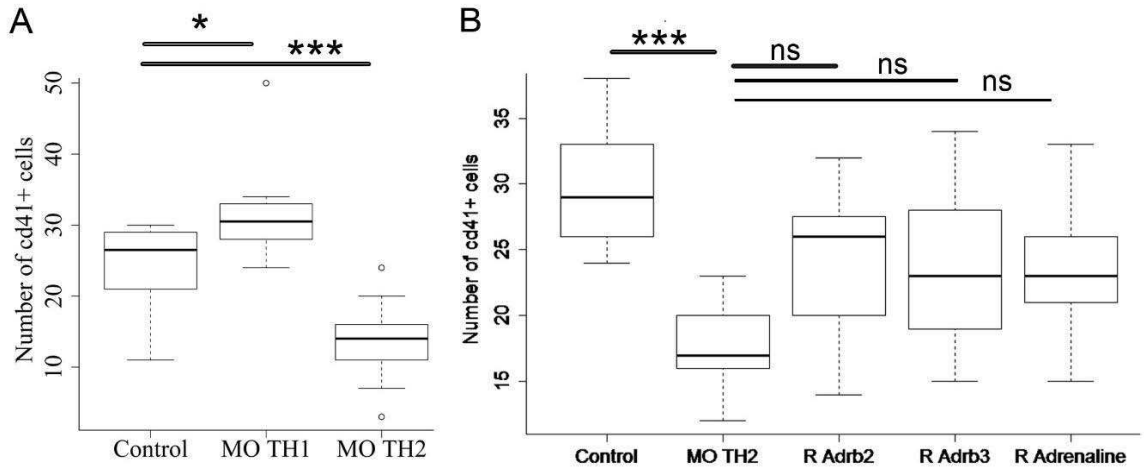

Figure 12: The tyrosine hydroxylase inhibition and rescue of haematopoiesis. (A) The decrease of HSC emergence in the AGM in the absence of TH2 but not TH1 expression. N=10 for control and MO TH1, N=18 embryos for MO TH2. (B) The rescue of haematopoiesis after TH2 inhibitor by catecholamines or specific pharmacological agonists – Adrb2 agonist, Adrb3 agonist or adrenaline. N=8 for each condition. HSC emergence is counted as the number of cd41+/HSCs in the AGM at 48 h.p.f. Data are represented in boxplots. *p < 0.05; *** p < 0.001; ns = not significant.

In order to inhibit the formation of all TH expressing cells, we repeated the same rescue experiment but during the step preceding the TH expression, which is neural crest cell specification. We inhibited the specification of the neural crest cells by using FoxD3 morpholino which impairs maintenance of the neural crest cells and development of the sympathetic nervous system (Stewart et al., 2006). The morphants exhibited disturbed EHT and the decreased number of cd41 cells in the AGM (**Figure 13A**). We performed the rescue assay of haematopoiesis using either Adrb2 or Adrb3 agonist. Adrenaline has not yet been tested in this condition. The adrb2 agonist did not exhibit any increase in the number of HSCs whereas adrb3 agonist showed a 70% increase of HSCs in the AGM compared to the morphants which indicates a partial rescue of the EHT (**Figure 13B**).

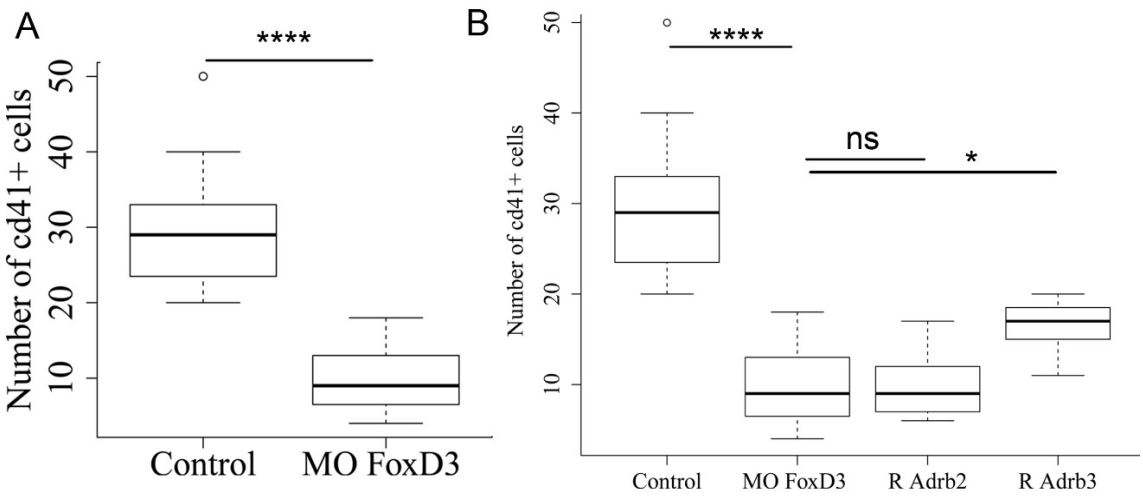

Figure 13: Neural crest inhibition affects HSC emergence in the AGM. (A) FoxD3 morpholino substantially reduces the number of HSCs emerged in the AGM. (B) The rescue of HSCs emergence is held by replacing the missing catecholamines by the specific pharmacological Adrb2 or Adrb3 agonists in the FoxD3 morphants. N = 23 for control and FoxD3 morphant, N=5 for R Adrb2 and N=7 for R Adrb3. HSC emergence is counted as the number of cd41+/HSCs in the AGM at 48 h.p.f. Data are represented in boxplots. * $p < 0.05$; **** $p < 0.0001$; ns= not significant.

Interestingly, it appears that only adrb3 receptor can mediate the rescue of haematopoiesis in FoxD3 morphants contrary to the TH morphants, where every condition

showed same tendency in the increased EHT. The absence of FoxD3 impairs the specification of most cells of neural crest origin (Stewart et al., 2006). Therefore, the adrb2 receptor might be expressed by one of the neural crest populations, for example stromal cells. The transversal sections of embryos after Adrb2b WISH could answer to this question.

Discussion

The studies described herein show the specific regulation of definitive haematopoiesis by the catecholamines through the adrenergic receptors beta 2b and 3 (Figure 14). In the absence of receptors the number of emerged HSCs decreases and several endothelial cells in the ventral wall of DA burst into pieces. The morphology of fragmented cells suggest that the cells undergo apoptosis, which remains to be directly demonstrated. In addition to the cells survival, several other mechanisms can play role in the establishment of definitive haematopoiesis. Few endothelial cells start to emerge in the same manner as in control. However, they fail to finish EHT process and single cells bend for longer time than in control. Moreover, aorta diameter changes that were demonstrated during HSC emergence and might be associated to the EHT process (Kissa and Herbomel, 2010) are impaired in the absence of adrb2b or adrb3 receptors. All these characteristics might be important for HSC emergence.

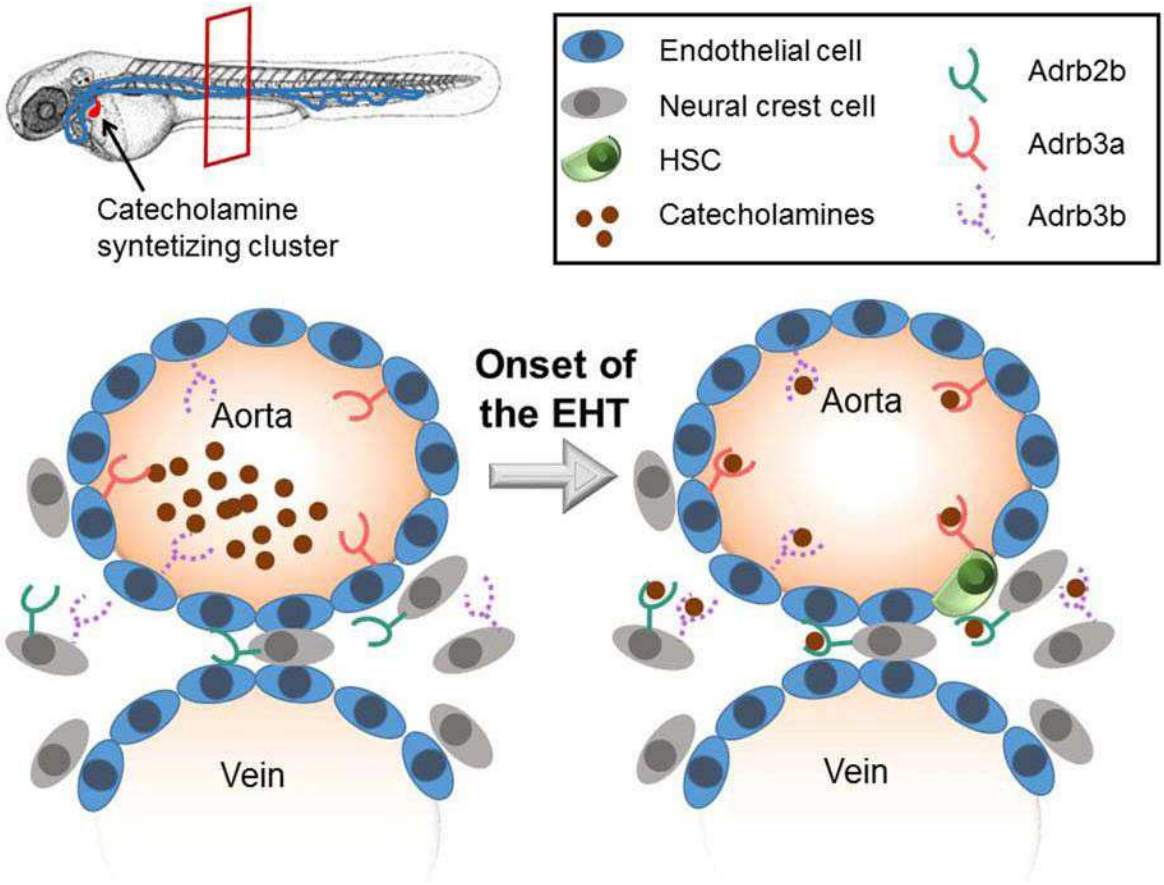

Figure 14 - Graphical abstract: Visual summary shows the localisation of cluster synthetizing catecholamines which are released to the blood circulation. They activate adrb2b and adrb3 receptors localised in the AGM, either on the surface of endothelial or surrounding cells to initiate the EHT process.

In mammals, previous studies have described the role of the sympathetic nervous system in HSC homeostasis. Catecholamines released from the sympathetic neurons in the vicinity of DA in mouse embryo regulate HSCs emergence while in the bone marrow they induce HSC mobilisation. Here, we show that the regulation of embryonic haematopoiesis through the adrenergic receptors is conserved in the zebrafish embryo which indicates that this mechanism may be common for several vertebrate species. Especially, analysis of adrenergic receptors in human embryos would bring an essential information regarding a translational use of the receptor.

Interestingly, few points differ in the sympathetic regulation between the mouse and zebrafish embryos. In the zebrafish embryo, Adrb3 receptors control HSCs emergence in addition to Adrb2b receptor. Each adrb3 receptor knock-down decreased the number of HSC in the AGM. As both receptors affected haematopoiesis it would be interesting to determine if the combined knock-down inhibited HSC emergence in synergic manner. The role of Adrb3 receptor during development has not been intensely analysed yet. In mouse embryo, Adrb3 receptor is expressed by stromal cell but its role was not associated with the embryonic haematopoiesis. On the other hand, Adrb3 receptor in adult mouse bone marrow controls HSC mobilisation upon its activation (Mendez-Ferrer et al., 2008). It would be of great interest to analyse the ADRB3 receptor expression and localisation during HSC emergence as well as in the adult bone marrow in human and compare to mouse and zebrafish. Detailed study in the embryonic and adult zebrafish will give first insights into the role of adrb3 receptor in embryonic haematopoiesis before investigating in mammals.

Another intriguing observation of this report is that the sympathetic innervation of the dorsal aorta is delayed in zebrafish embryo compared to the mouse development (An et al., 2002). The adrenergic receptors activation precedes the sympathetic specification in the AGM. We demonstrated lacking local innervation at the onset of haematopoiesis by using TH1 antibody. The expression of the TH2 in peripheral tissues still remains to be elucidated. Nevertheless, previous results showed that the both TH enzymes are expressed in the CNS and localised close to each other (Semenova et al., 2014).. Therefore, we can postulate that the expression of these two enzymes could be localised close to each other also in the peripheral tissues. Therefore we hypothesise that TH2 enzyme can be also found at the vicinity of a cardiovascular system but not in the AGM region. We propose that the receptors are activated by catecholamines delivered through the blood circulation from the TH expressing cells clusters

at the vicinity of aorta. If our hypothesis is validated, two interesting suggestions can be deduced from this result.

First, the role of the microenvironment in the haematopoiesis might be extended to the distant regions in the organism. The local innervation may not be required for the receptor activation. The sympathetic nervous system plays a role during the development and is also deregulated in several chronic pathologies including the tumour progression (Magnon et al., 2013). Thus, it will be interesting to evaluate if the catecholamines can regulate the physiological or pathological processes through the blood circulation in cases when the sympathetic local innervation was not described. The transport of catecholamines through the blood circulation have been already well described in human (Mccorry, 2007). The adrenal medulla synthetises adrenaline in stress situation and releases it to the blood circulation. The adrenaline released in the blood flow then acts on many tissues simultaneously to induce a systemic reaction. This process is mostly associated with ADRB2 receptor because adrenaline preferentially binds to this receptor.

Second, we propose that blood circulation is the way used for the delivery of the catecholamines. The importance of blood flow in the HSC emergence has been already described. The blood flow induces the shear stress on the endothelial cells and induce the EHT (Adamo et al., 2009; North et al., 2009). Considering the mechanism of the catecholamine delivery to the tissues, we can postulate an additional role of the blood circulation in the haematopoiesis. In addition to the mechanical forces, the blood can also deliver the signalling molecules, hormones and neurotransmitters.

It has been reported that activation of adrb receptor affect the HSC emergence and mobilisation (Fitch et al., 2012; Katayama et al., 2006). The exact mechanism behind the receptor activation still remains unclear. Consistent with the data in mouse embryo, we

demonstrate that the receptors play role at the onset of EHT event. Moreover, it appears that the activation of adrb receptor control the haemogenic endothelial cell survival. Interestingly, the proposition that adrb receptors can play role in cell survival, already appeared in pathological conditions. Beta blockers, which are the medicines used over 60 years in cardiovascular related pathologies, are now re-evaluated as the potential 'anti-cancer' drugs. The pre-clinical studies have shown that adrb2 receptor control the tumour cell survival in prostate cancer and sarcoma. The clinical studies with beta-blocker demonstrated increased patient survival (Tang et al., 2013). All the clinically used inhibitors preferentially block the adrb2 receptor. As the adbr3 receptor was also detected in the tumour (Magnon et al., 2013), it would be of great interest to see how the adrb3 specific inhibitor will end in the clinical studies and if they have a therapeutic potential.

Materials and Methods

Zebrafish husbandry

Wild-type and transgenic lines were maintained in compliance with the Institutional Animal Care and Use protocols. The following transgenic lines were used in this study: *Tg(cd41:eGFP)* to label HSCs (Lin et al., 2005), *Tg(kdrl:eGFP)* and *Tg(kdrl:Has.HRAS-mCherry)* (here cited as *kdrl:caax-mCherry*) (Chi et al., 2008) for the vessel endothelium marking (Beis et al., 2005) and *Tg(FoxD3:GFP)* for neural crest cell labelling (Gilmour et al., 2002). Embryos were kept in the presence of 1-phenyl-2-thiourea (PTU) to prevent melanin pigmentation (Westerfield, 2000) and staged as described by Kimmel et al (Kimmel et al., 1995). All experiments were performed in accordance with the protocol CEEA-LR-13007 approved by the Animal Care and Use Languedoc-Roussillon Committee.

Live Imaging

Zebrafish embryos (lateral views, rostral to the left) were embedded in 0.7% low melting agarose and imaged using a Zeiss LSM510 confocal microscope through a 20x air immersion or 40x water immersion objective. All real-time live imaging experiments were performed from 30 h.p.f. for 16-25 hours at an acquisition rate of 6-8 minutes at a 1µm z-interval.

HSC enumeration

For the HSCs quantification, 2 sets of z-stacks were acquired using the 20x air immersion objective and resolution of 1024x256 pixel with 1 µm z-interval. The maximum intensity projections were then used for the manual counting of cd41+ cells with the Fiji cell counter

plugin. The graphical representation of the data is shown in the box plot. Box plots show minimum (lower whisker) and maximum (upper whisker), as well as 1st and 3rd quartile (bottom and top of box, respectively), and median (central thicker line). The graphs were created using the R software.

Morpholino injection

Specific antisense targeting morpholinos (MO, Gene Tools) were resuspended in morpholino buffer – 12 mM KCl and 20 mM HEPES – in 2-3 mM stock concentration. The MO was injected at 1-4 cell stage in zebrafish embryos using the micro-injector system (Tritech Research Inc.). The MOs used in this study are listed in Table 1.

Name	5'-3' sequence	Type	Used concentration	Reference
Adrb1	GGT AGC CCG TCT CCC ATG ATT TGG A	ATG	0.4mM	(Wang et al., 2009)
Adrb2a	GTA TTG AGG ACC TTA TGT TTC CCA T	ATG	0.8mM	(Wang et al., 2009)
Adrb2b	TCA GCG TAT TCT CTC CCT CCA TGA G	ATG	0.3mM	(Wang et al., 2009)
Adrb3a	TCA TGG TGT GCA GCT TTT CAA GGC A	ATG	0.4mM	*Designed for the study*
Adrb3b	GTT GGC GCT CAT CCT GAG AGG AAG C	ATG	0.3mM	(Wang et al., 2009)
TH1	CAC AGG TTA ACA GAC TTA CAT TTG A	Splice	1mM	(Reimer et al., 2013)
TH2	CTG TTG TTC ACT TAC AGG GTG ATC C	Splice	0.6mM	(Semenova et al., 2014)
TH2 bis	TTA TGC ATT GTA CGT ACG GTT CAG G	Splice	0.6mM	(Semenova et al., 2014)
FoxD3	CAC CGC GCA CTT TGC TGC TGG AGC A	ATG	0.5mM	(Stewart et al., 2006)

Table 1: List of used morpholinos in this study

Inhibitor treatment

Manually dechorionated embryos were soaked in ICI-118,551 (Adrb2 inhibitor, 100µM, Abcam) or SR59230A (Adrb3 inhibitor, 40µM, Sigma) or DMSO 1% as a control from 18 h.p.f. until observation at 48 h.p.f.

Rescue assay

The morpholino injected embryos were manually dechorionated at 18 h.p.f. and transferred in the 24-well-plate. The morphants and corresponding controls were soaked in the procaterol (Adrb2 agonist, 100 µM, Abcam), BRL 37344 (Adrb3 agonist, 100 µM, Enzo Life Sciences), Adrenaline (physiological neurotransmitter, 100 µM, Sigma) or DMSO 1% as a control.

Immunostaining

Tg(FoxD3:GFP) embryos were fixed with 4% PFA 4% sucrose at 30 and 48 h.p.f. After the permeabilisation with 1% triton and saturation with 10% goat serum, the embryos were incubated with the TH1 (1/200, Merck Millipore) or TH2 (Semenova et al., 2014) antibody followed by Alexa Fluor 532 Goat Anti-Mouse or Goat Anti-Rabbit IgG antibody (1/1,000, Life Technologies). The embryos were imaged using a Zeiss LSM510 confocal microscope through a 20x air immersion and 40x water immersion objectives.

Whole mount in situ hybridisation (WISH) coupled with immunofluorescence staining

WISH of Adrenergic beta receptors was performed according to Thisse (). *Tg(kdrl:eGFP)* embryos at 30 and 48 h.p.f. were fixed, dehydrated with methanol, digested with proteinase K (New England Biolabs) and fixed again. Prehybridization was performed at 65 °C in HM+ buffer (50% formamide, 5x saline sodium citrate, 0.1% Tween-20, 50 µg ml-1 heparin, 500 µg ml-1 yeast tRNA) and followed by hybridization with 0.6 ng µl-1 digoxigenin labelled antisense RNA probe in HM+ buffer. The probes were detected with alkaline phosphatase-conjugated anti-digoxigenin antibodies (1/5,000, Roche Applied Science) using

nitro blue tetrazolium chloride/5-bromo-4-chloro-3-indolyl-phosphate, toluidine-salt (Roche Applied Science). After staining embryos were mounted in 90% glycerol prior imaging or the immunofluorescence staining was pursued. For immunostaining, embryos were incubated with anti-GFP antibody (1/500, BLM), followed by Alexa Fluor 488 Anti-Rabbit IgG antibody (1/1,000, Life Technologies). The embryos were transferred to 90% glycerol and imaged using a Zeiss AxioImager Z2 microscope through the 40x oil immersion objective. A Zeiss V12 microscope was used for WISH whole trunk images (Figures 1-4).

Catecholamines biochemical detection

The embryos at 30 h.p.f. were manually dechorionated and anesthetised with the cold Egg's water. The 200 embryos were decapitated using a pair of needles. The heads and the zebrafish bodies were snap-frozen separately. The 150 snap-frozen embryos were used to compare the whole organism with the peripheral part. The HPLC system consisted of an ESA liquid chromatography pump (ESA, Bedford, UK) coupled to an ESA Coulochem II detector (ESA, Chelmsford, USA) equipped with a 5014 high-performance analytic cell (ESA Bedford). The detector potential at the analytic cell was set at +0.4 V. HPLC analysis was performed on a C18 Spherisorb ODS2 Nucleosil HD reverse phase column (Macherey-Nagel EURL, France; 5 µm pore size, 4.6 mm internal diameter, 25 cm long). The mobile phase consisted of 0.1 M NaH_2PO_4, pH 3, containing 0.1 mM of EDTA, 1.7 mM 1-octane sulphonic acid sodium salt and 10% acetonitrile. The flow rate was 0.9 mL/min. Concentrations of NE were determined by comparison of chromatographic peak areas with calibration curves derived from authentic standards of NA, using data analysis software (Baseline 810, Waters).

Statistical analysis

Normal distributions were analysed using the Shapiro-Wilk test. Non-Gaussian data were analysed using the Wilcoxon test, Gaussian with Student t-test. $P<0.05$ was considered as statistically significant (symbols: ****$p<0.0001$ *** $p<0.001$; ** $p<0.01$; * $p<0.05$) Statistical analyses were performed using the R software.

Supplementary legends

Supplementary movie 1: HSC emergence is impaired in absence of Adrb2b expression. Combined representative time-lapse standard deviation projections of *Tg(kdrl:eGFP)* embryo at 30 h.p.f. draw a comparison between a physiological HSC emergence in the AGM (control, top) and in absence of Adrb2b expression (MO Adrb2b, bottom). The Adrb2b morphants show a decreased number of EHT events and several endothelial cell fragmentation in the ventral wall of dorsal aorta. Image stacks were acquired every 8 minutes over 16 hours with 1024x350 pixel resolution using the LSM Zeiss confocal microscope equipped with 40x water immersion objective. Scale bar 30 μm, time code in hours and minutes.

Supplementary movie 2: HSC emergence is impaired in absence of Adrb3a expression. Combined representative time-lapse standard deviation projections of *Tg(kdrl:eGFP)* embryo at 30 h.p.f. draw a comparison between a physiological HSC emergence in the AGM (control, top) and in absence of Adrb3a expression (MO Adrb3a, bottom). The Adrb3a morphants show a decreased number of EHT events and several endothelial cell fragmentation in the ventral wall of dorsal aorta. Image stacks were acquired every 6 minutes over 25 hours with 1024x256 pixel resolution using the LSM Zeiss confocal microscope equipped with 20x air immersion objective. Scale bar 30 μm, time code in hours and minutes. White asterisks point the fragmented cells.

Supplementary movie 3: HSC emergence is impaired in absence of Adrb3b expression. Combined representative time-lapse standard deviation projections of *Tg(kdrl:eGFP)* embryo

at 30 h.p.f. draw a comparison between a physiological HSC emergence in the AGM (control, top) and in absence of Adrb3b expression (MO Adrb3b, bottom). The Adrb3b morphants show a decreased number of EHT events and several endothelial cell fragmentation in the ventral wall of dorsal aorta. Image stacks were acquired every 8 minutes over 20 hours with 1024x350 pixel resolution using the LSM Zeiss confocal microscope equipped with 40x water immersion objective. Scale bar 30 μm, time code in hours and minutes.

Supplementary movie 4: 3D view of TH expressing cell cluster in *Tg(kdrl:eGFP)* embryo. 360° overview of 3D projection of TH immune-staining on the vessel endothelium background using *Tg(kdrl:eGFP)* embryo at 30 h.p.f. 3D projection was performed using Fiji plugin 3D viewer from a confocal image with 0.8 μm interval acquired using the LSM Zeiss confocal microscope through the 20x air immersion objective.

3.2. Peripheral nervous system in the AGM and definitive haematopoiesis: complementary results

In the manuscript in preparation "Catecholamines control definitive haematopoiesis in the zebrafish embryo" I introduced the role of the sympatho-adrenal system in the early steps of HSC emergence. Adrenergic receptors adrb2b and adrb3 were activated in the AGM region even though the sympathetic innervation was not yet established. However, this conclusion does not mean that the DA is not innervated at all. Using a pan-neuronal marker nbt revealed that the peripheral nerves migrate ventrally from the spinal cord in the whole trunk and tail region from early stage. At 25 h.p.f., which corresponds to the onset of blood circulation, the nerves reach the DA and continue to migrate ventrally toward the PCV. One symmetrical pair of neurons is placed per somite (**Figure 32**). These neurons are in direct contact to the DA as demonstrated from the orthogonal view.

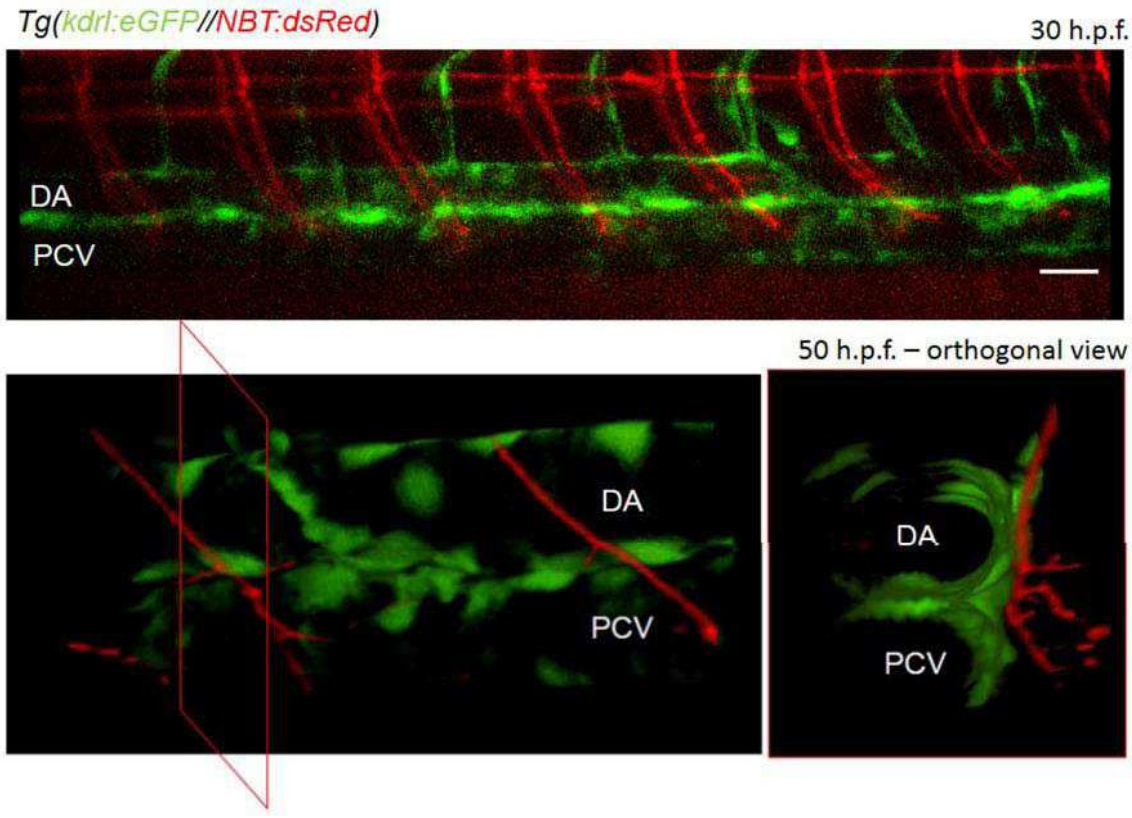

Figure 32 – Local innervation of the AGM:
A pair of nerves per somite migrates ventrally to reach the DA and later the PCV. 3D lateral and orthogonal views show the direct contact of the nerve axon with the vascular endothelium. Scale bar = 30 µm.

We then decided to characterise the neuron present in the AGM. A set of different neuronal markers demonstrated that the neurons are negative for sympathetic markers (TH), but positive for Islet1 – a motoneuron marker – and vesicular acetylcholine transporter (VAChT) – a parasympathetic marker (**Figure 33**). These markers indicate that the described neurons can be part either of somatic motoneuron population or of parasympathetic nervous system.

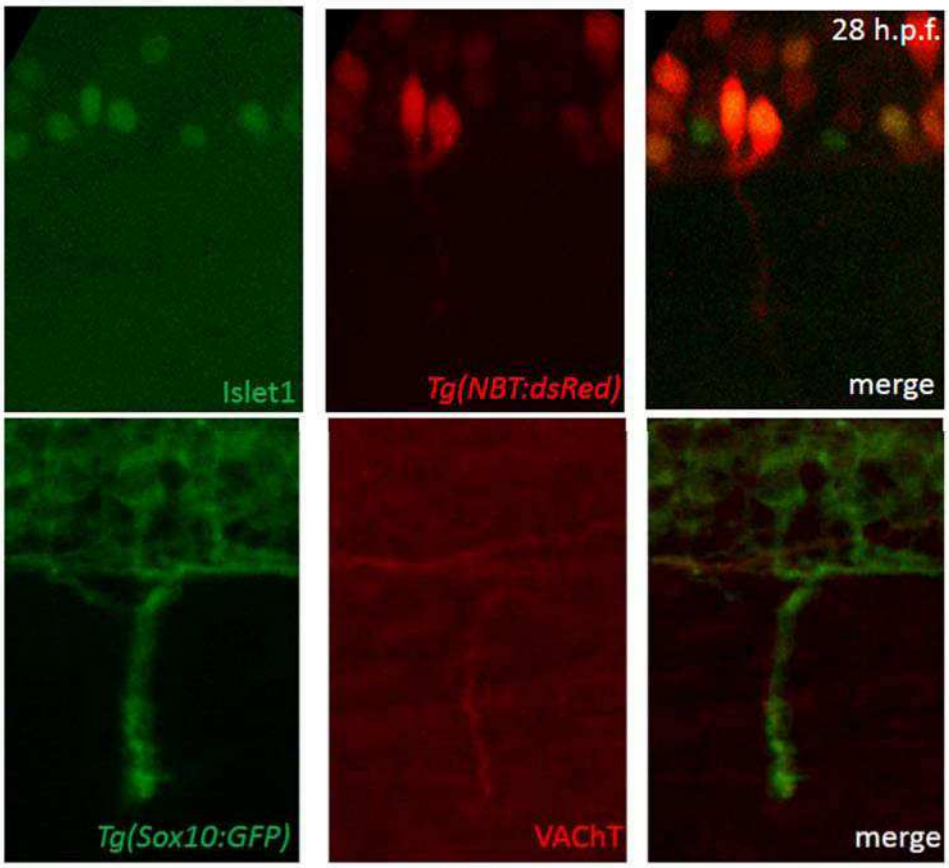

Figure 33 – The identity of the nerves present in the AGM:
The peripheral nerves localised in the AGM show expression of motoneuron Islet1 marker in the nucleus and Parasympathetic VAChT marker in the axon.

Concomitantly with the neuron migration, we observed that neural crest cells migrate through the same path established by neurons. Regarding their localisation around the nerves and their morphology we hypothesise that neural crest differentiated into Schwann cells ensheating the neurons (**Figure 34A**). Part of the neural crest derivatives continue the migration trough the AGM and settle between DA and PCV or around PCV. These cells stay positive for neural crest markers, for instance FoxD3, but do not exhibit neural character. We suggest that these cells could be neural crest derived stromal cells (**Figure 34B**).

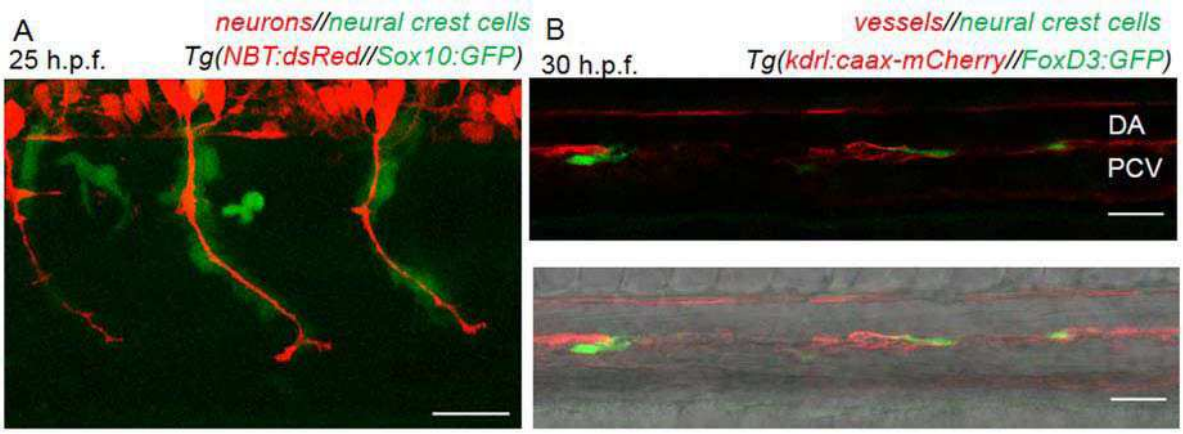

Figure 34 – Neural crest cells migration along the nerves present in the AGM:
(A) Neural crest cells enveloping the peripheral nerve in the AGM. (B) Neural crest cells localised between DA and PCV at 30 h.p.f. whose morphology suggest non-neuronal identity. Scale bar = 30 µm.

To evaluate the role of these neurons we performed live imaging of transgenic embryos highlighting the neurons and HSCs – *Tg(NBT:dsRed//cd41:eGFP)*. The time-lapse revealed interactions between nascent HSCs and neurons during their migration in the AGM. HSCs migrate actively toward the neurons and touch them or stay for some time in contact with them. Interestingly, HSCs did not touch the nerve at the terminal axon zone where the majority of synapsis is localised but at the central part of the main axon. This indicates that the HSCs might not react with the nerve itself but with the enveloping Schwann cell. The quantification of migrating HSC demonstrated that 75% of migrating HSCs interacted with the neural crest cell (**Figure 35**). Moreover, most HSCs intravasated shortly after their interaction with the neuron. As not all HSCs migrate in the AGM after the emergence, only the moving cells were taken in count for the quantification.

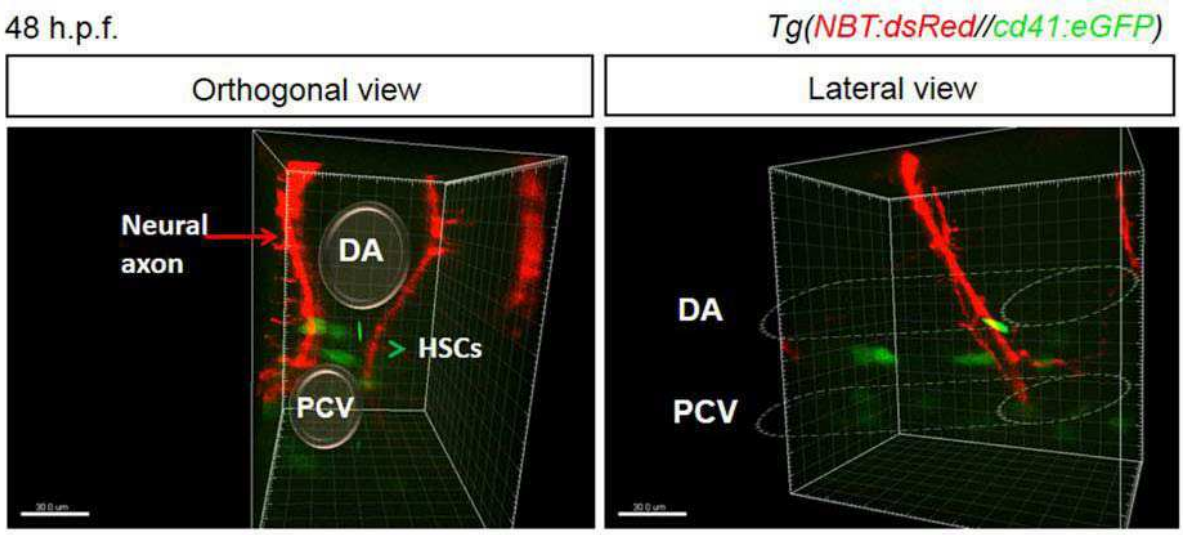

Figure 35 – HSCs in contact with the neural axons:
Orthogonal and lateral view of the AGM show nascent HSC which are localised in the direct contact with neural axon at 48 h.p.f. DA, dorsal aorta; PCV, posterior cardinal vein. Scale bar = 30 µm

The intravasation of HSCs shortly after the interaction suggest that the contact with Schwann cells can be required for this process. Therefore it would be interesting to further analyse this aspect and compare to the role of macrophages in HSC mobilisation that we described previously.

DISCUSSION AND CONCLUSION

Chapter 5: Discussion

The establishment of definitive haematopoiesis is a complex process controlled by several factors. HSCs require signalling from the surrounding microenvironment to emerge, mature and maintain their self-renewing potential. The definitive wave of haematopoiesis takes place in the AGM region, where HSCs emerge from the aortic endothelium by the EHT process. The AGM is composed of several cell types including vascular endothelial cells, blood cells, pronephric tubules or stromal cells, which express different factors necessary for the EHT process (Wilkinson et al., 2009). The results obtained during my thesis complete the description of the AGM region in the zebrafish embryo, identify its cell composition and investigate the role of each population. I have described two systems playing major roles in the establishment of haematopoiesis – macrophages and the sympatho-adrenal system.

1. Macrophages

We have identified the presence of primitive macrophages in the aorta local environment. Macrophages accumulate in the AGM of human and zebrafish embryo during the definitive wave of haematopoiesis. It was previously reported that HSCs enter the PCV circulation through particular structures, which facilitate HSPC intravasation (Kissa et al., 2008). In the first study of my thesis, we showed using live imaging that these tiny entry points are created by macrophages during their migration through the stroma, which allow HSPCs to join the PCV. Macrophage depletion using either L-clodronate injection or nitroreductase-transgenic embryos prevents the colonisation of haematopoietic organs without affecting EHT in the AGM. The entry points allowing HSPC intravasation are formed by Mmps-secreting macrophages. Specific Mmp inhibition with combined WISH and immunofluorescence staining established that macrophages are involved in HSPC mobilization via Mmp-9 secretion.

Several roles of macrophages have been described during embryogenesis. They phagocyte cellular debris of cells undergoing programmed cell death during organogenesis. They can also induce apoptosis, angiogenesis or cell proliferation and differentiation through specific signalling (Jones and Ricardo, 2013; Rae et al., 2007). Here, we show an additional role of macrophages during embryogenesis. ECM degradation was frequently associated with macrophages in pathological conditions. Macrophages mediate ECM degradation in chronic cardiovascular diseases such as atherosclerosis, where they remodel the sub-endothelial region

(Newby, 2007). Moreover, tumour-associated macrophages (TAM) play a role in ECM remodelling in tumour stroma through the release of proteases from invadopodia. These enzymes degrade the stroma of tumour and enable tumour cells to intravasate and seed secondary sites. Our study shows in real time how macrophages can mediate ECM degradation in physiological conditions *in vivo*.

Considering the number of roles that single macrophage can fulfil, it is questionable whether ECM degradation and mechanical mobilisation of HSCs is the only function of macrophages in the AGM niche. During EHT and following HSCs mobilisation, the tissue undergo substantial remodelling. We demonstrated that the ECM is degraded, but it has been shown before that macrophages are also able to induce the deposit of ECM proteins (Schnoor et al., 2008). The hypothesis that macrophages may induce the deposit of ECM protein in the AGM can be supported by the persisting accumulation of macrophages after the migration of HSCs to the haematopoietic organs. The intimate interactions between HSCs and macrophages indicate that specific inter-cellular signalling might be implied. It will be interesting to evaluate if macrophages mediate complementary signalling to activate HSCs, for instance by playing a trophic role. Further analysis of transcriptomics or proteomics of macrophages in the AGM could reveal their additional participation in HSC homeostasis.

Transversal study between the zebrafish and the human embryo revealed that a specific accumulation of primitive macrophages was also detected in the human embryo. Macrophages accumulated underneath the ventral wall of human embryonic aorta and in intra-aortic clusters. Even if in mammals HSCs mobilise and intravasate within DA circulation, we may hypothesise that macrophages can also contribute to the establishment of definitive haematopoiesis in these species. Therefore, we postulate that this mechanism is evolutionary conserved.

Macrophages were described to contribute to HSC homeostasis in the bone marrow. Interestingly, in the marrow, the role of macrophages can be defined as opposite to their role in the AGM. Indeed, macrophages retain HSCs in the bone marrow. Macrophages enhance CXCL12 expression through CAR cells. After macrophage depletion, HSCs mobilise and enter blood circulation to differentiate into blood cells. Those results demonstrate how every cell population can fulfil a distinct role in HSC homeostasis depending on the haematopoietic site microenvironment.

In the following parts, we have focused on detailed description of macrophages in the zebrafish embryo. We tried to answer two intriguing questions: 1) How do macrophages in the AGM behave and migrate and 2) Does an M1/M2 polarisation concept exist in the zebrafish?

Macrophages are involved in many acute and chronic pathologies. They can promote recovery but also enhance the pathological situation. The detailed description of macrophage phenotype and behaviour can help to predict which function macrophages will adopt in each situation. The zebrafish embryo represents an ideal candidate for real-time tracking and analysis of macrophage behaviour.

Different studies focused on macrophage shape and migration in different conditions *in vitro*. Two main types of migration have been described – amoeboid and mesenchymal (Friedl, 2004). While the first one uses the existing gaps in the matrix scaffold, the second one mediates ECM degradation to allow migration. Moreover, each migration mode has been described to adopt distinct morphologies – round in the amoeboid movement and elongated in the mesenchymal one (Friedl, 2004). *In vitro*, macrophages can adopt both types of migration – amoeboid and mesenchymal – depending on the type of artificial scaffold used (Van Goethem et al., 2010).

In the zebrafish embryo, we showed that macrophage morphology is more heterogeneous than expected. We categorised macrophages depending on their shape into 4 categories: round, amoeboid, star-like and elongated ones. Therefore, *in vivo* observations revealed the presence of more macrophage subgroups than the assays on 3D matrices, thereby showing the importance *of in vivo* modelling to complete results obtained *in vitro*. Real-time imaging and single macrophage-tracking then demonstrated the strong morphological plasticity of macrophages during their migration through the ECM in the AGM. They successively adopt different shapes while migrating through the matrix. In the results obtained in the first project of my thesis – macrophages in the AGM degrade the ECM – we propose that these macrophages use the mesenchymal migration for their moves. It would therefore indicate that macrophages display high morphological plasticity during mesenchymal migration.

We showed that the inhibition of either Rac or Mmp, which are the proteins involved in the mesenchymal migration, affected macrophage behaviour in the AGM. Rac inhibition is associated to podosome formation and actin polymerisation at the leading edge to

allow cell polarisation (Sanz-Moreno and Marshall, 2010). Our observations were in agreement with this mechanism. Macrophages failed to form the leading edge or to migrate. In addition, they formed protrusions toward opposite directions at the same time and ECM degradation was impaired. It would be interesting to evaluate by which mechanism Rac signalling affects ECM degradation. Mmp-9 appears to be expressed in Rac-inhibited embryos (data not shown). Therefore, one of the following steps, for instance protein translation, delivery to the membrane or release of mmp-9, could be affected after Rac inhibition.

We found that Mmp inhibition modifies macrophage shape as well as migration. Macrophages preferentially adopt a round shape and migrate much faster and along the vein. The characteristics of macrophage behaviour after Mmp inhibition – round shape, Mmp-independent migration, missing ECM degradation and fast movements – indicate that the migration switched to the amoeboid type. It would be the first *in vivo* demonstration of mesenchymal-to-amoeboid transition of macrophage migration. We evaluated the modifications of macrophage behaviour after inhibition of mesenchymal migration markers – Rac and Mmp. It would be interesting to analyse if macrophage behaviour remains unchanged after inhibition of signalling molecules inducing amoeboid migration, for instance ROCK protein. Considering the current results, we do not expect any substantial modifications of macrophage behaviour in the AGM following inactivation of amoeboid migration regulators.

Activation of macrophages toward a specific phenotype is one of the main characteristics that allowed to categorise mammalian macrophages. Macrophages start to express distinct cytokines, growth factors or metabolism-related markers in response to the local signalling and then polarise into M1 or M2 phenotype. Our collaborators have recently demonstrated that the concept of macrophage polarisation is conserved in the zebrafish larva. During inflammation, macrophages migrate toward the inflamed site and start to express pro-inflammatory factors such as *tnfa*. The use of the transgenic line *Tg(mpeg1:mCherry//TNFa:GFP-F)* permitted to observe in real-time the polarisation of macrophage into a pro-inflammatory M1 phenotype and at the same time to sort macrophages based on their *tnfa* positive or negative labelling. *Tnfa*$^{+}$ macrophages expressed significantly higher levels of other pro-inflammatory markers including *tnfb*, *il1b* and *il6,* associated with the M1 phenotype. On the other hand, *Tnfa*$^{-}$ macrophages showed higher expression of markers associated with the M2 phenotype, such as *tgfb1*, *ccr2* or *cxcr4b*. However, one of the most often used marker to identify M2 phenotype Arginase 1 was not detected in any of the subsets.

Difficulties to find a common M2 marker for human, murine and zebrafish macrophage, complicate accurate characterisation of macrophages. Moreover, it has been shown that the M2 phenotype is very heterogeneous and may include several distinct subsets of macrophages. Two solutions can be proposed to the current problem of macrophage categorisation: we either seek for a specific M2 marker conserved among species, or we try to establish a new way – probably more complex – to characterise macrophages. For example, it would be interesting to include the morphological and behavioural characteristics of macrophages into a new system of characterisation. Concerning the search of a new M2-specific marker, a transgenic zebrafish line would permit to analyse *in vivo* the dynamics of polarisation and determine if a single macrophage can pass from one phenotype to another or if several different subsets are required.

The concept of M1/M2 macrophage polarisation has been a promising way to categorise macrophages due to its relative simplicity. However, it is mainly based on *in vitro* or *ex vivo* results and does not consider embryonic macrophages. We attempted to analyse primitive macrophages in the AGM during the establishment of definitive haematopoiesis in order to see if macrophages are polarised into a specific phenotype and to compare their phenotype after different treatment affecting their behaviour. We found that macrophages expressed very low level of pro-inflammatory cytokines and *tnfa* was not even detected in macrophages in the AGM. This suggests that macrophages mobilising HSCs do not activate into a pro-inflammatory phenotype but it does not demonstrate their M2 phenotype either. In addition, we found that Rac inhibition enhanced the expression of pro-inflammatory cytokines, suggesting that macrophages polarised toward M1 phenotype. Despite this increase, *tnfa*$^{+}$ macrophages were still not detected while using the *Tg(mpeg1:mCherry//TNFa:GFP-F)* embryos (data not shown).

The initial aim of macrophage behaviour study was to correlate macrophage macroscopic changes – for instance shape plasticity and migration dynamics – with their molecular phenotype. We postulated that proteolytic macrophages would preferentially expressed anti-inflammatory markers and that elongated-shaped macrophages would be associated with an M2 phenotype as described *in vitro* (McWhorter et al., 2013). However, we encounter several challenges during this project. First, macrophages are much more dynamic during their migration than we expected. Second, the absence of specific M2 markers do not allow to visualise the shift from M1 to M2 phenotype *in vivo*. Finally, due to the technical

limitations, we were not able to associate the dynamics of macrophage changes with a modification at the molecular level.

In conclusion, embryonic yolk sac-originated macrophages are different from bone-marrow-derived macrophages. Thus, due to the differences between the two origins, we cannot conclude that the classical concept of M1/M2 activation is conserved in embryonic stages. We can still observe some similarities but macrophages are likely to be differentially diversified depending on the tissues in which they are localised.

2. Sympatho-adrenal system

In the second part of my work, I have shown that another cell population substantially influence the establishment of definitive haematopoiesis. These cells were neural crest cells, which differentiate into the sympatho-adrenal system. They produce and release catecholamines which then mediate HSC emergence through the Adrb2b and Adrb3 receptors.

In mammals, previous studies have described the role of the sympathetic nervous system in HSC homeostasis. In the mouse embryo, catecholamines released from the sympathetic neurons at the vicinity of the DA regulate HSCs emergence, while in the bone marrow they induce HSC mobilisation. Here, we propose that the regulation of embryonic haematopoiesis through adrenergic receptors is conserved among species. Interestingly, in the zebrafish embryo, we found that activation of the Adrb3 receptors is required for HSC emergence in addition to the Adrb2 receptor already described in the mouse embryo.

Previous studies showed that the two TH enzymes are expressed in the CNS of the zebrafish embryo in distinct but always neighbouring areas (Semenova et al., 2014). The TH2 expression in the periphery remains to be elucidated but we suppose that the pattern would be similar to TH1 enzyme. Therefore, we hypothesise that sympathetic innervation of the dorsal aorta is lacking during the initial steps of EHT process. Catecholamines synthesised in TH clusters in distant areas seem to be delivered to the adrb receptors through blood circulation. If TH2 localisation confirms this theory, a new role of blood circulation in EHT process would be established. It has been shown before that blood circulation induce EHT through flow-mediated shear stress (Adamo et al., 2009; North et al., 2009). Our observation indicates an additional

role of blood circulation, which might also be responsible for catecholamine delivery to initiate the EHT process. In conclusion of this study, we propose that the role of the local microenvironment is not complete and needs to be extended to distant regions of the organism including for example this cluster of cells synthetizing and secreting catecholamines. Moreover, because blood delivers a high variety of molecules including cytokines and hormones, other structures able to synthesise these molecules and localised at the vicinity of the circulation might be included into the notion of environment.

Despite the lack of sympathetic innervation of the dorsal aorta, other local nerves can play a role during the establishment of definitive haematopoiesis. Dorsal aorta is innervated by peripheral neurons expressing islet1 and VAChT markers, which are themselves enveloped by Schwann cells. Even though the role of these neurons has not yet been determined, live imaging revealed interaction of nascent HSCs with these nerves and/or Schwann cells respectively. We found that HSCs actively migrate toward the neural axons and stay in contact before intravasation. It suggests that these nerves may be involved in the step of HSC maturation or mobilisation. It would mean that several populations of neurons control multiple steps during the establishment of definitive haematopoiesis.

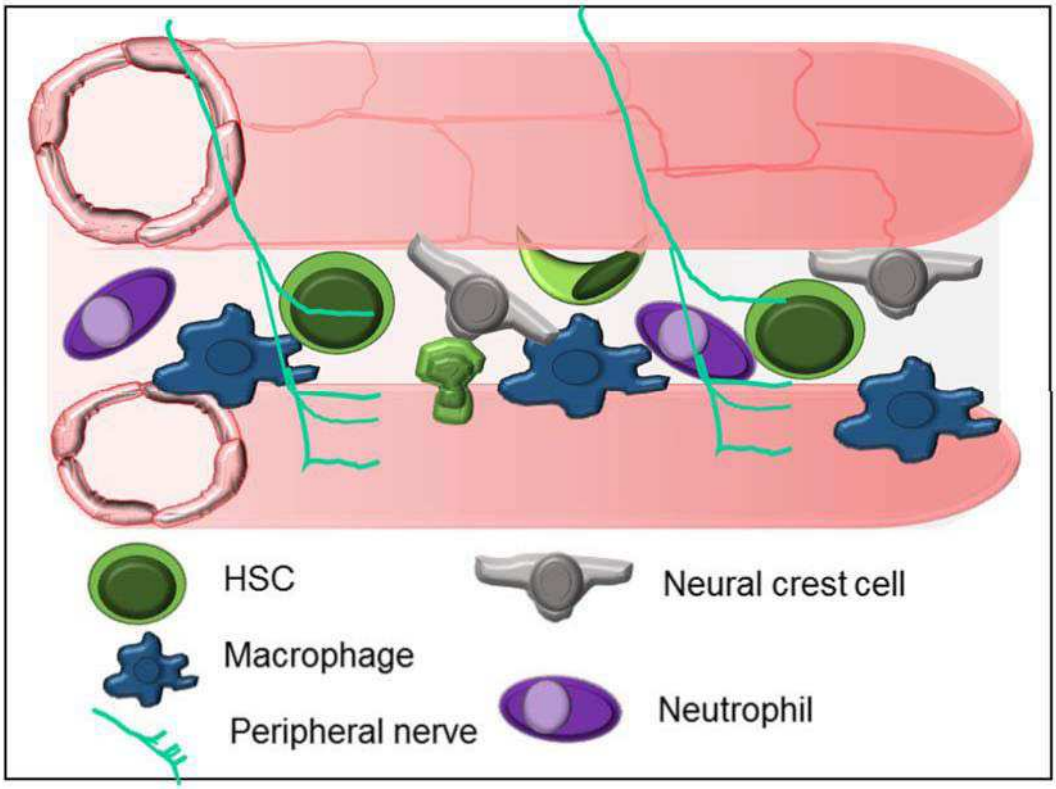

Figure 36 – Microenvironment in the AGM during definitive haematopoiesis:
Macrophages, neutrophils, neural crest cells and peripheral nerves are so far the cell populations identified in the AGM during HSC emergence.

3. General remarks

In the present study, we have extended the knowledge of the microenvironment surrounding the aorta in the AGM during HSC emergence (**Figure 36**). The detailed characterisation of the AGM allowed to identify two additional key players in the establishment of definitive haematopoiesis. In addition to our results, other cells have been described in the zebrafish AGM recently. Neutrophils arisen from the primitive wave are one of the cells identified in the AGM. They release tnfa, which induces EHT through the tnfr2 receptor activation (Espín-Palazón et al., 2014). It demonstrates that the haematopoietic cells originated from the primitive wave substantially regulates several steps of definitive haematopoiesis. Therefore, the two haematopoietic waves are tightly connected despite distinct location and timing of emergence.

In addition to macrophages and neutrophils, we have detected other cells whose role needs to be determined. In part 3, we have described that sympathetic innervation of DA

is missing during the first steps of EHT. However, it does not mean that the AGM region is not innervated at all. We have reported that nerves together with neural crest cells migrate ventrally from spinal cord and reach the DA at the time at which blood circulation starts. Although the identification of these neurons and their role in the establishment of definitive haematopoiesis needs to be fully determined, preliminary results suggest that nascent HSCs are attracted to the neurons prior their intravasation.

We detected cells of neural crest origin between DA and PCV and around the vein whose morphology indicate non-neuronal character. These cells could be stromal cells of neural crest origin, which were described in other haematopoietic sites, for instance in the bone marrow. In light of these new results, the AGM microenvironment shows high heterogeneity. Many cell populations are present and each contribute to HSC development by a specific mechanism. The tight regulation of haematopoiesis requires an organised collaboration within the niche to achieve temporal and spatial restriction of each signalling. It would be very interesting to assess if a single conductor controls this whole process or if a precise coordination of several factors is required.

During the ontogeny of haematopoiesis, HSCs go through or home in successive haematopoietic organs or tissues with different structures. Although each environment fulfils distinct role in HSC homeostasis, we can observe similarities in the composition of niches. We have identified macrophages and nervous system, which play role in the HSC emergence and mobilisation. Several studies have demonstrated that in the bone marrow, macrophages and sympathetic nervous system are also present. Although the composition is in part conserved, the cell populations play distinct roles in the bone marrow. Macrophages retain HSCs in the bone marrow niche while adrenergic receptor activation mobilise HSC to intravasate (Chow et al., 2011; Katayama et al., 2006). In addition to AGM and bone marrow, macrophages are also part of foetal liver environment and contribute to blood cell differentiation (Payushina, 2012). In the thymus, both populations, macrophages and sympathetic system, are present and are involved in thymocyte maturation (Leposavić et al., 2008). General description of each environment shows similar cell composition while performing different roles. It indicates how complex the regulation of the local environment is.

The characterisation of the AGM microenvironment allowed to identify the different cell populations contributing to HSC homeostasis. However, the establishment of

definitive haematopoiesis is a very complex process and further analysis will be required for potential translational use. In addition to the identification of the AGM cell composition, the temporal and spatial restrictions need to be considered. For instance, we observed specific accumulation of macrophages in the AGM from 40 to 60 h.p.f. This timing corresponds to the peak of HSC emergence and following colonisation of the CHT. Therefore, the initial steps of EHT can be accomplished without macrophage participation, which we later confirmed. As another example, adrenergic receptors, are expressed in the AGM at 30 h.p.f., which corresponds to the onset of EHT process. At 48 h.p.f., which is the peak of HSC emergence, the expression of most of the receptor decreases in the AGM. This observation indicates that Adrb2b and Adrb3 receptors play an important role in the initial steps of EHT but are optional during maturation and mobilisation of HSC. Deciphering the specific role of every niche components during each step of haematopoiesis would permit to generate fully functional HSCs *in vitro* and to use them for clinical applications.

Interestingly, several aspects of the haematopoiesis that occurs in the AGM show similarities with the initiation of tumour metastasis. Like the AGM, the primary tumour is a complex structure composed of tumour cells, vasculature, innervation, immune cells and stromal cells. Recent studies revealed that the initiation of metastasis is a highly organised mechanism (Joyce and Pollard, 2009). A first common aspect between tumour and AGM environments is the presence of adrenergic beta 2 and 3 receptors. Both receptors have been shown to play role in tumour expansion. While adrb2 receptor is expressed by tumour cells and surrounding stroma, adrb3 receptor is exclusively localised in the stroma (Magnon et al., 2013). These receptors regulate tumour cell survival and proliferation. Interestingly, control of cell survival is one of the mechanisms that we proposed in regulation of HSC emergence by adrb2b and adrb3 receptors.

Translational application of inhibitors of beta receptors is now developed for cancer treatment. Beta 2 inhibitors were approved by the FDA more than 60 years ago for cardiovascular disease treatment. Today, these medicines are re-evaluated in clinical studies for the use as cancer treatment (Tang et al., 2013). Beta 3 inhibitors have never been used so far, but *in vitro* assays showed a promising effect on tumour reduction. Therefore, similar to our experimental model, it is intriguing to see that these two receptors are also associated with tumour progression.

If we correlate our results with studies performed in cancer research, one intriguing observation emerge. We propose that adrenergic receptors could be activated in the absence of local sympathetic innervation through catecholamines delivered by blood circulation. Currently, not all solid tumours have been described to be innervated but the majority is vascularised. It would be interesting to evaluate if the sympatho-adrenal system can play a role in tumours where the local innervation is missing.

The second common aspect between the establishment of definitive haematopoiesis and tumour development is the presence of macrophages degrading the ECM. In both situations, macrophages degrade the ECM around the target cell – HSC or tumour cell – and promote its mobilisation and intravasation to seed distant areas (Pollard, 2004).

Translational application using depletion of macrophages to reduce tumour cell mobilisation did not succeed. This could be explained by the multiple roles of macrophages in the organism (Panni et al., 2013; Turk, 2006). Macrophages as the main players in innate immunity are crucial for proper functioning of the organism. Using general inhibition or depletion of macrophages do not specifically affect tumour-associated macrophage (TAM) but all macrophages in the organism and therefore adverse effects exceed the benefits. Affecting macrophages in a more specific manner would allow to develop a new treatment which would specifically target metastasis process. Our *in vivo* results concerning macrophage behaviour and the factors influencing macrophage migration and proteolytic activity could complement the existing studies and enable to develop more targeted immunotherapeutic strategies.

Chapter 6: Conclusion

During my PhD thesis, I have studied the AGM microenvironment during the establishment of definitive haematopoiesis in the zebrafish embryo. I have identified and described several cell populations and in particular focused on two of them, macrophages and sympatho-adrenal nervous system.

Each cell population demonstrated a specific role during the different steps of the establishment of definitive haematopoiesis. Chronologically, catecholamines control the initiation of the EHT process whereas macrophages mobilise nascent HSCs after their emergence. Concretely, we identified the expression of adrenergic beta receptors in the AGM at the onset of definitive haematopoiesis. Three of them, Adrb2b, Adrb3a and Adrb3b were found to control the first steps of EHT. Catecholamines synthetized in a distant area from the AGM are likely to be released to the blood circulation and to mediate EHT through the activation of adrb2b and adrb3 receptors.

We showed that macrophages degrade the ECM surrounding nascent HSCs in the AGM and allow their mobilisation. After HSC mobilisation, macrophages appeared to form a path for HSCs to reach the vein and intravasate. We also characterised this population of macrophages in the AGM, showing that they use the mesenchymal type of migration and exhibit a high morphological plasticity during migration. Macrophage migration and role was impaired after either Rac or Mmp signalling inhibition, which are two factors required for proper mesenchymal migration.

In conclusion, these findings showed that the microenvironment can substantially influence definitive haematopoiesis in the zebrafish embryo by distinct mechanisms.

APPENDIX

Appendix

Article 4: Identification of polarized macrophage subsets in zebrafish

Identification of polarized macrophage subsets in zebrafish

Mai Nguyen-Chi, Beryl Laplace-Builhe, Jana Travnickova, Patricia Luz-Crawford, Gautier Tejedor, Quang Tien Phan, Isabelle Duroux-Richard, Jean-Pierre Levraud, Karima Kissa, Georges Lutfalla, Christian Jorgensen, Farida Djouad

eLife, 2015, 4:e07288, DOI: 10.7554/eLife.07288

Graphical abstract:

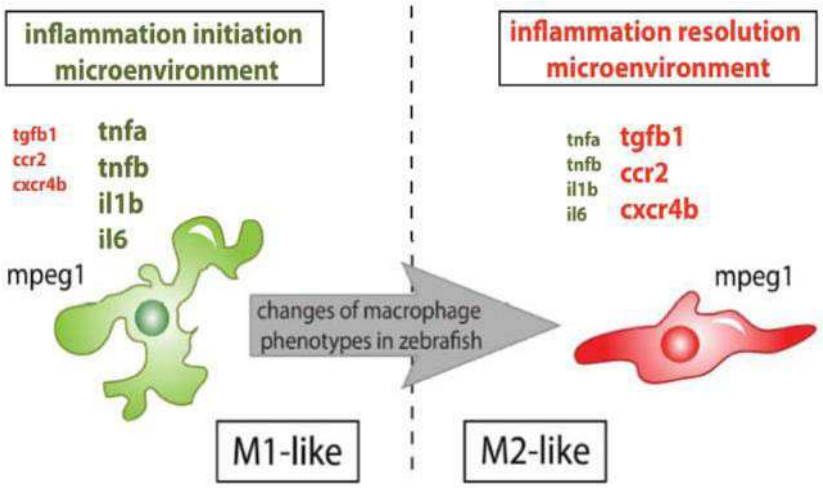

eLIFE elifesciences.org

RESEARCH ARTICLE

Identification of polarized macrophage subsets in zebrafish

Mai Nguyen-Chi[1,2†], Beryl Laplace-Builhe´[1,2†], Jana Travnickova[2,3], Patricia Luz-Crawford[1,2], Gautier Tejedor[1,2], Quang Tien Phan[3], Isabelle Duroux-Richard[1,2], Jean-Pierre Levraud[4,5], Karima Kissa[2,3], Georges Lutfalla[2,3], Christian Jorgensen[1,2,6‡], Farida Djouad[1,2*‡]

[1]Institut de Medecine Régénérative et Biothérapies, Institut national de la santé et de´ la recherche médicale, Montpellier, France;´ [2]Universite de Montpellier, Montpellier, France; [3]Dynamique des Interactions Membranaires Normales et Pathologiques, Centre national de la recherche scientifique, Montpellier, France; [4]Macrophages et Developpement de l'Immunité, Institut Pasteur, Paris, France; [5]Departement de Biologie du Developpement et Cellules Souches, Institut Pasteur, Paris, France; [6]Clinical unit for osteoarticular diseases and Department for Biotherapy, Centre Hospitalier Universitaire, Montpellier, France

Abstract While the mammalian macrophage phenotypes have been intensively studied in vitro, the dynamic of their phenotypic polarization has never been investigated in live vertebrates. We used the zebrafish as a live model to identify and trail macrophage subtypes. We generated a transgenic line whose macrophages expressing tumour necrosis factor alpha (tnfa), a key feature of classically activated (M1) macrophages, express fluorescent proteins Tg(mpeg1:mCherryF/tnfa: eGFP-F). Using 4D-confocal microscopy, we showed that both aseptic wounding and Escherichia coli inoculation triggered macrophage recruitment, some of which started to express tnfa. RT-qPCR on Fluorescence Activated Cell Sorting (FACS)-sorted tnfa$^+$ and tnfa$^-$ macrophages showed that they, respectively, expressed M1 and alternatively activated (M2) mammalian markers. Fate tracing of tnfa$^+$ macrophages during the time-course of inflammation demonstrated that pro-inflammatory macrophages converted into M2-like phenotype during the resolution step. Our results reveal the diversity and plasticity of zebrafish macrophage subsets and underline the similarities with mammalian macrophages proposing a new system to study macrophage functional dynamic.
DOI: 10.7554/eLife.07288.001

*For correspondence: farida. djouad@inserm.fr

†These authors contributed equally to this work

‡These authors also contributed equally to this work

Competing interests: The authors declare that no competing interests exist. Funding: See page 13

Received: 03 March 2015 Accepted: 07 July 2015 Published: 08 July 2015

Reviewing editor: Utpal Banerjee, University of California, Los Angeles, United States

Introduction

Behind the generic name 'macrophage' hides various cell types with distinct phenotypes and functions. Currently, it is well established that macrophages are not just important immune effector cells but also cells with critical homeostatic roles, exerting a myriad of functions in development, homeostasis, and tissue repair and playing a pivotal role in disease progression (Wynn et al., 2013). Therefore, there is a high interest in a better characterization of these cells to establish an early and accurate diagnosis. The wide variety of macrophage functions might be explained by the outstanding plasticity and versatility of macrophages that efficiently respond to environmental challenges and changes in tissue physiology by modifying their phenotype (Mosser and Edwards, 2008). Although there is a consensus that macrophages are a diversified set of cells, macrophage subtypes are still poorly characterized. Indeed, although these cell populations have been extensively investigated in mouse and human, these studies were mostly performed in vitro using monocyte-derived macrophages induced under specific stimuli. A comprehensive characterization of macrophage

eLife digest Inflammation plays an important role in helping the body to heal wounds and fight off certain diseases. Immune cells called macrophages—which are perhaps best known for their ability to engulf and digest microbes and cell debris—help to control inflammation. In mammals, different types of macrophage exist; the most functionally extreme of which are the M1 macrophages that stimulate inflammation and M2 macrophages that reduce the inflammatory response.

Macrophages acquire different abilities through a process called polarization, which is controlled by signals produced by a macrophage's environment. Polarization has been well investigated in human and mouse cells grown in the laboratory, but less is understood about how this process occurs in live animals.

Nguyen Chi, Laplace-Builhe et al. investigated whether zebrafish larvae (which are naturally transparent) could form an experimental model in which to investigate macrophage polarization in living animals. Zebrafish were first genetically engineered to produce two fluorescent proteins: one that marks macrophages and one that marks M1 macrophages. These fluorescent proteins allow the movement and polarization of macrophages to be tracked in real time in living larvae using a technique called confocal microscopy. Nguyen Chi, Laplace-Builhe et al. also isolated macrophage cells from these zebrafish at different times during the inflammatory process to identify which macrophage subtypes form and when.

The results show that unpolarized macrophages move to the sites of inflammation (caused by wounds or bacterial infection), where they become polarized into M1 cells. Over time, these M1 macrophages progressively convert into an M2-like macrophage subtype, presumably to help clear up the inflammation.

Furthermore, Nguyen Chi, Laplace-Builhe et al. show that the M1 and M2 macrophage subtypes in zebrafish are similar to those found in mammals. Therefore, genetically engineered zebrafish larvae are likely to prove useful for studying macrophage activity and polarization in living animals. DOI: 10.7554/eLife.07288.002

subsets that takes into account their specific behaviour, phenotypic diversity, functions, and modulation shall rely on a real-time tracking in the whole organism in response to environmental challenges.

Mouse and human macrophages have been classified according to their polarization state. In this classification, M1 macrophages, also referred as classically activated macrophages, are proinflammatory cells associated with the first phases of inflammation, while M2 macrophages, also known as alternatively activated macrophages, are involved in the resolution of inflammation and tissue remodelling (Gordon, 2003; Biswas and Mantovani, 2010; Sica and Mantovani, 2012). Differential cytokine and chemokine production and receptor expression define the polarization state of macrophages. However, it is worthwhile to note that such binary naming does not fully reflect the diversity of macrophage phenotypes in complex in vivo environments in which several cytokines and growth factors are released and adjust the final differentiated state (Chazaud, 2013; Thomas and Mattila, 2014). Macrophages might adopt intermediate activation phenotypes classified by the relative levels of macrophage subset-specific markers. Therefore, macrophage plasticity results in a full spectrum of macrophage subsets with a myriad of functions (Mosser and Edwards, 2008; Xue et al., 2014). Although the possible phenotype conversion of macrophages from M1 to M2 has been suggested in in vitro studies, a recent study argues for the sequential homing of M1 and M2 macrophages to the site of injury (Stout et al., 2005; Sica and Mantovani, 2012; Shechter et al., 2013). Such controversies highlight the lack of accurate real-time tracing of macrophage subtypes in vivo in the entire animal.

Inflammation is a model of choice to study the wide range of macrophage subsets involved from its initiation to its resolution. Therefore, in the present study, we propose to decipher in vivo in real time the kinetic of macrophage subset recruitment, their behaviour and their phenotypic plasticity at the molecular level during a multiple-step inflammatory process. We used the zebrafish larvae model for its easy genetic manipulation, transparency, and availability of fluorescent reporter lines to track macrophages (Ellett et al., 2011). While the existence of macrophage subtypes in zebrafish embryos

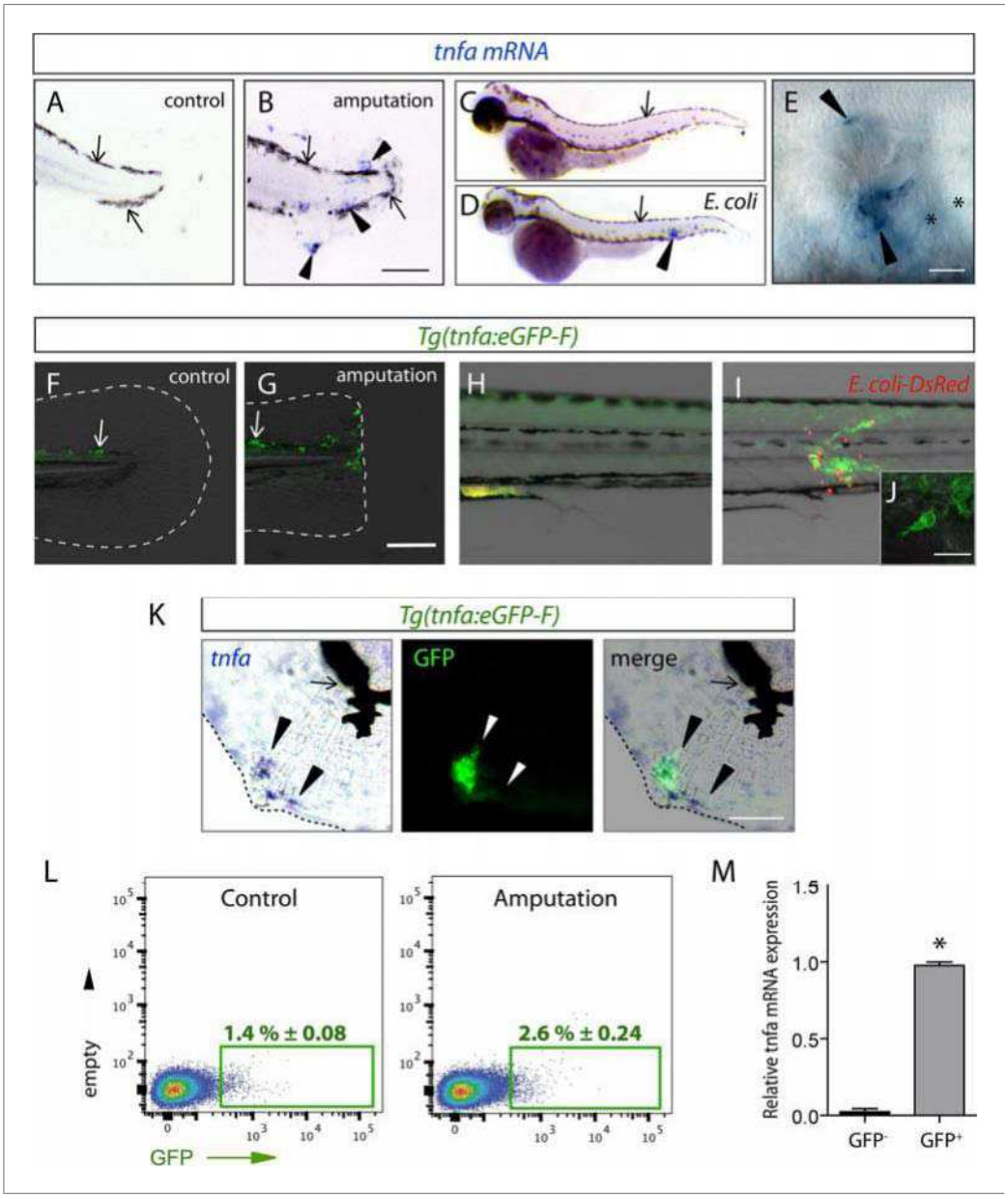

Figure 1. The (tnfa:eGFP-F) reporter line recapitulates transcriptional activation of tnfa upon wound-induced inflammation and Escherichia coli infection. (A–E) Tumour necrosis factor alpha (tnfa) mRNA expression (blue, arrowhead) was detected by in situ hybridization using tnfa anti-sense probe: at 6 hpA in (A) intact (control) and (B) amputated fins from 3 dpf WT larvae, (C) in uninfected larvae (54 hpf, hours post-fertilization) and (D, E) E. coli infected larvae (24 hpi, 54 hpf). Arrows show melanocytes (black). (E) Imaging of tnfa mRNA expression in the muscle at higher magnification, asterisks show muscle fibres, scale bar in (B) = 100 µm and in (E) = 50 µm. (F, G) eGFP fluorescence (green) was analyzed by fluorescent microscopy in (F) intact (control) and (G) amputated Tg(tnfa:eGFP-F) fins at 6 hpA, dotted lines outline the caudal fin, scale bar = 100 µm and at 16 hpi in Tg(tnfa:eGFP-F) larvae injected with (H) PBS or (I, J) E. coli (red) in the muscle. Arrows show auto-fluorescent xanthophores. (J) Multi-scan confocal analysis of GFP expression in E. coli-infected Tg(tnfa:eGFP-F) larvae, scale bar = 20 µm. (K) tnfa mRNA and eGFP-F expressions were analyzed using microscopy at 6 hpA in amputated fins from 3 dpf Tg(tnfa:eGFP-F) larvae. Dotted lines delimit the caudal fin, arrowheads show overlapping signals, and arrows show the pigments. Scale bar = 100 µm. (L) Graphed data of representative fluorescence-activated flow cytometry analysis of $eGFP^+$ cells in upon amputation. Tg(tnfa:eGFP-F) larvae were either kept intact (control) or amputated at 3 dpf, and cells were collected at 6 hr post-treatment. Green gates represent $eGFP^+$ population and mean percentage of $eGFP^+$

Figure 1. continued on next page

Figure 1. Continued

population ±s.e.m is indicated. (M) Relative expression of tnfa in eGFP- and GFP$^+$ cells in amputated larvae. Realtime RT-PCR on separated cells using EF1a as a reference gene. Graph represents the mean value of three independent experiments ±s.e.m. *$p < 0.05$. DOI: 10.7554/eLife.07288.003

has been suggested, they have not been fully characterized (Herbomel et al., 1999; Ellett et al., 2011; Cambier et al., 2013; Petrie et al., 2014). Here, we report a new reporter transgene for TNFa, a central inflammatory cytokine and well-established marker of M1 macrophages, instrumental to discriminate macrophage subsets during intravital imaging.

Results and discussion

In vivo visualization of macrophage activation and polarization

Fin wounding-induced inflammation and Escherichia coli inoculation in zebrafish larvae of 3 dpf are two well-established models triggering macrophage recruitment. Using in situ hybridization, we observed that the expression of the tumour necrosis factor alpha (tnfa), a consensus marker of M1 macrophages, was induced in cells accumulated in the caudal fin and the muscle following amputation (n_{larvae} = 29/33) and E. coli inoculation (n_{larvae} = 12/12), respectively (Figure 1A–E). To study the cells that express the tnfa transcripts, we established the Tg(tnfa:eGFP-F) transgenic zebrafish line expressing a farnesylated (membrane-bound) eGFP (eGFP-F) under the control of the tnfa promoter. While eGFP-F was undetectable in intact fins of Tg(tnfa:eGFP-F) larvae (n_{larvae} = 10/10), it was expressed in cells recruited to the wound at 6 hr post-amputation (hpA) (n_{larvae} = 16/16, Figure 1F,G). Similarly, eGFP-F expression was upregulated in cells accumulated in the muscle of Tg(tnfa:eGFP-F) larvae at 16 hr post-inoculation (hpi) of DsRed-expressing E. coli (n_{larvae} = 8/8), compared to Phosphate-buffered saline (PBS) injection (n_{larvae} = 3/3, Figure 1H,I). Confocal analysis confirmed the presence of a membrane-bound eGFP in cells displaying a typical myeloid morphology (Figure 1J). To demonstrate that the Tg(tnfa:eGFP-F) line recapitulates transcriptional activation of tnfa, we performed a simultaneous detection of tnfa mRNA by in situ hybridization and GFP-F protein by immunofluorescence in amputated larvae 6 hpA. We observed a consistent overlap between tnfa and GFP-F signal in the fin (n_{larvae} = 11/11), showing the direct correlation of eGFP-F and tnfa transcriptional activation in the fin of the reporter line (Figure 1K). In addition, we FACS-sorted GFP$^+$ cells from wounded Tg(TNFa:eGFP-F) larvae 6 hpA and performed RT-qPCR to analyze tnfa expression. We observed a significant increase of tnfa mRNA level in eGFP$^+$ cells as compared to eGFP$^-$ cells (Figure 1L,M). All together these results indicate that the Tg(TNFa:eGFP-F) reporter line recapitulates transcriptional activation of tnfa. Then, with the ability to specifically track tnfa-expressing cells, we used Tg(tnfa:eGFP-F) fish to study macrophage activation by mating them with Tg(mpeg1:mCherryF) fish in which macrophages express farnesylated mCherry (mCherryF) under the control of the macrophagespecific mpeg1 promoter (Ellett et al., 2011; Nguyen-Chi et al., 2014). In intact Tg(tnfa:eGFP-F/ mpeg1:mCherryF) larvae, no eGFP-F was observed in macrophages (Figure 2A). We imaged double transgenic larvae Tg(tnfa:eGFP-F/mpeg1:mCherryF) using 4D confocal microscopy from 45 min postamputation and found that macrophages were recruited to the wound from 1 hpA, some starting to express eGFP from 3 hpA (Figure 2B,C and Video 1). From 5 hpA already activated macrophages, that is, expressing tnfa arrived at the wound (Video 1 and Figure 2C). Similarly, infection with a crimsonexpressing E. coli in the muscle induced the expression of tnfa in phagocytes few hours following the infection (Figure 2—figure supplement 1, Video 2). Imaging of the double transgenic larvae Tg(tnfa: eGFP-F/mpeg1:mCherryF) showed that tnfa-expressing phagocytes were mainly macrophages (Figure 2—figure supplement 1, Video 2). These results show the dynamic macrophage activation in real-time in vivo including recruitment and rapid phenotypic change. During the revision of this paper, a similar result has been published (Sanderson et al., 2015).

Morphology and behaviour of macrophage phenotypes

To test whether tnfa$^+$ and tnfa$^-$ macrophages harboured different cellular characteristics, we first analyzed their morphology in fin-wounded Tg(tnfa:eGFP-F/mpeg1:mCherryF) larvae. tnfa$^+$mpeg1$^+$ cells displayed flattened and lobulated morphology (Figure 2D), while tnfa$^-$mpeg1$^+$ were elongated

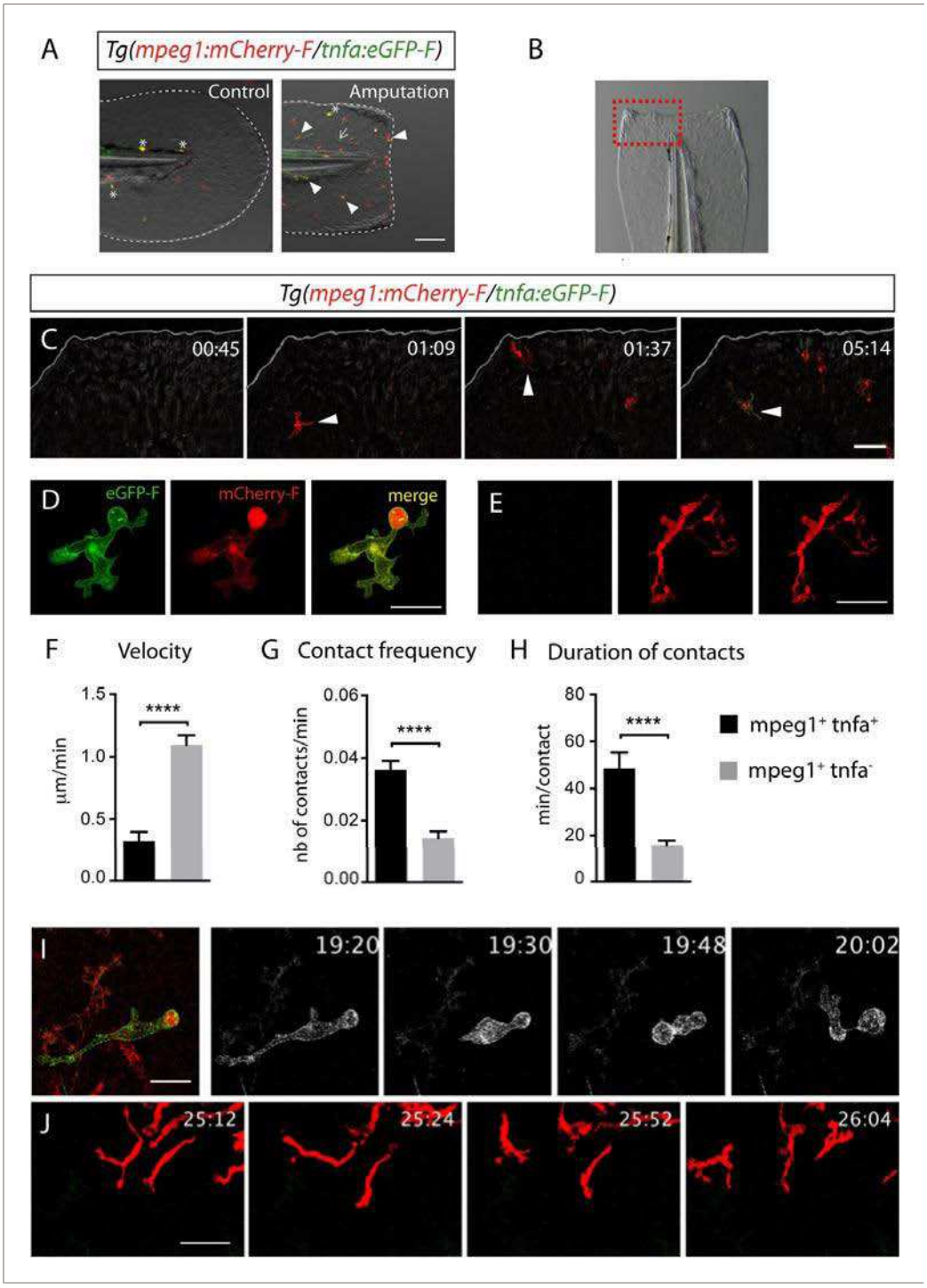

Figure 2. Activation, morphology, and behaviour of TNF-α+ macrophages in (tnfa:eGFP-F/mpeg1:mCherry-F) transgenic larvae upon wound-induced inflammation. (A) eGFP-F (green) and mCherryF (red) fluorescence was analyzed by fluorescent microscopy in intact (control) and amputated Tg(mpeg1:mCherryF/tnfa:eGFP-F) fins at 6 hpA of 3 dpf larvae. Arrowheads show recruited macrophages that express tnfa, arrows show tnfa+ cells that are not macrophages, and asterisks show auto-fluorescent pigments. Dotted lines outline the caudal fin, scale bar = 100 µm. (B) Bright-field image of the wounded fin of a 3 dpf Tg(mpeg1:mCherryF/tnfa:eGFP-F) larva. Dotted red box shows the region imaged in C. (C) Representative time-lapse maximum projections show the activation of macrophages arriving at the wound in 3 dpf amputated Tg(mpeg1:mCherryF/tnfa:eGFP-F). The time pA is shown on top right

Figure 2. continued on next page

Figure 2. Continued

corner and indicated in hours and minutes, white lines outline the caudal fin. The transcriptional activation of tnfa (green) in recruited macrophage (red, arrowhead) was first observed from 3 hpA. Scale bar = 30 µm. White lines outline the caudal fin. (D, E) Maximum projections of confocal analysis of eGFP-F (green) and mCherryF (red) expressions in recruited macrophages at (D) 18 hpA and (E) 24 hpA in Tg(mpeg1:mCherryF/tnfa:eGFP-F). tnfa$^+$mpeg1$^+$ macrophages exhibit a round and protrusive morphology, while tnfa$^-$mpeg1$^+$ macrophages exhibit a dendritic morphology. (F) Velocity of tnfa$^+$mpeg1$^+$ and tnfa$^-$mpeg1$^+$ macrophages (N = 18). (G) Frequency of macrophage–macrophage contacts and (H) time length of the contacts of tnfa$^-$mpeg1$^+$ and tnfa$^+$mpeg1$^+$ cells. Measurements were extracted from three independent videos of amputated Tg(mpeg1:mCherryF/tnfa:eGFP-F), for contact frequency, N = 15 and for duration of the interaction, N = 11 macrophages. ****p < 0.0001. (I) Representative time-lapse maximum projections show the behaviour of tnfa$^+$mpeg1$^+$ macrophages, starting

19h20 pA during 42 min. Two macrophages (green + red) interact by cell–cell contact. These macrophages (eGFP in grey) remain attached up to 40 min. Scale bar 20 =µm. (J) Representative time-lapse maximum projections show the behaviour of tnfa$^-$mpeg1$^+$ macrophages, starting 25h12 pA during 52 min. Macrophages (red) barely establish cell–cell contact. Scale bar = 30 µm.

DOI: 10.7554/eLife.07288.004

The following figure supplement is available for figure 2:

Figure supplement 1. Activation of tnfa$^+$ macrophages in (tnfa:eGFP-F/mpeg1:mCherry-F) transgenic larvae upon E. coli infection.

DOI: 10.7554/eLife.07288.005

and dendritic (Figure 2E). As we observed that tnfa$^+$mpeg1$^+$ cells were predominant at the wound at 18 hpA and tnfa$^-$mpeg1$^+$ cells at 24 hpA (data not shown), we imaged the behaviour of these macrophage populations in wounded fins from Tg(tnfa:eGFP-F/mpeg1:mCherryF) larvae at these time points. tnfa$^+$mpeg1$^+$ cells presented a lower velocity (0.32 µm/min) than tnfa$^-$mpeg1$^+$ macrophages (1.09 µm/min, Figure 2F) but a higher cell–cell contact frequency (0.036 VS 0.016 contacts/min) with other macrophages (Figure 2G,I,J and Videos 3, 4). Measurements of the duration of macrophage–macrophages contacts showed that these contacts lasted longer (48.6 min/contact) than that of tnfa$^-$mpeg1$^+$ macrophages (15.9 min/contact, Figure 2H–J and Videos 3, 4). All together these data highlight different morphology and behaviour of macrophage phenotypes in live zebrafish suggesting the existence of macrophage subsets exhibiting different functions.

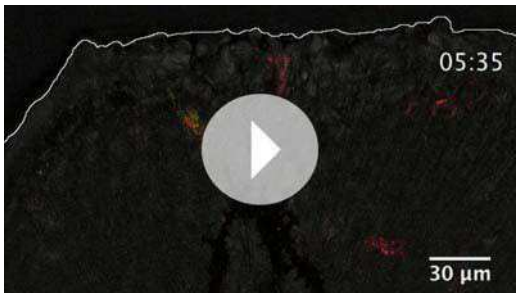

Video 1. Transcriptional activation of tnfa in macrophages of (tnfa:eGFP-F/mpeg1:mCherry-F) transgenic larvae upon amputation. Representative time-lapse maximum projections show the transcriptional activation of tumour necrosis factor alpha (tnfa) in macrophages arriving at the wound in 3 dpf amputated Tg(mpeg1: mCherryF/tnfa:eGFP-F). The time pA is shown on top right corner, white line outline the caudal fin. Scale bar = 30 µm. Image stacks were acquired every 3 min 30 s from 45 min pA to 7 hr 48 min pA at 2-µm intervals, 1024 × 512 pixel resolution using a confocal microscope

TCSSP5 SP5 inverted equipped with a HCXPL APO 40×/1.25–0.75 oil objective (Leica). Excitation wavelengths used were 488 nm for EGFP-F and 570 nm for mCherryF.

DOI: 10.7554/eLife.07288.006

Macrophages phenotypes are activated in a time-dependant manner

To quantify the respective frequency of tnfa$^+$ macrophages (mCherry$^+$eGFP$^+$ referred as dbl$^+$) and tnfa$^-$ macrophages (mCherry$^+$eGFP$^-$ referred as mCh$^+$), we performed flow cytometry analysis on cells isolated from Tg(tnfa:eGFP-F/ mpeg1:mCherryF) larvae at different time points following caudal fin amputation or E. coli. inoculation (Figure 3A,B). While only 5.6% ± 1.9 (s.e.m.) dbl$^+$ cells were detected in the mpeg1$^+$ population of the intact larvae, a steady increase of the dbl$^+$ population from 6 to 20 hpA (up to 27.33 ± 0.2%) was observed. This percentage decreased dramatically at 26 hpA to 8.75 ± 1%. In E. coli inoculation experiments, the frequency of dbl$^+$ cells increased as soon as 3 hpi (55.60 ± 0.6%) and remained stable until

26 hpi. These results demonstrate that wound-induced macrophage activation is transient compared to infection-induced macrophage activation.

Video 2. Transcriptional activation of tnfa of (tnfa: eGFP-F/mpeg1:mCherry-F) transgenic larvae upon E. coli infection. Tg(mpeg1:mCherryF/tnfa:eGFP-F) larvae were infected with crimson-expressing E. coli (blue) at 3 dpf in the muscle and imaged from 30 min pi to 10 hr 30 min pi. Representative time-lapse maximum projections show the expression of tnfa (green) induced in myeloid-like cells at the infection site from 3 hpA. The time pA is shown on top right corner, scale bar = 25 µm. Image stacks were acquired every acquired 3 min 30 s at 2-µm intervals, 512 × 512 pixel resolution with a X2 zoom using a confocal microscope TCSSP5 SP5 inverted equipped with a APO 20× objective (Leica). Excitation wavelengths used were 488 nm for EGFP-F and 580 nm for Crimson. To distinguish Crimson from mCherry, emission filter was adjusted from 630 to 750 nm.

DOI: 10.7554/eLife.07288.007

Video 3. tnfa$^+$ macrophage behaviour following amputation.

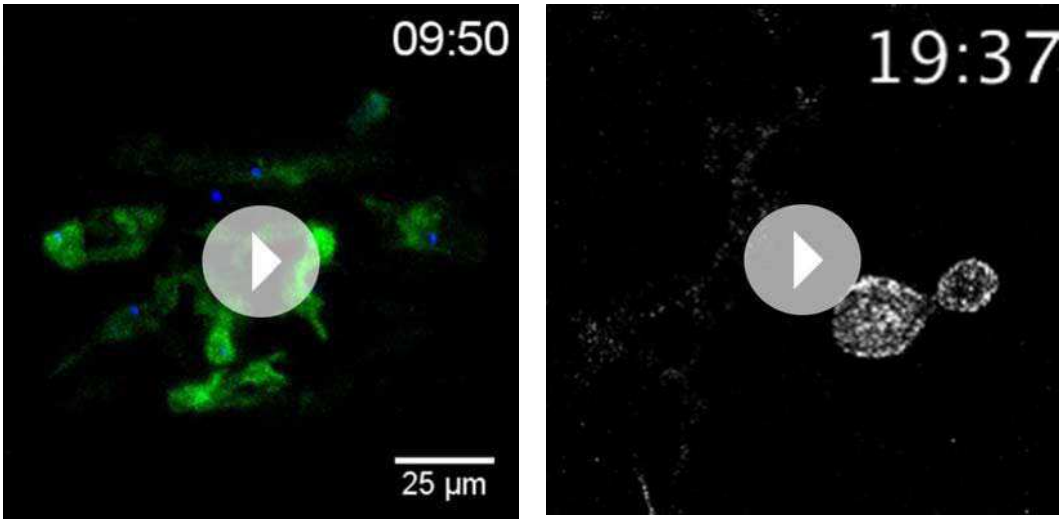

To characterize at the molecular level tnfa$^-$ and tnfa$^+$ macrophage populations during early and late phases of inflammation, we FACS-sorted dbl$^+$ and mCh$^+$ cells from Tg(tnfa:eGFP-F/mpeg1:mCherryF) tail-amputated larvae (Figure 3C) and analyzed them by qRT-PCR. In mammals, M1 and M2 macrophages are reported to be involved, respectively, in the initial phase of inflammation and in the resolution phase. Cell sorting was thus performed at 6 hpA and 26 hpA following caudal fin amputation since the kinetic analysis of macrophage subset activation (Figure 3B) suggested that these two time points correspond to initiation and resolution of inflammation, respectively. As expected, high levels of mpeg1 expression was observed in the mCh$^+$ and dbl$^+$ sorted cells at 6 and 26 hpA (Figure 3D), and high levels of tnfa expression was detected in double-positive populations at 6 hpA (Figure 3E). These observations demonstrated that fluorescence of these transgenes can be efficiently used to track and separate macrophage sub-populations. At 6 hpA, dbl$^+$ macrophages expressed high levels of tnfb, il1b, and il6 compared to mCh$^+$ macrophages (Figure 3F,G) that are well-known markers of M1 macrophages in mammals (Mantovani et al., 2002; Martinez et al., 2006). By contrast, mCh$^+$ macrophages expressed low levels of these pro-inflammatory cytokines at both 6 and 26 hpA (Figure 3F,G), but expressed high levels of tgfb1, ccr2, and cxcr4b (Figure 3H), that are specifically expressed in mammalian M2 macrophages (Mantovani et al., 2002; Martinez et al., 2006; Hao et al., 2012; Beider et al., 2014; Machado et al., 2014). Of note, neither Arginase 1 (Arg1), which is largely used as a M2 marker in mouse but not in human (Chinetti-Gbaguidi and Staels, 2011; Pourcet and Pineda-Torra, 2013), nor il10 (data not shown), a known M2 marker in mammals (Mantovani et al., 2002), was detected in zebrafish macrophages. Importantly, based on

Representative time-lapse maximum projections show the behaviour of tnfa$^+$mpeg1$^+$ macrophages in Tg(mpeg1:mCherryF/tnfa:eGFP-F) larvae following amputation, starting 19h20 pA during 42 min. Two macrophages tnfa$^+$mpeg1$^+$ interact by cell–cell contact. These macrophages (GFP in grey) remain attached up to 40 min. Scale bar = 20 µm. Image stacks were acquired every 3 min 30 s at 2 µm-intervals, 1024 × 512 pixel resolution using a confocal microscope
TCSSP5 SP5 inverted equipped with a HCXPL APO
40×/1.25–0.75 oil objective (Leica). Excitation wavelengths used were 488 nm for EGFP-F and 570 nm for mCherryF.

DOI: 10.7554/eLife.07288.008

Molecular signature of tnfa+ and tnfa− macrophage populations

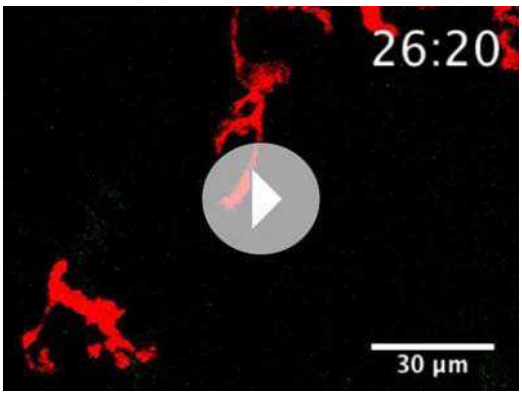

Video 4. tnfa$^-$ macrophage behaviour following amputation. Tg(mpeg1:mCherryF/tnfa:eGFP-F) caudal fins were amputated at 3 dpf. Representative time-lapse maximum projections show the behaviour of tnfa$^-$ mpeg1$^+$ macrophages, starting 25h12 pA during 42 min. Macrophages (red) scarcely establish cell–cell contact.

Scale bar = 30 µm. Image stacks were acquired every 4 min at 2 µm-intervals at 1024 × 512 pixel resolution using a confocal microscope TCSSP5 SP5 inverted equipped with a HCXPL APO 40×/1.25–0.75 oil objective (Leica). Excitation wavelengths used were

488 nm for EGFP-F and 570 nm for mCherryF.

DOI: 10.7554/eLife.07288.009

the stability of the eGFP in Tg(tnfa:eGFP-F/mpeg1:mCherryF) larvae allowing us to specifically track the behaviour and fate of proinflammatory macrophages, we found that the dbl$^+$ pro-inflammatory macrophages changed their phenotype at 26 hpA. Indeed, dbl$^+$ macrophages negative for M2 markers at 6 hpA, displayed at 26 hpA, in parallel to a significant decrease of tnfa, il1b, and il6 expression level, a significant increased expression level of ccr2 and cxcr4b (Figure 3E,H). Of note, a tendency toward differential expression level was observed for tnfb and tgfb1 between 6 and 26 hpA. To go further and demonstrate that the same macrophages are present at the wound site during inflammation and its resolution, we generated the Tg(mpeg1:GAL4/UAS:Kaede) larvae to track macrophages exploiting the conversion of the native green fluorescence of Kaede into red fluorescence under UV light. Recruited macrophages were photoconverted 6 hpA and imaged at 26 hpA revealing that early recruited macrophages were still present at the wound area 20 hr later (Figure 4—figure supplement 1). Then, GFP$^+$ macrophages were specifically tracked using time-lapse imaging of wounded Tg (mpeg1:mCherryF/TNFa:GFP-F) fins from 6 to 26 hpA. We show that initially recruited eGFP$^+$ macrophages remain at the injury site and still express the GFP (Figure 4A–C and Video 5). The analysis of macrophage behaviour over time shows that among eGFP$^+$ macrophages displaying an amyboid phenotype at the wound edge 6 hpA, 50% change toward a fibroblastic phenotype from 11 hpA when they moved distally (Video 5). All together these data show that pro-inflammatory macrophages underwent a phenotypic conversion toward an intermediate phenotype in which both M1 and M2 markers are expressed. In addition, this molecular characterization of macrophages in zebrafish reveals the conservation of macrophage subtypes between zebrafish and human.

In conclusion, we identified macrophage subsets in zebrafish and described their behaviour and fate during a process of inflammation (Figure 4D). Live imaging of transparent transgenic zebrafish larvae allowed the first real-time visualization of macrophage activation and polarization. In parallel, a molecular analysis of macrophage sub-populations highlights the evolutionary conservation of macrophages from fish to mammals. We propose that in response to wounding zebrafish, unpolarized macrophages are recruited to the inflammation site and adopt a M1-like phenotype. Subsequently, they progressively convert their functional phenotype from M1-like to M2-like in response to progressive inflammatory microenvironment changes within the tissue (Figure 4D). Live imaging of the new transgenic line we generated opens new avenues to study in real time in live vertebrates the full spectrum of macrophage activation, polarization, and functions.

Materials and methods

Ethics statement

All animal experiments described in the present study were conducted at the University of Montpellier according to European Union guidelines for handling of laboratory animals (http://ec.europa.eu/environment/chemicals/lab_animals/home_en.htm) and were approved by the Direction Sanitaire et Vet´erinaire de l'H´erault and Comit´e d'Ethique pour l'Exp´erimentation Animale under reference´ CEEA-LR-13007.

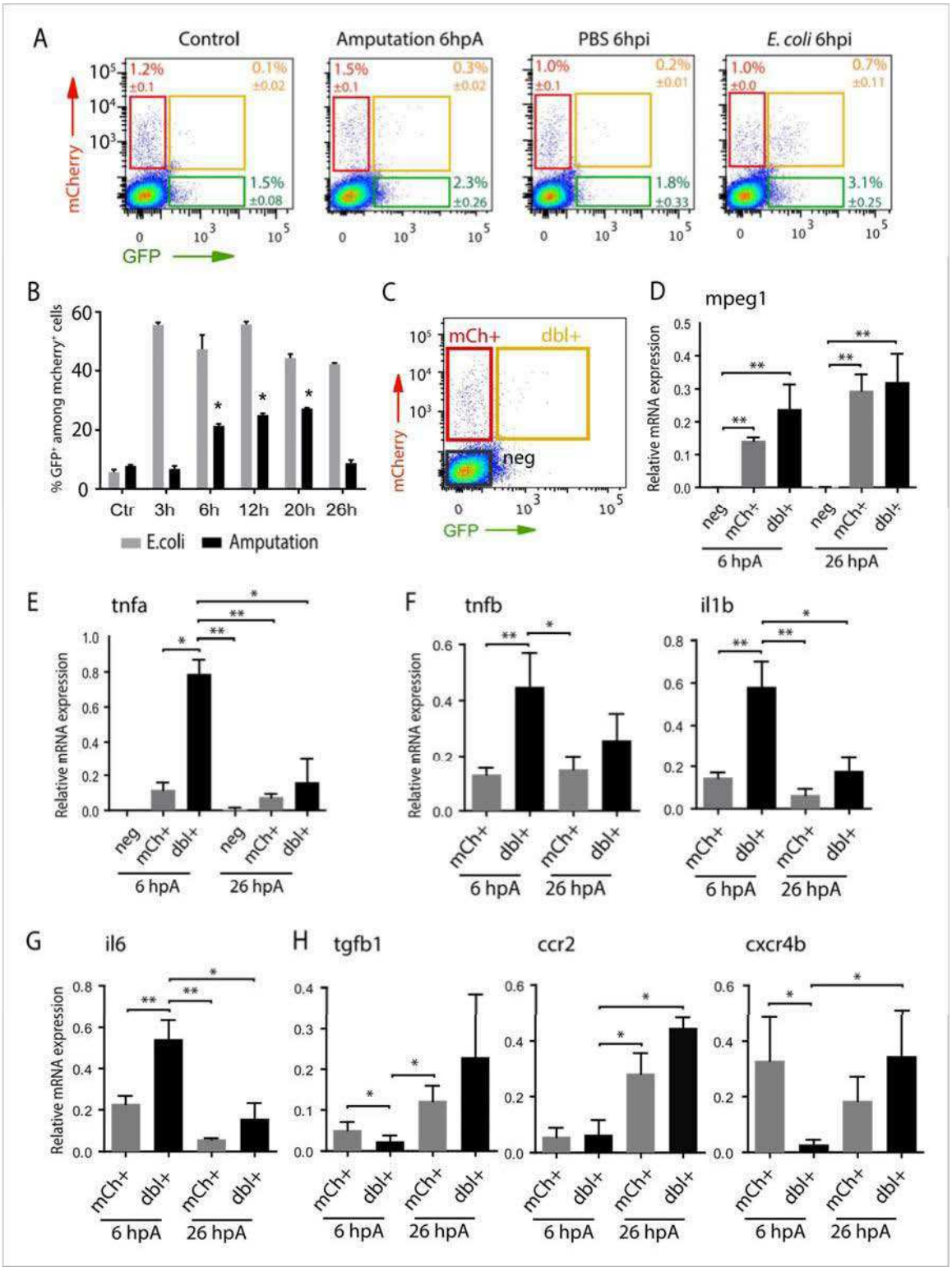

Figure 3. Isolation and molecular characterization of macrophage phenotypes. (A) Graphed data of representative fluorescence-activated flow cytometry analysis of tnfa$^+$ and tnfa$^-$ macrophages upon inflammatory stimulations. Tg(mpeg1:mCherryF/tnfa:eGFP-F) larvae were either kept intact (control), or amputated, or injected with PBS or with E. coli at 3 dpf, and cells were collected at 6 hr post-treatment. Red, green, and yellow gates represent mCherry$^+$, eGFP$^+$, and mCherry$^+$eGFP$^+$ populations, respectively. (B) Graph represents the kinetic of the frequency of mpeg1$^+$tnfa$^+$ macrophages in macrophage population (mpeg1$^+$) in three independent experiments following stimulation: amputation and E. coli infection (E. coli) at indicated time points. *$p < 0.05$ Figure 3. continued on next page

Figure 3. Continued

vs 3 hpA, mean value of three experiments ±s.e.m. (C) Gating strategy to isolate control cells (mCherry$^-$ eGFP$^-$, neg), tnfa$^-$ macrophages (mCherry$^+$ eGFP$^-$, mCh$^+$), tnfa$^+$ macrophages (mCherry$^+$eGFP$^+$, dbl$^+$). (D–H) Relative expression of (D) mpeg1, (E) tnfa, (F) tnfb, il1b, (G) il6, (H) tgfb1, ccr2, and cxcr4b in cells neg, mCh$^+$, and dbl$^+$. Tg(mpeg1:mCherryF/tnfa:eGFP-F) were amputated at 3 dpf and cells were collected and separated at 6 hpA and 26 hpA.

Real-time RT-PCR on separated cells using EF1a as a reference gene. Graph represents the mean value of five independent experiments ±s.e.m. Statistical significance between bars are indicated *$p < 0.05$, **$p < 0.01$. DOI: 10.7554/eLife.07288.010

Zebrafish line and maintenance

Fish and embryo maintenance, staging, and husbandry were as previously described (Nguyen-Chi et al., 2014). Experiments were performed using the AB zebrafish strain (ZIRC) and the transgenic line Tg(mpeg1:mCherryF) to visualize macrophages. For the photoconversion experiments, a cross of Tg (mpeg1:Gal4)^{gl25} and Tg(UAS:kaede)^{rk8} lines was used, using breeders selected for progeny with negligible silencing of the UAS transgene.

Transgenic line construction

The TNFa promoter (Gene ID: 405785) was amplified from zebrafish genomic DNA using primers zTNFaP4 (CCCGCATGCTCCACGTCTCC) and zTNFaE11N (TTATAGCGGCCGCCCGACTCTCAAGCTTCA). The resulting fragment was phosphorylated using T4PNK, digested by NotI and cloned in a farnesylated eGFP (eGFP-F) derivative of pBSKI2 (Thermes et al., 2002). The resulting plasmid (pI2promTNFa: eGFP-F) harbours a 3.8-kb fragment of the zebrafish tnfa promoter, including part of the first coding exon. It uses the endogenous ATG codon of tnfa to drive the translation of eGFP-F. The expressed eGFP-F harbours the first 7 amino acids of zebrafish TNFa at its N-terminus (MKLESRA). The expression cassette is flanked by two I-SceI sites. pI2promTNFa:eGFP-F was co-injected in fertilized eggs with the enzyme I-SceI (New England Biolabs, France). Developing embryos were injected with non-pathogenic E. coli at 3 dpf (days post-fertilization), and those that developed a specific green fluorescence were raised as putative founders. The offspring of putative founders was tested the same way in order to establish the stable transgenic line. Low expression of eGFP in the pharynx at 3 dpf was used to check larvae for the presence of the transgene.

Larva manipulation for inflammation assays and imaging

Caudal fin amputation was performed on 3 dpf larvae as described in Pase et al. (2012). The caudal fin was transected with a sterile scalpel, posterior to muscle and notochord under anaesthesia with 0.016% Tricaine (ethyl 3-aminobenzoate, Sigma Aldrich, France) in zebrafish water. Larvae were inoculated at 3 dpf by 2.10^3 CFU E. coli K12 bacteria harbouring either DsRed (van der Sar et al., 2003) or Crimson (Clontech, France) expression plasmid or no plasmid. Imaging was performed as previously described (Nguyen-Chi et al., 2014) using a confocal TCS SP5 inverted microscope with a HCXPL APO 40×/1.25–0.75 oil objective (Leica, France). Image stacks for time-lapse videos were acquired every 3–5 min, typically spanning 30–60 µm at 2-µm intervals, 1024 × 512 or 512 × 512 pixel resolution. The 4D files generated from time-lapse acquisitions were processed using Image J. They were compressed into maximum intensity projections and cropped. Brightness, contrast, and colour levels were adjusted for maximal visibility. Velocity of macrophages was measured using Manual Tracking Image J plugin. Frequency of macrophage–macrophage interaction and duration of interactions were measured manually on stack images. For tracking of macrophages, eGFP-F$^+$ mCherryF$^+$ cells from Tg(mpeg1:mCherryF/tnfa:eGFP-F) wounded fins were tracked using timelapse image series from 6 hpA (hours post-amputation) to 26 hpA.

FACS analysis, isolation of mRNA from macrophages and RT-qPCR

300 Tg(tnfa:eGFP-F/mpeg1:mCherryF) larvae were either amputated or infected as described above, then crushed on a 70-µm cell strainer (Falcon, France). Isolated cells were washed in PBS/2 mM ethylenediaminetetraacetic acid (EDTA)/2% Foetal Calf Serum (FCS), filtered through a 40-µm cell strainer, and counted. Counting of mCherry$^+$eGFP$^-$ and mCherry$^+$eGFP$^+$ cells was performed on LSRFortessa (BD Bioscience, France), and data analyzed using the Flowjo software (Tree start, Ashland, Or, USA). Sorting was done using FACS

ARIA (BD Bioscience, France) and collected in 50% FCS/50% Leibovitz L-15 medium (21083-027, Gibco, France) on ice. To isolate total RNA, cells were

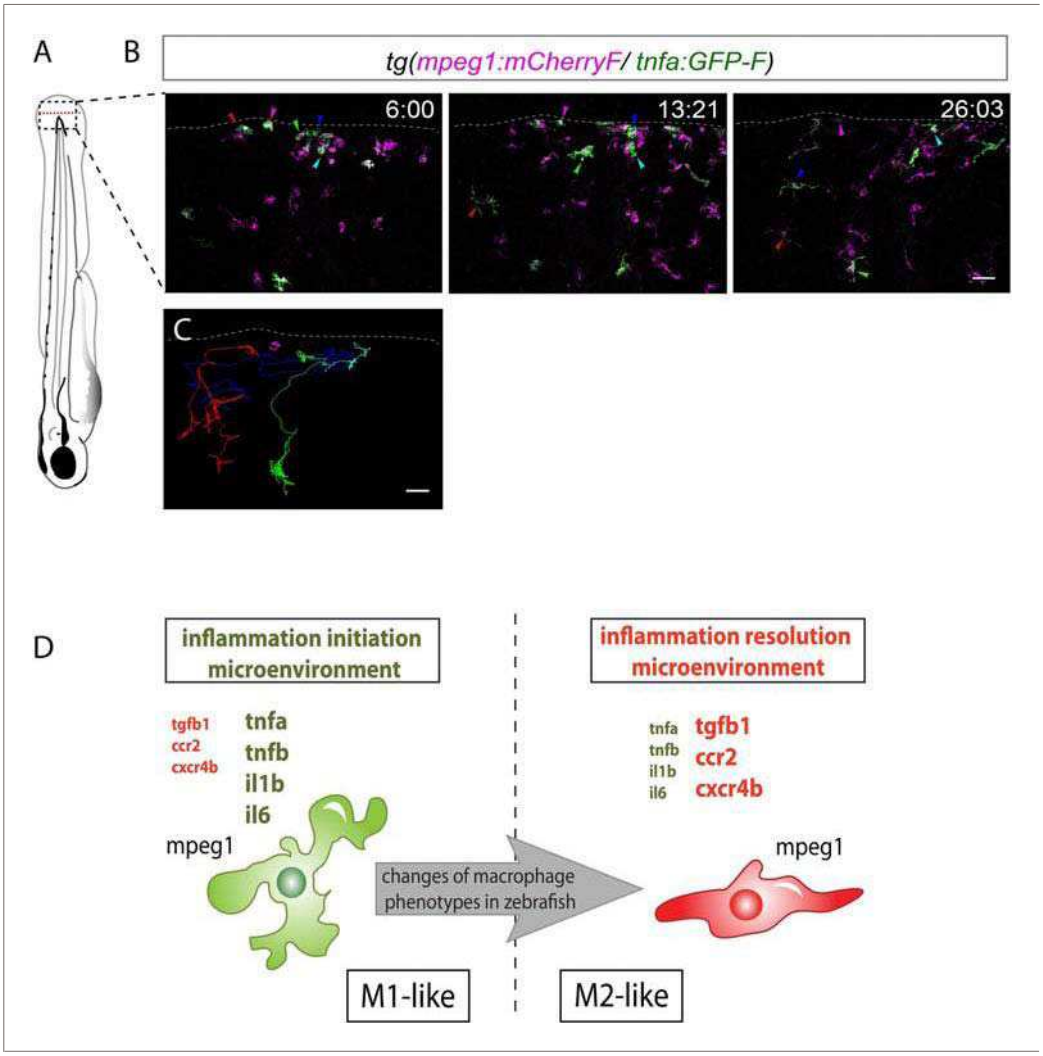

Figure 4. M1-like macrophages convert their phenotype toward M2-like phenotype in the wounded fin. (A) Diagram showing the site where caudal fin was transected (dotted red line) in 3 dpf Tg(mpeg1:mCherryF/tnfa:eGFP-F) larvae. The black dotted box represents the region imaged by confocal microscopy. (B) Representative time-lapse maximum projections of 3 dpf Tg(mpeg1:mCherryF/tnfa:eGFP-F) amputated fins showing the fate of tnfa$^+$ macrophages (magenta + green) at the indicated times pA (hours:minutes) from 6 hpA to 26 hpA. White lines delimit the caudal fin. Scale bar = 30 µm. (C) Tracking of tnfa$^+$ macrophages from 6 to 26 hpA. The distinct colours of the lines correspond to the distinct macrophages that were indicated with an arrowhead in B. (D) Diagram representing macrophage activation and polarization in zebrafish. Unpolarized macrophages (mpeg1$^+$) are mobilized and recruited to the wound following fin amputation. They are activated and polarized toward a M1-like phenotype (pro-inflammatory) few hours following fin amputation. After 24 hpA, in response to changes in environmental cues, the same macrophages progressively change their phenotype toward intermediate phenotypes and maybe fully polarized M2-like phenotype (non-inflammatory). Main markers of macrophage subtypes are indicated and resemble those found in human (tnfa/b indicates tumour necrosis factor alpha; il1b, interleukin 1-beta; il6, interleukin 6; tgfb1, tumour growth factor beta 1; ccr2, c–c chemokine receptor type 2; cxcr4b, chemokine (C-X-C motif) receptor 4b).
DOI:10.7554/eLife.07288.011

The following figure supplement is available for figure 4:

Figure supplement 1. Recruited macrophages remain in the region of tissue injury at 26 hpA.
DOI:10.7554/eLife.07288.012

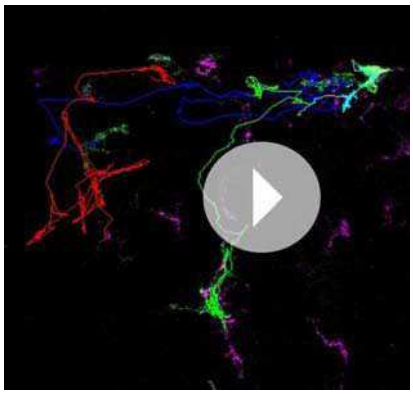

Video 5. Recruited GFP$^+$ macrophages persist in the region of tissue injury at 26 hpA. Tg(mpeg1:mCherryF/ tnfa:eGFP-F) caudal fins were amputated at 3 dpf. Representative time-lapse maximum projections show the movements of tnfa$^+$mpeg1$^+$ macrophages (green + magenta), starting 6 hpA to 26 hpA. Coloured lines correspond to eGFP$^+$ macrophage tracking that stay in the wounded fin and still express eGFP at 26 hpA. Scale bar = 30 μm. Image stacks were acquired every 4 min 40 s at 3.5-μm intervals at 512 × 512 pixel resolution using a confocal microscope TCSSP5 SP5 inverted equipped with a HCXPL APO 40×/1.25–0.75 oil objective (Leica). Excitation wavelengths used were 488 nm for EGFP-F and 570 nm for mCherryF. DOI: 10.7554/eLife.07288.013

lysed in QIAzol Lysis Reagent (Qiagen, France) and RNA extracted using miRNeasy mini kit (Qiagen-21704, France). 20 ng of total RNA was reverse transcribed using High Capacity RNA Reverse Transcription kit (Applied Biosystems, France). QPCR were performed on a LightCycler 480 system (Roche, France), following manufacturer's instructions (SYBR Green format, Roche Applied Science, Meylan, France) and using primers in Supplementary file 1: denaturation 15 s at 95˚C, annealing 10 s at 64˚C, and elongation 20 s at 72˚C. Expression levels were determined with the LightCycler analysis software (version-3.5) from 5 independent experiments. The relative amount of a given mRNA was calculated by using the formulae $2^{-\Delta Ct}$ with ef1a as reference.

Statistical analysis

Significance testing for Figures 1M, 3D–H was done using Mann–Whitney unpaired t-test, one-tail and Figure 2F–H using Mann–Whitney unpaired t-test, two-tails using GraphPad Prism 6 Software. *p < 0.05, **p < 0.01, ****p < 0.0001.

In situ hybridization

A tnfa probe was amplified from total cDNA by PCR using tnfa.55 and tnfa.58 primers (Supplementary file 1) and cloned in plasmid pCRII-TOPO. Digoxigenin (DIG)-labelled (Roche, France) sense and anti-sense RNA probes were in vitro transcribed (Biolabs, France). In situ hybridizations on whole-mount embryos were as previously described (Nguyen-Chi et al., 2012). For simultaneous detection of eGFP-F proteins and tnfa mRNA by immuno-detection and in situ hybridization, fixed and rehydrated Tg(tnfa:eGFP-F) larvae were permeabilised in ice in 100% ethanol for 5 min, then in a mixture of 50% Xylene-50% ethanol for 1 hr and in 80% acetone for 10 min at −20˚C as described in Nagaso et al. (2001). After washes in PBS0.1% Tween, larvae were post-fixed in 4% paraformaldehyde (PFA) for 20 min. Subsequent steps of hybridization, washes, and staining with NBT-BCIP (Roche, France) were as previously described in Nguyen-Chi et al. (2012). Next, unspecific-binding sites were saturated in PBS-1% bovin serum albumin (BSA)-1% lamb serum-10% Goat serum and larvae incubated 3 days with an anti-GFP antibody (MBL, 1/500). After extensive washes, larvae were incubated with a goat anti-rabbit antibody. Stained embryos were imaged using a MVX10 Olympus microscope with MVPLAPO 1× objective and XC50 camera and using a Zeiss Axioimager with a Zeiss 40× Plan-Apo 1.3 oil objective.

Photoconversion of macrophage-specific Kaede protein

Tg(mpeg1:GAL4/UAS:Kaede) embryos were raised to 3 dpf in the dark, and caudal fin was transected as described above. At 6 hpA, larvae were mounted in 1% low-melting point agarose. A 405-nm Laser Cube 405-50C on a confocal TCS SP5 inverted microscope with a HCXPL APO 40×/1.25–0.75 oil objective (Leica) was used to photoconvert the Kaede-labelled cells using 6% laser power scanning for 60 s (optimized before the experiments; data not shown). Fins were imaged before and after the photoconversion (at 6 and 26 hpA) in the green and red channels.

Acknowledgements

This work was supported by Inserm and grants from the Medical Research Foundation (projet FRM 2011 'Comite Languedoc-Roussillon-Rouergue (LRR)'), from 'La region Languedoc-Roussillon projet´ Chercheurs d'avenir 2011'

(chercheur avenir 2012-Q-173), from the French National Research Agency for 'Zebraflam' program n˚ ANR-10-MIDI-009. We thank Myriam Boyer-Clavel from the Montpellier RIO Imaging platform (MRI) for their help with cytometry and Pr Christine Dambly-Chaudiere, U5235/` CNRS, France for their help with in situ hybridization.

Additional information

Funding

Funder	Grant reference	Author
Conseil Regional´	chercheur avenir 2012-Q-173	Farida Djouad Languedoc-Roussillon
Agence Nationale de la Recherche	ANR-10-MIDI-009	Jean-Pierre Levraud, Georges Lutfalla

Conseil Regional Languedoc-Roussillon: supported Farida Djouad's work by covering´ the expenses for reagent, imaging and animal facilities as well as the salary for an engineer. Agence Nationale de la Recherche: supported Jean-Pierre Levraud's work by covering animal facility expenses and expenses for reagent and Georges Lutfalla's work by covering animal facility expenses and some expenses for reagents. The funders had no role in study design, data collection and interpretation, or the decision to submit the work for publication.

Author contributions

MN-C, BL-B, FD, Conception and design, Acquisition of data, Analysis and interpretation of data, Drafting or revising the article; JT, PL-C, GT, QTP, ID-R, J-PL, GL, Acquisition of data, Analysis and interpretation of data; KK, CJ, Conception and design, Drafting or revising the article

Ethics

Animal experimentation: All animal experiments described in the present study were conducted at the University Montpellier 2 according to European Union guidelines for handling of laboratory animals (http://ec.europa.eu/environment/chemicals/lab_animals/home_en.htm) and were approved by the Direction Sanitaire et Vet´ erinaire de l'H´ erault and Comit´ e d'Ethique pour l'Exp´ erimentation´ Animale under reference CEEA-LR-13007.

Additional files

Supplementary file

- Supplementary file 1. Genes, accession numbers, and sequences of the primers.

DOI:10.7554/eLife.07288.014

References

Beider K, Bitner H, Leiba M, Gutwein O, Koren-Michowitz M, Ostrovsky O, Abraham M, Wald H, Galun E, Peled A, Nagler A. 2014. Multiple myeloma cells recruit tumor-supportive macrophages through the CXCR4/CXCL12 axis and promote their polarization toward the M2 phenotype. Oncotarget 5:11283–11296.

Biswas SK, Mantovani A. 2010. Macrophage plasticity and interaction with lymphocyte subsets: cancer as a paradigm. Nature Immunology 11:889–896. doi: 10.1038/ni.1937.

Cambier CJ, Takaki KK, Larson RP, Hernandez RE, Tobin DM, Urdahl KB, Cosma CL, Ramakrishnan L. 2013. Mycobacteria manipulate macrophage recruitment through coordinated use of membrane lipids. Nature 505: 218–222. doi: 10.1038/nature12799.

Chazaud B. 2013. Macrophages: supportive cells for tissue repair and regeneration. Immunobiology 219:172–178. doi: 10.1016/j.imbio.2013.09.001.

Chinetti-Gbaguidi G, Staels B. 2011. Macrophage polarization in metabolic disorders: functions and regulation. Current Opinion in Lipidology 22:365–372. doi: 10.1097/MOL.0b013e32834a77b4.

Ellett F, Pase L, Hayman JW, Andrianopoulos A, Lieschke GJ. 2011. mpeg1 promoter transgenes direct macrophage-lineage expression in zebrafish. Blood 117:e49–e56. doi: 10.1182/blood-2010-10-314120.

Gordon S. 2003. Alternative activation of macrophages. Nature Reviews. Immunology 3:23–35. doi: 10.1038/ nri978.

Hao NB, Lu MH, Fan YH, Cao YL, Zhang ZR, Yang SM. 2012. Macrophages in tumor microenvironments and the progression of tumors. Clinical & Developmental Immunology 2012:948098. doi: 10.1155/2012/948098.

Herbomel P, Thisse B, Thisse C. 1999. Ontogeny and behaviour of early macrophages in the zebrafish embryo. Development 126:3735–3745.

Machado CM, Andrade LN, Teixeira VR, Costa FF, Melo CM, dos Santos SN, Nonogaki S, Liu FT, Bernardes ES, Camargo AA, Chammas R. 2014. Galectin-3 disruption impaired tumoral angiogenesis by reducing VEGF secretion from TGFbeta1-induced macrophages. Cancer Medicine 3:201–214. doi: 10.1002/cam4.173.

Mantovani A, Sozzani S, Locati M, Allavena P, Sica A. 2002. Macrophage polarization: tumor-associated macrophages as a paradigm for polarized M2 mononuclear phagocytes. Trends in Immunology 23:549–555. doi: 10.1016/S1471-4906(02)02302-5.

Martinez FO, Gordon S, Locati M, Mantovani A. 2006. Transcriptional profiling of the human monocyte-tomacrophage differentiation and polarization: new molecules and patterns of gene expression. The Journal of Immunology 177:7303–7311. doi: 10.4049/jimmunol.177.10.7303.

Mosser DM, Edwards JP. 2008. Exploring the full spectrum of macrophage activation. Nature Reviews. Immunology 8:958–969. doi: 10.1038/nri2448.

Nagaso H, Murata T, Day N, Yokoyama KK. 2001. Simultaneous detection of RNA and protein by in situ hybridization and immunological staining. The Journal of Histochemistry and Cytochemistry 49:1177–1182. doi: 10.1177/002215540104900911.

Nguyen-Chi ME, Bryson-Richardson R, Sonntag C, Hall TE, Gibson A, Sztal T, Chua W, Schilling TF, Currie PD. 2012. Morphogenesis and cell fate determination within the adaxial cell equivalence group of the zebrafish myotome. PLOS Genetics 8:e1003014. doi: 10.1371/journal.pgen.1003014.

Nguyen-Chi M, Phan QT, Gonzalez C, Dubremetz JF, Levraud JP, Lutfalla G. 2014. Transient infection of the zebrafish notochord with E. coli induces chronic inflammation. Disease Models & Mechanisms 7:871–882. doi: 10. 1242/dmm.014498.

Pase L, Nowell CJ, Lieschke GJ. 2012. In vivo real-time visualization of leukocytes and intracellular hydrogen peroxide levels during a zebrafish acute inflammation assay. Methods Enzymol 506:135–156. doi: 10.1016/B9780-12-391856-7.00032-9.

Petrie TA, Strand NS, Tsung-Yang C, Rabinowitz JS, Moon RT. 2014. Macrophages modulate adult zebrafish tail fin regeneration. Development 141:2581–2591. doi: 10.1242/dev.098459.

Pourcet B, Pineda-Torra I. 2013. Transcriptional regulation of macrophage arginase 1 expression and its role in atherosclerosis. Trends in Cardiovascular Medicine 23:143–152. doi: 10.1016/j.tcm.2012.10.003.

Sanderson LE, Chien AT, Astin JW, Crosier KE, Crosier PS, Hall CJ. 2015. An inductible transgene reports activation of macrophages in live zebrafish larvae. Developmental and Comparative Immunology 53:63–69. doi: 10.1016/j.dci.2015.06.013.

Shechter R, Miller O, Yovel G, Rosenzweig N, London A, Ruckh J, Kim KW, Klein E, Kalchenko V, Bendel P, Lira SA, Jung S, Schwartz M. 2013. Recruitment of beneficial M2 macrophages to injured spinal cord is orchestrated by remote brain choroid plexus. Immunity 38:555–569. doi: 10.1016/j.immuni.2013.02.012.

Sica A, Mantovani A. 2012. Macrophage plasticity and polarization: in vivo veritas. The Journal of Clinical Investigation 122:787–795. doi: 10.1172/JCI59643.

Stout RD, Jiang C, Matta B, Tietzel I, Watkins SK, Suttles J. 2005. Macrophages sequentially change their functional phenotype in response to changes in microenvironmental influences. The Journal of Immunology 175: 342–349. doi: 10.4049/jimmunol.175.1.342.

Thermes V, Grabher C, Ristoratore F, Bourrat F, Choulika A, Wittbrodt J, Joly JS. 2002. I-SceI meganuclease mediates highly efficient transgenesis in fish. Mechanisms of Development 118:91–98. doi: 10.1016/S0925-4773 (02)00218-6.

Thomas AC, Mattila JT. 2014. 'Of mice and men': arginine metabolism in macrophages. Front Immunol 5:479. doi: 10.3389/fimmu.2014.00479.

van der Sar AM, Musters RJ, van Eeden FJ, Appelmelk BJ, Vandenbroucke-Grauls CM, Bitter W. 2003. Zebrafish embryos as a model host for the real time analysis of Salmonella typhimurium infections. Cellular Microbiology 5: 601–611. doi: 10.1046/j.1462-5822.2003.00303.x.

Wynn TA, Chawla A, Pollard JW. 2013. Macrophage biology in development, homeostasis and disease. Nature 496:445–455. doi: 10.1038/nature12034.

Xue J, Schmidt SV, Sander J, Draffehn A, Krebs W, Quester I, De Nardo D, Gohel TD, Emde M, Schmidleithner L, Ganesan H, Nino-Castro A, Mallmann MR, Labzin L, Theis H, Kraut M, Beyer M, Latz E, Freeman TC, Ulas T, Schultze JL. 2014. Transcriptome-based network analysis reveals a spectrum model of human macrophage activation. Immunity 40:274–288. doi: 10.1016/j.immuni.2014.01.006

References

Acar, M., Kocherlakota, K.S., Murphy, M.M., Peyer, J.G., Oguro, H., Inra, C.N., Jaiyeola, C., Zhao, Z., Luby-Phelps, K., and Morrison, S.J. (2015). Deep imaging of bone marrow shows non-dividing stem cells are mainly perisinusoidal. Nature *526*, 126–130.

Adameyko, I., Lallemend, F., Furlan, A., Zinin, N., Aranda, S., Kitambi, S.S., Blanchart, A., Favaro, R., Nicolis, S., Lübke, M., et al. (2012). Sox2 and Mitf cross-regulatory interactions consolidate progenitor and melanocyte lineages in the cranial neural crest. Development *139*, 397–410.

Adamo, L., Naveiras, O., Wenzel, P.L., McKinney-Freeman, S., Mack, P.J., Gracia-Sancho, J., Suchy-Dicey, A., Yoshimoto, M., Lensch, M.W., Yoder, M.C., et al. (2009). Biomechanical forces promote embryonic haematopoiesis. Nature *459*, 1131–1135.

Adams, G.B., Chabner, K.T., Alley, I.R., Olson, D.P., Szczepiorkowski, Z.M., Poznansky, M.C., Kos, C.H., Pollak, M.R., Brown, E.M., and Scadden, D.T. (2006). Stem cell engraftment at the endosteal niche is specified by the calcium-sensing receptor. Nature *439*, 599–603.

Al-Drees, M.A., Yeo, J.H., Boumelhem, B.B., Antas, V.I., Brigden, K.W.L., Colonne, C.K., and Fraser, S.T. (2015). Making Blood: The Haematopoietic Niche throughout Ontogeny. Stem Cells Int. *2015*, 1–14.

An, M., Luo, R., and Henion, P. (2002). Differentiation and maturation of zebrafish dorsal root and sympathetic ganglion neurons. J. Comp. Neurol. *275*, 267–275.

Apostolova, G., and Dechant, G. (2009). Development of neurotransmitter phenotypes in sympathetic neurons. Auton. Neurosci. *151*, 30–38.

Arvidsson, U.L.F., Riedl, M., and Elde, R. (1997). (VAChT) Protein : A Novel and Unique Marker for Cholinergic Neurons in the. *467*, 454–467.

Becker, A.J., McCulloch, E.A., and Till, J.E. (1963). Cytological demonstration of the clonal nature of spleen colonies derived from transplanted mouse marrow cells. Nature *197*, 452–454.

Beis, D., Bartman, T., Jin, S.-W., Scott, I.C., D'Amico, L. a, Ober, E. a, Verkade, H., Frantsve, J., Field, H. a, Wehman, A., et al. (2005). Genetic and cellular analyses of zebrafish atrioventricular cushion and valve development. Development *132*, 4193–4204.

Bertrand, J.Y., Kim, A.D., Violette, E.P., Stachura, D.L., Cisson, J.L., and Traver, D. (2007). Definitive hematopoiesis initiates through a committed erythromyeloid progenitor in the zebrafish embryo. Development *134*, 4147–4156.

Bertrand, J.Y., Chi, N.C., Santoso, B., Teng, S., Stainier, D.Y.R., and Traver, D. (2010a). Haematopoietic stem cells derive directly from aortic endothelium during development. Nature *464*, 108–111.

Bertrand, J.Y., Cisson, J.L., Stachura, D.L., and Traver, D. (2010b). Notch signaling

distinguishes 2 waves of definitive hematopoiesis in the zebrafish embryo. Blood *115*, 2777–2783.

Bigas, A., and Espinosa, L. (2012). Hematopoietic stem cells: to be or Notch to be. Blood *119*, 3226–3235.

Boisset, J., Clapes, T., and Klaus, A. (2014). Progressive maturation towards hematopoietic stem cells in the mouse embryo aorta. Blood *125*, 465–470.

Boisset, J.-C., van Cappellen, W., Andrieu-Soler, C., Galjart, N., Dzierzak, E., and Robin, C. (2010). In vivo imaging of haematopoietic cells emerging from the mouse aortic endothelium. Nature *464*, 116–120.

Bonifer, C., Faust, N., Geiger, H., and Müller, A.M. (1998). Developmental changes in the differentiation capacity of haematopoietic stem cells. Immunol. Today *19*, 236–241.

Boyer, S.W., Schroeder, A. V., Smith-Berdan, S., and Forsberg, E.C. (2011). All Hematopoietic Cells Develop from Hematopoietic Stem Cells through Flk2/Flt3-Positive Progenitor Cells. Cell Stem Cell *9*, 64–73.

Bruijn, M.F.T.R. De, Ma, X., Robin, C., Ottersbach, K., Sanchez, M., and Dzierzak, E. (2002). to the Endothelial Cell Layer in the Midgestation Mouse Aorta. *16*, 673–683.

Bylund, D.B. (1992). Subtypes of a1- and a2-adrenergic receptors. FASEB J *6*, 832–839.

Calvi, L.M., and Link, D.C. (2014). Cellular complexity of the bone marrow hematopoietic stem cell niche. Calcif Tissue Int. *94*, 112–124.

Lo Celso, C., Fleming, H.E., Wu, J.W., Zhao, C.X., Miake-Lye, S., Fujisaki, J., Côté, D., Rowe, D.W., Lin, C.P., and Scadden, D.T. (2009). Live-animal tracking of individual haematopoietic stem/progenitor cells in their niche. Nature *457*, 92–96.

Ceredig, R., Rolink, A.G., and Brown, G. (2009). Models of haematopoiesis: seeing the wood for the trees. Nat. Rev. Immunol. *9*, 293–300.

Chen, J.Y., Miyanishi, M., Wang, S.K., Yamazaki, S., Sinha, R., Kao, K.S., Seita, J., Sahoo, D., Nakauchi, H., and Weissman, I.L. (2016). Hoxb5 marks long-term haematopoietic stem cells and reveals a homogenous perivascular niche. Nature *530*, 223–227.

Chen, M.J., Yokomizo, T., Zeigler, B., Dzierzak, E., and Speck, A. (2009). Runx1 is required for the endothelial to hematopoietic cell transition but not thereafter. Nature *457*, 887–891.

Chi, N.C., Shaw, R.M., De Val, S., Kang, G., Jan, L.Y., Black, B.L., and Stainier, D.Y.R. (2008). Foxn4 directly regulates tbx2b expression and atrioventricular canal formation. Genes Dev. *22*, 734–739.

Chow, A., Lucas, D., Hidalgo, A., Méndez-Ferrer, S., Hashimoto, D., Scheiermann, C., Battista, M., Leboeuf, M., Prophete, C., van Rooijen, N., et al. (2011). Bone marrow CD169+ macrophages promote the retention of hematopoietic stem and progenitor cells in the mesenchymal stem cell niche. J. Exp. Med. *208*, 261–271.

Ciau-Uitz, a, Walmsley, M., and Patient, R. (2000). Distinct origins of adult and embryonic blood in Xenopus. Cell *102*, 787–796.

Clarke, R.L., Yzaguirre, A.D., Yashiro-Ohtani, Y., Bondue, A., Blanpain, C., Pear, W.S., Speck, N. a, and Keller, G. (2013). The expression of Sox17 identifies and regulates haemogenic

endothelium. Nat. Cell Biol. *15*, 502–510.

Clements, W.K., Kim, A.D., Ong, K.G., Moore, J.C., Lawson, N.D., and Traver, D. (2011). A somitic Wnt16/Notch pathway specifies haematopoietic stem cells. Nature *474*, 220–224.

Coman, O.A., Păunescu, H., Ghiţă, I., Coman, L., Bădărău, A., and Fulga, I. (2008). Beta 3 adrenergic receptors: Molecular, histological, functional and pharmacological approaches. Rom. J. Morphol. Embryol. *50*, 169–179.

Condeelis, J., and Pollard, J.W. (2006). Macrophages: obligate partners for tumor cell migration, invasion, and metastasis. Cell *124*, 263–266.

Cougoule, C., Van Goethem, E., Le Cabec, V., Lafouresse, F., Dupré, L., Mehraj, V., Mège, J.-L., Lastrucci, C., and Maridonneau-Parini, I. (2012). Blood leukocytes and macrophages of various phenotypes have distinct abilities to form podosomes and to migrate in 3D environments. Eur. J. Cell Biol. *91*, 938–949.

Crawford, B.D., and Pilgrim, D.B. (2005). Ontogeny and regulation of matrix metalloproteinase activity in the zebrafish embryo by in vitro and in vivo zymography. Dev. Biol. *286*, 405–414.

Crisan, M., Kartalaei, P.S., Neagu, A., Karkanpouna, S., Yamada-inagawa, T., Purini, C., Vink, C.S., Linden, R. Van Der, Ijcken, W. Van, Chuva, S.M., et al. (2016). BMP and Hedgehog Regulate Distinct AGM Hematopoietic Stem Cells Ex Vivo. Stem Cell Reports *6*, 383–395.

Cumano, A., and Godin, I. (2007). Ontogeny of the hematopoietic system. Annu. Rev. Immunol. *25*, 745–785.

Cumano, A., Dieterlen-Lievre, F., and Godin, I. (1996). Lymphoid potential, probed before circulation in mouse, is restricted to caudal intraembryonic splanchnopleura. Cell *86*, 907–916.

Dale, L., Howes, G., Price, B.M., and Smith, J.C. (1992). Bone morphogenetic protein 4: a ventralizing factor in early Xenopus development. Development *115*, 573–585.

Dar, a, Schajnovitz, a, Lapid, K., Kalinkovich, a, Itkin, T., Ludin, a, Kao, W.-M., Battista, M., Tesio, M., Kollet, O., et al. (2011). Rapid mobilization of hematopoietic progenitors by AMD3100 and catecholamines is mediated by CXCR4-dependent SDF-1 release from bone marrow stromal cells. Leukemia *25*, 1286–1296.

Dieterlen-Lievre, F. (1975). On the origin of haematopoietic stem cells in the avian embryo: an experimental approach. J Embryol Exp Morphol *33*, 607–619.

Dieterlen-Lièvre, F., Pouget, C., Bollérot, K., and Jaffredo, T. (2006). Are intra-aortic hemopoietic cells derived from endothelial cells during ontogeny? Trends Cardiovasc. Med. *16*, 128–139.

DiMascio, L., Voermans, C., Uqoezwa, M., Duncan, A., Lu, D., Wu, J., Sankar, U., and Reya, T. (2007). Identification of Adiponectin as a Novel Hemopoietic Stem Cell Growth Factor. J. Immunol. *178*, 3511–3520.

Douarin, N.M. Le, and Smith, J. (1988). Development of the peripheral nervous system from the neural crest. Ann.Rev.Cell Biol. *4*, 375–404.

Durand, C., Robin, C., Bollerot, K., Baron, M.H., Ottersbach, K., and Dzierzak, E. (2007). Embryonic stromal clones reveal developmental regulators of definitive hematopoietic stem cells.

Proc. Natl. Acad. Sci. U. S. A. *104*, 20838–20843.

Dutton, J.R., Antonellis, A., Carney, T.J., Rodrigues, F.S.L.M., Pavan, W.J., Ward, A., and Kelsh, R.N. (2008). An evolutionarily conserved intronic region controls the spatiotemporal expression of the transcription factor Sox10. BMC Dev. Biol. *8*, 105.

Dyachuk, V., Furlan, A., Shahidi, M.K., Giovenco, M., Kaukua, N., Konstantinidou, C., Pachnis, V., Memic, F., Marklund, U., Müller, T., et al. (2014). Parasympathetic neurons originate from nerve-associated peripheral glial progenitors. Science *345*, 82–87.

Dzierzak, E., and Robin, C. (2010). Placenta as a source of hematopoietic stem cells. Trends Mol. Med. *16*, 361–367.

Ebert, R.H., and Florey, H.W. (1939). The Extravascular Development of the Monocyte Observed In vivo. Br. J. Exp. Pathol. *20*, 342.

Ellett, F., and Lieschke, G.J. (2010). Zebrafish as a model for vertebrate hematopoiesis. Curr. Opin. Pharmacol. *10*, 563–570.

Ellett, F., Pase, L., Hayman, J.W., Andrianopoulos, A., and Lieschke, G.J. (2011). Mpeg1 Promoter Transgenes Direct Macrophage-Lineage Expression in Zebrafish. Blood *117*, e49-56.

Ema, H., and Nakauchi, H. (2015). Expansion of hematopoietic stem cells in the developing liver of a mouse embryo. *95*, 2284–2289.

Espinosa-Medina, I., Outin, E., Picard, C.A., Chettouh, Z., Dymecki, S.Consalez, G.G., Coppola, E., and Brunet, J.-F. (2014). Parasympathetic ganglia derive from Schwann cell precursors. Science (80-.). *345*, 87–90.

Espín-Palazón, R., Stachura, D.L., Campbell, C.A., García-Moreno, D., Del Cid, N., Kim, A.D., Candel, S., Meseguer, J., Mulero, V., and Traver, D. (2014). Proinflammatory Signaling Regulates Hematopoietic Stem Cell Emergence. Cell *159*, 1070–1085.

Fairchild, K.D., and Shea, T.M.O. (2011). Heart Rate Characteristics: Physiomarkers for Detection of Late- Onset Neonatal Sepsis. Clin Perinatol *37*, 581–598.

Fitch, S.R., Kimber, G.M., Wilson, N.K., Parker, A., Mirshekar-Syahkal, B., Göttgens, B., Medvinsky, A., Dzierzak, E., and Ottersbach, K. (2012). Signaling from the sympathetic nervous system regulates hematopoietic stem cell emergence during embryogenesis. Cell Stem Cell *11*, 554–566.

Friedl, P. (2004). Prespecification and plasticity: Shifting mechanisms of cell migration. Curr. Opin. Cell Biol. *16*, 14–23.

Friedl, P., and Weigelin, B. (2008). Interstitial leukocyte migration and immune function. Nat. Immunol. *9*, 960–969.

Friedl, P., and Wolf, K. (2010). Plasticity of cell migration: a multiscale tuning model. J. Cell Biol. *188*, 11–19.

Frielle, T., Kobilka, B., Lefkowitz, R.J., and Caron, M.G. (1988). Human B1 and B2-adrenergic receptors: strudurally and fund nally related receptors derived from distind genes. TINS *11*, 321–324.

Gekas, C., Dieterlen-Li??vre, F., Orkin, S.H., and Mikkola, H.K.A. (2005). The placenta is a niche for hematopoietic stem cells. Dev. Cell *8*, 365–375.

Gering, M., and Patient, R. (2005). Hedgehog signaling is required for adult blood stem cell formation in zebrafish embryos. Dev. Cell *8*, 389–400.

Gering, M., Rodaway, a R., Göttgens, B., Patient, R.K., and Green, a R. (1998). The SCL gene specifies haemangioblast development from early mesoderm. EMBO J. *17*, 4029–4045.

Gilmour, D.T., Maischein, H.-M., and Nüsslein-Volhard, C. (2002). Migration and Function of a Glial Subtype in the Vertebrate Peripheral Nervous System. Neuron *34*, 577–588.

Goessling, W., North, T.E., Loewer, S., Lord, A.M., Lee, S., Stoick-Cooper, C.L., Weidinger, G., Puder, M., Daley, G.Q., Moon, R.T., et al. (2009). Genetic interaction of PGE2 and Wnt signaling regulates developmental specification of stem cells and regeneration. Cell *136*, 1136–1147.

Van Goethem, E., Poincloux, R., Gauffre, F., Maridonneau-Parini, I., and Le Cabec, V. (2010). Matrix Architecture Dictates Three-Dimensional Migration Modes of Human Macrophages: Differential Involvement of Proteases and Podosome-Like Structures. J. Immunol. *184*, 1049–1061.

Gomez Perdiguero, E., Klapproth, K., Schulz, C., Busch, K., Azzoni, E., Crozet, L., Garner, H., Trouillet, C., de Bruijn, M.F., Geissmann, F., et al. (2014). Tissue-resident macrophages originate from yolk-sac-derived erythro-myeloid progenitors. Nature *518*, 547–551.

Gong, Y., Hart, E., Shchurin, A., and Hoover-Plow, J. (2008). Inflammatory macrophage migration requires MMP-9 activation by plasminogen in mice. J. Clin. Invest. *118*, 3012–3024.

Goodell, B.M.A., Brose, K., Paradis, G., Conner, A.S., and Mulligan, R.C. (1996). Isolation and Functional Properties o f Murine Hematopoietic Stem Cells that are Replicating In Vivo. J. Exp. Med. *183*.

Gordon, S., and Taylor, P.R. (2005). Monocyte and macrophage heterogeneity. Nat. Rev. Immunol. *5*, 953–964.

Goridis, C., and Rohrer, H. (2002). Specification of catecholaminergic and serotonergic neurons. Nat. Rev. Neurosci. *3*, 531–541.

Graf, T. (2002). Differentiation plasticity of hematopoietic cells Review article Differentiation plasticity of hematopoietic cells. Blood *99*, 3089–3101.

Granneman, J.G. (2001). The putative B4-adrenergic receptor is a novel state of the B1-adrenergic receptor. Am J Physiol Endocrinol Metab *43*, E199–E202.

Green, S. a., Simoes-Costa, M., and Bronner, M.E. (2015). Evolution of vertebrates as viewed from the crest. Nature *520*, 474–482.

Gritz, E., and Hirschi, K.K. (2016). Specification and function of hemogenic endothelium during embryogenesis. Cell. Mol. Life Sci. *73*, 1547–1567.

Grosselin, J., Sii-Felice, K., Payen, E., Chretien, S., Roux, D.T. Le, and Leboulch, P. (2013). Arrayed lentiviral barcoding for quantification analysis of hematopoietic dynamics. Stem Cells *31*, 2162–2171.

Guiet, R., Van Goethem, E., Cougoule, C., Balor, S., Valette, A., Al Saati, T., Lowell, C. a, Le Cabec, V., and Maridonneau-Parini, I. (2011). The process of macrophage migration promotes matrix metalloproteinase-independent invasion by tumor cells. J. Immunol. *187*, 3806–

3814.

Guiet, R., Vérollets, C., Lamsoul, I., Cougoule, C., Poincloux, R., Labrousse, A., Calderwood, D.A., Glogauer, M., Lutz, P.G., and Maridonneau-Parini, I. (2012). Macrophage mesenchymal migration requires podosome stabilization by filamin A. J. Biol. Chem. *287*, 13051–13062.

Herbomel, P., Thisse, B., and Thisse, C. (1999). Ontogeny and behaviour of early macrophages in the zebrafish embryo. Development *126*, 3735–3745.

Hoppe, P., Schwarzfischer, M., Loeffler, D., Kokkaliaris, K., Hilsenbeck, O., Moritz, N., Endele, M., Filipczyk, A., Gambardella, A., Ahmed, N., et al. (2016). Early myeloid lineage choice is not initiated by random PU.1 to GATA1 protein ratios. Nature *535*, 299–302.

Howard, M.J. (2005). Mechanisms and perspectives on differentiation of autonomic neurons. Dev. Biol. *277*, 271–286.

Howe, K., Clark, M.D., Torroja, C.F., Torrance, J., Berthelot, C., Muffato, M., Collins, J.E., Humphray, S., McLaren, K., Matthews, L., et al. (2013). The zebrafish reference genome sequence and its relationship to the human genome. Nature *496*, 498–503.

Hsu, Y.-C., and Fuchs, E. (2012). A family business: stem cell progeny join the niche to regulate homeostasis. Nat. Rev. Mol. Cell Biol. *13*, 103–114.

Hung, S.-I., Chang, A.C., Kato, I., and Chang, N.-C.A. (2002). Transient expression of Ym1, a heparin-binding lectin, during developmental hematopoiesis and inflammation. J. Leukoc. Biol. *72*, 72–82.

Iacovino, M., Chong, D., Szatmari, I., Hartweck, L., Rux, D., Caprioli, A., Cleaver, O., and Kyba, M. (2011). HoxA3 is an apical regulator of haemogenic endothelium. Nat. Cell Biol. *13*, 72–78.

Ishibashi, T., Yokota, T., Tanaka, H., Ichii, M., Sudo, T., Satoh, Y., Doi, Y., Tanimura, A., Hamanaka, Y., Ezoe, S., et al. (2015). Endothelial cell-selective adhesion molecule is a novel human hematopoietic stem cell marker associated with a subset of human leukemias. Exp. Hematol. *43*, S69.

Itoi, M., Kawamoto, H., Katsura, Y., and Amagai, T. (2001). Two distinct steps of immigration of hematopoietic progenitors into the early thymus anlage. Int. Immunol. *13*, 1203–1211.

Jaffredo, T., Gautier, R., Eichmann, A., and Dieterlen-Lievre, F. (1998). Intraaortic hemopoietic cells are derived from endothelial cells during ontogeny. Development *125*, 4575–83.

Jaffredo, T., Richard, C., Pouget, C., Teillet, M.-A., Bollérot, K., Gautier, R., and Drevon, C. (2010). Aortic remodelling during hemogenesis: is the chicken paradigm unique? Int. J. Dev. Biol. *54*, 1045–1054.

Johnson, M. (2006). Molecular mechanisms of B2-adrenergic receptor function, response, and regulation. J. Allergy Clin. Immunol. *117*, 18–24.

Jones, G.E. (2000). Cellular signaling in macrophage migration and chemotaxis. J. Leukoc. Biol. *68*, 593–602.

Jones, C. V, and Ricardo, S.D. (2013). Macrophages and CSF-1: implications for

development and beyond. Organogenesis *9*, 249–260.

Jordan, H.E. (1916). Evidence of hemogenic capacity of endothelium. Anatatomical Rec. *10*, 417–420.

Joyce, J. a, and Pollard, J.W. (2009). Microenvironmental regulation of metastasis. Nat. Rev. Cancer *9*, 239–252.

Kabrun, N., Bühring, H.J., Choi, K., Ullrich, a, Risau, W., and Keller, G. (1997). Flk-1 expression defines a population of early embryonic hematopoietic precursors. Development *124*, 2039–2048.

Katayama, Y., Battista, M., Kao, W.-M., Hidalgo, A., Peired, A.J., Thomas, S.A., and Frenette, P.S. (2006). Signals from the sympathetic nervous system regulate hematopoietic stem cell egress from bone marrow. Cell *124*, 407–421.

Keely, P.J., Westwick, J.K., Whitehead, I.P., Der, C.J., and Parise, L. V (1997). Cdc42 and Rac1 induce integrin-mediated cell motility and invasiveness through PI(3)K. Nature *390*, 632–636.

Khan, J.A., Mendelson, A., Kunisaki, Y., Birbrair, A., Kou, Y., Arnal-Estape, A., Pinho, S., Cierl, P., Nakahara, F., Ma'ayan, A., et al. (2016). Fetal liver hematopoietic stem cell niches associate with portal vessels. Science *351*, 176–180.

Kiel, M.J., Yilmaz, ??mer H., Iwashita, T., Yilmaz, O.H., Terhorst, C., and Morrison, S.J. (2005). SLAM family receptors distinguish hematopoietic stem and progenitor cells and reveal endothelial niches for stem cells. Cell *121*, 1109–1121.

Kim, A.D., Melick, C.H., Clements, W.K., Stachura, D.L., Distel, M., Panáková, D., MacRae, C., Mork, L.A., Crump, J.G., and Traver, D. (2014). Discrete Notch signaling requirements in the specification of hematopoietic stem cells. EMBO J. *33*, 2363–2373.

Kim, J., Lo, L., Dormand, E., and Anderson, D.J. (2003). SOX10 maintains multipotency and inhibits neuronal differentiation of neural crest stem cells. Neuron *38*, 17–31.

Kim, P.G., Albacker, C.E., Lu, Y., Jang, I., Lim, Y., Heffner, G.C., Arora, N., Bowman, T. V, Lin, M.I., Lensch, M.W., et al. (2013). Signaling axis involving Hedgehog, Notch, and Scl promotes the embryonic endothelial-to-hematopoietic transition. Proc. Natl. Acad. Sci. U. S. A. *110*, E141-50.

Kimmel, C.B., Ballard, W.W., Kimmel, S.R., Ullmann, B., and Schilling, T.F. (1995). Stages of embryonic development of the zebrafish. Dev. Dyn. *203*, 253–310.

Kissa, K., and Herbomel, P. (2010). Blood stem cells emerge from aortic endothelium by a novel type of cell transition. Nature *464*, 112–115.

Kissa, K., Murayama, E., Zapata, A., Cortés, A., Perret, E., Machu, C., and Herbomel, P. (2008). Live imaging of emerging hematopoietic stem cells and early thymus colonization. Blood *111*, 1147–1156.

Kumai, Y., Ward, M. a R., and Perry, S.F. (2012). β-Adrenergic regulation of Na+ uptake by larval zebrafish Danio rerio in acidic and ion-poor environments. Am. J. Physiol. Regul. Integr. Comp. Physiol. *303*, R1031-41.

Lam, E.Y.N., Chau, J.Y.M., Kalev-Zylinska, M.L., Fountaine, T.M., Mead, R.S., Hall, C.J.,

Crosier, P.S., Crosier, K.E., and Flores, M.V. (2009). Zebrafish runx1 promoter-EGFP transgenics mark discrete sites of definitive blood progenitors. Blood *113*, 1241–1249.

Lam, E.Y.N., Hall, C.J., Crosier, P.S., Crosier, K.E., and Flores, M.V. (2010). Live imaging of Runx1 expression in the dorsal aorta tracks the emergence of blood progenitors from endothelial cells. Blood *116*, 909–915.

Lancrin, C., Sroczynska, P., Stephenson, C., Allen, T., Kouskoff, V., and Lacaud, G. (2009). The haemangioblast generates haematopoietic cells through a haemogenic endothelium stage. Nature *457*, 892–895.

Lancrin, C., Mazan, M., Stefanska, M., Patel, R., Lichtinger, M., Costa, G., Vargel, O., Wilson, N.K., Moroy, T., Bonifer, C., et al. (2012). GFI1 and GFI1B control the loss of endothelial identity of hemogenic endothelium during hematopoietic commitment. Blood *120*, 314–322.

Lapidot, T. (2001). Mechanism of human stem cell migration and repopulation of NOD/SCID and B2mnull NOD/SCID mice. The role of SDF-1/CXCR4 interactions. Ann. N. Y. Acad. Sci. *938*, 83–95.

Lapidot, T., Dar, A., and Kollet, O. (2005). How do stem cells nd their way home? Blood *106*, 1901–1910.

Larochelle, A., Savona, M., Wiggins, M., Anderson, S., Ichwan, B., Keyvanfar, K., Morrison, S.J., and Dunbar, C.E. (2011). Human and rhesus macaque hematopoietic stem cells cannot be purified based only on SLAM family markers. Blood *117*, 1550–1554.

Leposavić, G., Pilipović, I., Radojević, K., Pešić, V., Perišić, M., and Kosec, D. (2008). Catecholamines as immunomodulators: A role for adrenoceptor-mediated mechanisms in fine tuning of T-cell development. Auton. Neurosci. Basic Clin. *144*, 1–12.

Li, Z.J., and Cho, C.H. (2011). Neurotransmitters, more than meets the eye--neurotransmitters and their perspectives in cancer development and therapy. Eur. J. Pharmacol. *667*, 17–22.

Li, Y., Esain, V., Teng, L., Xu, J., Kwan, W., Frost, I.M., Yzaguirre, A.D., Cai, X., Cortes, M., Maijenburg, M.W., et al. (2014). Inflammatory signaling regulates embryonic hematopoietic stem and progenitor cell production. 2597–2612.

Lim, Y., and Matsui, W. (2010). Hedgehog Signaling in Hematopoiesis. Crit Rev Eukaryot Gene Expr. *20*, 129–139.

Lim, W.F., Inoue-Yokoo, T., Tan, K.S., Lai, M., and Sugiyama, D. (2013). Hematopoietic cell differentiation from embryonic and induced pluripotent stem cells. Stem Cell Res. Ther. *4*, 71.

Lin, H.-F., Traver, D., Zhu, H., Dooley, K., Paw, B.H., Zon, L.I., and Handin, R.I. (2005). Analysis of thrombocyte development in CD41-GFP transgenic zebrafish. Blood *106*, 3803–3810.

Ling, K.-W., Ottersbach, K., van Hamburg, J.P., Oziemlak, A., Tsai, F.-Y., Orkin, S.H., Ploemacher, R., Hendriks, R.W., and Dzierzak, E. (2004). GATA-2 plays two functionally distinct roles during the ontogeny of hematopoietic stem cells. J. Exp. Med. *200*, 871–882.

Lugus, J.J., Chung, Y.S., Mills, J.C., Kim, S.-I., Grass, J.A., Kyba, M., Doherty, J.M., Bresnick, E.H., and Choi, K. (2007). GATA2 functions at multiple steps in hemangioblast development and differentiation. Development *134*, 393–405.

Magnon, C., Hall, S.J., Lin, J., Xue, X., Gerber, L., Freedland, S.J., and Frenette, P.S. (2013). Autonomic nerve development contributes to prostate cancer progression. Science *341*, 1236361.

Marshall, C.J., Kinnon, C., and Thrasher, A.J. (2000). Polarized expression of bone morphogenetic protein-4 in the human aorta- gonad-mesonephros region. Blood *96*, 1591–3.

Maximov, A. (1909). Der lymphozyt als gemeinsame stammzelle der verschiedenen blutelemente in der embryonalen entwicklung und im postfetalen leben der saugetiere. Fol. Haematol. *8*, 125–134.

Mccorry, L.K. (2007). TEACHERS ' TOPICS Physiology of the Autonomic Nervous System. *71*.

McKinney-Freeman, S.L., Naveiras, O., Yates, F., Loewer, S., Philitas, M., Curran, M., Park, P.J., and Daley, G.Q. (2009). Surface antigen phenotypes of hematopoietic stem cells from embryos and murine embryonic stem cells. *114*, 268–278.

McWhorter, F.Y., Wang, T., Nguyen, P., Chung, T., and Liu, W.F. (2013). Modulation of macrophage phenotype by cell shape. Proc. Natl. Acad. Sci. U. S. A. *110*, 17253–17258.

Medvinsky, A., and Dzierzak, E. (1996). Definitive Hematopoiesis Is Autonomously Initiated by the AGM Region. Cell *86*, 897–906.

Medvinsky, A., Rybtsov, S., and Taoudi, S. (2011). Embryonic origin of the adult hematopoietic system: advances and questions. Development *138*, 1017–1031.

Mendelson, A., and Frenette, P.S. (2014). Hematopoietic stem cell niche maintenance during homeostasis and regeneration. Nat. Med. *20*, 833–846.

Mendez-Ferrer, S., Lucas, D., Battista, M., and Frenette, P.S. (2008). Haematopoietic stem cell release is regulated by circadian oscillations. Nature *452*, 442–447.

Metchnikoff, É. (1892). Leçons sur la pathologie comparée de l ' inflammation : faites à l ' Institut Pasteur en avril et mai 1891 / par Élie Metchnokoff (Paris: Librairie de l'académie de médecine, 120, Boulevard Saint-Germain, Paris).

Miiller, A.M., Medvinsky, A., Strouboulis, J., Grosveld, F., and Dzierzak, E. (1994). Development of Hematopoietic Stem Cell Activity in the Mouse Embryo. Immunity *1*, 291–301.

Mikkola, H.K. a, and Orkin, S.H. (2006). The journey of developing hematopoietic stem cells. Development *133*, 3733–3744.

Mikkola, H.K.A., Fujiwara, Y., Schlaeger, T.M., Traver, D., and Orkin, S.H. (2003). Expression of CD41 marks the initiation of definitive hematopoiesis in the mouse embryo. Blood *101*, 508–516.

Minot, C.S. (1912). The origin of the Angioblast and the Development of the blood. In Manual of Human Embryology, F. Keibel, and F.P. Mall, eds. (Philadelphia & London: J.B. Lippincott Company), p.

Monypenny, J., Chou, H.C., Bañón-Rodríguez, I., Thrasher, A.J., Antón, I.M., Jones, G.E., and Calle, Y. (2011). Role of WASP in cell polarity and podosome dynamics of myeloid cells. Eur. J. Cell Biol. *90*, 198–204.

Moore, M., and Metcalf, D. (1970). Ontogeny of the haemopoietic system: yolk sac origin

of in vivo and in vitro colony forming cells in the developing mouse embryo. Br J Haematol *18*, 279–296.

Morikawa, Y., Zehir, A., Maska, E., Deng, C., Schneider, M.D., Mishina, Y., and Cserjesi, P. (2009). BMP signaling regulates sympathetic nervous system development through Smad4-dependent and -independent pathways. Development *136*, 3575–3584.

Murayama, E., Kissa, K., Zapata, A., Mordelet, E., Briolat, V., Lin, H.-F., Handin, R.I., and Herbomel, P. (2006). Tracing hematopoietic precursor migration to successive hematopoietic organs during zebrafish development. Immunity *25*, 963–975.

Murayama, E., Sarris, M., Redd, M., Le Guyader, D., Vivier, C., Horsley, W., Trede, N., and Herbomel, P. (2015). NACA deficiency reveals the crucial role of somite-derived stromal cells in haematopoietic niche formation. Nat. Commun. *6*, 8375.

Muthu, K., Iyer, S., Szilagyi, A., Gamelli, R.L., Shankar, R., and Jones, S.B. (2007). Murine Hematopoietic Stem cells and Progenitors Express Adrenergic Receptors. J Neuroimmunol. *186*, 27–36.

Namikawa, R., Muench, M.O., and Roncarolo, M.G. (1996). Regulatory roles of the ligand for Flk2/Flt3 tyrosine kinase receptor on human hematopoiesis. Stem Cells *14*, 388–395.

Naveiras, O., Nardi, V., Wenzel, P.L., Hauschka, P. V, Fahey, F., and Daley, G.Q. (2009). Bone-marrow adipocytes as negative regulators of the haematopoietic microenvironment. Nature *460*, 259–263.

Newby, A.C. (2007). Metalloproteinases and Vulnerable Atherosclerotic Plaques. Trends Cardiovasc. Med. *17*, 253–258.

Nombela-Arrieta, C., Pivarnik, G., Winkel, B., Canty, K.J., Harley, B., Mahoney, J.E., Park, S.-Y., Lu, J., Protopopov, A., and Silberstein, L.E. (2013). Quantitative imaging of haematopoietic stem and progenitor cell localization and hypoxic status in the bone marrow microenvironment. Nat. Cell Biol. *15*, 533–543.

North, T., Gu, T.L., Stacy, T., Wang, Q., Howard, L., Binder, M., Marín-Padilla, M., and Speck, N.A. (1999). Cbfa2 is required for the formation of intra-aortic hematopoietic clusters. Development *126*, 2563–2575.

North, T.E., De Bruijn, M.F.T.R., Stacy, T., Talebian, L., Lind, E., Robin, C., Binder, M., Dzierzak, E., and Speck, N.A. (2002). Runx1 expression marks long-term repopulating hematopoietic stem cells in the midgestation mouse embryo. Immunity *16*, 661–672.

North, T.E., Goessling, W., Walkley, C.R., Lengerke, C., Kopani, K.R., Lord, A.M., Weber, G.J., Bowman, T. V, Jang, I.-H., Grosser, T., et al. (2007). Prostaglandin E2 regulates vertebrate haematopoietic stem cell homeostasis. Nature *447*, 1007–1011.

North, T.E., Goessling, W., Peeters, M., Li, P., Ceol, C., Lord, A.M., Weber, G.J., Harris, J., Cutting, C.C., Huang, P., et al. (2009). Hematopoietic stem cell development is dependent on blood flow. Cell *137*, 736–748.

Oberlin, E., Tavian, M., Blazsek, I., and Péault, B. (2002). Blood-forming potential of vascular endothelium in the human embryo. Development *129*, 4147–4157.

Ogawa, M., Matsuzaki, Y., Nishikawa, S., Hayashi, S.-I., Kunisada, T., Sudo, T., Kina, T., Nakauchi, H., and Nishikawa, S.-I. (1991). Expression and Function of c-kit in Hemopoietic

Progenitor Cells. J. Exp. Med. *174*, 63–71.

Oguro, H., Ding, L., and Morrison, S.J. (2013). SLAM family markers resolve functionally distinct subpopulations of hematopoietic stem cells and multipotent progenitors. Cell Stem Cell *13*, 102–116.

Osawa, M., Hanada, K., Hamada, H., and Nakauchi, H. (1996). Long-Term Lymphohematopoietic Reconstitution by a Single CD34-Low/Negative Hematopoietic Stem Cell. Science (80-.). *273*, 242–245.

Palha, N., Guivel-Benhassine, F., Briolat, V., Lutfalla, G., Sourisseau, M., Ellett, F., Wang, C.-H., Lieschke, G.J., Herbomel, P., Schwartz, O., et al. (2013). Real-time whole-body visualization of Chikungunya Virus infection and host interferon response in zebrafish. PLoS Pathog. *9*, e1003619.

Palis, J., Robertson, S., Kennedy, M., Wall, C., and Keller, G. (1999). Development of erythroid and myeloid progenitors in the yolk sac and embryo proper of the mouse. Development *126*, 5073–5084.

Panni, R.Z., Linehan, D.C., and DeNardo, D.G. (2013). Targeting tumor-infiltrating macrophages to combat cancer. Immunotherapy *5*, 1075–1087.

Pappenheim, A. (1896). Ueber Entwickelung und Ausbildung der Erythroblasten. Virchows Arch. *145*, 587–643.

Paul, F., Arkin, Y., Giladi, A., Jaitin, D.A., Kenigsberg, E., Keren-Shaul, H., Winter, D., Lara-Astiaso, D., Gury, M., Weiner, A., et al. (2015). Transcriptional Heterogeneity and Lineage Commitment in Myeloid Progenitors. Cell *163*, 1663–1677.

Payushina, O. V. (2012). Hematopoietic Microenvironment in the Fetal Liver: Roles of Different Cell Populations. ISRN Cell Biol. *2012*, 1–7.

Peeters, M., Ottersbach, K., Bollerot, K., Orelio, C., Bruijn, M. De, Wijgerde, M., and Dzierzak, E. (2009). Ventral embryonic tissues and Hedgehog proteins induce early AGM hematopoietic stem cell development. *2621*, 2613–2621.

Peri, F., and Nüsslein-Volhard, C. (2008). Live imaging of neuronal degradation by microglia reveals a role for v0-ATPase a1 in phagosomal fusion in vivo. Cell *133*, 916–927.

Pollard, J.W. (2004). Tumour-educated macrophages promote tumour progression and metastasis. Nat. Rev. Cancer *4*, 1–8.

Pollard, J.W. (2009). Trophic macrophages in development and disease. Nat. Rev. Immunol. *9*, 259–270.

Pouget, C., Gautier, R., Teillet, M.-A., and Jaffredo, T. (2006). Somite-derived cells replace ventral aortic hemangioblasts and provide aortic smooth muscle cells of the trunk. Development *133*, 1013–1022.

Prashad, S.L., Calvanese, V., Yao, C.Y., Kaiser, J., Wang, Y., Sasidharan, R., Crooks, G., Magnusson, M., and Mikkola, H.K.A. (2015). GPI-80 defines self-renewal ability in hematopoietic stem cells during human development. Cell Stem Cell *16*, 80–87.

Quillard, T., Croce, K., Jaffer, F.A., Weissieder, R., and Libby, P. (2011). Molecular imaging of macrophage protease activity in cardiovascular inflammation in vivo. Thromb Haemost

105, 828–836.

Rae, F., Woods, K., Sasmono, T., Campanale, N., Taylor, D., Ovchinnikov, D.A., Grimmond, S.M., Hume, D.A., Ricardo, S.D., and Little, M.H. (2007). Characterisation and trophic functions of murine embryonic macrophages based upon the use of a Csf1r-EGFP transgene reporter. Dev. Biol. *308*, 232–246.

Ramalho-Santos, M., and Willenbring, H. (2007). On the Origin of the Term "Stem Cell." Cell Stem Cell *1*, 35–38.

Ramond, C., Berthault, C., Burlen-Defranoux, O., de Sousa, A.P., Guy-Grand, D., Vieira, P., Pereira, P., and Cumano, A. (2014). Two waves of distinct hematopoietic progenitor cells colonize the fetal thymus. Nat. Immunol. *15*, 27–35.

Ransom, D.G., Bahary, N., Niss, K., Traver, D., Burns, C., Trede, N.S., Paffett-Lugassy, N., Saganic, W.J., Anthoney Lim, C., Hersey, C., et al. (2004). The Zebrafish moonshine gene encodes transcriptional intermediary factor 1??, an essential regulator of hematopoiesis. PLoS Biol. *2*.

Reimer, M.M., Norris, A., Ohnmacht, J., Patani, R., Zhong, Z., Dias, T.B., Kuscha, V., Scott, A.L., Chen, Y.-C., Rozov, S., et al. (2013). Dopamine from the brain promotes spinal motor neuron generation during development and adult regeneration. Dev. Cell *25*, 478–491.

Renshaw, S. a, Loynes, C. a, Trushell, D.M.I., Elworthy, S., Ingham, P.W., and Whyte, M.K.B. (2006). A transgenic zebrafish model of neutrophilic inflammation. Blood *108*, 3976–3978.

Ridley, A.J. (2001). Rho GTPases and cell migration. J Cell Sci *114*, 2713–2722.

Robin, C., Ottersbach, K., Durand, C., Peeters, M., Vanes, L., Tybulewicz, V., and Dzierzak, E. (2006). An Unexpected Role for IL-3 in the Embryonic Development of Hematopoietic Stem Cells. Dev. Cell *11*, 171–180.

Robin, C., Bollerot, K., Mendes, S., Haak, E., Crisan, M., Cerisoli, F., Lauw, I., Kaimakis, P., Jorna, R., Vermeulen, M., et al. (2009). Human Placenta Is a Potent Hematopoietic Niche Containing Hematopoietic Stem and Progenitor Cells throughout Development. Cell Stem Cell *5*, 385–395.

Robin, C., Ottersbach, K., and Boisset, J. (2011). CD41 is developmentally regulated and differentially expressed on mouse hematopoietic stem cells. Blood *117*, 5088–5092.

Rohrer, H. (2011). Transcriptional control of differentiation and neurogenesis in autonomic ganglia. Eur. J. Neurosci. *34*, 1563–1573.

Roques, M., Durand, C., Gautier, R., Canto, P.Y., Petit-Cocault, L., Yvernogeau, L., Dunon, D., Souyri, M., and Jaffredo, T. (2012). Endoglin expression level discriminates long-term hematopoietic from short-term clonogenic progenitor cells in the aorta. Haematologica *97*, 975–979.

Rőszer, T. (2015). Understanding the Mysterious M2 Macrophage through Activation Markers and Effector Mechanisms. Mediators Inflamm. *2015*, 816460.

Ruiz-Herguido, C., Guiu, J., D'Altri, T., Inglés-Esteve, J., Dzierzak, E., Espinosa, L., and Bigas, A. (2012). Hematopoietic stem cell development requires transient Wnt/β-catenin activity. J. Exp. Med. *209*, 1457–1468.

Sadlon, T.J., Lewis, I.D., and Andrea, R.J.D. (2004). BMP4: Its role in development of the hematopoietic system and potential as a hematopoietic growth factor. Stem Cells *22*, 457–474.

Saito, D., and Takahashi, Y. (2015). Sympatho-adrenal morphogenesis regulated by the dorsal aorta. Mech. Dev. *138 Pt 1*, 2–7.

Saito, D., Takase, Y., Murai, H., and Takahashi, Y. (2012). The dorsal aorta initiates a molecular cascade that instructs sympatho-adrenal specification. Science *336*, 1578–1581.

Sanz-Moreno, V., and Marshall, C.J. (2010). The plasticity of cytoskeletal dynamics underlying neoplastic cell migration. Curr. Opin. Cell Biol. *22*, 690–696.

Schnoor, M., Cullen, P., Lorkowski, J., Stolle, K., Robenek, H., Troyer, D., Rauterberg, J., and Lorkowski, S. (2008). Production of type VI collagen by human macrophages: a new dimension in macrophage functional heterogeneity. J. Immunol. *180*, 5707–5719.

Schofield, R. (1978). The relationship between the spleen colony-forming cell and the haemopoietic stem cell. Blood Cells *4*, 7–25.

Semenova, S.A., Chen, Y.C., Zhao, X., Rauvala, H., and Panula, P. (2014). The tyrosine hydroxylase 2 (TH2) system in zebrafish brain and stress activation of hypothalamic cells. Histochem. Cell Biol. *142*, 619–633.

Shi, X., Richard, J., Zirbes, K.M., Gong, W., Lin, G., Kyba, M., Thomson, J.A., Koyano-Nakagawa, N., and Garry, D.J. (2014). Cooperative interaction of Etv2 and Gata2 regulates the development of endothelial and hematopoietic lineages. Dev. Biol. *389*, 208–218.

Song, H.-D., Sun, X.-J., Deng, M., Zhang, G.-W., Zhou, Y., Wu, X.-Y., Sheng, Y., Chen, Y., Ruan, Z., Jiang, C.-L., et al. (2004). Hematopoietic gene expression profile in zebrafish kidney marrow. Proc. Natl. Acad. Sci. U. S. A. *101*, 16240–16245.

Souilhol, C., Gonneau, C., Lendinez, J.G., Batsivari, A., Rybtsov, S., Wilson, H., Morgado-Palacin, L., Hills, D., Taoudi, S., Antonchuk, J., et al. (2016). Inductive interactions mediated by interplay of asymmetric signalling underlie development of adult haematopoietic stem cells. Nat. Commun. *7*, 10784.

Spangrude, G.J., Heimfeld, S., and Weissman, I.L. (1988). Purification and Characterization of Mouse Hematopoietic Stem Cells. Science (80-.). *241*, 58–62.

Stanke, M., Duong, C.V., Pape, M., Geissen, M., Burbach, G., Deller, T., Parlato, R., Schütz, G., Development, H.R., Otto, C., et al. (2005). Target-dependent specification of the neurotransmitter phenotype: cholinergic differentiation of sympathetic neurons is mediated in vivo by gp130 signaling. Development *133*, 383–383.

Steele, S.L., Ekker, M., and Perry, S.F. (2011). Interactive effects of development and hypoxia on catecholamine synthesis and cardiac function in zebrafish (Danio rerio). J. Comp. Physiol. B Biochem. Syst. Environ. Physiol. *181*, 527–538.

Stein, M., Keshav, S., Harris, N., and Gordon, S. (1992). Interleukin 4 potently enhances murine macrophage mannose receptor activity: a marker of alternative immunologic macrophage activation. J. Exp. Med. *176*, 287–292.

Stewart, R.A., Arduini, B.L., Berghmans, S., George, R.E., Kanki, J.P., Henion, P.D., and Look, A.T. (2006). Zebrafish foxd3 is selectively required for neural crest specification, migration and survival. Dev. Biol. *292*, 174–188.

Sudo, T., Yokota, T., Ishibashi, T., Ichii, M., Doi, Y., and Oritani, K. (2013). Canonical HSC markers and recent achievements. In Stem Cell Biology in Normal Life and Diseases, K. Alimoghaddam, ed. (Intech), pp. 51–64.

Sugiyama, D., Inoue-Yokoo, T., Fraser, S.T., Kulkeaw, K., Mizuochi, C., and Horio, Y. (2011). Embryonic regulation of the mouse hematopoietic niche. ScientificWorldJournal. *11*, 1770–1780.

Sugiyama, T., Kohara, H., Noda, M., and Nagasawa, T. (2006). Maintenance of the Hematopoietic Stem Cell Pool by CXCL12-CXCR4 Chemokine Signaling in Bone Marrow Stromal Cell Niches. Immunity *25*, 977–988.

Takahashi, Y., Sipp, D., and Enomoto, H. (2013). Tissue interactions in neural crest cell development and disease. Science *341*, 860–863.

Tamplin, O.J., Durand, E.M., Carr, L.A., Childs, S.J., Hagedorn, E.J., Li, P., Yzaguirre, A.D., Speck, N.A., and Zon, L.I. (2015). Hematopoietic stem cell arrival triggers dynamic remodeling of the perivascular niche. Cell *160*, 241–252.

Tang, J., Li, Z., Lu, L., and Cho, C.H. (2013). β-Adrenergic system, a backstage manipulator regulating tumour progression and drug target in cancer therapy. Semin. Cancer Biol. *23*, 533–542.

Tavian, M., Biasch, K., Sinka, L., Vallet, J., and Péault, B. (2010). Embryonic origin of human hematopoiesis. Int. J. Dev. Biol. *54*, 1061–1065.

Theveneau, E., and Mayor, R. (2012). Neural crest delamination and migration: from epithelium-to-mesenchyme transition to collective cell migration. Dev. Biol. *366*, 34–54.

Till, J.E., and McCulloch, E.A. (1961). A direct measurement of the radiation sensitivity of normal bone marrow cells. Radiat Res *Feb*, 213–222.

Travnickova, J., Tran Chau, V., Julien, E., Mateos-Langerak, J., Gonzalez, C., Lelièvre, E., Lutfalla, G., Tavian, M., and Kissa, K. (2015). Primitive macrophages control HSPC mobilization and definitive haematopoiesis. Nat. Commun. *6*, 6227.

Turk, B. (2006). Targeting proteases: successes, failures and future prospects. Nat. Rev. Drug Discov. *5*, 785–799.

Vérollet, C., Charrière, G.M., Labrousse, A., Cougoule, C., Le Cabec, V., and Maridonneau-Parini, I. (2011). Extracellular proteolysis in macrophage migration: losing grip for a breakthrough. Eur. J. Immunol. *41*, 2805–2813.

Visnjic, D., Kalajzic, Z., Rowe, D.W., Katavic, V., Lorenzo, J., and Aguila, H.L. (2004). Hematopoiesis is severely altered in mice with an induced osteoblast deficiency. Blood *103*, 3258–3264.

Vu, T.H., and Werb, Z. (2000). Matrix metalloproteinases : effectors of development and normal physiology. Genes Dev. *14*, 2123–2133.

Wang, Z., Nishimura, Y., Shimada, Y., Umemoto, N., Hirano, M., Zang, L., Oka, T., Sakamoto, C., Kuroyanagi, J., and Tanaka, T. (2009). Zebrafish beta-adrenergic receptor mRNA expression and control of pigmentation. Gene *446*, 18–27.

Welgus, H.G., Campbell, E.J., Cury, J.D., Eisen, A.Z., Senior, R.M., Wilhem, S.M., and

Goldberg, G.J. (1990). Neutral metalloproteinases produced by human mononuclear phagocytes. J Clin.Invest. *86*, 1496–1502.

Westerfield, M. (2000). The Zebrafish book. A guide for the laboratory use of zebrafish (Danio rerio), 4th edition (Eugene).

Wheeler, A.P., Wells, C.M., Smith, S.D., Vega, F.M., Henderson, R.B., Tybulewicz, V.L., and Ridley, A.J. (2006). Rac1 and Rac2 regulate macrophage morphology but are not essential for migration. J. Cell Sci. *119*, 2749–2757.

Whetton, A.D., and Graham, G.J. (1999). Homing and mobilization in the stem cell niche. Trends Cell Biol. *9*, 233–238.

Wiesner, C., Le-Cabec, V., El Azzouzi, K., Maridonneau-Parini, I., and Linder, S. (2014). Podosomes in space: Macrophage migration and matrix degradation in 2D and 3D settings. Cell Adhes. Migr. *8*, 179–191.

Wikberg, J.E. (1982). Adrenergic receptors: classification, ligand binding and molecular properties. Acta Med. Scand. Suppl. *665*, 19–36.

Wilkinson, R.N., Pouget, C., Gering, M., Russell, A.J., Davies, S.G., Kimelman, D., and Patient, R. (2009). Hedgehog and Bmp Polarize Hematopoietic Stem Cell Emergence in the Zebrafish Dorsal Aorta. Dev. Cell *16*, 909–916.

Winkler, I.G., Sims, N. a, Pettit, A.R., Barbier, V., Nowlan, B., Helwani, F., Poulton, I.J., van Rooijen, N., Alexander, K. a, Raggatt, L.J., et al. (2010). Bone marrow macrophages maintain hematopoietic stem cell (HSC) niches and their depletion mobilizes HSCs. Blood *116*, 4815–4828.

Winkler, I.G., Barbier, V., Nowlan, B., Jacobsen, R.N., Forristal, C.E., Patton, J.T., Magnani, J.L., and Lévesque, J.-P. (2012). Vascular niche E-selectin regulates hematopoietic stem cell dormancy, self renewal and chemoresistance. Nat. Med. *18*, 1651–1657.

Wu, C., Li, B., Lu, R., Koelle, S.J., Yang, Y., Jares, A., Krouse, A.E., Metzger, M., Liang, F., Lor??, K., et al. (2014). Clonal tracking of rhesus macaque hematopoiesis highlights a distinct lineage origin for natural killer cells. Cell Stem Cell *14*, 486–499.

Wyatt, R. a, Keow, J.Y., Harris, N.D., Haché, C. a, Li, D.H., and Crawford, B.D. (2009). The zebrafish embryo: a powerful model system for investigating matrix remodeling. Zebrafish *6*, 347–354.

Wynn, T. a, Chawla, A., and Pollard, J.W. (2013). Macrophage biology in development, homeostasis and disease. Nature *496*, 445–455.

Xie, Y., Yin, T., Wiegraebe, W., He, X.C., Miller, D., Stark, D., Perko, K., Alexander, R., Schwartz, J., Grindley, J.C., et al. (2009). Detection of functional haematopoietic stem cell niche using real-time imaging. Nature *457*, 97–101.

Yamazaki, S., Ema, H., Karlsson, G., Yamaguchi, T., Miyoshi, H., Shioda, S., Taketo, M.M., Karlsson, S., Iwama, A., and Nakauchi, H. (2011). Nonmyelinating Schwann cells maintain hematopoietic stem cell hibernation in the bone marrow niche. Cell *147*, 1146–1158.

Yang, J., Zhang, L., Yu, C., Yang, X.-F., and Wang, H. (2014). Monocyte and macrophage differentiation: circulation inflammatory monocyte as biomarker for inflammatory diseases. Biomark. Res. *2*, 1.

Yokomizo, T., and Dzierzak, E. (2010). Three-dimensional cartography of hematopoietic clusters in the vasculature of whole mouse embryos. Development *137*, 3651–3661.

Yokota, T., Oritani, K., Butz, S., Ewers, S., Vestweber, D., and Kanakura, Y. (2012). Markers for Hematopoietic Stem Cells : Histories and Recent Achievements. In Advances in Hematopoietic Stem Cell Research, R. Pelayo, ed. (InTech), pp. 77–88.

Yoong, S., O'Connell, B., Soanes, A., Crowhurst, M.O., Lieschke, G.J., and Ward, A.C. (2007). Characterization of the zebrafish matrix metalloproteinase 9 gene and its developmental expression pattern. Gene Expr. Patterns *7*, 39–46.

Young, H.M., Cane, K.N., and Anderson, C.R. (2011). Development of the autonomic nervous system: a comparative view. Auton. Neurosci. *165*, 10–27.

Zhang, C.C., and Lodish, H.F. (2004). Insulin-like growth factor 2 expressed in a novel fetal liver cell population is a growth factor for hematopoietic stem cells. Growth (Lakeland) *103*, 2513–2521.

Zhang, C.C., Kaba, M., Ge, G., Xie, K., Tong, W., Hug, C., and Lodish, H.F. (2006). Angiopoietin-like proteins stimulate ex vivo expansion of hematopoietic stem cells. Nat. Med. *12*, 240–245.

Zhang, Y., Bai, X.-T., Zhu, K.-Y., Jin, Y., Deng, M., Le, H.-Y., Fu, Y.-F., Chen, Y., Zhu, J., Look, a T., et al. (2008). In vivo interstitial migration of primitive macrophages mediated by JNK-matrix metalloproteinase 13 signaling in response to acute injury. J. Immunol. *181*, 2155–2164.

Zovein, A.C., Hofmann, J.J., Lynch, M., French, W.J., Turlo, K.A., Yang, Y., Becker, M.S., Zanetta, L., Dejana, E., Gasson, J.C., et al. (2008). Fate Tracing Reveals the Endothelial Origin of Hematopoietic Stem Cells. Cell Stem Cell *3*, 625–636.

Résumé

L'hématopoïèse est le processus de formation des cellules souches hématopoïétiques (CSH); elle est conservée au cours d'évolution. Durant l'hématopoïèse embryonnaire, deux vagues hématopoïétiques se succèdent, la vague primitive et la vague définitive. La vague primitive produit des macrophages, des neutrophiles et des érythrocytes. Au cours de la vague définitive, les CSH émergent du plancher de l'aorte dorsale par une transition endothélio-hématopoïétique ou TEH, dans une région appelée aorte-gonades-mesonephros (AGM).

Ces dernières années, des études des organes hématopoïétiques chez les mammifères ont démontré que le microenvironnement joue un rôle crucial dans l'émergence et le devenir des CSH. Pendant ma thèse, je me suis intéressée au rôle du microenvironnement dans la mise en place de l'hématopoïèse définitive chez l'embryon de zebrafish. Dans l'AGM, j'ai caractérisé et évalué la contribution de différents acteurs dont deux populations en particulier, les macrophages et le système neuronal sympathique. Chacune de ces cellules joue un rôle spécifique durant la vague définitive de l'hématopoïèse. Les macrophages mobilisent des CSH de l'AGM afin de permettre leur intravasation et la colonisation des organes hématopoïétiques. Les catécholamines synthétisées par le système neuronal sympathique quant à elles contrôlent la TEH par l'activation des récepteurs beta2b et beta3 dans l'AGM.

En conclusion, nous avons démontré que le microenvironnement influence l'hématopoïèse définitive chez le zebrafish par différents mécanismes. Ces travaux ont pour objectif d'améliorer la compréhension du mécanisme de genèse des CSH et potentiellement de permettre un jour la production de CSH *in vitro*.

Abstract

Haematopoiesis is the process of haematopoietic stem cell (HSC) generation conserved in all vertebrates. During the embryonic development, two successive waves of haematopoiesis occur – the primitive and the definitive wave. The first one gives rise to erythrocytes, macrophages and neutrophils. During the second one, HSCs emerge from the ventral wall of dorsal aorta (DA) in the aorta-gonads-mesonephros (AGM) region by a process called endothelial-to-haematopoietic transition or EHT.

In the last years, several studies performed in mammals have shown that the microenvironment plays a key role in haematopoiesis. During my thesis I have studied the role of the microenvironment in definitive haematopoiesis in the zebrafish embryo. I have described several cell components present in the AGM and evaluated their contribution to the haematopoiesis. I further analysed two of those players: macrophages and sympathetic nervous system. Each of them plays a specific role during the definitive wave of haematopoiesis. Macrophages mobilise nascent HSCs from the AGM to allow their intravasation and colonisation of haematopoietic organs. Catecholamines synthetized by sympathetic nervous system control EHT through the activation of beta2b and beta3 receptors in the AGM.

In conclusion, we have shown that the microenvironment can substantially influence the definitive haematopoiesis in the zebrafish by distinct mechanisms. These findings would help to understand the mechanism of HSC generation and potentially to allow *in vitro* HSC production.